Prediction of Rainfall Runoff in Geoenvironmental Engineering Practice

by

Ahlam Abdulnabi

A thesis submitted in partial fulfillment of the requirements for the degree of

Doctor of Philosophy

in

Geoenvironmental Engineering

Department of Civil and Environmental Engineering
University of Alberta

ABSTRACT

Soil cover systems are engineered barriers designed to isolate hazardous mine waste from climatic water and oxygen. Assessment of water flow at the interface between the atmosphere and the ground surface is paramount to successful cover design. For decades, cover systems were designed based on infiltration and evaporation models often overlooking surface runoff. Runoff is a fundamental part of the rainwater cycle intertwined with both infiltration and evaporation but rarely adequately examined in the context of cover system design.

This thesis provides a laboratory and numerical modelling program for comprehensive physical evaluation of rainfall runoff responses in soil cover systems. In the laboratory, rainfall runoff tests were conducted using a specially designed rainfall simulator apparatus. A series of controlled rainfall experiments targeted at low permeability and capillary barrier profiles were completed. The experiments focused on observing the runoff phenomenon and quantifying the volume, rate, and time until runoff occurred in response to variation of applied rainfall intensities. Changes in matric suction and volumetric water content were monitored as wetting fronts propagated through the soil profiles. Soil profiles were investigated under different saturation states. The study focused on one central question: is it possible to predict rainfall runoff based on measurable soil properties? Laboratory observations suggest that yes, rainfall runoff rates and volumes are primarily governed by the applied rainfall intensity and saturated hydraulic conductivity in the case of saturated soil surfaces, whereas rainfall runoff rates are governed by the applied rainfall intensity and infiltration capacity for unsaturated soil profiles.

The laboratory experiments were numerically replicated for each profile using the SVFlux model. One- and three-dimensional models were assessed for saturated and unsaturated initial states. One-dimensional models produced runoff cumulative volume results within 6% accuracy for most low permeability profiles. Less rigorous results were observed in the capillary barrier profiles, where accuracy varied between 1% and 32%. Three-dimensional models marginally improved the results for capillary barrier profiles. Overall, the results of numerical predictions testify to a reasonably good capability to predict runoff fluxes for controlled laboratory conditions.

Lastly, a case study of the Savage River mine in Australia was evaluated to ascertain temporal and spatial variability effects on numerical predictions in field settings. Comparisons of field measured rainfall, and runoff volumes with predictions made by SVFlux were discussed. Both non-vegetated water-shedding cover system and uncovered tailings dam were examined. The study encompassed detailed sensitivity analyses of surface runoff predictions in response to the changing input of rainfall intensity resolution and saturated hydraulic conductivity. The results showed that runoff predictions were highly sensitive to both the resolution of precipitation rate and change in saturated hydraulic conductivity input. Close attention to site conditions is vital when choosing soil parameters to attain meaningful results.

PREFACE

This thesis is an original work by Ahlam Abdulnabi under the supervision of Dr. G. Ward Wilson. The literature review in Chapter 2 is a summary of a comprehensive report Ahlam submitted in partial fulfillment of the Master of Engineering degree at the University of Alberta in 2015. Chapter 3 is a summary of classical theories in unsaturated soil mechanics pertinent to the current work. All laboratory data acquisition and analysis in Chapter 4 were designed, constructed, and conducted by Ahlam. Input data in Chapter 4 for the field case study were collected by S. K. Jubinville as part of an MSc program at the University of Alberta. However, all SVFlux simulations and sensitivity analyses were completed by Ahlam.

The results of the laboratory study were published in the proceedings of the 68th Canadian Geotechnical Conference, GeoQuebec 2015. The field case study results were published in the proceedings of the 69th Canadian Geotechnical Conference, GeoVancouver 2016. The results of numerical modelling of laboratory tests were published in the proceedings of the 70th Canadian Geotechnical Conference, GeoOttawa 2017. The practical recommendations pertinent to runoff prediction in soil cover systems were published in the proceedings of the 71st Canadian Geotechnical Conference, GeoEdmonton 2018.

To Yusef and Haytham, my favourite beings in the Cosmos

ACKNOWLEDGMENTS

I would like to gratefully acknowledge the financial support of the National Science and Engineering Research Council of Canada (NSERC) and the University of Alberta.

I am grateful beyond measure to my supervisor, Dr. Ward Wilson, for his guidance, counsel, constant encouragement, and inexorable positive influence throughout my tenure as a graduate student. Studying under a world-class expert has been an immense privilege that has profoundly defined the researcher, the academic and, indeed, the person I have become. Without Dr. Wilson's moral and financial support, I would not have been able to complete this degree.

I extend my genuine appreciation to my supervisory committee, Dr. Dave Sego, and Dr. Michael Hendry for their encouragement, invaluable technical insight, and constant support. Thank you to my candidacy examiners, Dr. Derek Martin and Dr. Del Fredlund for stimulating discussions. My heartfelt thanks go to Dr. Mohamad Kayyal for his active support since the days of my bachelor's degree to this day.

I am overwhelmed with the amount of support and encouragement I received over the years here at the University of Alberta. Thank you to everyone who crossed paths with me, stood by me and encouraged me. Special thanks to Christine Hereygers for her unwavering assistance during the laboratory program that will be forever appreciated. Many thanks to the fantastic administrative team at the University of Alberta – Sally Petaske, Annette Busenius, Vivian Giang and Jen Stogowski – for their continued willingness to help. I would also like to acknowledge the fabulous team of researchers at the geotechnical centre – Sarah, Louis, Jorge, Juan, Chao, Neeltje, Bereket, David, Ralph - thank you for your ongoing friendship.

I will forever cherish the time spent with my family that has always revived my soul and helped me persevere toward the completion of this thesis. For that, I thank my son, Yusef, my inquisitive and stellar companion who illuminates my world with endless laughs, hugs, and love. And, my husband, Haytham, you are one of a kind partner. We have been through so many terrific times and milestones together and made it through the tough times. Your unparalleled support has afforded me to chase my dreams and make them a reality. I cannot thank you enough for all you have been and done. Mom and Dad, you both worked so hard to see us succeed and I hope this makes you proud. I will never forget where I come from or what it took to get here. My fellow Syrians have endured years of hardships and suffering, but I am hopeful that the day will come to rebuild and prosper.

Post Manuscript

Sincere thank you to Dr. Dirk van Zyl and Dr. Nicholas Beier whose detailed insightful comments helped me greatly in preparing this final version of my thesis following my defence.

TABLE OF CONTENTS

LIST OF FIGURES

LIST OF TABLES

LIST OF SYMBOLS AND ACRONYMS

ARD	Acid rock drainage
AE	Actual evaporation
AEV	Air entry value
K_a	Apparent dielectric constant
P	Campbell parameter
CB	Capillary barrier
h_c	Capillary rise
CU	Christensen uniformity coefficient
Mv	Coefficient of compressibility
ρ_w	Density of water
DC	Direct current
y	Elevation head
FEM	Finite element method
n	Fitting parameter related to rate of water extraction beyond air entry value.
a	Fitting parameter related to the air entry value of the soil
m	Fitting parameter related to the residual water content of the soil.
GARD	Global acid rock drainage
g	Gravitational acceleration
i	Hydraulic gradient
I	Infiltration

I_C	Infiltration capacity
$(u_a - u_w)$	Matric suction
OTD	Old tailings dam
π	Osmotic suction
PSD	Particle size distribution
PVC	Polyvinyl chloride
u_a	Pore-air pressure
u_w	Pore-water pressure
PE	Potential evaporation
R	Rainfall
REV	Referential element volume
θ_{ar}.	Residual air content
θ_r	Residual volumetric water content.
$(u_a - u_w)_r$	Residual matric suction
RO	Runoff
K_{sat}	Saturated hydraulic conductivity
θ_s	Saturated volumetric water content.
SRRP	Savage river rehabilitation program
SWCC	Soil water characteristics curves
ψ	Soil total suction
Gs	Specific gravity
α	The angle at which surface tension occurs

t	Time
TDR	Time domain reflectometry
h_w	Total hydraulic head
USCS	Unified soil classification system
γ_w	Unit weight of water
K_{unsat}	Unsaturated hydraulic conductivity
v_w	Velocity of water
Vwc	Volumetric water content
ρ_w	Water density
m_2^w	Water storage coefficient related to soil suction
T_s	Water surface tension

CHAPTER 1. Introduction

1.1. General Background

The analysis of water flow both at the ground surface and in the subsurface is crucial for various problems encountered by geotechnical and geoenvironmental engineers. Problems such as the design of earth-fill dams, highways, airport runways, slope stability, and environmental structures such as mine waste cover systems, and landfills, and the like require a profound understanding of water flow. Furthermore, water balance is a significant topic in mine waste management facilities such as tailings and waste rock depositories. The primary motivation for this study was to form an understanding of water flow in the context of soil cover systems. Soil cover systems are engineered barriers designed as containment to prevent Acid Rock Drainage (ARD) in potentially acid forming waste rock and tailings minerals.

The primary process responsible for the generation of acid rock drainage is weathering of sulphide minerals when exposed to atmospheric oxygen and meteoric water. The drainage effluent resulting from the weathering process with pH below 4.5 is termed ARD. The acid-forming process is a complex combination of physical, chemical, and biological factors. The oxidation rate is highly dependent on surface area exposed to weathering, grain size, presence of oxygen and water, the presence of other oxidizing agents like iron, current acidity, temperature, and the presence of certain bacteria, (i.e. Thiobacillus ferrooxidans). The reaction occurs slowly at first. However, once underway, the rate of acid production progressively increases with time through both chemical and biological oxidation. The chain reaction accelerates as lower pH develops, and consequently cause increased concentrations of dissolved heavy metals as described in the global acid rock drainage (GARD) guide (2018).

Even though ARD can occur naturally, anthropogenic activities such as mining activities can accelerate the weathering process through earthmoving operations. Global existing liability due to ARD neutralization and hydrolysis are excessively costly and perpetual nature of the treatment creates an added complexity to what is already a severe and enduring issue. Therefore, proactive safe disposal of sulphide-bearing minerals is critical. One of the most effective and widely spread techniques for ARD prevention is the construction of soil cover systems to restrict contact of oxygen and water with the waste repository, thus interrupting the onset of ARD.

1.2. Statement of Problem

Subaqueous disposal of acid generating minerals is a preferred strategy for the long-term closure of reactive minerals worldwide as outlined by the global acid rock drainage (GARD) guide. Submergence of ARD generating materials severely limits oxygen transport thus limiting ARD generation over the long term (GARD Guide, 2017).

However, a few key challenges arise from water covers that might limit the use of subaqueous disposal strategies and necessitate alternative techniques. Some of these issues are summarized below:

1. Water covers are only feasible for climates with a positive water balance. Potential periods of prolonged drought may render cover system ineffective in limiting oxygen ingress and require alternative measures. Moreover, mine sites located in an arid climate cannot utilize water cover techniques.

2. A sufficient water level must be maintained to prevent resuspension by wind and wave action concerning tides and currents.

3. Following the catastrophic failures of Mount Polley Tailings Dam in 2014 and Samarco Dam in 2015, the long-term physical stability of containment facilities with large volumes of fluids became a growing concern of geo-professionals worldwide. This is especially crucial when mining void is not available for waste storage as in-pit lakes, but instead, require engineered structures such as dams and embankments.

4. The conflicting priorities of chemical stability that considers water cover an adequate solution for limiting oxidation versus physical stability that considers large water bodies as a perpetual geohazard.

Considering all those challenges associated with water covers, soil covers provide an alternative ARD prevention technique. Soil covers are engineered earthen barriers placed over mine waste; those covers are termed dry covers to distinguish them from water covers. The primary goal of placing dry covers over reactive waste material is to minimize ARD and metal leaching production and to minimize its transport as outlined in the GARD Guide. Furthermore, dry covers help provide an apt rooting zone for vegetation, limiting landforms erosion. Soil covers also help divert meteoric water and limit water infiltration.

The design of soil cover systems is flux driven. In other words, the design regards the ground surface as a boundary across which there is a constant water movement. Water fluxes can either be upward in the form of evaporation, downward in the form of infiltration or across in the form of runoff. Understanding and quantifying those three fluxes of infiltration, evaporation and runoff is paramount. The optimum design of a cover system is case specific. Furthermore, it is highly climate dependent and is generally governed by the quantity of these three components of the rainwater cycle.

Introduction

Numerous models exist for predicting infiltration, such as Green and Ampt (1911), Mein and Larsen (1978) and Philip (1957). This topic is well understood at the point scale and has been extensively covered in the literature. The success of infiltration models, however, is inevitably bound by the ability to calibrate these models. Surface runoff measurements are essential for the calibration process, yet these measurements are rarely completed.

In the absence of runoff measurements, runoff prediction represents the necessary means to calibrate infiltration models. Rainfall-runoff can be the most significant component of the water budget that directly influences the amount of net infiltration, which in turn governs the design and performance of cover systems. The rainwater partitioning between runoff and infiltration is a multifaceted process that has rarely been addressed in the context of geoenvironmental structures highly contingent on these processes such as soil cover systems.

Prediction of rainfall runoff is not adequately addressed in the literature at the field scale. Accurate runoff estimates improve the level of confidence in predicted infiltration, thus enhancing confidence in the cover system design. Although the need to develop a reliable method of predicting rainfall runoff for soil cover systems was the primary motivation for this research, the application can extend well beyond this point, for example, but not limited to operational water balance calculations for tailings facilities, rainfall-induced slope instability, and the like.

In soil /atmospheric modelling, prediction of both evaporation (Penman 1948 and Wilson et al. 1994), and infiltration (Green and Ampt 1911; Horton 1939; Philip 1957; Mein and Larsen 1978) are well addressed in the literature. The same, however, cannot be said about predicting rainfall-runoff. Available models for predicting rainfall runoff at the field scale are rare and require improvements (Schmocker- Fackel et al. 2007, Benson, 2010 and Jubinville 2013). The reader is kindly referred to Abdulnabi (2015) for detailed understanding of the available models to predict runoff and the missing link in these models.

Surface runoff measurements are not only necessary to perform water balance controls, but also a fundamental entity in the practice of geoenvironmental engineering. The general knowledge concerning the prediction of rainfall runoff under different climatic conditions, rainfall intensities, storm events, surface characteristics, profiles types, slopes and topographies, and vegetation is by far under-represented in the geotechnical and geoenvironmental literature.

The intertwined nature of the rainwater, runoff and infiltration cycle is complex and dependent on a range of factors most of which are not covered in literature as will be discussed in later sections. Factors such as saturation conditions of the profiles are often overlooked. Nevertheless, individual understanding of saturated and unsaturated responses is key to understanding the water flow.

This thesis focuses on the examination of rainfall runoff fluxes in a controlled laboratory setting. Effects of different rainfall intensities and different initial conditions are quantified. The advance of an unsaturated front may allow oxygen ingress to underlying waste. The specific objectives of the research are discussed in the following sections.

1.3. Research Objectives

Water balance is a significant concern during and after mining activities. During mining processes, water balance calculations are crucial for proper machine operation and extraction. After mining has been complete, environmental risks, such as ARD associated with closure are critically linked to water flow. How much we know about runoff as part of the water balance cycle dramatically influences these aspects of operation and closure, giving this research its significance.

The primary objective of this research is to examine the phenomenon of rainfall runoff in soil covers systems. The research emphasizes the following specific objectives:

1. Identify physical processes operating at and below the ground surface when rainfall occurs.

2. Identify appropriate soil parameters that control rainfall runoff in different saturation conditions.

3. Formulate a theoretical framework for predicting rainfall runoff in soil profiles at different saturation conditions.

4. Carry out laboratory tests that investigate the theoretical approach regarding different initial conditions and profile types exposed to controlled and variable rainfall intensities.

5. Conduct numerical simulations to investigate how accurate numerical prediction is compared to the laboratory results.

6. Demonstrate the practical significance of the current research in a field case study.

1.4. Thesis Outline

This thesis encompasses seven chapters. The research is introduced in Chapter 1 including a description of the research scope, a general background, and statement of the research problem and research objectives.

Chapter 2 provides a brief summary of a comprehensive review of literature that was submitted in partial fulfillment of MEng degree at the University of Alberta (Abdulnabi 2015), which is publicly available. Topic related to soil cover systems, rainfall runoff generation mechanism, and current approaches of runoff prediction are summarized. Furthermore, the chapter recaps a discussion of the use of a rainfall simulator apparatus to investigate rainfall runoff phenomenon and classifies the factors influencing runoff onset.

Chapter 3 describes the theoretical considerations related to the current research and presents the fundamentals of unsaturated soil mechanics. Moreover, it summarizes the laws of water flow through saturated and unsaturated media and discusses the available numerical solutions.

Chapter 4 is dedicated to the research methodology. The design elements of the rainfall simulator apparatus are discussed. The testing procedure of the laboratory program is presented. Moreover, description of the input and procedure for numerical simulations of the laboratory tests are presented. Lastly, elements of the sensitivity analyses and the numerical simulations of a field case study are discussed.

Chapter 5 presents the results of the laboratory rainfall runoff experiments for each profile type and each saturation scenario. Moreover, the numerical modelling results of replicating those experiments using the model SVFlux. Results of the field case study are presented along with their sensitivity analyses.

Chapter 6 presents a comprehensive discussion of the results and data analyses. Lastly, Chapter 7 encapsulates the summary, conclusions and recommendations for further research.

1.5. Publications Related to This Research

Articles, reports and conference papers were published based on the results of this research work. The following is a summary of the publications:

Abdulnabi, A. Wilson, G. W. 2015. Laboratory Testing Program for the Prediction of Rainfall Runoff from Soil Cover Systems. Proceedings of the 68th Canadian Geotechnical Conference and 7th Canadian Permafrost Conference GeoQuebec 2015, Quebec City. September 20 - 23 2015.

Abdulnabi, A. 2015. A Comprehensive Literature Review for Soil Covers and the Role of Rainfall Runoff in Soil Atmospheric Modelling. MEng. report, University of Alberta, Canada. pp42.

Abdulnabi, A. 2015. Prediction of Rainfall Runoff for Soil Cover Systems: A Laboratory Approach. Geotechnical News Vol. 33 no. 04 P 50. December 2015.

Abdulnabi, A. Jubinville, S. K. Wilson, G. W. 2016. A Case Study of Numerical Prediction of Rainfall Runoff for Soil Cover Systems. Proceedings of the 69th Canadian Geotechnical Conference. GeoVancouver 2016, Vancouver, October 2 - 5 2016.

Abdulnabi, A. Wilson, G. W. 2017. Rainfall Runoff in Cover Systems Design: Are Numerical Predictions and Observational Science Reconcilable? Proceedings of the 70th Canadian Geotechnical Conference and the 12th Joint CGS/IAH-CNC Groundwater Conference. GeoOttawa 2017, Ottawa. October 1 - 4 2017.

Abdulnabi, A. Wilson, W. 2018 Two New Models to Predict Rainfall Runoff in Soil Cover Systems. Proceedings of the 71st Canadian Geotechnical Conference and the 13th Joint CGS/IAH-CNC Groundwater Conference. GeoEdmonton 2018, Edmonton September 23 – 26 2018 (accepted).

CHAPTER 2. Literature Review

2.1. Soil Covers

The selection of waste containment type is based on site-specific conditions and governed by a regulatory framework (O'Kane and Wels 2003). Several types of cover systems exist depending on a range of factors such as climate and specific site conditions. The cover design can have different objectives as listed by O'Kane and Wels (2003) and summarized in Abdulnabi (2015).

Conventional soil covers involve creating a physical hydraulic barrier on top of the containment facility. The conventional barrier comprises a compacted clay barrier to shut off infiltration. We use properties of unsaturated soil to contain water and manage it in a much more natural way works harmoniously with nature.

Water-balance soil covers are a low-cost technique to prevent the onset of ARD proactively. Water-balance covers utilize unsaturated soil behaviour as means of controlling hydrology. The primary purpose of water balance covers is to control the ingress of water thereby keeping precipitation separate from potentially acid forming waste. This eliminates generating leachate that may contaminate groundwater.

The design of water-balance covers is conceptually simple. The layer thickness required for storage can be estimated based on extreme meteorological events and the energy required to remove water by either evaporation or evapotranspiration (Benson 2014). Figure 2.1 illustrates a conceptual schematic of a soil cover system and controlling water fluxes.

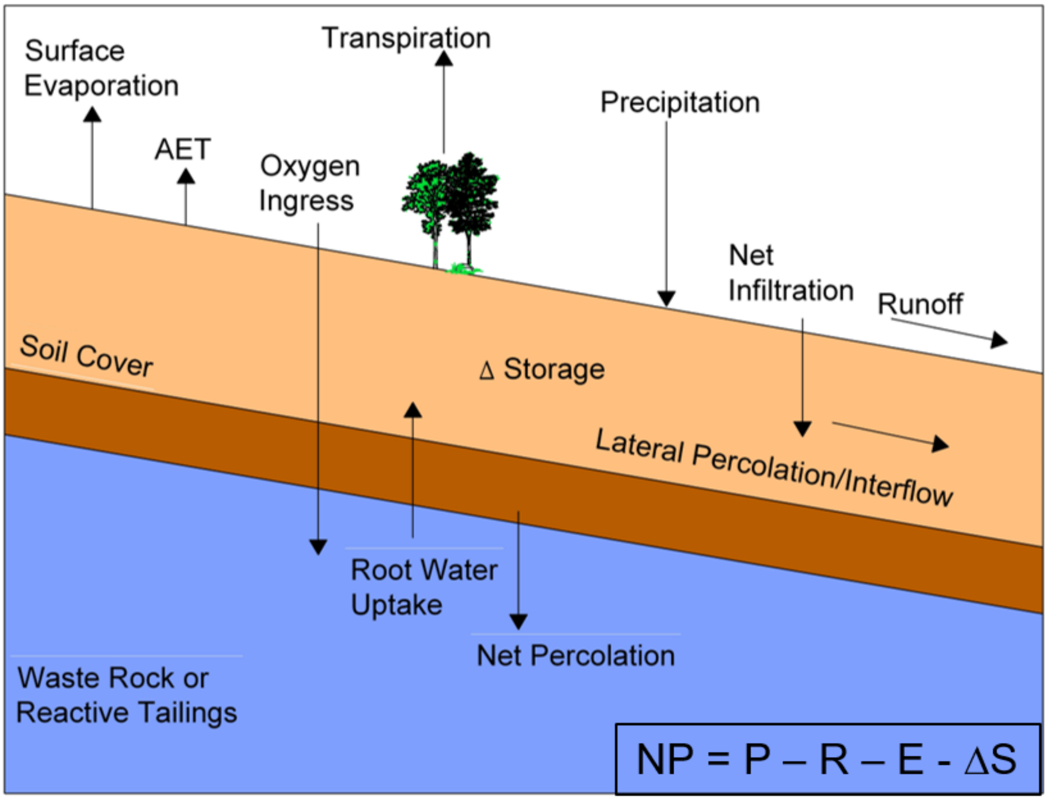

Figure 2.1 Conceptual Schematic of a soil cover system (after GARDGuide 2018)

However, the current state of design overlooks a vital component of the water cycle, i.e. surface runoff. Infiltration and runoff have similar interdependency much like a DNA double helix. One cannot overlook runoff without compromising the engineered design. Thinking of soil covers as barriers to restrict the contact of water and oxygen with potentially reactant minerals makes accounting for all water fluxes crucial in the design. Abdulnabi (2015) discuss in detail the types of cover systems based on climate regime and other controlling criteria. Figure 2.2 illustrates a summary of the design process of dry covers systems.

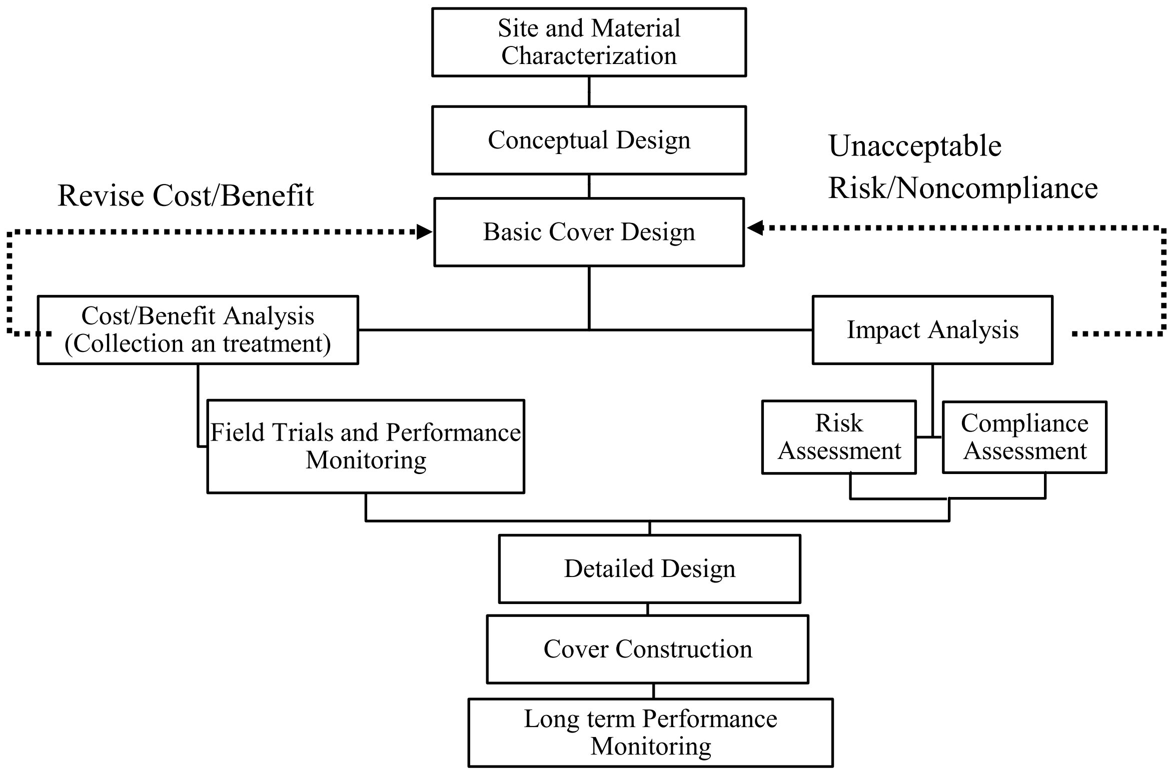

Figure 2.2 Cover Design Process (after GARD Guide 2017).

2.2. Rainfall Runoff

The water balance equation, in simple terms, represents the difference between water inflow and water losses. Despite the mathematical simplicity, the equation remains an indeterminate equation so long as the rainfall runoff is not measured. The entwined nature of infiltration and runoff is confirmed by numerous studies on soil cover systems such as Wilson et al. (2006) and Miskolczi (2007). These studies concluded that net infiltration quantities were significantly influenced by surface runoff quantities, which in turn control the design and long-term performance of water balance covers. Therefore, having reliable runoff predictions have direct implications for soil covers systems performance.

Surface runoff generation mechanisms are discussed in detail in Schmocker-Fackel et al. (2007) and Beven (2012). In the context of soil covers the dominant runoff mechanism is argued to be the *Hortonian Overland Flow*, after Horton (1933), and is also referred to as *the infiltration-excess runoff*. Three critical aspects of the Hortonian Overland Flow need to be considered. The first is that rain falling at rates less than the infiltration capacity of the soil would all infiltrate into the soil. The second is that when infiltration capacity decreases to the point where it is lower than the rainfall intensity, surface depressions begin to fill. The third is that runoff is only generated once the rainfall intensity exceeds the infiltration capacity and all surface depressions are filled.

Horton (1933) introduced "the 'infiltration capacity' concept that considers the soil as a separating surface that divides rainfall water into two portions. One portion is initially absorbed by the soil (infiltration) and then percolates into groundwater. The other portion does not infiltrate into the soil but runs off in the form of surface runoff." "Beven (2004) describes that this function starts at a maximum value when the rainfall begins and then decrease with time nonlinearly down to a minimum value related to the saturated hydraulic conductivity of the soil. After rain ends, restoration of the infiltration capacity begins." (Abdulnabi 2015).

Similarly, "Stone et al. (1996) describe that after the rainfall begins, infiltration capacity is at its maximum, and the potential infiltration rate is greater than the rainfall rate. Nevertheless, the actual infiltration rate is equal to the rainfall rate, since the water can only enter the soil at the application rate. At a certain point in time, referred to as *the time to ponding*, the water begins to pond, and accordingly, the excess water overflows." (Abdulnabi 2015).

For infiltration excess runoff, the quantity of runoff is governed by both the rainfall intensity and soil infiltration capacity. Furthermore, the distribution of rainfall-excess runoff with time depends on the rainfall intensity. (Stone et al. 1996).

2.2.1. Rainfall-Runoff Prediction Approaches

The literature about the prediction of rainfall runoff is broadly multidisciplinary. The topic is addressed in research in hydrology, agriculture, soil erosion, flood management, environmental engineering, and the like. The existing models for runoff prediction range from point scale to the watershed scale.

Abdulnabi (2015) provides a comprehensive review of available techniques for rainfall-runoff modelling categorized by discipline. The report broadly classifies runoff models either empirically or conceptually, then breaks down conceptual approaches into three subclasses of deterministic, parametric, and stochastic models. Furthermore, the report lists and discusses critiques of each method.

2.3. Rainfall Simulators in Rainfall-Runoff Research

The logical evolution of rainfall runoff research to solve practical, multidisciplinary problems is thoroughly described in Abdulnabi (2015). Often, diverse disciplines resort to physically simulate the rainfall runoff to investigate specific aspects of the runoff phenomenon. The research objective often drives the design of the simulator apparatus. For instance, simulators used to assess soil erosion often focus on the raindrop size and kinematic energy to displace soil particles Navas et al. (1990) More details on the diverse types of rainfall simulators and their design objectives are described in Abdulnabi (2015).

Furthermore, Abdulnabi (2015) gives the full particulars of the factors that influence runoff characteristics. These factors were classified into precipitation characteristics, initial conditions of the soil surface, soil properties, vegetation cover, slope gradient and scale effects. Moreover, surface roughness has direct impact on runoff generation and quantities, which will be discussed in Section 6.3.2. Table 2.1 summarizes the significant factors influencing rainfall runoff.

Table 2.1 A summary of the factors that influence rainfall runoff (after Abdulnabi 2015).

Factor	Details
Precipitation	quantity, intensity, duration, and distribution
Initial Conditions	initial suction state, antecedent water content
Material Properties	hydraulic conductivity of the material
Vegetation Cover	if present, more infiltration less runoff
Slope Gradient Effects	slope gradient increases the time to runoff decrease
Scale Effects	spatial and temporal variability in rainfall and soil properties

2.4. Numerical Models for Prediction of Rainfall-Runoff

The laws that control water flow in saturated and unsaturated conditions i.e., Darcy's Law for water flow; and Modified Fick's Law for water vapour diffusion, are described by nonlinear partial differential equations (e.g., Richards' equation) that are not easily solved using analytical approach (discussed further in Section 3.4). The best method to obtain a solution to such complex equations is using finite element analysis. Numerical models deliver a solution to such an analysis, which can be utilized for predicting water balance components in geo-environmental engineering.

Abdulnabi (2015) discuss the numerous studies that have attempted to replicate field measurements of water balance parameters in soil cover systems utilizing different commercial numerical models available in the industry. The unanimous conclusion of all investigated studies was that numerical models must be calibrated to yield accurate results. Scanlon et al. (2002), Swanson et al. (2003), Benson et al. (2004 and 2005), Scanlon et al. (2005), Bohnhoff et al. (2009) Benson (2010), systematically illustrate the significance of model calibration when numerical models are utilized in prediction of water balance components.

Moreover, sensitivity assessment of numerical models to input parameters such as surface hydraulic conductivity was reported by Fayer et al. (1992), Roesler et al. (2002), Scanlon et al. (2002), and Bohnhoff et al. (2009). Furthermore, numerical runoff predictions have also proven sensitive to rainfall resolution Wainwright and Parsons (2002), Bronstert and Bardossy (2003), Benson et al. (2004), Benson et al. (2005), Bohnhoff et al. (2009), and Jubinville (2013).

Rainfall runoff and infiltration have a unique interdependency. One cannot design a system such as a soil cover system which is primarily based on water balance without confidently being able to account for rainfall-runoff fluxes. Thus far, there does not seem to be a conclusive model to predict runoff fluxes at the field scale with adequate assurance to be used in practical studies.

2.5. Research Contributions Related to Earlier Work

The literature review summarized in the previous sections indicates that a conclusive model for the evaluation of rainfall runoff suitable for geotechnical and geoenvironmental engineers is not available. Operational models for rainfall-runoff prediction are indeed limited. Some approaches were only appropriate for fully saturated surfaces. Others were less rigorously developed and, thus, require a significant amount of data before the model can be employed.

Furthermore, most of the mechanisms and actual physical processes within cover systems such as capillary barriers have not been thoroughly tested in a controlled setting. The specific contributions of this thesis to previous work and the collective multidisciplinary knowledge are as follows:

1. Identify physical processes operating at and below the ground surface when rainfall occurs.

2. Identify appropriate soil parameters that control rainfall runoff in different saturation conditions.

3. Formulate a theoretical framework for predicting rainfall runoff in soil profiles at different saturation conditions.

4. Carry out laboratory tests that investigate the theoretical approach regarding different initial conditions and profile types exposed to controlled and variable rainfall intensities.

5. Conduct numerical simulations to investigate how accurate numerical prediction is compared to the laboratory results.

6. Demonstrate the practical significance of the current research in a field case study.

CHAPTER 3. Theoretical Prologue

3.1. Introduction

This chapter explains the theoretical aspects of the present research. Applicable theories on laws of water flow in saturated and unsaturated soils are presented. Furthermore, the chapter discusses the fundamentals of physics that govern the phenomenon of capillary barrier effect. Lastly, the chapter presents the theories related to finite element modelling of water flow in saturated and unsaturated soils.

3.2. Unsaturated Soils

The science of unsaturated soil mechanics is well developed for a degree of saturation ranges between 20% and 80% (Tami 2004). Fredlund et al. (2012) provide a comprehensive reference for unsaturated soil mechanics including laws, theories, and practical problems. This section summarizes theories and defines fundamentals essential to the research scope mostly from Fredlund et al. 2012 unless otherwise noted.

When operating in the unsaturated soils realm, the soil matrix is no longer a two-phase system, but rather a four-phase system consisting of water, air, soil particles and contractile skin. Generally, the portion of soil above the water table is referred to as *the vadose zone* and is usually considered unsaturated. The portion of the vadose zone closer to the water table is referred to as *the capillary fringe* and is, mostly, saturated despite negative pore-water pressure (Tami 2004).

Potential pore-water pressures distribution in the unsaturated zone is illustrated in Figure 3.1. The pressure distribution is hydrostatic in the absence of water flux, i.e., static equilibrium with water table as shown in curve 1. When water is removed from the soil either by evaporation or evapotranspiration, the distribution is shifted to the left as in curve 2 to reach a steady state upward flow of water eventually. Conversely, when water is added to the system by rainfall, the curve shifts to the right as in curve 3 to eventually reach a steady state flow downward.

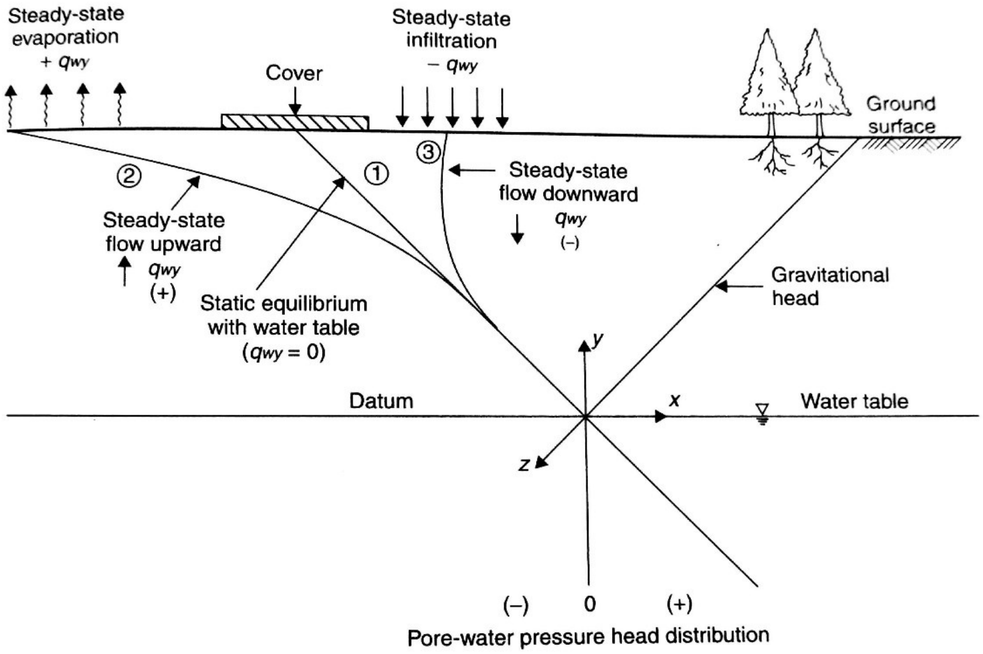

Figure 3.1 Potential pore-water pressure distribution in the vadose zone (from Fredlund et al. 2012).

3.2.1. Soil Suction

The total suction in soil comprises two components, the matric and osmotic suction. The relationship defining total suction can be written as follows:

$$\psi = (u_a - u_w) + \pi \tag{3.1}$$

where:

ψ	=	soil total suction
$(u_a - u_w)$	=	matric suction
u_a	=	pore-air pressure
u_w	=	pore-water pressure
π	=	osmotic suction

The osmotic suction is associated with dissolved ions in pore-water of the soil. Change in ion type or concentration incites change in the osmotic suction. However, change in osmotic suction has less impact on the total suction relative to the matric suction. Therefore, it is often assumed that a change in the total suction equals the change in matric suction (Tami 2004).

The matric suction is defined as the difference between pore-air pressure and pore-water pressure $(u_a - u_w)$. “The matric suction is commonly associated with the capillary phenomenon arising from surface tension of water. This surface tension is caused by intermolecular forces acting on molecules in the contractile skin. The capillary phenomenon can be illustrated by rise of water in a capillary tube.” “The pores in a soil are analogue to capillary tubes with small radii. Soil-water rises above the water table because of the capillaries created by the soil. The capillary water has a negative pressure with respect to the air pressure” (Fredlund et al. 2012). Figure 3.2 illustrates the capillary model of matric suction in soil.

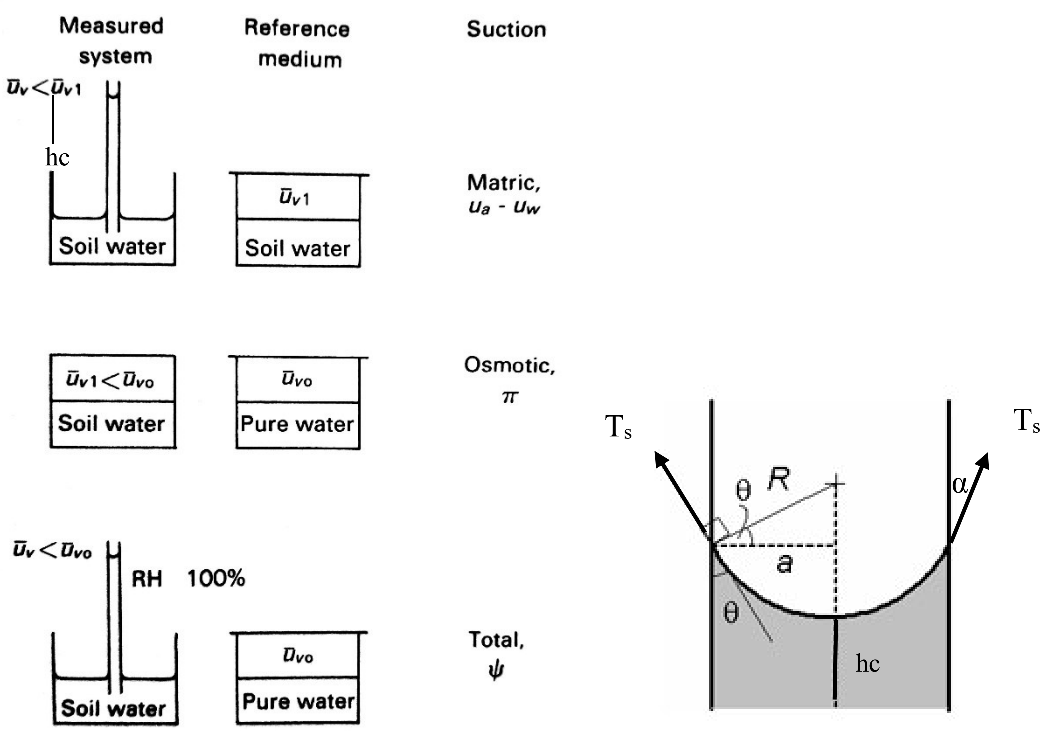

Figure 3.2 The capillary model of matric suction in soil (after Fredlund et al. 2012).

Soil capillarity can be evaluated using the surface tension T_s acting upon the surface meniscus at an angle α with the vertical axis. The capillary rise can be derived from vertical equilibrium of the surface tension force and weight of the column of water in the capillary tube as follows:

$$h_c = \frac{2\pi\ T_s \cos\alpha}{\pi R\ \rho g} \tag{1.2}$$

where:

R = tube radius

T_s = water surface tension

α = the angle at which surface tension occurs

h_c = capillary rise

ρ = water density

The negative pressure of the capillary water relative to the atmospheric pressure can be accentuated at low degrees of saturation, and sustained by adsorption forces between soil particles. Further details on degree of saturation and implication on unsaturated properties of soils are described in the following sections.

3.2.2. Soil Water Characteristics Curve (SWCC)

In simple terms, the soil water characteristics curve (SWCC) defines the relationship between water content (gravimetric, volumetric or degree of saturation) and soil matric suction. The choice of appropriate representation of water content depends on whether the soil undergoes significant volume change (Fredlund et al. 2012). SWCCs are indispensable tools to characterize properties of unsaturated soils.

Typical SWCC shape illustrated in Figure 3.3 is defined by the following parameters: the saturated water content θ_s, air entry value ψ_a, water entry value ψ_w, residual water content θ_r, and residual air content θ_{ar}.

Air entry value is the matric suction where water first enters the soil in the desorption or drying SWCC curve. Starting with full saturation, as matric suction increases, the water content seems unchanged up to the air entry value where the water content decreases nonlinearly with the increase of matric suction. The residual water content is defined as the water content after which change in matric suction does not induce a notable change in water content; the corresponding matric suction is termed *residual matric suction*.

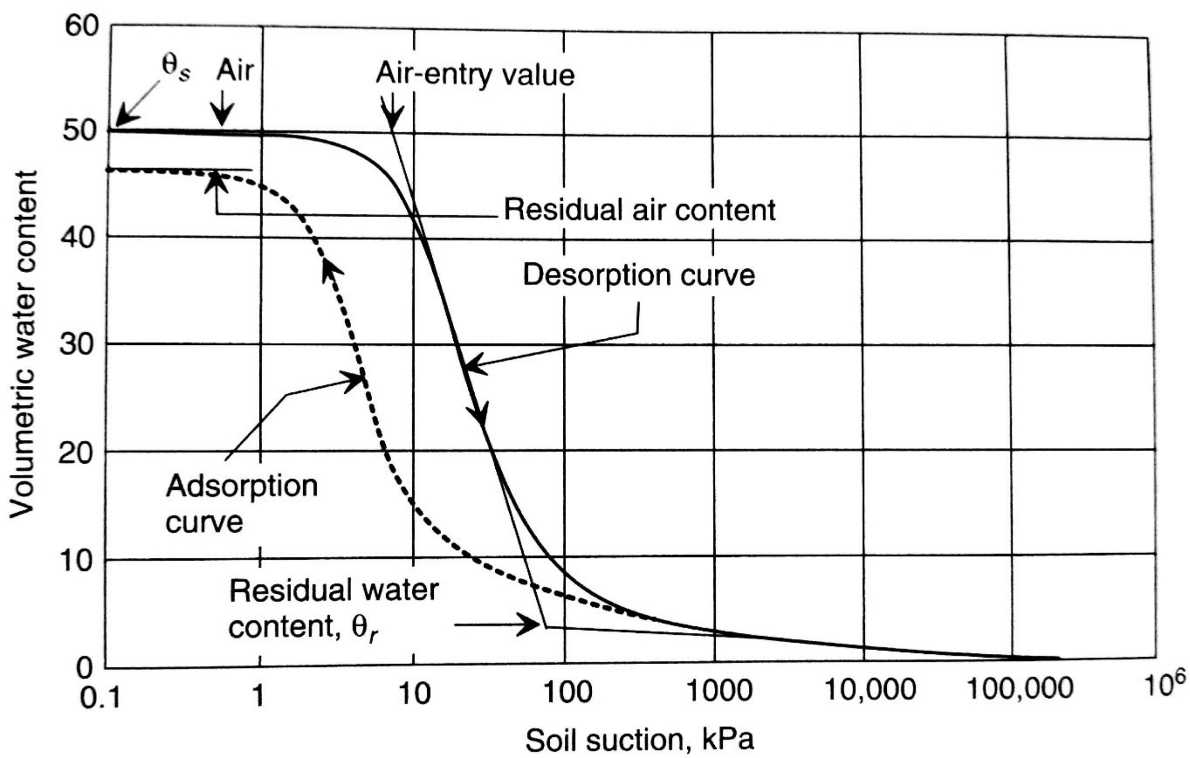

Figure 3.3 Typical SWCC for silty soil with defining parameters (from Fredlund et al. 2012).

3.2.2.1. Effect of Hysteresis of SWCC

The SWCC is not a single value unique relationship, but is rather a hysteretic property. In simple terms, the hysteresis effect of SWCC means that drying (desorption) and wetting (adsorption) paths are significantly different.

The phenomenon causing this can be described as the ink bottle effect (Taylor 1948), and is illustrated in Figure 3.4. A clean capillary tube of radius r allows pure water to rise to a maximum capillary height h_e, which is a function of the tube radius. Nonuniform openings along the capillary tube (as is the case in soil pores) can prevent the full development of capillary height. Figure 3.4 c shows that during the wetting cycle, the portion of the tube with radius $r_1>r$ prevents water from rising to full h_c. The capillary height h_c can only be fully developed if the entire tube is filled by submerging the soil below the water surface and then allowing for equilibrium during the drying cycle (Figure 3.4 d). Similarly, the development of capillary rise in the soil is influenced by the pore size distribution in the soil, creating hysteretic effect with scanning curves between drying and wetting curves as seen in Figure 3.5.

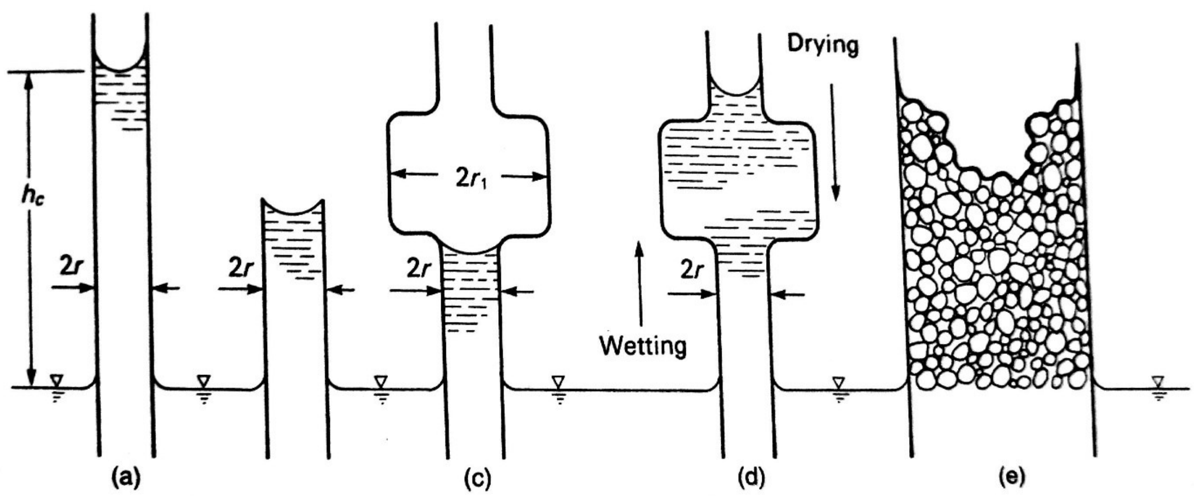

Figure 3.4 Ink bottle effect in capillary tube (from Fredlund et al. 2012).

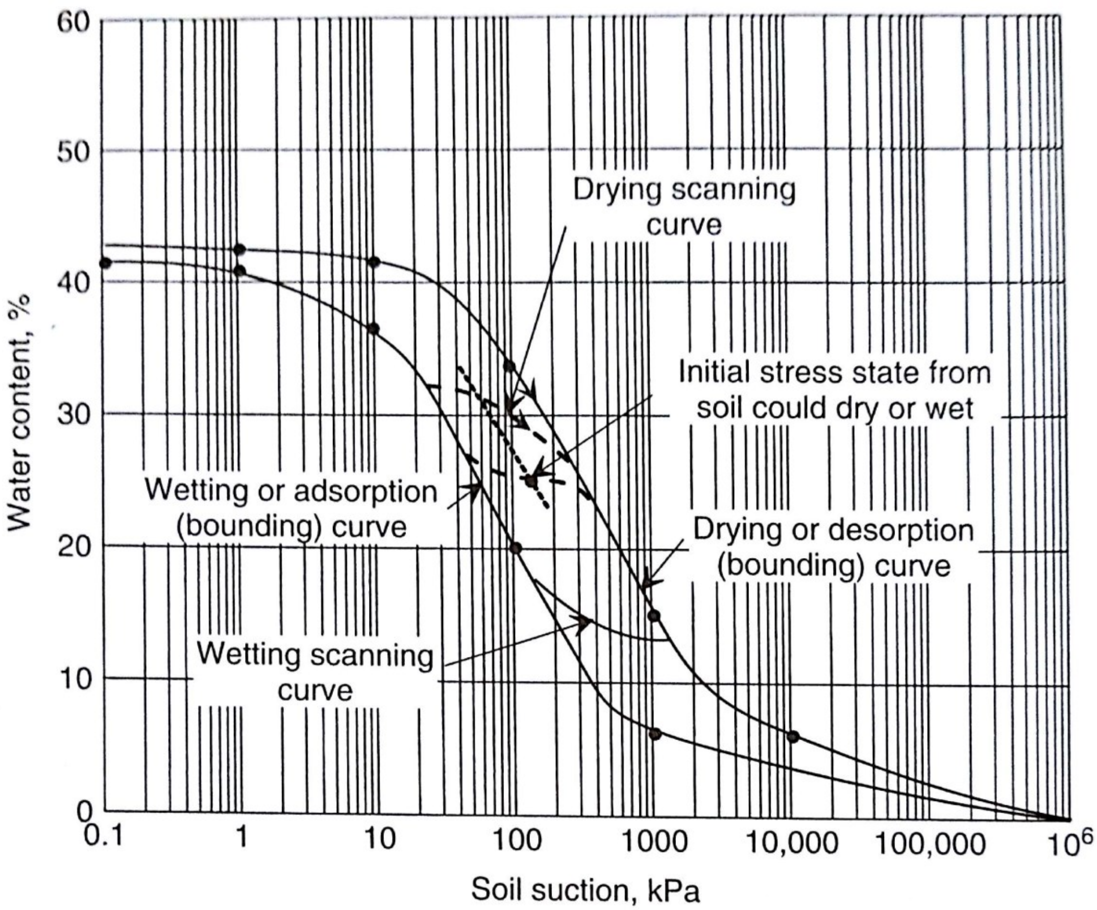

Figure 3.5 Typical wetting and drying scanning curves (from Fredlund et al. 2012).

Sometimes it may be necessary to distinguish the soil properties associated with the drying/wetting curves. This demands that the geotechnical engineer decide which appropriate process to simulate (i.e., the drying or wetting process), and then use the corresponding estimated unsaturated soil property function (Tami et al., 2004). It is not uncommon to use an average SWCC (i.e., between the drying and wetting SWCCs) when estimating unsaturated soil property functions.

3.2.2.2. Mathematical representation of SWCC

The evolution of mathematical representation of the SWCC is described in (Fredlund et al. 2012). The most common empirical correlation in geotechnical engineering practice is the one developed in (Fredlund and Xing 1994); it can be written as follows:

$$\theta_w = \theta_s\, C\,(\psi) \left\{ \frac{1}{\left(\ln\left(e + \left(\frac{(u_a - u_w)}{a} \right)^n \right) \right)^m} \right\} \tag{3.3}$$

where:

$C\,(\psi)$ = correction factor related to the suction matching to the residual water content.

= $1 - \frac{ln\left(1+\frac{(u_a-u_w)}{(u_a-u_w)_r}\right)}{ln\left(1+\frac{10^6}{(u_a-u_w)_r}\right)}$

θ_w = volumetric water content.

θ_s = saturated volumetric water content.

a = fitting parameter related to the air entry value of the soil (kPa)

n = fitting parameter related to rate of water extraction beyond air entry value.

m = fitting parameter related to the residual water content of the soil.

$(u_a - u_w)$ = matric suction (kPa)

$(u_a - u_w)_r$ = residual matric suction (kPa)

u_a = pore-air pressure (kPa)

u_w = pore-water pressure (kPa)

Depending on the soil type, SWCC shape and the air entry value may vary up to a few orders of magnitude. Figure 3.6 illustrates comparative desorption SWCCs for sand, silt and clay soils. The SWCC is an essential representative property of unsaturated soil that is correlated to strength and permeability parameters. The following section provides more details on estimation of permeability functions based on SWCCs.

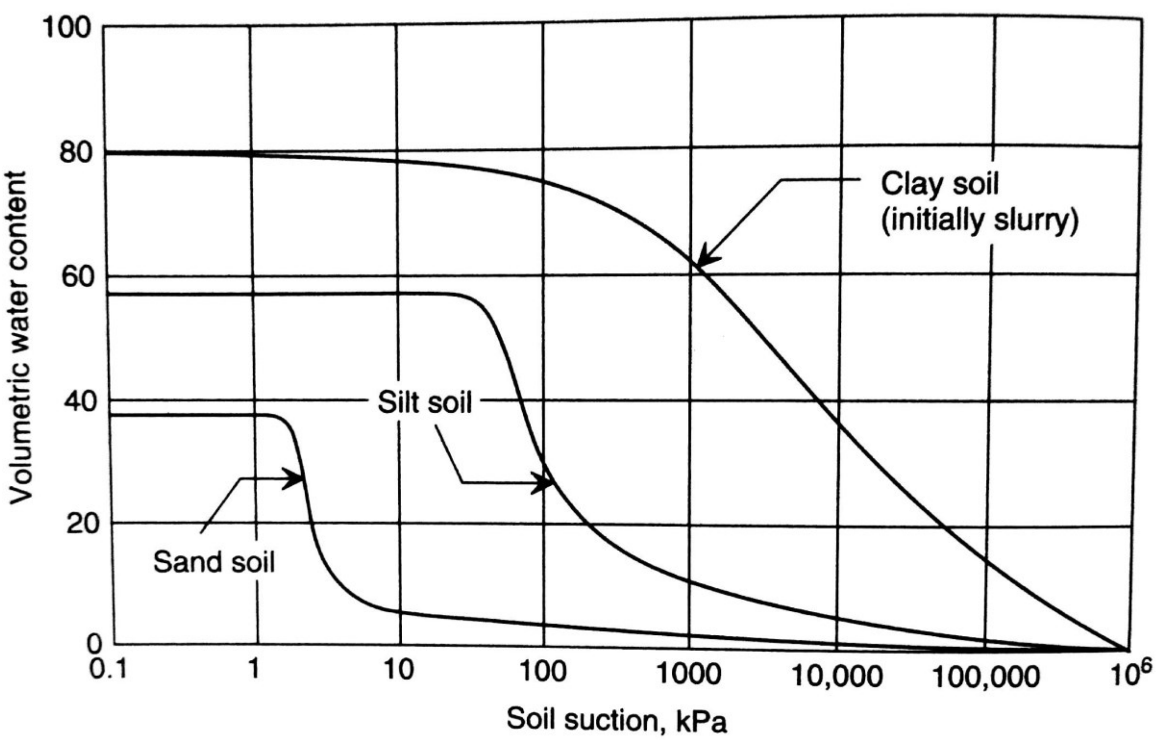

Figure 3.6 Comparative desorption SWCCs for sand silt and clay soils (from Fredlund et al. 2012).

3.2.3. Soil Unsaturated Permeability Functions

The rate at which water flows through soils is regulated by the hydraulic conductivity of the soil. Generally, the hydraulic conductivity or coefficient of permeability of saturated soils is considered constant. However, in the unsaturated realm, the hydraulic conductivity can decrease several orders of magnitude with matric suction as the soil desaturates as illustrated in Figure 3.7. The reason is that water can only flow through pores filled with water, and as the soil desaturates, there is less continuous body of water within the soil matrix, which causes thereby, the coefficient of permeability to decrease significantly.

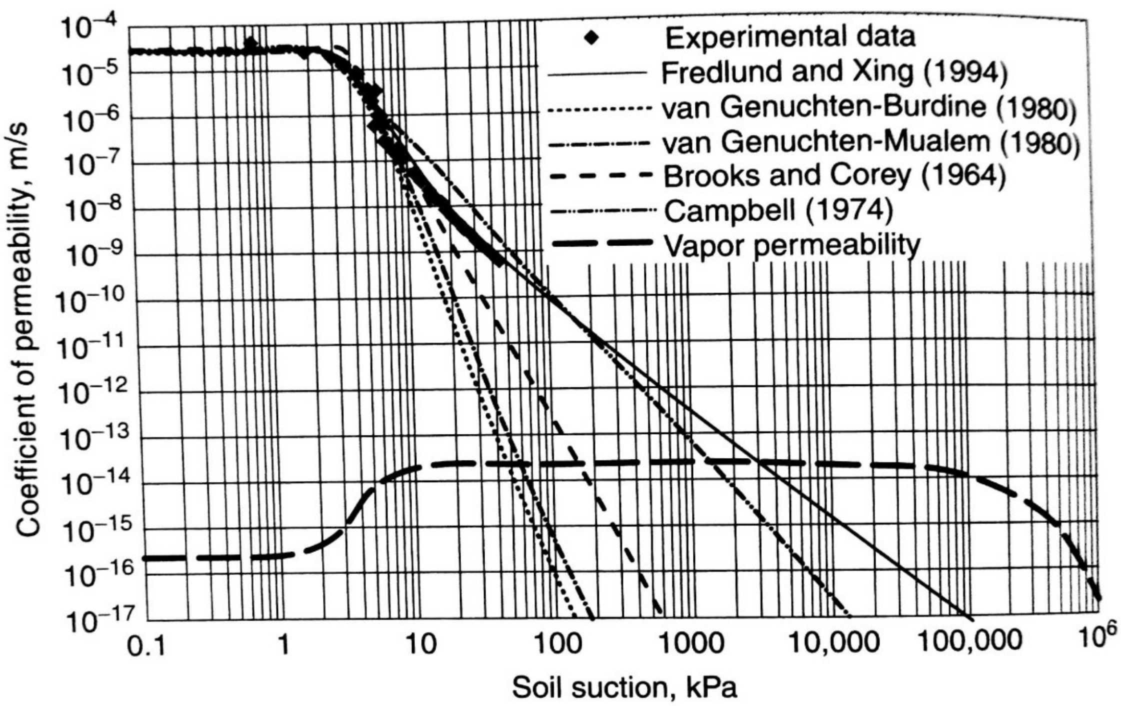

Figure 3.7 Unsaturated permeability functions for silty sand (from Fredlund et al. 2012).

Laboratory measurements of unsaturated hydraulic conductivity are both a time- and cost-intensive task. Hence, correlation models exist between SWCC and the unsaturated hydraulic conductivity functions. In this study, the permeability functions used in the numerical analysis were determined using the correlation by Campbell (1974). The equation for the permeability function can be written as follows:

$$k = k_s \left[\frac{\theta}{\theta_s}\right]^w \tag{3.4}$$

where:

$\frac{\theta}{\theta_s}$ = dimensionless water content from SWCC

w = fitting parameter related to soil type

k = relative coefficient of permeability

k_s = saturated coefficient of permeability

The unsaturated hydraulic conductivity function is a primary soil property governing water flow through unsaturated soils. During this research, correlations between SWCC were used to estimate the unsaturated permeability function.

3.3. Capillary Barrier Effect

The capillary barrier phenomenon usually takes place when a layer of fine-textured soil is placed on top of a layer of the coarse-textured soil. Figure 3.8 illustrates the typical soil water characteristic curves and permeability functions of appropriate soils that can be utilized to create a capillary barrier.

When saturated, the coarse soil has a higher saturated hydraulic conductivity compared to the fine soil. However, as soil desaturates, water is extracted from pores (bigger pores drain first), all the while maintaining the water content relatively unchanged. Once the matric suction for the coarse soil exceeds the air entry value of the soil, the hydraulic conductivity of the coarse soil decreases by several orders of magnitude becoming lower than that of the fine textured soil. Since fine soils have higher entry value, point (a) in Figure 3.8 shows that fine soil is still saturated and possesses a higher coefficient of permeability compared to coarse soil. This contrast of permeability creates a hydraulic impedance at the interface limiting downward infiltration. The permeability functions of fine-grained and coarse-grained layers are the key to successful capillary barriers design.

The capillary break continues until the matric suction at the interface between the fine and coarse soil layers falls below residual suction of the coarse layer during the drying cycle. During the wetting cycle, the capillary barrier continues to limit downward seepage of water until matric suction at the interface exceeds water entry value of the coarse-grained layer. The laboratory program provides a solid verification of this theoretical model as discussed in later sections.

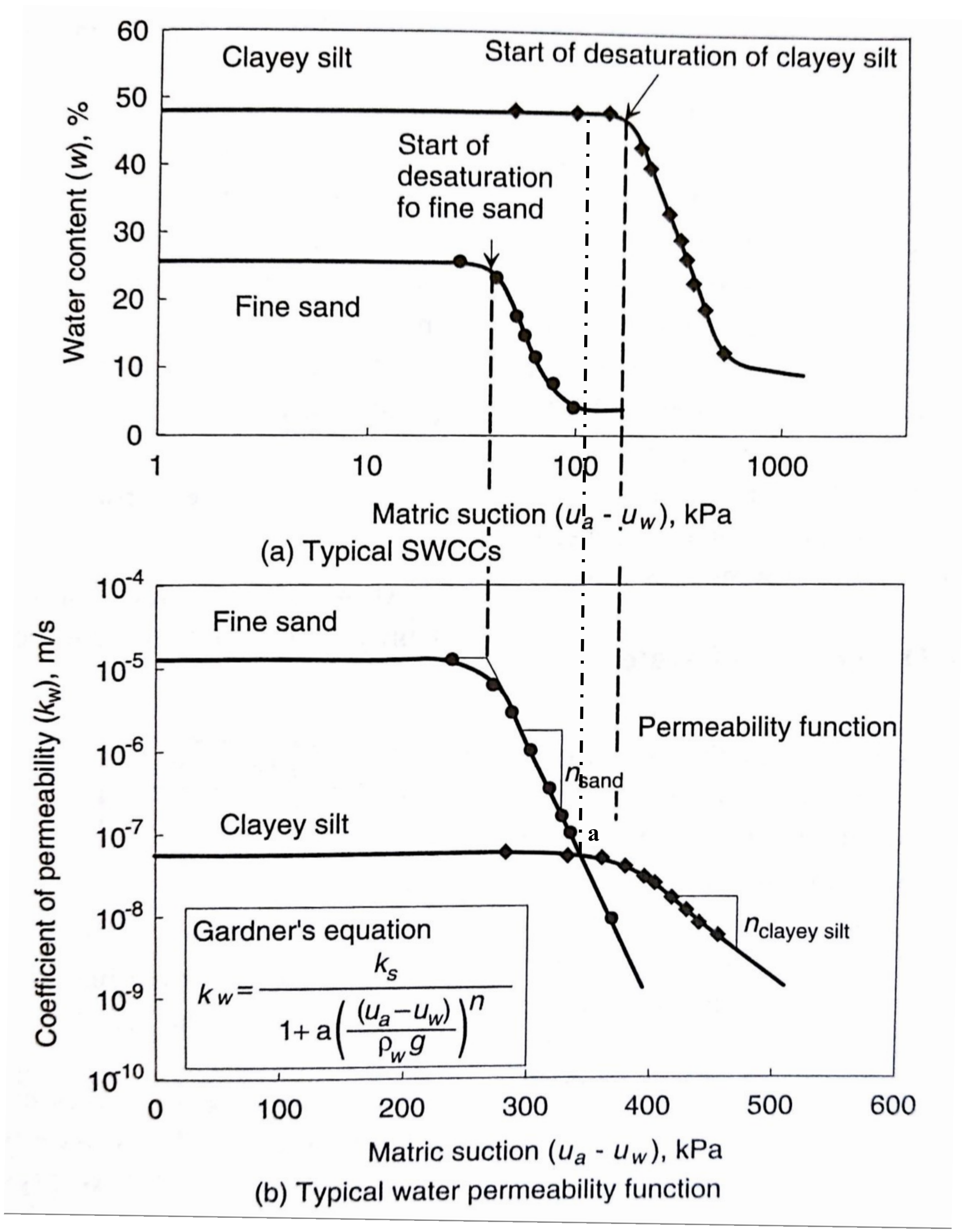

Figure 3.8 Typical permeability and SWCC functions of unsaturated sand and silt soil (after Fredlund et al. 2012).

3.4. Laws of Water Flow in Unsaturated Soils

Solving steady-state and transient seepage through saturated and unsaturated soils requires solving the governing partial differential equations. The one common denominator between saturated and unsaturated world is the driving potential being the hydraulic head gradient for both cases. The hydraulic head can be understood in terms of energy. The total head being the summation of elevation, pressure, and velocity, which can be written as follows:

$$h_w = y + \frac{u_w}{\gamma_w\, g} + \frac{v_w^2}{2g} \tag{3.5}$$

where:

h_w	=	total hydraulic head [L]
y	=	elevation head [L]
u_w	=	pore-water pressure [ML^{-2}]
γ_w	=	unit weight of water [ML^{-3}]
g	=	gravitational acceleration [LT^{-2}]
v_w	=	velocity of water (i.e., flow rate) [LT^{-1}]

The velocity head ($\frac{v_w^2}{2g}$) can be negligible compared to the elevation head y, therefore, rendering equation 3.5 into:

$$h_w = y + \frac{u_w}{\gamma_w\, g} \tag{2.6}$$

In saturated soils under steady-state flow, Darcy's law adequately describes the flow of water through the soil matrix. Darcy's law postulates that the rate of water flow through a porous medium is directly proportional to the hydraulic gradient and coefficient of permeability as follows:

$$v_w = -k_w \, i \qquad (3.7)$$

where:

v_w = flow rate [LT^{-1}]

i = hydraulic gradient = $\frac{\Delta h}{\Delta l}$

The negative sign indicates that water flows from high to low gradient. For unsaturated soils, Darcy's law is still operational, with one exception – the coefficient of permeability is no longer a single value but rather a function of matric suction of the soil.

3.4.1. Governing Equations for Water Flow in Soils

Let us consider a referential element volume (REV) of soil as illustrated in Figure 3.9. The law of mass conservation postulates that no mass can be gained or lost of the system irrespective of the flow patterns. Hence, as described in Fredlund et al. (2012), the net flux of water through the element in the y-direction can be expressed as follows:

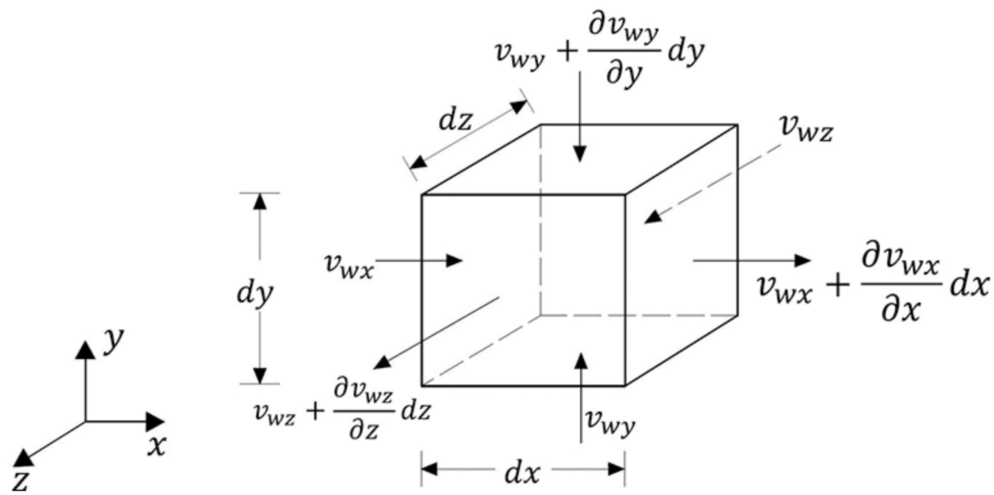

Figure 3.9 Water flow through a referential element in unsaturated soil.

$$\frac{\partial V_w}{\partial t} = \left(v_{wx} + \frac{\partial v_{wx}}{\partial x}\, dx\right) dy\, dz - v_{wx}\, dy\, dz + \left(v_{wy} + \frac{\partial\, v_{wy}}{\partial y}\, dy\right) dx\, dz - v_{wx}\, dx\, dz + \left(v_{wz} + \frac{\partial\, v_{wz}}{\partial z}\, dz\right) dx\, dy - v_{wz}\, dx\, dy \tag{3.8}$$

where:

$\partial\, v_{ij}$ = change in volume of water in the soil element over time in j-direction

v_{ij} = flow rate in the j direction

By expressing the change in volume of water in terms of change in volumetric water content, and then substituting Darcy's law into the equation, the following basic equation for water flow in the soil can be written:

$$\frac{\partial \theta_w}{\partial t} = \frac{\partial}{\partial x}\left(-k_{wx}\, \frac{\partial h_w}{\partial x}\right) + \frac{\partial}{\partial y}\left(-k_{wy}\, \frac{\partial h_w}{\partial y}\right) + \frac{\partial}{\partial z}\left(-k_{wz}\, \frac{\partial h_w}{\partial z}\right) \tag{3.9}$$

where:

$\frac{\partial \theta_w}{\partial t}$ = net flux of water per unit volume of the REV soil

k_{wi} = coefficient o permeability in the i direction

h_w = hydraulic head

The substitution of constitutive behaviour of the water flow and water storage and conservation of mass leads the governing partial differential equation for transient liquid flow through saturated and unsaturated soils to be written as follows:

$$m_2^w \rho_w \, g \, \frac{\partial h_w}{\partial t} = k_{wx} \frac{\partial^2 h_w}{\partial x} + \frac{\partial k_{wx}}{\partial x} \frac{\partial h_w}{\partial x} + k_{wy} \frac{\partial^2 h_w}{\partial y} + \frac{\partial k_{wy}}{\partial y} \frac{\partial h_w}{\partial y} + k_{wz} \frac{\partial^2 h_w}{\partial z} + \frac{\partial k_{wz}}{\partial z} \frac{\partial h_w}{\partial z} \tag{3.10}$$

where:

m_2^w = water storage coefficient related to soil suction

ρ_w = density of water

g = gravitational acceleration

h_w = total hydraulic head

t = time

k_{wx} = water coefficients of permeability in the x-direction (a function of soil suction in unsaturated soils)

$\frac{\partial h_w}{\partial x}$ = hydraulic head gradient in the x-direction

3.4.2. Numerical Solutions of the Governing Partial Differential Equations for Water Flow through Soils

The governing equations of water flow through saturated and unsaturated soils are second-degree Partial Differential Equations (PDE) that are non-linear especially in unsaturated soils. The most appropriate means of solving such an equation are numerical solutions with finite element or finite difference methods. This research utilized the finite element method (FEM) to solve the flow equations. Following is the standard process and basic formulation utilized in FEM.

1. To discretize the geometry of the problem into finite element mesh;
2. To determine the permeability matrix of each finite element;
3. To integrate the permeability matrix over the entire geometry;
4. To set appropriate initial and boundary conditions for the first solution;
5. To iterate by solving the total head equation at each node.

The finite element formulation for steady state seepage has been derived using the Galerkin principle of weighted residuals as follows:

$$\int_A [B]^T [k_w][B] dA\{h_{wn}\} - \int_A [L]^T \bar{v}_w \, dS_p = 0 \tag{3.11}$$

where:

$[B]$	=	gradient matrix
$[k_w]$	=	hydraulic conductivity matrix of an element
$\bar{v}_w$	=	external water flow rate perpendicular to the boundary of the considered element
$[L]$	=	matrix of interpolating function

A = area on the considered element

$\{h_{wn}\}$ = matrix of hydraulic head at nodal points

S_p = perimeter of the considered element

For transient flow, the formulation in Eq 3.11 becomes:

$$\int_A [B]^T [k_w][B] dA \{h_{wn}\} + \int_A [L]^T \lambda [L] dA \frac{\partial \{h_{wn}\}}{\partial t} - \int_A [L]^T \bar{v}_w \, dS_p = 0 \qquad (3.12)$$

where:

λ = $m_2^w \rho_w \, g$

This equation is the general finite element equation for water flow through saturated and unsaturated soil in transient and steady state. The current research utilized SVFlux (Soil Vision 2009) to conduct the analyses.

3.5. Summary

Chapter 3 provided the theoretical framework and background philosophy of unsaturated soil mechanics relevant to the current research. The pore pressure distribution in a three-phase system was discussed. The necessary parameters that define behaviour in unsaturated soils were introduced. These include the soil water characteristics curve and the unsaturated hydraulic conductivity. Mathematical representations of each function were defined and discussed.

The concept of capillary barrier effect was introduced. The laws that govern water flow through saturated and unsaturated soils were discerned. The chapter concludes that the most appropriate method of solving the highly nonlinear partial differential equations that govern water flow through unsaturated soils is by utilizing Finite Element Method. Finally, the universal steps for FEM using the Galerkin principle of weighted residuals were discussed.

CHAPTER 4. Methodology: Laboratory and Numerical Program

4.1. Introduction

The methodology framework for this research is a three tiers system. The first tier encompasses the apparatus design and the laboratory experiments. The second tier includes the numerical simulations of the laboratory experiments. The third and final tier consists of the numerical simulation of field cover system. SVFlux software was utilized for finite element simulations of both the laboratory experiments and the field case study. The following sections describe in detail the aspects of each stage of the research.

4.2. Rainfall Simulator Design and Construction

The laboratory program was established to investigate the relationship between simulated rainfall of different intensities, and the subsequent runoff response in both low permeability and capillary barrier covers. The laboratory tests were performed using a specially designed rainfall simulator apparatus.

The main components of the rainfall simulator were a water circulation system, a spraying system, and a flume to accommodate the soil and the measuring devices. The measuring devices were installed in the sidewalls of the flume to monitor changes in volumetric water content and matric suction. A view of the overall setup of the rainfall simulator is illustrated in Figure 4.1.

Prior to the design of the apparatus, a comprehensive literature review was conducted to obtain the sufficient dimensions, the most appropriate location of instruments, the appropriate soils for the capillary barrier system, and the factors that govern the runoff phenomenon when using rainfall simulators. These include precipitation characteristics, initial conditions, slope gradient effects, vegetation cover, material properties and scale effects. The spraying system design described herein is relatively parallel to that of (Tami 2004). However, the design objectives and desired data are different. An important point to highlight is that Tami (2004) focuses on the slope instability induced by rainfall and does not attempt to predict or quantify runoff.

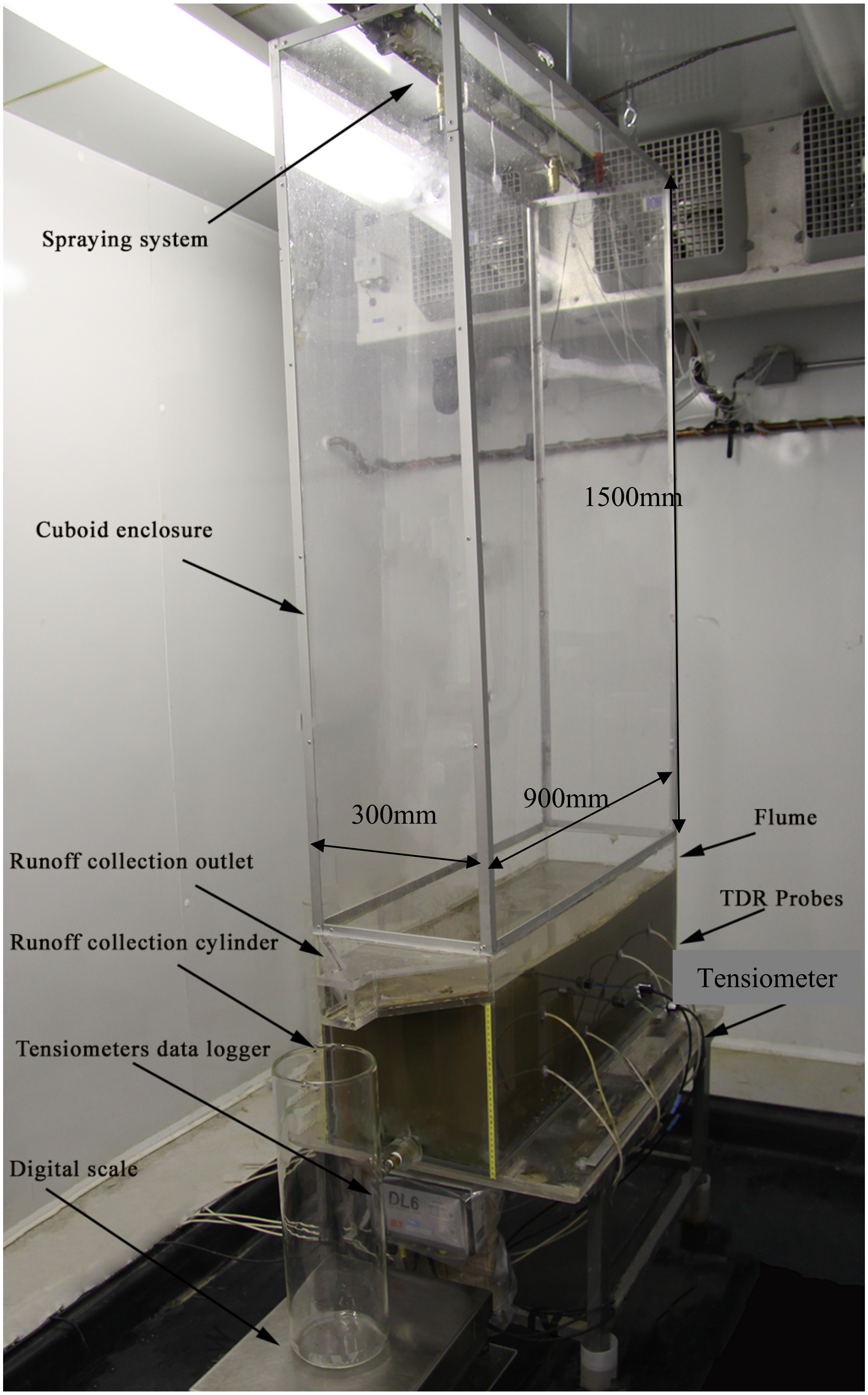

Figure 4.1 Rainfall simulator apparatus components.

4.2.1. Water Circulation System

The water circulation system included a water reservoir of one cubic meter in volume that contained a submersible constant-rate pump (Sta-Rite - high-head filtered). The pump directed the water from the reservoir to the spraying arm by a set of PVC pipes 25 mm in diameter. The pump provided an adequate constant pressure to overcome both head losses and friction losses in the pipes and to operate the nozzles properly.

An overflow system was designed to direct drainage back to the water reservoir to ensure proper functioning of the pump since some rainfall intensities were well below the capacity of the pump. A view of the water circulation system is shown in Figure 4.2. Filtered tap water was used for the simulated rainfall events.

4.2.2. Spraying System

The spraying system consisted of a set of nozzles (Veejet) of different orifices. Each set of nozzles produced different simulated rainfall intensity. Configuration of the spraying system is shown in Figure 4.2 featuring the following components: a) control valve to regulate inflow into the system, b) pressure gauge to monitor water pressure, c) flowmeter to measure volume and rate of applied rainfall, d) set of manifolds that have several appropriate openings for the intended nozzles, and e) release valve at the end of the arm for de-airing the system.

The most appropriate type of nozzles for this study was one that provided an even distribution of medium-sized raindrops throughout a rectangular spray pattern. The height of the spraying arm was obtained by iteration trials to achieve the correct spray pattern, the optimum rainfall coverage of the plot, and the maximum uniformity of simulated rainfall. Similarly, the spacing between the nozzles was attained to eliminate overlapping of raindrops and to ensure concordant coverage of the flume.

The uniformity of each set of simulated precipitations was assessed using Christensen Uniformity coefficient, CU[1].

For each rainfall intensity scenario, CU was assessed by collecting rainfall volume measurements from various locations in the flume as illustrated in Figure 4.3. The results for CU ranged between 74% and 85% indicating uniformity of rainfall over the soil profiles.

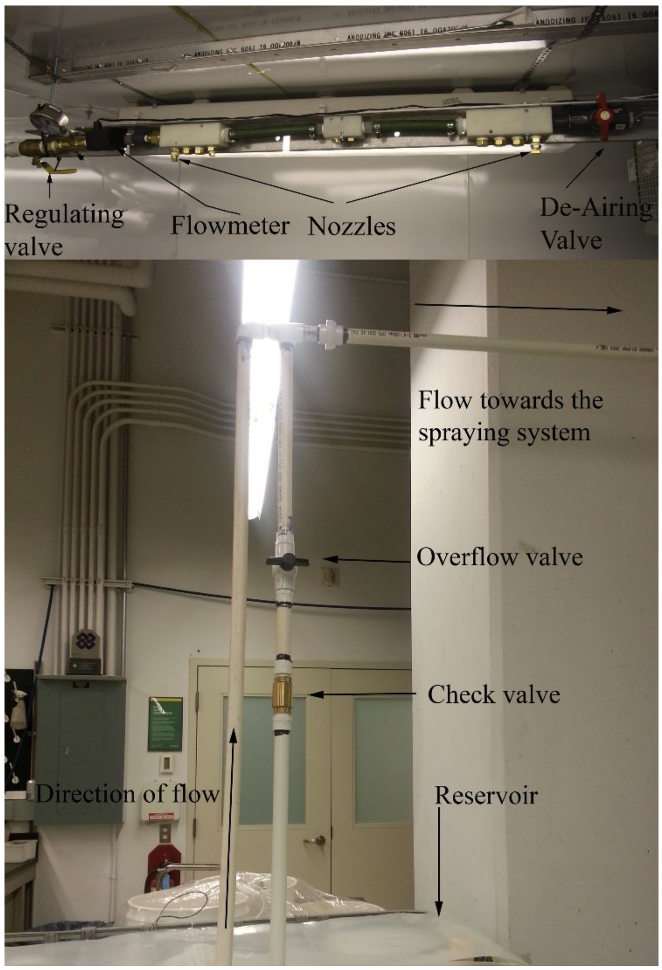

Figure 4.2 Spraying system components (top), and water circulation system (bottom).

[1] Christensen Uniformity Coefficient CU=100*$\left[1-\frac{\sum|\bar{x}-x_i|}{\sum x_i}\right]$ $\bar{x}$ is the arithmetic mean of all equally measured observations of magnitude.

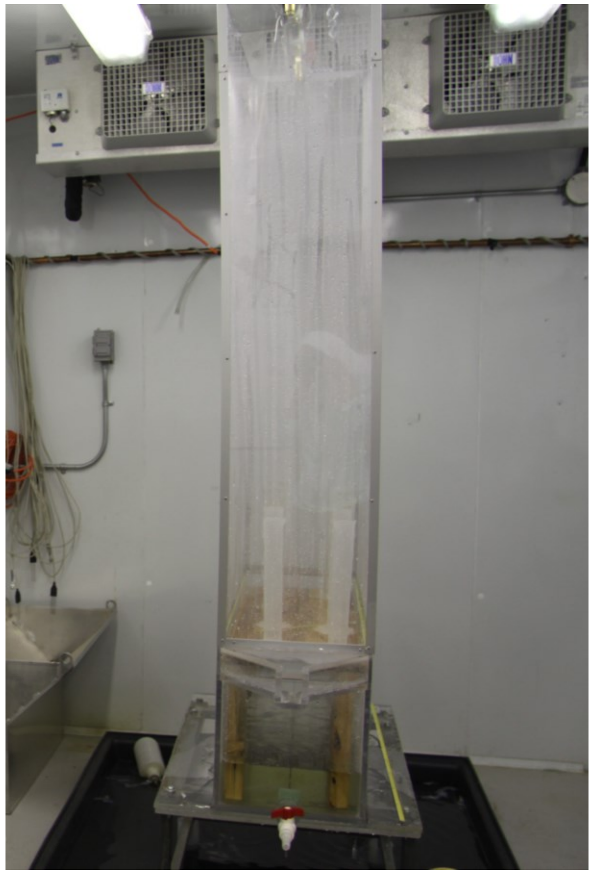

Figure 4.3 Setup for verification of the Christensen Uniformity coefficient.

4.2.3. Flume and Measuring Devices

The soil was contained inside a specially designed flume, which was built of 10 mm thick Plexiglas® sheets to enable observing the wetting-fronts propagation as the tests progressed. The dimensions of the flume were: 900 mm in length, 300 mm in width, and 350 mm in height. The flume had a runoff collection spout at the top and a 25 mm in diameter drainage orifice equipped with a regulating valve at the toe.

A cuboid enclosure made of 2 mm thick Plexiglas® sheets was placed directly on top of the flume to ensure a complete water budget during testing. Water tightness was paramount; thus, the entire structure was conservatively designed and constructed to avoid leakage. All joints between the flume and the cuboid enclosure were carefully sealed with silicone, and allowed to set before testing took place.

Measurements of surface runoff volume and rate were achieved using an electronic scale linked to a data acquisition system. Continuous manual monitoring of cumulative runoff volumes was conducted to ensure accuracy.

Measurements of applied rainfall volume and rate were achieved using a turbine flowmeter mounted onto the spraying system. The flowmeter utilized infrared light beam technology. This technology can be explained as follows: as the fluid passes through the meter body along the paddle axle, the paddle wheel spins. The paddle wheel contains six holes to allow infrared light to pass through. Each time the wheel rotates, a DC square wave is output from the sensor. The generated signal is then sent into the electronic light-detecting circuit to be processed; accordingly, the volume and rate are measured and displayed. The flowmeter uses a factor to calculate the flow rate and total volume passing through the meter. The factor is defined as the number of pulses generated by the paddle per volume of fluid flow. There are six different body sizes at different operating flow ranges and several factors. The flowmeter was reprogrammed and calibrated to represent the appropriate flow range.

Measurements of the internal water and matric suction changes within the profiles were achieved using Time Domain Reflectometry (TDR) (Cambell-CS640) probes, and Tensiometers (UMS-T5). The instruments were distributed evenly at two elevations. Figure 4.4 illustrates the general setup of the flume and measuring devices during testing one of the saturated silt profiles.

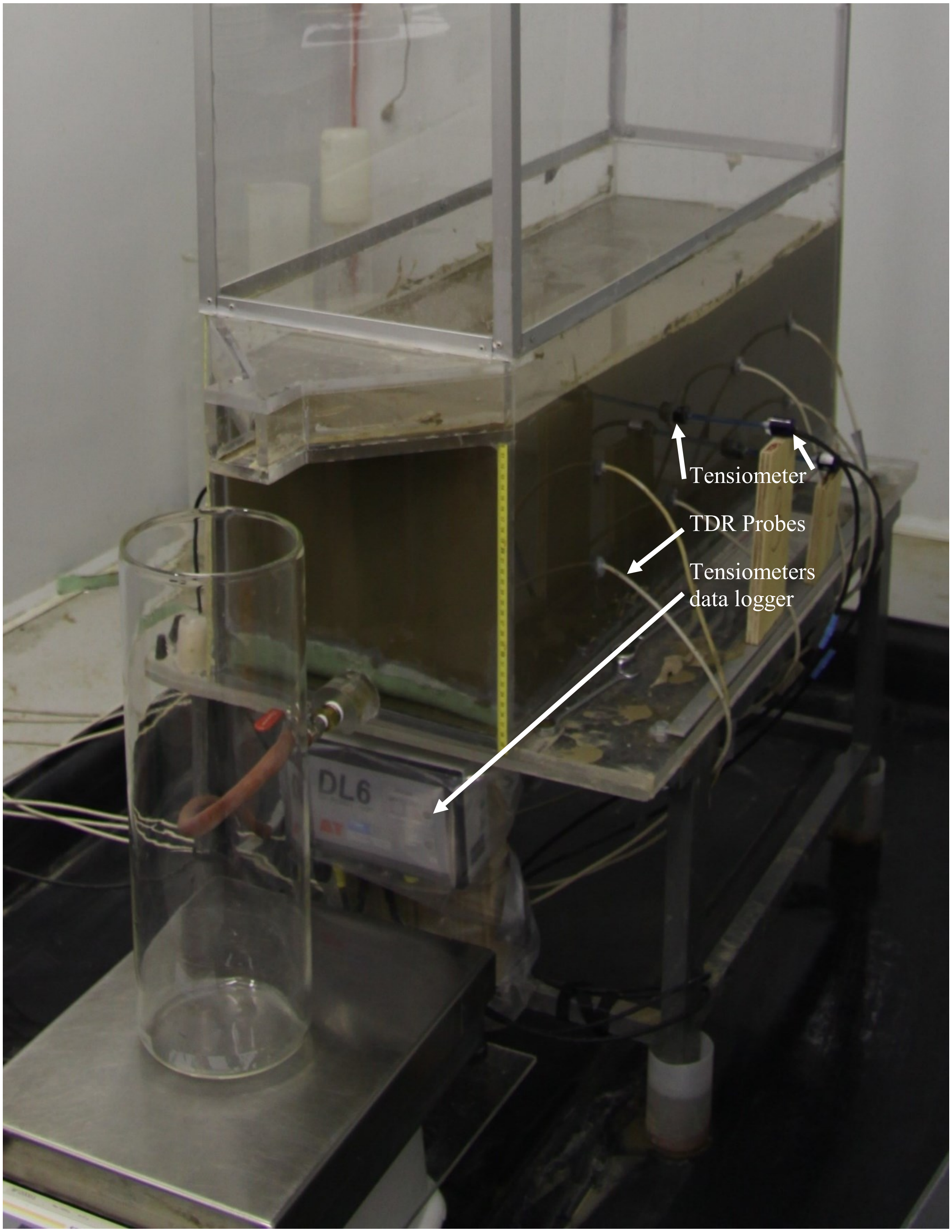

Figure 4.4 A close look at the flume and measuring device illustrating TDR probes and tensiometers.

4.2.3.1. Time Domain Reflectometry (TDR)

Twelve TDR probes were installed along the sidewall of the flume. Each probe consists of a coaxial cable that connects the probe to the data acquisition system and a metal three-rod waveguide. The waveguide is the sensor that conveys the pulse to the surrounding soil to detect changes in volumetric water content. The specifications of the TDR probes are: 75, 22, 4.8, and 35 mm for rod length, spacing, diameter and offset, respectively. Figure 4.5 shows a typical TDR used in the laboratory study.

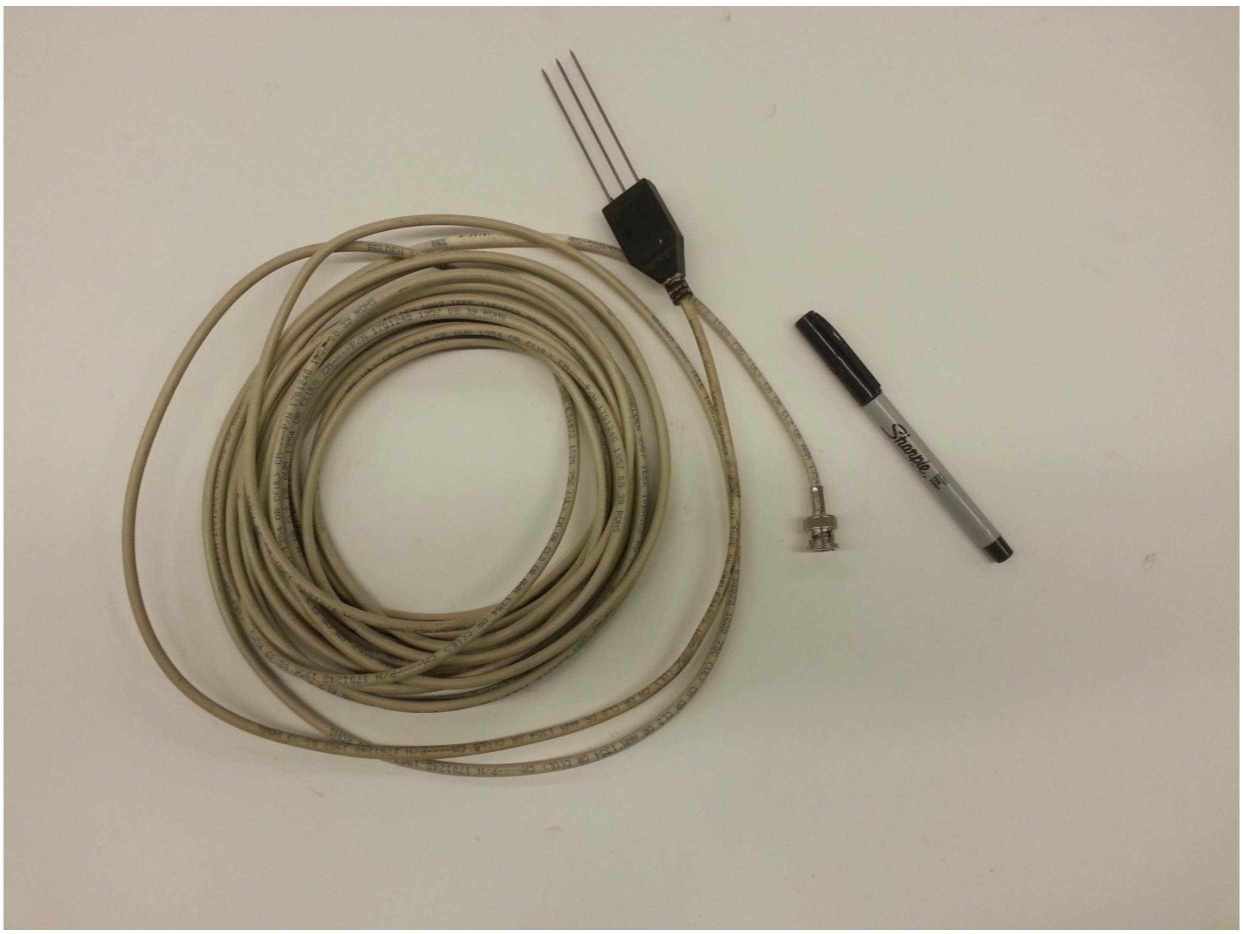

Figure 4.5 A typical CS640 TDR probe used in the laboratory program.

The data acquisition system consisted of: a power supply, a data logger board (CR1000), a pulse generator (TDR100), and two 8-channel multiplexers to which all TDR probes were connected. Data from the TDR probes can be retrieved from the data logger referred to as *TDR100*, which is connected to a personal computer running the PC400 software.

The principle of TDR is such that TDR100 generates a fast short-rise-time electromagnetic pulse through a coaxial cable to a probe (waveguide) buried in the medium of interest. The probe consists of three metal rods as seen previously in Figure 4.5. The transmitted electromagnetic pulse reflects to the source due to the rod impedance.

The travel time of this pulse and its reflection depends on the velocity of the signal and the length of the waveguide. The velocity of the signal is a function of the dielectric constant of the material surrounding the probe.

While the velocity of the applied pulse along a waveguide depends on the dielectric constant of the material surrounding the waveguide, the amplitude of the reflected voltage depends on the electrical conduction of the applied signal between probe rods.

The dielectric constant of water relative to other soil constituents is high. Therefore, change in volumetric water content can readily change the dielectric properties. Accordingly, changes in volumetric water content can be directly related to the change in the dielectric constant of bulk soil. In general, as the water content increases, the travel time of the applied pulse increases.

The relationship between apparent dielectric constant, Ka, apparent TDR probe rod length, La is expressed in Equation. Furthermore, the actual rod length L is given as follows:

$$\mathrm{Ka} = \sqrt{\frac{\mathrm{La}}{\mathrm{L}}} \tag{4.1}$$

where:

Ka = the dielectric constant

La = the apparent TDR probe rod length

L = the actual rod length.

The difference between the apparent and actual rod length is the portion of the rod embedded within the probe head. The reason is that the probe head is made of a block of epoxy or other material that holds the rods rigidly spaced. The part of the rod rooted inside the probe head is referred to as *the probe offset*.

The volumetric water content of the tested soil is strongly related to the dielectric constant, Ka. Therefore, empirical correlations between the soil dielectric constant and the volumetric water content of the soil are established by Topp et al. (1980), Ledieu et al. (1986) and a few other researchers. Although these correlations are empirical, they seem to cover a wide range of soils.

4.2.3.2. Tensiometers

Soil matric-suction measurements were obtained using fine tip tensiometers with a flexible coaxial cable, also referred to as a *pressure transducer tensiometer*. Figure 4.6 shows the typical tensiometer used in the laboratory program. Four UMS T5 tensiometers were used during the laboratory program. All tensiometers were connected to a data logger referred to as *DL6-te*, which was used for data acquisition.

Figure 4.6 Tensiometer probe and readout device.

Each tensiometer probe consists of five main components, namely: a high-grade porous ceramic tip, acrylics glass shaft, a sensor body, a flexible sealed cable, and a readout device (referred to as *INFIELD7*). It is also possible to connect the tensiometers to a data logger (UMS DL6-te) for continuous measurements of matric suction.

The operation principle for this type of tensiometer is based on the contact between the tensiometer water and the water in the soil. The contact is achieved through the ceramic tip, which is highly porous and permeable to water. A wetted porous ceramic tip creates an ideal pore/water interface. The soil matric suction is directly conducted to the pressure transducer that offers a continuous signal to be retrieved by either a readout device or a data logger – in this program, a DL6-te data logger was utilized.

The piezoelectric pressure sensor measures the soil matric suction against the atmospheric pressure. The atmospheric pressure is conducted through a watertight diaphragm in the cable to the reference side of the pressure sensor.

4.2.4. Calibration of Measuring Devices

Accurate monitoring system is crucial for the success of the experimental study. Accordingly, calibrations of all devices were conducted prior to installing. Appendix I includes all calibration curves for every measuring device employed in the laboratory program.

4.2.4.1. Flowmeter Calibration

The selected flowmeter uses a factor to calculate the flow rate and the total volume of water passing through the body of the meter. The factor is defined as the number of pulses generated by the paddle per volume of passing fluid flow (Omega Engineering User's Guide 2013). The amount of fluid that flows through the meter during the calibration procedure was measured.

During the calibrations, the flowmeter operated as intended for up to six hours. During each calibration run, water volumes were collected and measured independently. As water flowed through the meter, pulses accumulated in the display screen. Following each calibration run, the flow was stopped, and the amount of water that passed through the meter was determined using a scale. Moreover, the number of pulses and the corresponding factor were recorded. The procedure was repeated twenty times with varying duration to ensure consistency. The measured volumes were plotted with the flowmeter readings to obtain calibration factors. Later, the calibration factors were programmed into the flowmeter and were validated by repeating a portion of the calibration process to check whether measured volumes and those read by the flowmeter were identical.

4.2.4.2. Time Domain Reflectometry (TDR)

TDR probes calibration procedure was a two-phase process. In the first phase, the proper probe offset was determined; in the second phase, the proper empirical correlation between the dielectric constant and the volumetric water content of the material was established.

During phase 1, one TDR probe was immersed in water, and dielectric constant readings were collected by PC400 software. Since water is known to have a dielectric constant of 81, the probe offset was calibrated to produce this value. The probe offset accounts for the portion of rods that is embedded by a block of epoxy and not exposed to soil. Calibration accounts for the distance the signal travels thru the length of rod that is embedded within the probe head. Therefore, all twelve probes were immersed in water to obtain the individual actual probe offset. The test was performed at a controlled temperature.

During phase 2, twenty samples were prepared to ten volumetric water contents. Each sample was thoroughly mixed in a PVC cylinder container measuring 100 mm in diameter and 200 mm in height. Readings of volumetric water content, as well as the dielectric constant, were collected by PC400 software. Furthermore, three gravimetric water content samples were taken from each container to determine the average gravimetric water content in each sample. The relationship between the volumetric and gravimetric water content of the mixed samples compared to the TDRs readings of volumetric water content were plotted.

4.2.5. Distribution of Instruments

Prior to placing the soil, the measuring devices were installed and secured in place through the openings in the sidewalls of the flume using rubber stoppers. The TDR probes and tensiometers had to be in good contact with the soil to produce excellent quality measurements. Figure 4.7 shows a top view of the measuring devices within the testing flume as distributed during the tests. A simplified schematic of the distribution of the instruments is illustrated in Figure 4.8.

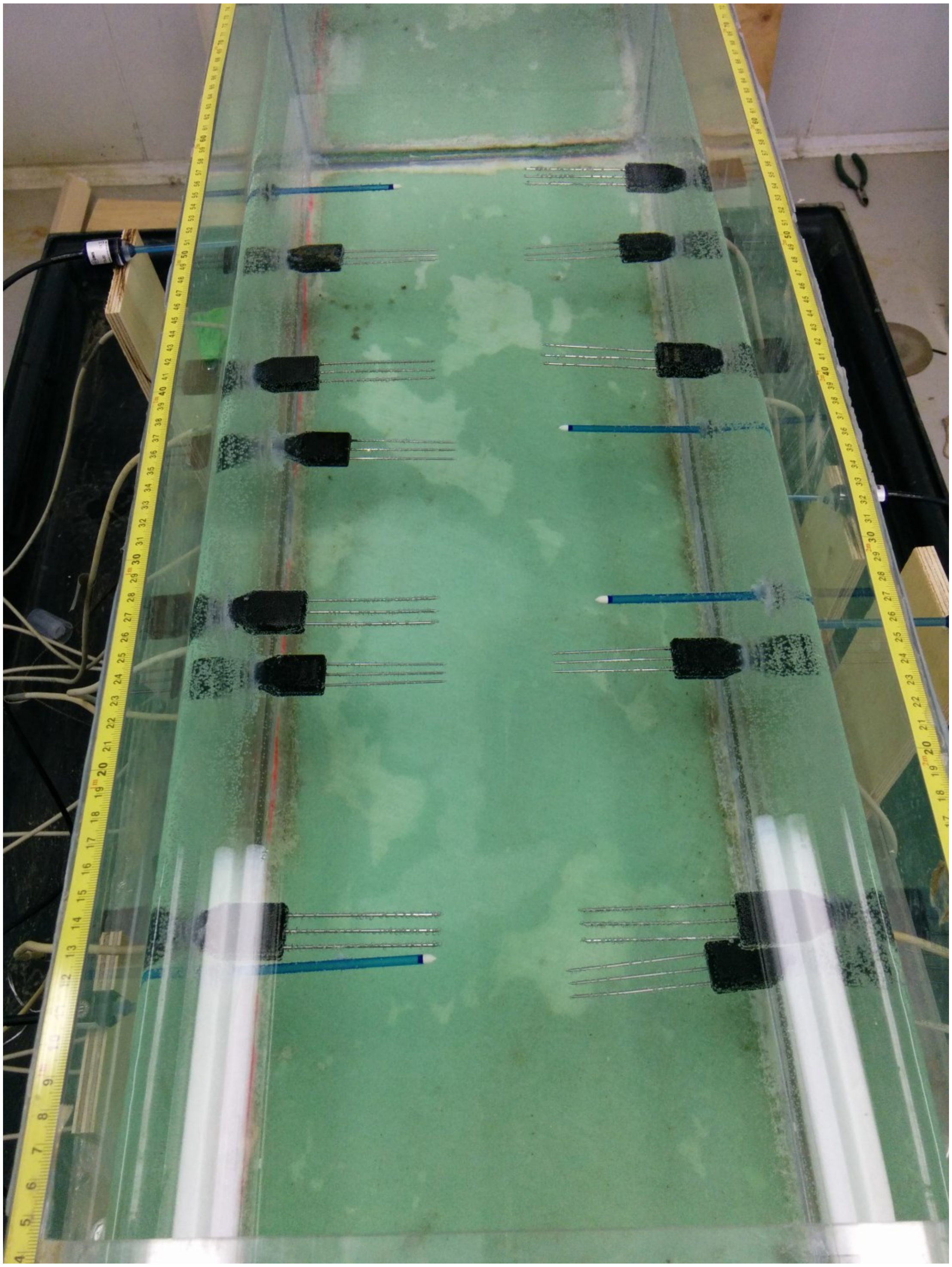

Figure 4.7 Measuring instruments distribution within the flume profile submerged in water during the calibration procedure.

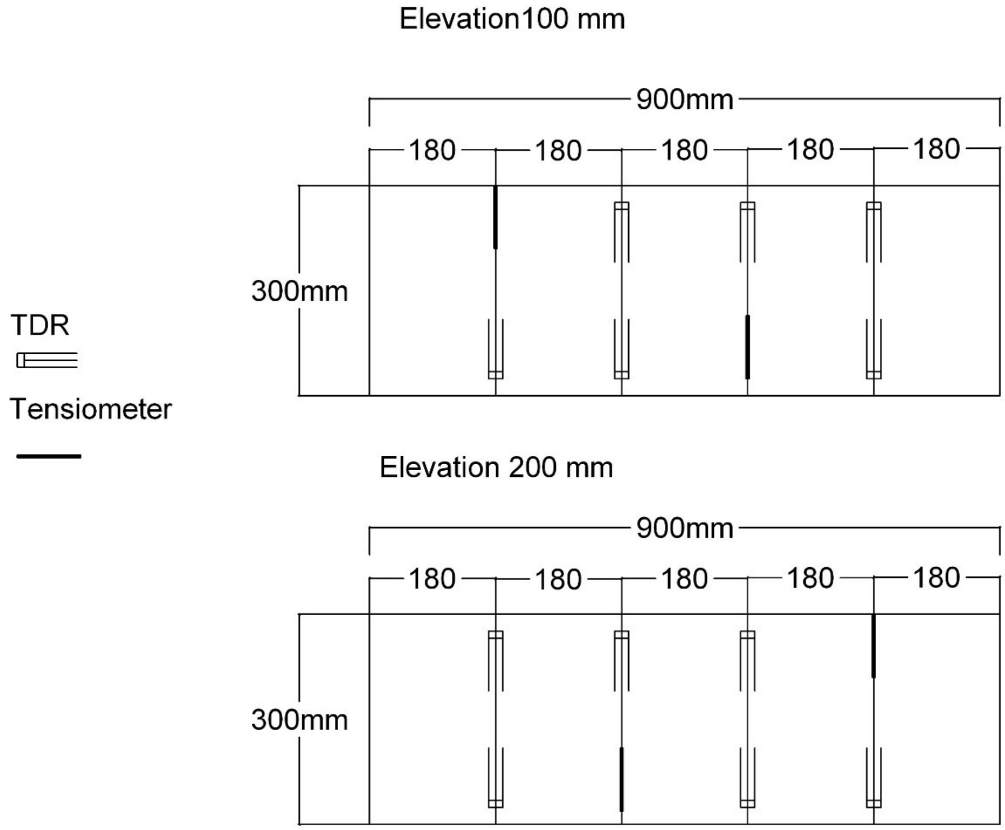

Figure 4.8 Instruments' distribution within the soil profile.

4.3. Materials

Both low permeability profiles and capillary barrier profiles were investigated during the laboratory study. The low permeability profiles were represented by a single layer of Devon silt, while the capillary barrier profiles consisted of two approximately equally thick layers of Devon silt overlaying Tailings Beach sand.

4.3.1. Basic Characterization of Soils

Prior to conducting the simulated rainfall runoff tests, the basic and advanced hydraulic characteristics of both soils were thoroughly investigated. The following sections describe the test procedures and standards corresponding to each soil property determined in the laboratory.

4.3.1.1. Particle Size Distribution and Hydrometer Analyses

Sieve analyses were completed for each soil type to determine the particle-size distribution per the ASTM D6913 (2009) standard. Hydrometer analyses were completed per ASTM D4221 (2011) standard for Devon silt samples.

Hydrometer analyses were completed to determine the grain size distribution for particles smaller than 75 μm. The hydrometer analysis is based on Stokes' Law for sedimentation. This law governs the relationship among the velocity of fall of spheres in a fluid, the diameter of the sphere, the specific weights of the sphere and of the fluid, and the fluid viscosity. Accordingly, the diameter of soil particles in suspension and the percent of soil in suspension were calculated.

Oven-dried specimens were soaked in 125 mL of sodium hexametaphosphate dispersing agent for 72 hours. The sample slurry was then poured into a dispersion cup and dispersed for one minute using an electric mixer. Later, the dispersed slurry was transferred into the sedimentation cylinder, filled with distilled water, capped, and shaken up and down for one minute.

The correction factor of hydrometer reading was determined using a distilled water control. A hydrometer cylinder was filled with 125 mL of the dispersing agent. The solution was left to equilibrate at room temperature. The Hydrometer test setup is shown in Figure 4.9.

Hydrometer readings and corresponding slurry temperature measurements were recorded at 1, 2, 5, 10, 15, 30, 60, 250, and 1440 cumulative minutes, as directed by ASTM D422 (2007). The readings were then corrected using the meniscus and solution correction factors.

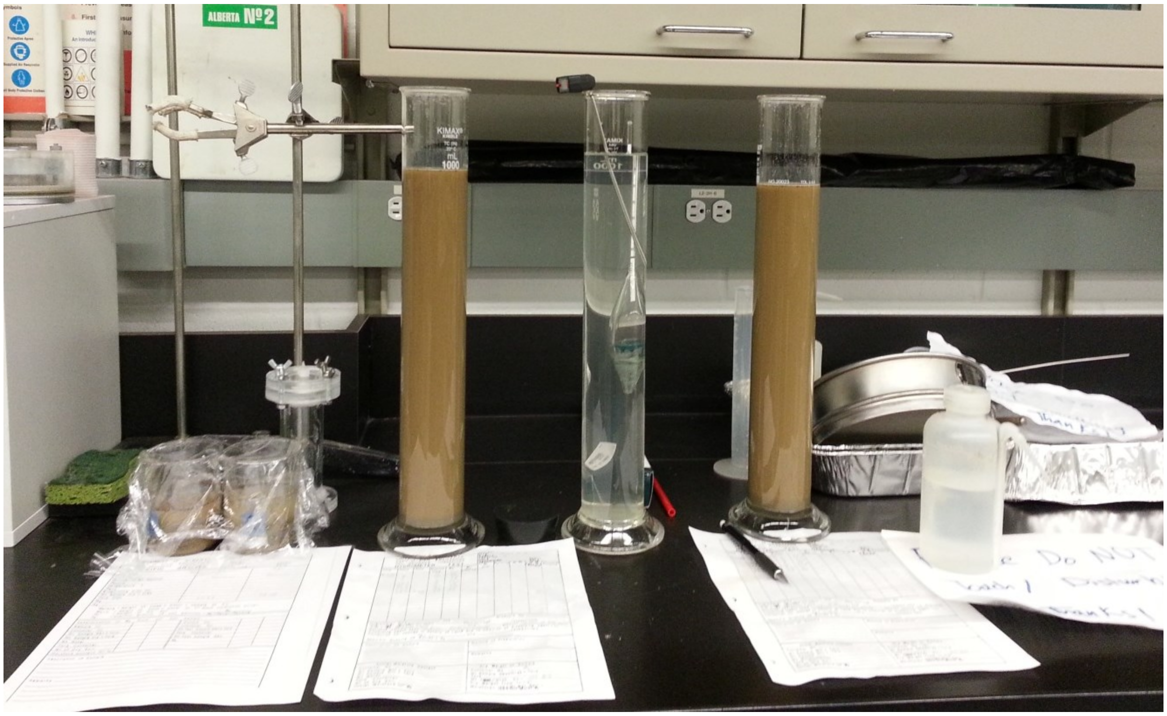

Figure 4.9 Typical setup of the hydrometer test.

4.3.1.2. Saturated Hydraulic Conductivity Analyses

The saturated hydraulic conductivity of sand was investigated in accordance with ASTM D2434-68 (2006) standard. The saturated hydraulic conductivity for silt was determined using the falling head test. A modified version of ASTM D2434-68 was adopted as follows: after the steady state flow was achieved in the sample, the head drop and the corresponding time interval were used to calculate the saturated hydraulic conductivity.

After the sample had achieved a steady state flow, the head at the manometer was marked, and a stopwatch timer was started simultaneously. After the head dropped sufficiently, the stopwatch was stopped, and the time and the new head were recorded. The saturated hydraulic conductivity was calculated using the head difference and the corresponding time interval. Figure 4.10 illustrates permeameter cells used for testing along with a basic schematic of the parameters used to calculate the flow rate required to conclude the saturated hydraulic conductivity.

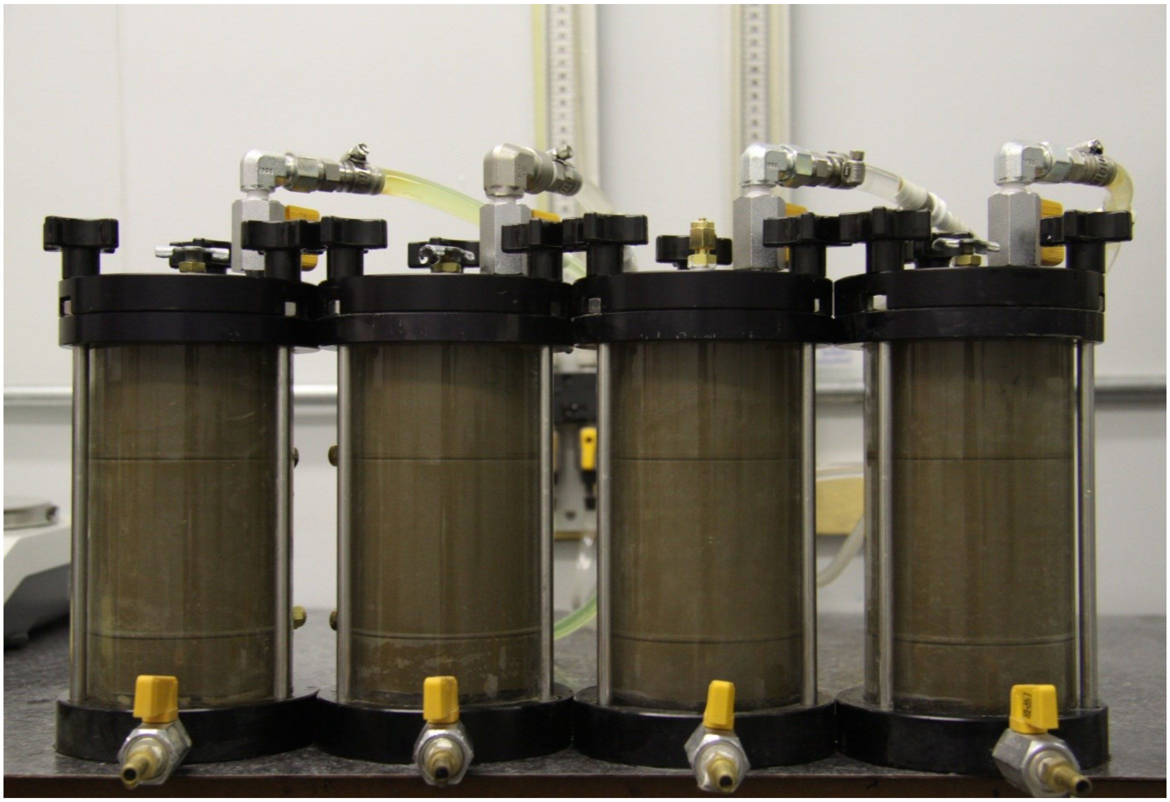

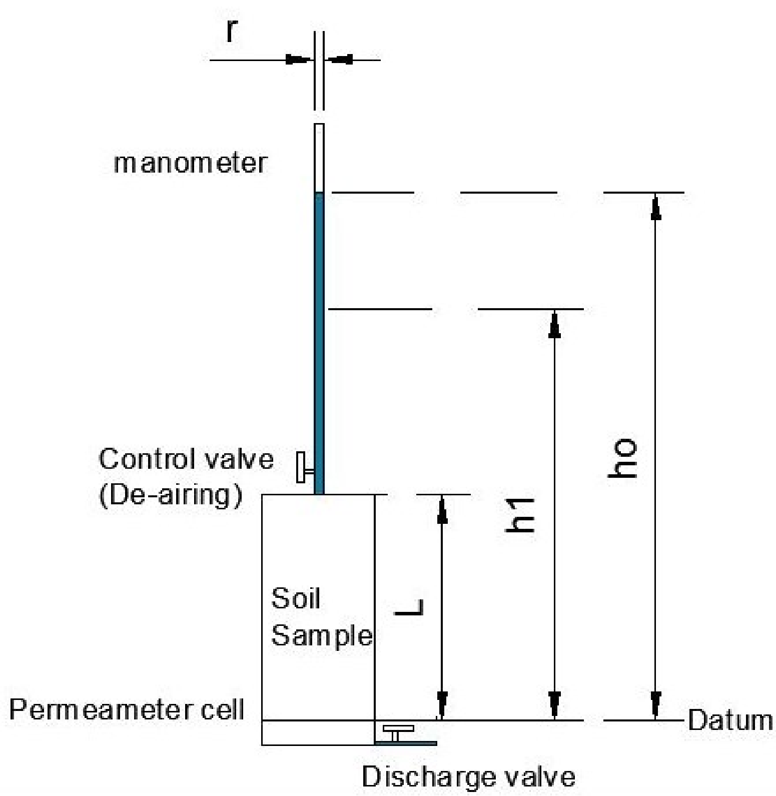

Figure 4.10 Typical permeameter cells used for hydraulic conductivity determination (top) and schematic of testing (bottom).

4.3.2. Advanced Water Retention Testing

A detailed characterization of the soils' water retention properties was essential to the scope of the laboratory program. Therefore, soil water characterization and infiltration capacity tests were conducted on each soil.

4.3.2.1. Soil Water Characteristics Curves

The soil water characteristic curve (SWCC) describes the relationship between soil suction and volumetric water content for a soil (Fredlund and Xing 1994). The SWCC can be used to predict other unsaturated soil parameters, including unsaturated hydraulic conductivity (Fredlund et al. 1994).

Soil-water characteristic curves were determined for tailings beach sand and Devon silt using Tempe cell according to the ASTM D6836-16 standard. Plexiglas® Tempe cells measuring 70 mm in diameter and 100 mm in height with 1-bar ceramic porous stones were utilized. Figure 4.11 illustrates the general setup during the SWCC tests.

Specimens were saturated in the Tempe cell at atmospheric pressure from the bottom up with distilled water and then left at saturation for a minimum of 48 hours. Following saturation, initial sample height and mass were recorded. For tailings beach sand samples, low matric suction range was determined using the hanging column method.

The hanging column method can be summarized as follows: The datum of Tempe cell discharge was selected, and then the discharge tubing was lowered by 10 mm to represent the application of 0.1 kPa of matric suction. The applied suction induced water discharge through a capillary needle placed in the tube and drained water was collected in a container. The mass of the sample and cell was monitored during each increment until no further change in mass was observed, which signified equilibrium. The discharge tubing was lowered incrementally, applying additional suction pressures, and the equilibrated mass recorded for each increment was used up to a maximum of 10 kPa.

Air pressure was used to apply suction for Devon silt samples and tailings beach sand samples at matric suction exceeding 10 kPa. Following testing, the gravimetric water content was determined for the specimens. The water content of the specimen could be back-calculated for each pressure increment using the final water content and recorded changes in mass. The volumetric water content and matric suction were then plotted to create the SWCC for each specimen. Curve fitting of the experimental data was generated using the Fredlund and Xing (1994) method in the SVFlux software.

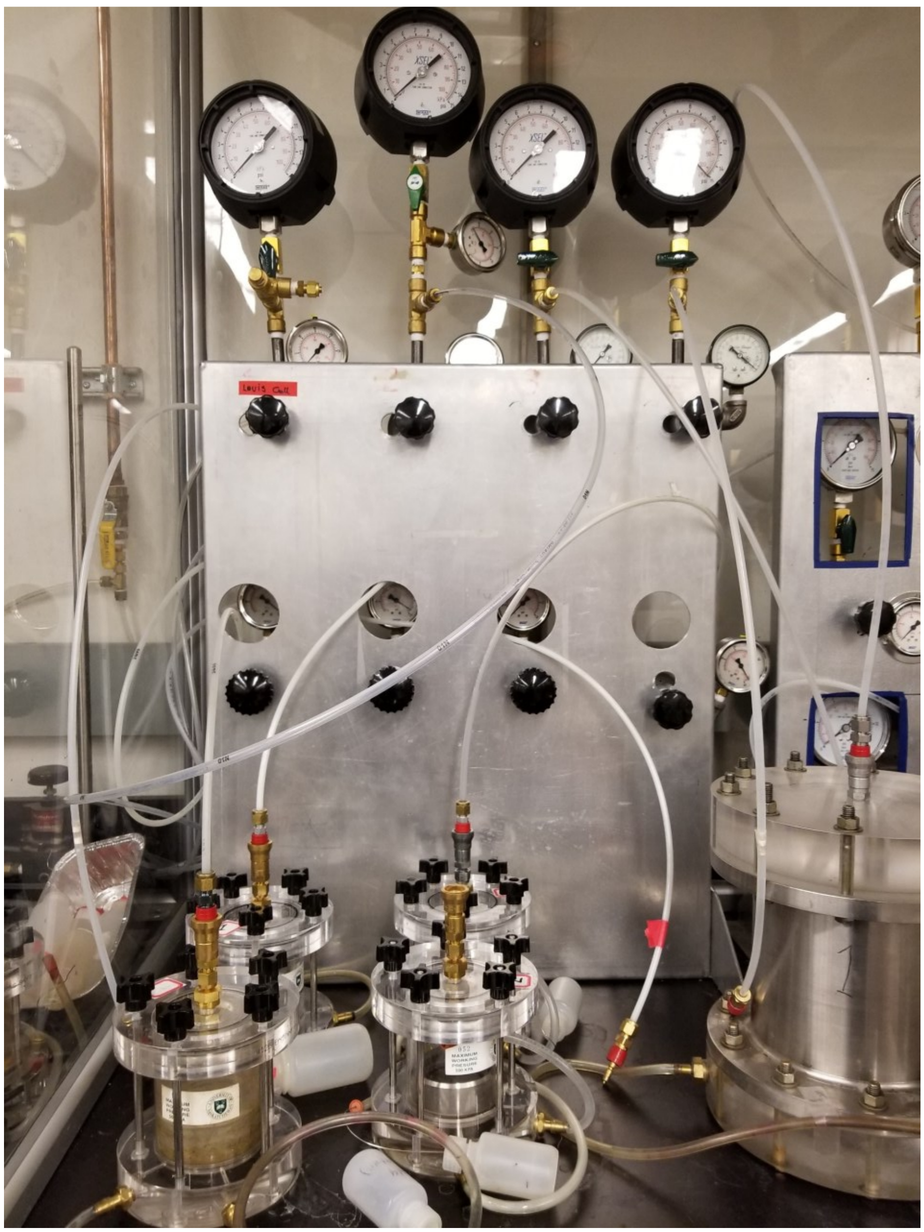

Figure 4.11 The general setup of the SWCC test in the air pressure chamber.

4.3.2.2. Infiltration Capacity Functions

Infiltration capacity function captures the change in infiltration rate with time. This function is known to start at a maximum value and then decrease nonlinearly with time down to a minimum value related to the saturated hydraulic conductivity of the soil (Horton 1939 and Beven 2002).

There is no standard test method to determine the infiltration capacity function of soil. Nevertheless, the standard test method for infiltration rate of soils in the field using double-ring infiltrometer (ASTM D3385 2009) was implemented with adjustments. The test was converted into a column test subjected to a sufficient ponding depth to generate the maximum infiltration rate. The column boundary conditions mirrored those of the flume test. For each soil type, four samples were prepared at four dry densities inside plexiglass cylinders. The tests started at a known ponding depth. While the time was being recorded, each cylinder was manually refilled with water to keep the ponding depth constant. The volume of water needed to maintain a constant ponding depth and elapsed time were recorded. The volume of water added during each time interval was converted to water depth, and incremental infiltration rate was calculated and then plotted with time. During each test, photographs were taken at a constant interval to observe the change in wetting front propagation. Details on how infiltration capacity functions are impacted by bulk density and void ratio can be found in Appendix I.

4.4. Soil Placement Procedure

The soil was placed in the flume using a funnel deposition method described by Yamamuro and Wood (2004). A specially designed funnel was employed for the procedure. The funnel was lifted using a mechanical movement facilitated by a wall mounted hand winch connected to a set of double pulleys to maintain uniformity of each profile. The funnel dimensions are illustrated in Figure 4.12.

Placement of soil inside the flume was performed by initially placing the spout of the funnel at the bottom of the flume. The funnel was filled with soil, and then slowly raised along the flume's axes of symmetry. This procedure ensured that the soil was deposited in a low-energy state without any drop height.

The velocity of lifting the funnel controls the density of the soil profile. The faster the funnel was raised, the denser the soil became (although still without a drop height). The rate of lifting the funnel was maintained at around 100 mm/min throughout all tests.

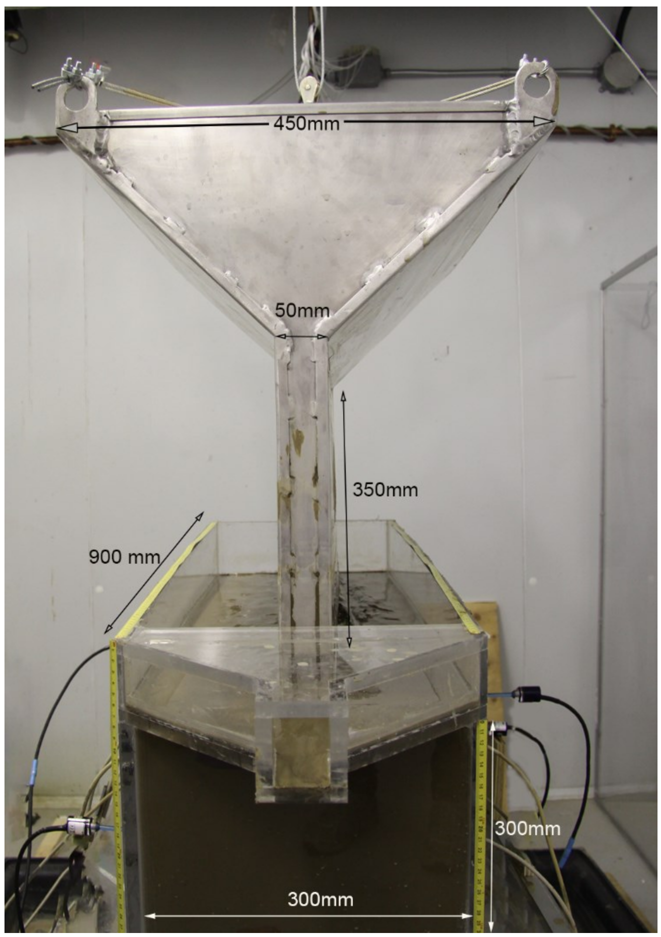

Figure 4.12 A view of the funnel used for soil placement procedure.

4.5. Laboratory Tests Procedures

The experiments on both silt and capillary barrier profiles adhered to the same regimen. In short, a rainfall flux was applied to the top surface of each profile at the designated rainfall intensity. Rainfall intensities ranging between 40 and 260 mm/hr were applied. This range ensured assessment of typical rainstorm event and extreme rainfall events. Rainfall intensities were changed by replacing the appropriate set of nozzles in the spraying system.

In terms of boundary conditions, both sides and base of the flume were impermeable. A discharge outlet 25 mm in diameter at the toe allowed for drainage. The flume had a slope of 1%. Saturated and unsaturated responses of each profile type were separately investigated.

In terms of initial conditions, unsaturated profiles were deposited in an oven-dry state using the placement procedure described earlier. Saturated profiles, on the other hand, utilized the same profile allowing full saturation for at least 24 hours prior to testing.

In terms of profile type, two soil profiles were established to represent two types of soil cover systems. Low permeability covers were represented by profiles of Devon silt 300 mm in thickness. Capillary barrier covers were represented by two-layer profiles consisting of Devon silt overlaying tailings beach sand 150 mm in thickness each.

In terms of rainfall intensities, rates were maintained constant throughout each experiment. The duration of each experiment ranged between thirty-three and one hundred and thirty hours of simulation conducted under a given rainfall intensity.

Table 4.1 summarizes detailed durations and intensities corresponding to each initial state including the stages and controlling parameters. The sequence of testing ensured that comparisons between saturated and unsaturated behaviours were possible for each profile type throughout the same duration. In other words, this ensured that data were available to compare initial conditions' influence on the quantity of measured runoff. The pillars of analyses are listed as follows:

1. initial conditions (saturated, unsaturated)
2. rainfall intensity (six different intensities)
3. profile type (low permeability, capillary barrier)
4. rainfall duration (six different durations)

The nature of flow (i.e., steady state/ transient) was defined when no further change in the measured data (volumetric water content, matric suction, water balance) was recorded. Moreover, transient flow tests were conducted to investigate the behaviour of both profiles.

During each test, rainfall and cumulative runoff volumes were measured simultaneously every 15 minutes. Plots of rainfall and runoff cumulative volumes and rates versus time were established using these measurements. Infiltration volumes were determined using equilibrium equation for the water balance components, which can be expressed as follows:

$$I = P - R - AE \tag{4.2}$$

where:

I	=	surface infiltration
P	=	cumulative precipitation
R	=	cumulative runoff

AE = cumulative actual evaporation

Complete water budget calculations were possible during each test since the tests were conducted in a controlled environment where no evaporation or outflows were therefore permitted. Equation 4.2 can be reduced as follows:

$$I = P - R \tag{4.3}$$

Table 4.1 The stages and controlling parameters of the laboratory testing program.

Cover Type	Initial state	Stages and duration of the experiments (hr)					
		I 40 mm/hr	II 55 mm/hr	III 90 mm/hr	IV 140 mm/hr	V 190 mm/hr	VI 260 mm/hr
Silt profiles	saturated	55	33	33	130	80	33
	dry	55	103	103	33	33	33
Capillary barrier profiles	saturated	103	55	55	33	45	33
	dry	103	55	55	55	55	55

For simplicity, the following is a summary of the conditions under evaluation after twenty-four data sets were collected during the experiments.

1. Comparisons of the effect of different initial conditions on surface runoff when the same profile type was exposed to the same rainfall intensity and the same rainfall duration.

2. Comparisons of the effect of different initial conditions on surface runoff when the same profile type was exposed to the same rainfall intensity but on different for rainfall duration.

3. Comparisons of the effect of profile type on surface runoff when exposed to the same rainfall intensity and duration under the same initial condition.

4. Comparisons of the effect of rainfall duration on surface runoff when the same profile type was exposed to the same rainfall intensity initial condition.

5. Comparisons of the effect of rainfall intensity on surface runoff when the same profile type was exposed to the same initial conditions and rainfall duration.

4.6. Numerical Simulations of Laboratory Experiments

Soil cover systems design is predicated on numerical modelling to determine both infiltration and evaporation fluxes, which are both intertwined with surface runoff. How representative are the numerical models that we use? Are the processes upon which models built physically correct? And if we eliminate field temporal and spatial variability, how representative would the results be? The present section examines these questions by modelling a series of controlled laboratory experiments.

The methodology of the numerical analyses of laboratory experiments on low permeability and capillary barrier profiles is described and discussed. Section 3.4. discusses the theory behind the governing equation of water flow. One-dimensional (1D) and three-dimensional (3D) analyses were performed. Input parameters for SVFlux include geometry, soil properties, and boundary and initial conditions. Each component of the input parameters is discussed in detail in the following sections.

4.6.1. The Numerical Model SVFlux

The numerical model SVFlux was used to reproduce the laboratory results. SVFlux is a multi-dimensional finite-element model that analyzes saturated and unsaturated seepage through soils (SoilVision Systems Ltd. 2009). The software solves the governing partial differential equations for groundwater flow using the following laws: for liquid flow, with hydraulic head as a driving force, Darcy’s Law is used as a flow law; for water vapour diffusion, where mass concentration of vapour per volume of soil is the driving potential, Modified Fick’s Law is utilized. These flow laws and a water volume-change constitutive equation are combined assuming the continuity of the water mass equation (SoilVision Systems Ltd. SVFlux theory manual 2012).

4.6.2. Geometry and Mesh

The geometry of the models in 1D analyses was entered as a single soil column for each profile type. For low permeability covers, the profile consisted of a single layer of silt of 350 mm in thickness to reflect the laboratory profile thickness. Similarly, the capillary barrier covers comprised two 150 mm-thick layers of silt overlaying sand. Each model contained an average of 209 nodes. The node spacing ranged between 3 mm and 5 mm. SVFlux automatically refined finite element mesh when needed.

In 3D analyses, the actual 3D matrix of the flume was analyzed. The dimensions of the flume were 300 mm in width, 300 mm in height, and 900 mm in length. For low permeability profiles, Devon silt constituted the entire thickness the entire profile thickness. For capillary barrier profiles, the thickness was equally distributed between tailings beach sand and Devon silt, totalling 150 mm each. The mesh generation and node spacing were set to a maximum possible level to ensure the quality of results. Figure 4.13 illustrates the typical mesh 3D analysis scenarios at time t = 0. The purpose of completing a 3D analysis can be understood upon reviewing the 1D analysis results in unsaturated capillary barrier profiles, which is discussed in further details in Section 5.4.2.

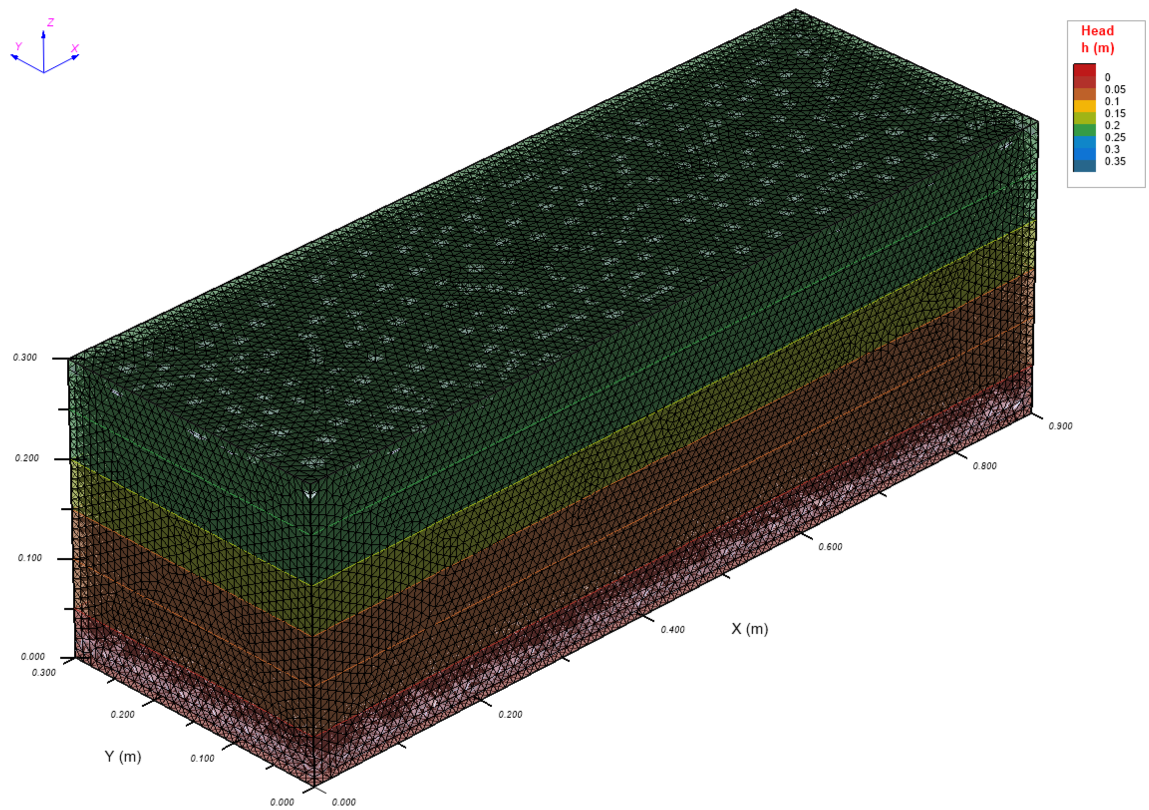

Figure 4.13 A view of the typical mesh in 3D analyses of the laboratory program.

4.6.3. Soils' Properties Input

Soil characteristics required for inputs include the saturated hydraulic conductivity (K_{sat}), unsaturated hydraulic conductivity function (K_{unsat}), soil water characteristic curve (SWCC), saturated volumetric water content (vwc), the coefficient of compressibility (m_v), and specific gravity (G_s).

The saturated hydraulic conductivity for Devon silt and tailings beach sand was obtained from laboratory characterization. The unsaturated hydraulic conductivity function was generated by SVFlux using the modified Campbell estimation. The Campbell (P) parameter was concluded for each material from the grain size distribution curve. The SWCC curves were generated in SVFlux using the Fredlund and Xing fit (1994). The saturated volumetric water content (vwc) was extrapolated from the SWCC. The coefficient of compressibility (mv), representing the slope of change in volumetric water content versus a change in pore-water pressure in the region of positive pore-water pressures, was also extrapolated from SWCC for each soil.

4.6.4. Initial and Boundary Conditions

Initial conditions reflected the state of saturation for each scenario. Laboratory measurements from Time Domain Reflectometry (TDR) probes and tensiometers were used to input the initial matric suction for the saturated and unsaturated profiles.

A climate boundary condition was applied at the top of each model to represent the precipitation and evaporation fluxes. Precipitation data were obtained from the laboratory program. Rainfall volumes were entered as 15-minute increment fluxes. Please refer to Table 4.1 for a summary of rainfall intensity scenarios corresponding to each profile type and each saturation state. The evaporation component of the climate data was eliminated since during the study, a closed water cycle was achieved in the testing chamber, and no evaporation was allowed.

4.7. The Case Study of the Savage River Mine

This section attempts to answer the following question: can we predict runoff for soil cover design models with reasonable confidence? To answer this question, numerical predictions of runoff fluxes for soil cover systems at the field scale were conducted. A case study for the Savage River mine in Tasmania, Australia, is presented. Comparisons of field-measured data and predictions made using the numerical model SVFlux are discussed. The feasibility and fallibility of such models are discerned.

4.7.1. Site Description

The Savage River mine, Northwestern Tasmania, Australia, is located in a pristine environment and a temperate climate with average annual rainfall and evaporation of 1938 mm and 902 mm, respectively. The maximum average monthly rainfall occurs in July, exceeding 234 mm, and the lowest in January with 78 mm. The average monthly evaporation is 146 mm in January and 27 mm in June. In general, rainfall amounts exceed evaporation from March to November. Mean temperatures reach a daily maximum (minimum) values of 20.1°C (9.9°C) in February and drop to 9.4°C (3.3°C) in July.

During previous mine operations, tailings were deposited in an uncovered impoundment referred to as *the Old Tailings Dam* (OTD), which has a history of generating Acid Rock Drainage (ARD). Figure 4.14 shows a visible sign of rusty colour associated with mineral oxidation and ARD. The waste rock was stored in a waste rock repository referred to as *the B-Dump*, which was capped with a cover system comprised two portions. The first portion is a low hydraulic conductivity water-shedding cover that limits infiltration by directing precipitation away as surface runoff, while the second is an alkaline side-hill cover that allows precipitation to percolate through the alkaline material to increase acid neutralization. The water-shedding cover comprised alkaline calcite chlorite schist run-of-mine waste rock and silty overburden. Both portions of the B-Dump cover were primarily non-vegetated.

The Savage River Rehabilitation Program (SRRP) initiative was instigated to address the historic ARD problem from the waste rock and tailings stored at the mine, and to identify options for long-term reclamation (Grange Resources 2012). Five catchment boundaries can be identified on the B-Dump cover. Two boundaries were equipped to measure the amount of rainfall and the resulting runoff as a part of the SRRP program.

The water-shedding portion encompasses the entire area of Catchment 1, which slopes between 3.5% and 8.8%. Conversely, Catchment 2 consists of approximately 81% water-shedding cover (the remainder is an alkaline side-hill portion), with gentle slopes between 0% and 4.0%. The total surface area of the B-Dump and the OTD is approximately 22.6 ha and 60 ha, respectively (Jubinville 2013). An aerial view of the B-Dump and the OTD showing ARD impacted drainage is illustrated in Figure 4.14.

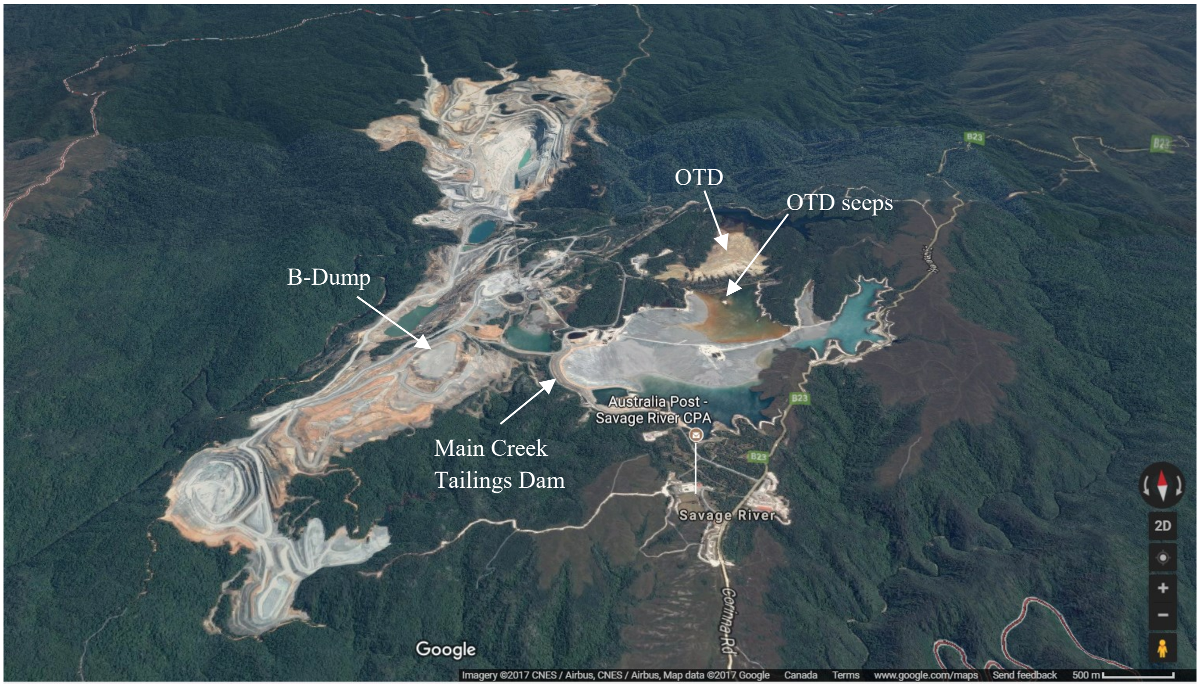

Figure 4.14 Aerial photograph of the Savage River mine (Google maps 2017).

4.7.2. Materials

Soil characteristics for the OTD and the B-Dump were obtained from a geochemical assessment of the near-surface tailings (SRK Consulting 2010), and (Jubinville 2013). B-Dump Catchment 1 consists of run-of-mine fine waste rock, and coarse and fine silt overburden. Catchment 2 consists of fine and coarse run-of-mine waste rock, as well as fine and coarse silt overburden. The fine waste rock, coarse waste rock, fine silt and coarse silt rock fit the USCS classification of GM, GP-GM, ML to SM and SM to GM, respectively.

Catchment A in the OTD comprised fine tailings and hardpan, which can be classified as SM and ML, respectively using the USCS classification. The corresponding particle size distribution and soil water characteristic curves for B-Dump and OTD materials as obtained from Jubinville (2013) are presented in Figure 4.15 and Figure 4.16, respectively.

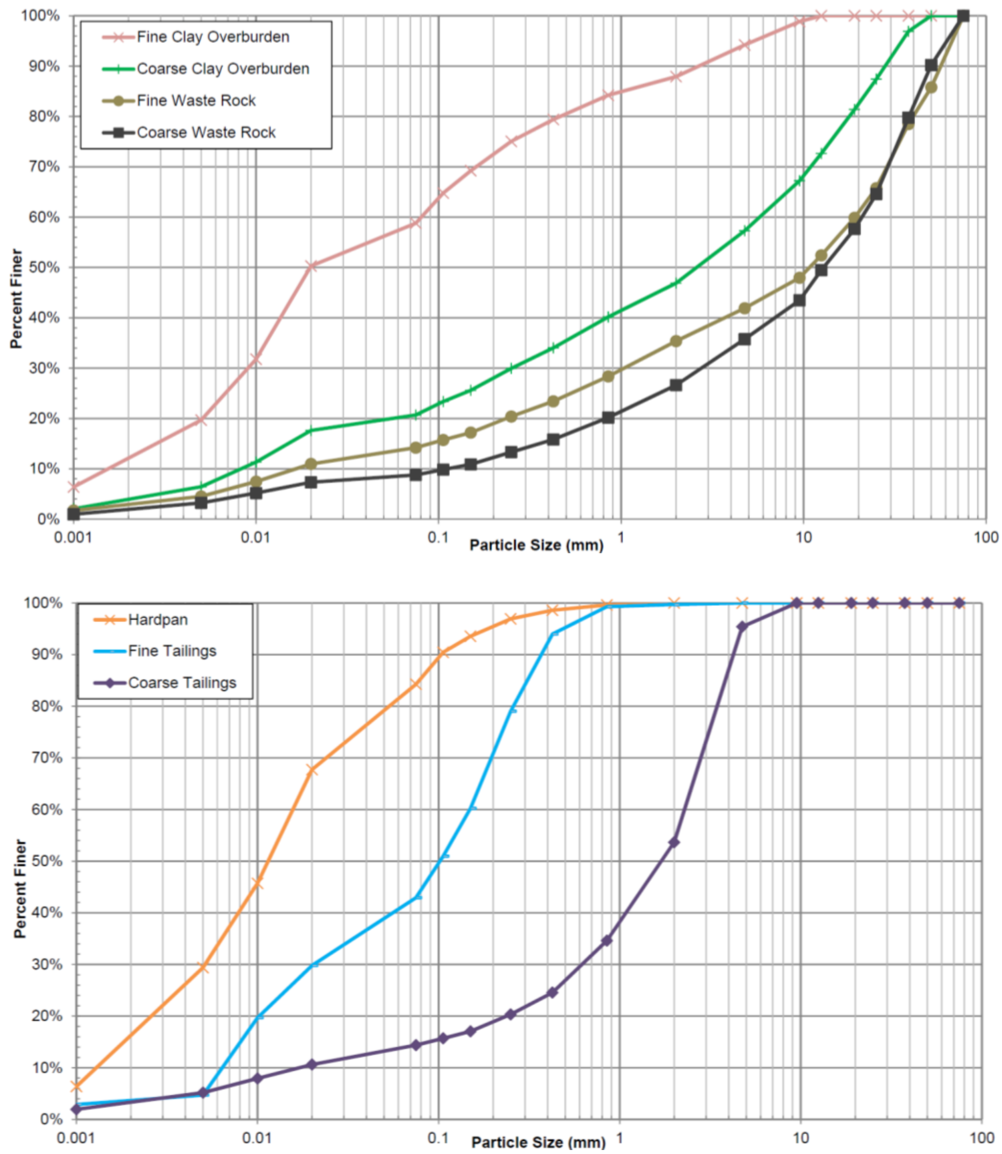

Figure 4.15 Representative particle size distributions for B-Dump materials (top) and OTD materials (bottom) (from Jubinville 2013).

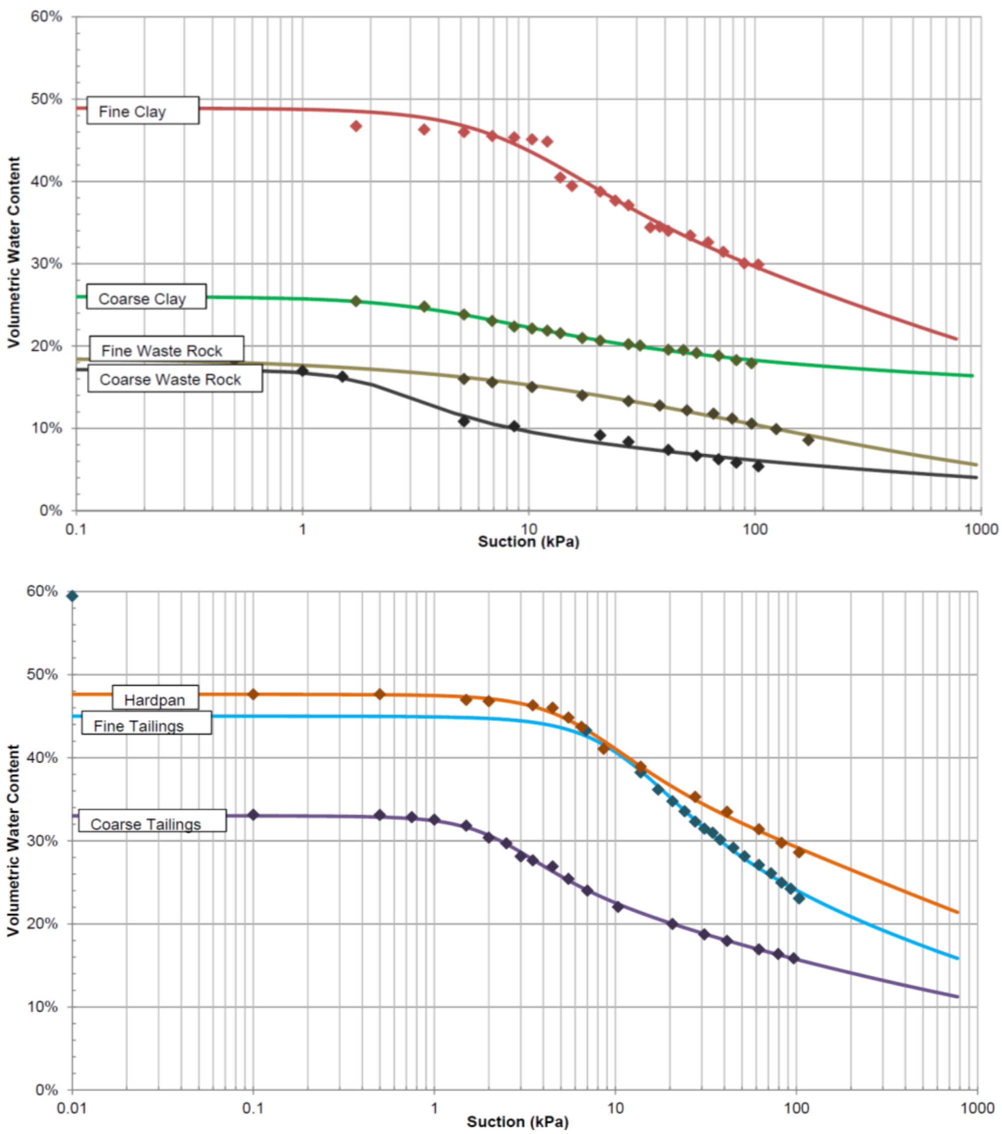

Figure 4.16 Soil-water characteristic data points and fitted Fredlund and Xing (1994) curves for B-Dump materials (top) and OTD materials (bottom) (from Jubinville 2013).

4.7.3. Model's Input Parameters

The focus of the numerical simulation program was to examine the sensitivity of numerical predictions of surface runoff to different input parameters. Climate data and soil properties were used to replicate field-measured data of runoff volumes using SVFlux.

Input parameters for SVFlux included the geometry of the model, soil properties, and boundary and initial conditions. Each component of the input parameters is discussed in detail in the following sections.

4.7.3.1. Geometry

The geometry of the models was entered as a one-dimensional soil profile for each material in the B-Dump and the OTD. The profile thickness was one meter and 0.6 meters for B-Dump and OTD, respectively, reflecting the in-field cover thickness.

In SVFlux, each model contained an average of 209 nodes. The node spacing ranged between three and five mm (SVFlux automatically refines finite element mesh when needed).

4.7.3.2. Soil Properties Input

Soil properties required for input for each material were the saturated hydraulic conductivity (K_{sat}), unsaturated hydraulic conductivity function (K_{unsat}), soil water characteristic curve (SWCC), saturated volumetric water content (vwc), coefficient of compressibility (mv), and specific gravity (Gs).

The saturated hydraulic conductivity was one of the parameters selected for the sensitivity analysis, allowing for an investigation of the effect of the natural variation of measured hydraulic conductivity on the numerically predicted results. Three cases of highest measured, lowest measured, and average K_{sat} were considered as reported by Jubinville (2013).

The unsaturated hydraulic conductivity function was generated by SVFlux using modified Campbell estimation (Campbell fitting parameter was concluded for each material from the grain size distribution curve). The SWCC curves were generated in SVFlux using Fredlund and Xing (1994).

Measured volumetric water content and specific gravity for each material were taken from Jubinville (2013). The coefficient of compressibility (mv) represents the slope of change in volumetric water content versus a change in pore-water pressure in the region of positive pore-water pressures; mv was extrapolated from SWCC curves for each soil.

4.7.3.3. Initial and Boundary Conditions

A climate boundary condition was applied at the top of each model to represent the precipitation and evaporation fluxes. Input details of climate parameters included such components as 1) precipitation data were obtained from field measured rainfall volumes, 2) evaporation data were extrapolated using net radiation, winds speed and air temperature and relative humidity. These data were obtained from publicly available meteorological information. A summary of climate data input is provided in Table 4.2.

Table 4.2 A summary of climate data parameters input into SVFlux.

Parameter	Input details
Precipitation	Measured rainfall volumes were converted to rainfall intensity using catchment area, and were input as global intensity in three different scenarios as described in Table 4.3 (from Jubinville (2013)
Air Temperature	Mean daily minimum, and maximum air temperatures were input using averages over the years 1966 – 1989 (from Commonwealth of Australia 2012)
Relative Air Humidity	Mean 9 a.m. and 3 p.m. relative humidity values were input using averaged values (over the years 1966 – 1989) (from Commonwealth of Australia 2012)
Net Radiation	Calculated using Penman approximation by inputting average daily global solar exposure (from Commonwealth of Australia 2012)
Winds Speed	Average monthly wind velocity distribution and magnitude were input (from Commonwealth of Australia 2012)
Potential Evaporation	Penman (1948) method was used to calculate the evaporative fluxes. Wilson-Penman’s (1994) method was used to estimate actual evaporation.

4.7.4. Sensitivity Analyses

Thirty-two modelling scenarios were conducted to assess the sensitivity of runoff predictions. Sensitivity analyses of runoff predictions were assessed in terms of the resolution of rainfall intensity input, and the variation in hydraulic conductivity. Further details on input are presented in the following sections.

4.7.4.1. Rainfall Intensity

Rainfall volumes were available from tipping bucket rain gauges in 15-minute increments from the SRRP program. The rainfall volumes were converted into rainfall intensity for input in climate boundary conditions.

SVFlux examined three scenarios of 15-minute, event-averaged, and 24-hour rainfall intensity input. In the event-averaged intensity, the duration and total rainfall from the storm event were defined each day from the raw data. An average rainfall intensity for the storm event was calculated based on the total rainfall volume and the duration of the event. In the 24-hour scenario, the measured rainfall amounts were totalled for each day, and the precipitation was entered as an intensity based on a 24-hour period.

4.7.4.2. Saturated Hydraulic Conductivity

The variation in the saturated hydraulic conductivity K_{sat} input reflects the natural variation in measured values. Three scenarios of the highest measured, lowest measured, and average K_{sat} were considered. Corresponding values shown in Table 4.3 were reported by Jubinville (2013).

Table 4.3 Saturated hydraulic conductivity values used in numerical modelling (from Jubinville 2013).

B-Dump Materials			
B-Dump Material	Lowest Measured[2] K_{sat} (m/s)	Average K_{sat} (m/s)	Highest Measured K_{sat} (m/s)
Fine Waste Rock	8×10^{-8}	2×10^{-7}	4×10^{-7}
Coarse Waste Rock	1×10^{-6}	1×10^{-6}	2×10^{-6}
Fine Clay Overburden	8×10^{-7}	2×10^{-6}	3×10^{-6}
Coarse Clay Overburden	3×10^{-7}	5×10^{-7}	9×10^{-7}
Old Tailings Dam materials			
OTD Material	Lowest Measured K_{sat} (m/s)	Average K_{sat} (m/s)	Highest Measured K_{sat} (m/s)
Fine Tailings	5×10^{-6}	9×10^{-6}	2×10^{-5}
Hardpan	2×10^{-7}	4×10^{-7}	9×10^{-7}

4.8. Summary

Chapter 4 covered three tiers of research methodology linking physical and numerical models. The chapter explored the design, construction and calibration of the laboratory rainfall simulator apparatus. The systems comprising the apparatus and measuring devices were discussed. Furthermore, the profiles considered to conduct the laboratory rainfall runoff experiments were revealed. Test procedures for basic and advanced characterization of each soil were outlined.

[2] Measured by Jubinville 2013

For the laboratory program component, the stages and controlling parameters of the experiments were detailed. Tests were performed on low permeability and capillary barrier profiles in saturated and unsaturated initial state. Six rainfall intensities were applied to each profile spanning different durations. Rainfall and runoff volumes and rates were measured simultaneously in 15-minute increments. Internal volumetric water content and matric suction were also recorded throughout each experiment.

For the numerical predictions component, the methods and input parameters for the one- and three-dimensional simulations of laboratory results were presented. Details on the theory and fundamental flow laws used in SVFlux were described.

Furthermore, for the field component, the case study of the Savage River Mine was discussed. Detailed sensitivity assessment of numerical runoff predictions in a field setting was presented. The sensitivity analyses were based on multiple scenarios for two significant parameters controlling numerical predictions. Three scenarios of intensity resolution were examined. Moreover, three scenarios of saturated hydraulic conductivity were investigated.

CHAPTER 5. Presentation of Results

5.1. Introduction

This chapter presents the experimental and numerical modelling results of the testing program described in Chapter 4. The data presented include the results of:

1. Testing for soil properties for Devon silt and tailings beach sand including saturated hydraulic conductivity values, particle size distributions, soil water characteristics curves and infiltration capacity functions.

2. The rainfall runoff laboratory tests for low permeability and capillary barrier profiles. Results are presented individually for saturated and unsaturated profiles. Groups in terms of volumes versus time and rates and internal matric suction and water content measurements are provided.

3. The numerical simulation of each scenario examined in the laboratory tests. Comparisons between 1D and 3D simulations conducted using SVFlux.

4. The numerical simulations for the Savage River mine. Detailed sensitivity analyses of runoff predictions to rainfall input saturated hydraulic conductivity performed for two locations.

A brief description of the implementation and operation of each test is provided along with tests results.

5.2. Soil Properties

The soils' basic and hydraulic characteristics of both soils were investigated according to test procedures and standards described in Section 4.3. Corresponding results for each soil are presented in the following sections.

5.2.1. Saturated Hydraulic Conductivity

The saturated hydraulic conductivity of Devon silt and tailings beach sand were investigated using the methods described in Section 4.3.1.1 The average saturated hydraulic conductivity values were $4x10^{-8}$ and 10^{-3} m/sec for Devon silt and tailings beach sand, respectively.

5.2.2. Particle Size Distribution

Sieve and hydrometer analyses were completed for particle-size distribution of soils following the standards described in Section 4.3.1.2, to determine the grain size distribution. A representative particle size distribution for each soil is illustrated in Figure 5.1.

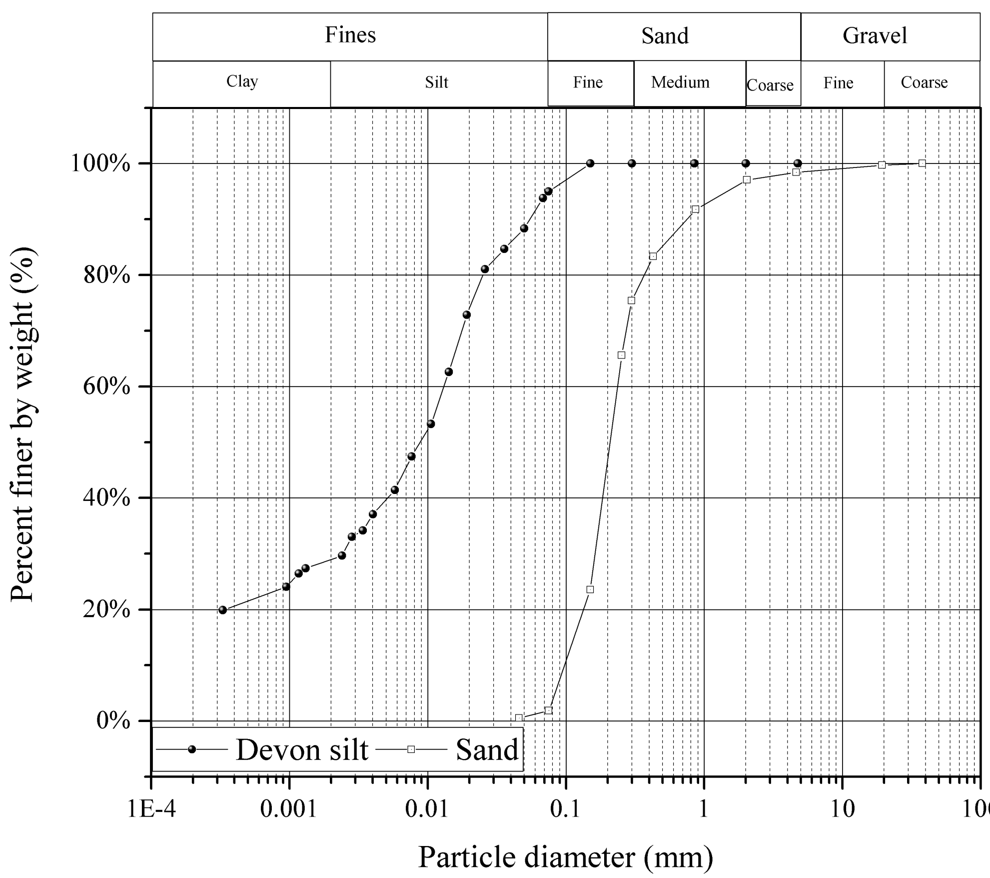

Figure 5.1 Representative particle size distribution of tested soils.

5.2.3. Soil Water Characteristics Curves

The soil water characteristics curves for Devon silt and tailings beach sand were determined using the methods described in Section 4.3.2.1. Fredlund and Xing (1994) fit was generated using SVFlux as illustrated in Figure 5.2.

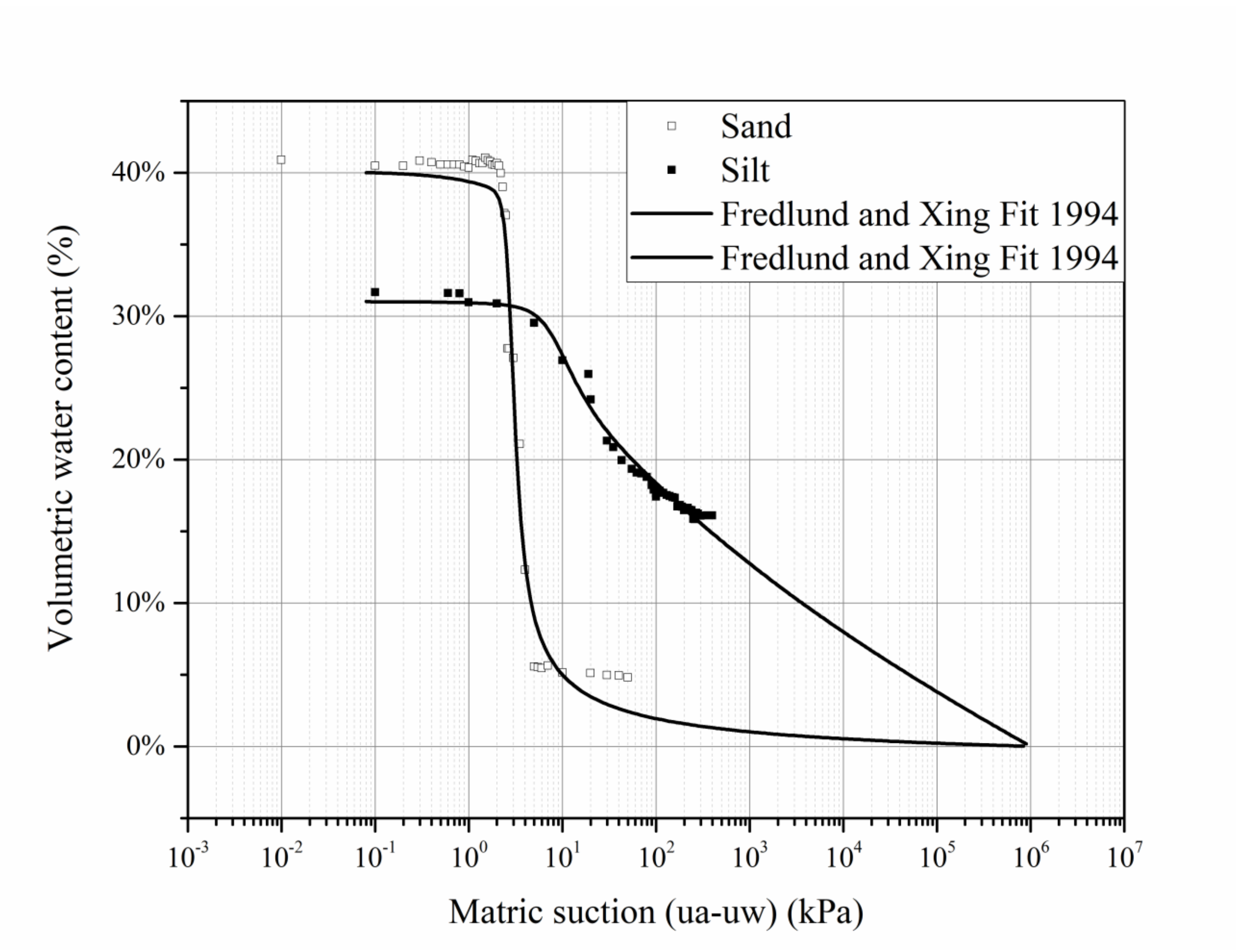

Figure 5.2 Representative soil water characteristics curve of each soil.

5.2.4. Infiltration Capacity Functions

Infiltration capacity functions capture the limit for the change in infiltration rate with time in unsaturated soils. The infiltration capacity function is known to start at a maximum value and then decrease nonlinearly with time down to a minimum value related to the saturated hydraulic conductivity of the soil (Horton 1939 and Beven 2002).

Infiltration capacity tests were conducted as described in Section 4.3.2.2. Plexiglass columns measuring 500 mm in height and 100 mm in diameter were used to investigate the infiltration capacity of soils employed in the laboratory program. The incremental infiltration rate was measured, and then plotted with time for each soil. Four samples were prepared for each soil at four different dry densities.

Measured infiltration capacity functions with time for both Devon silt and tailings beach sand exhibited a nonlinear decrease of infiltration rate with time following the theoretical assumption. The rate changed more rapidly reaching constant values in the sand specimens relative to the silt specimens. A representative illustration of the measured infiltration capacity functions for sand and silt is presented in Figure 5.3.

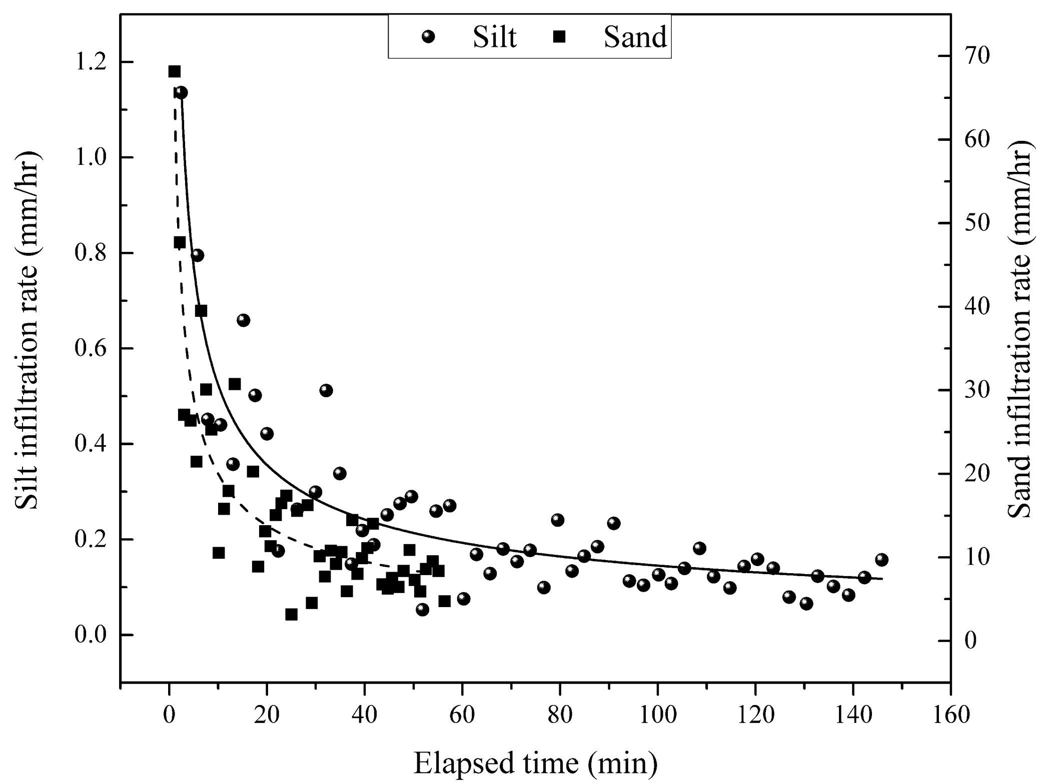

Figure 5.3 Typical measured infiltration capacity functions of tested soils.

5.2.4.1. Infiltration Capacity Functions of Devon Silt

During infiltration capacity tests, the wetting fronts' propagation was observed and recorded using time-lapse photography. A typical wetting front propagation for Devon silt samples is illustrated in Figure 5.4. The depicted column is 100 mm in diameter and 500 mm in height. Soil height in the column is 270 mm. The depth of the wetting front is noted on the photo along with the corresponding point in time. The results of the wetting fronts' propagation suggest that the infiltration rate is decreasing with time, as has been established from measured data. The rate decreases about an order of magnitude within an hour. The theoretical explanation is that dry soil is a two-phase matrix, and water easily displaces air at the beginning. As time progresses, more pores are filled with water and soil becomes a three-phase system. Water can only flow through pores that are filled with water. Therefore, lower flow rates ensue.

5.2.4.2. Infiltration Capacity Functions of Tailings Beach Sand

Like Devon silt samples, the wetting front propagation during infiltration capacity tests on tailing beach sand was observed and recorded using time-lapse photography. Typical wetting front propagation for tailings beach sand samples is illustrated in Figure 5.5. The depicted column is 100 mm in diameter and 500 mm in height. Soil depth in the column is 228 mm. The depth of the wetting front is noted on each photo along with the corresponding elapsed time. Results of wetting front propagation suggest that the infiltration rate trend is comparable to the trend observed in the silt specimen. The only distinction was that the rate change occurred faster than what had been observed in the Devon silt specimen. The wetting front propagated through the entire depth of soil within ten minutes of testing. More frequent readings had to be taken during the infiltration capacity tests, and less interval in time-lapse photography had to be implemented to capture the quick change in rate. Inability to do so might result in a misrepresentation of the infiltration capacity function as a linear function. Similar reasoning to that discussed in Section 5.2.4.1 could explain the physics of water flow causing the nonlinear rate change.

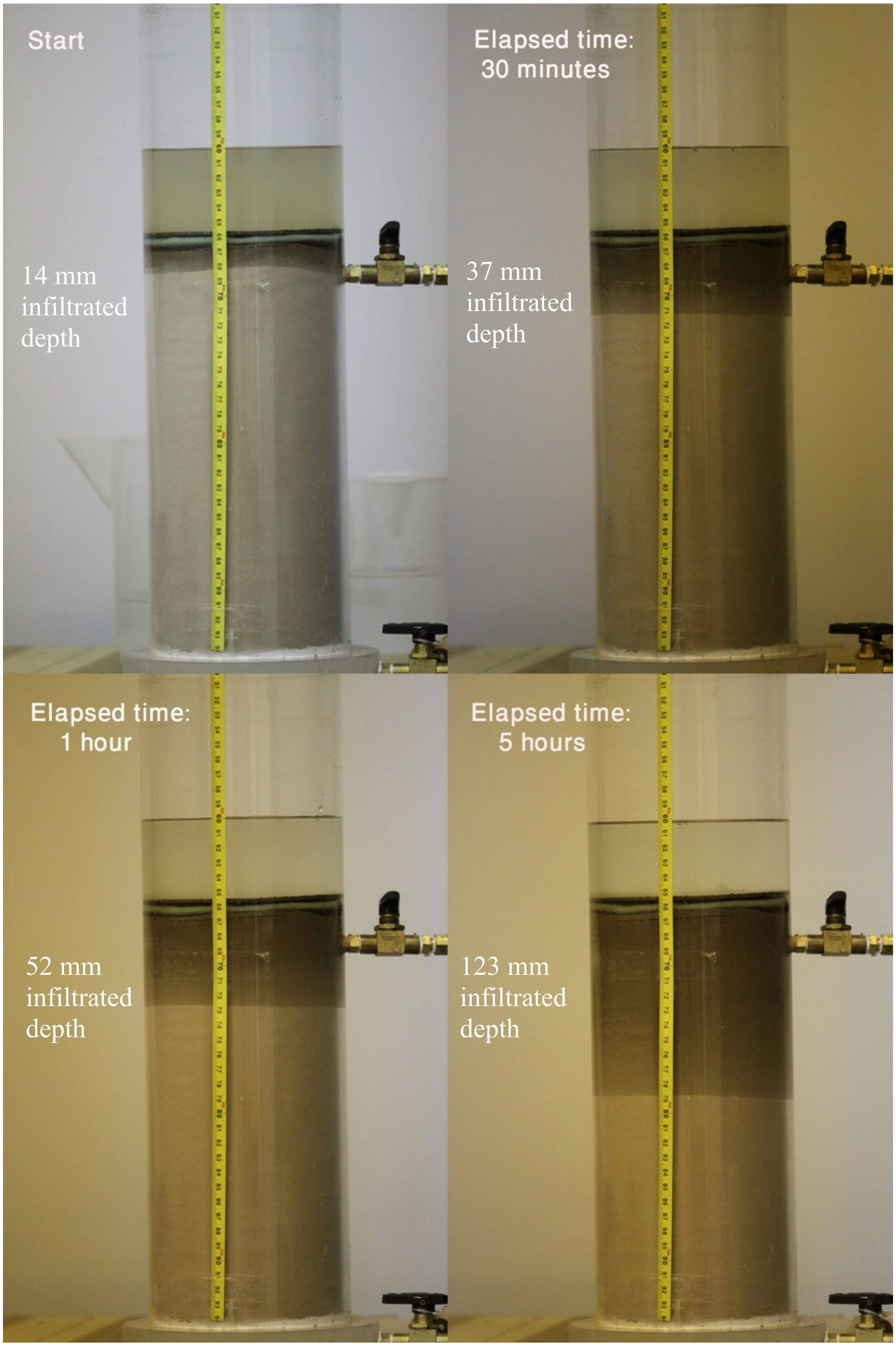

Figure 5.4 Typical stages of infiltration capacity test along with the wetting front propagation with time in the silt samples.

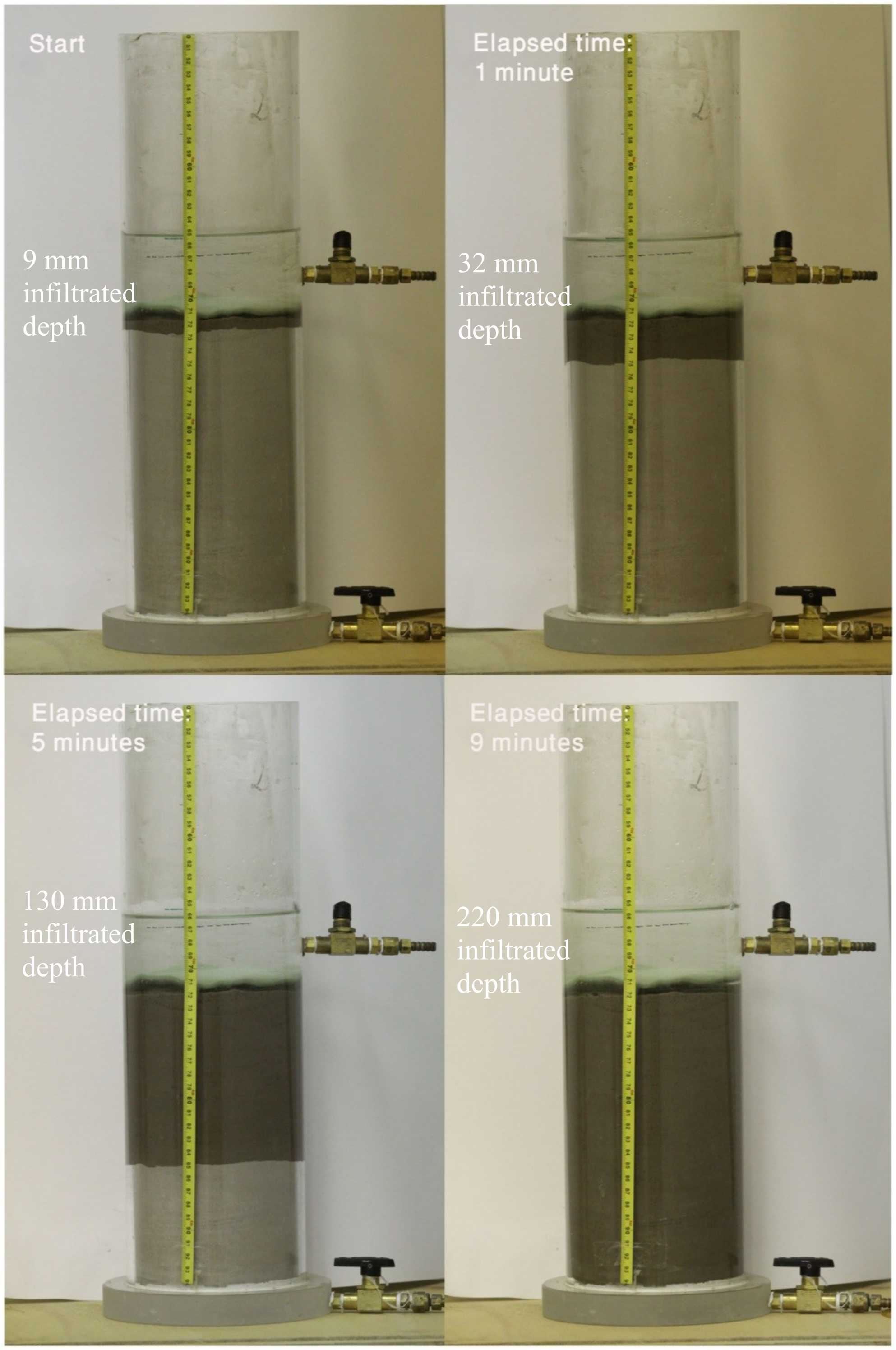

Figure 5.5 Typical stages of infiltration capacity test along with the wetting front propagation with time in the sand samples.

5.3. Laboratory Program Results

Two types of soil profiles were established to represent two types of cover systems. A single layer of Devon silt and two-layer Devon silt overlaying tailings beach sand profiles represented low permeability and capillary barrier systems, respectively. Runoff responses of six laboratory-simulated rainfall intensities were observed for each profile in each initial saturation state (i.e., saturated and unsaturated). Testing details and procedures were described in Section 4.5. The results for each profile type are grouped into the following categories: cumulative volumes, rates, and changes in volumetric water content and matric suction.

5.3.1. Silt Profiles

A single layer of Devon silt was established to represent low permeability cover systems. During unsaturated state tests, the profiles were initially deposited as oven-dry profiles into the testing flume using the funnel deposition method described in Section 4.4. For each rainfall intensity scenario, a new profile of oven-dry silt had to be prepared. Whereas for saturated profiles, the soil was allowed to saturate fully and then the same profile was utilized for all rainfall scenarios. After equilibrium was attained, testing took place as described earlier in Section 4.5. The results presented in this section summarize the response of saturated silt profiles compared to unsaturated silt profiles at respectively applied rainfall intensities in terms of change in cumulative volumes and rates with time.

5.3.1.1. Volumes

Rainfall, runoff, and infiltration cumulative volumes plotted with time during each experiment for saturated and unsaturated silt profiles, are presented in Figures 5.6 through 5.11. Rainfall volumes were measured via the flowmeter mounted on the spraying system. Runoff volumes were collected in containers placed below the flume's runoff spout and continuously measured using an electronic scale. Infiltration volumes were determined by conducting water balance calculations as described in Section 4.5.

In the saturated silt profiles, up to 98% of the entire applied rainfall volume eventually converted to runoff in all rainfall intensities scenarios. The cumulative runoff volume increased with time, consistent with the applied rainfall cumulative volume. Increase in the applied rainfall intensities produced a corresponding increase in both rainfall and runoff volumes; and as expected, the infiltration volumes remained virtually unaffected.

Measurements of water balance components for unsaturated silt profiles were observed in the same manner as in saturated silt profiles. At the beginning of each test, the entire rainfall infiltrated into the profile with no runoff generation. The patterns observed in Figure 5.6 b, where infiltration overlaps with rainfall at the beginning stages of the test, can be understood as such. Appendix II provides a close insight into the first couple of hours of testing where these two curves overlap. The time to runoff onset was inversely proportional to applied rainfall intensity. A detailed discussion of the variation in water balance components during the first couple of hours of testing is presented in Section 5.3.3.

The unsaturated silt profiles produced lower percentages of runoff, and, subsequently, higher infiltration volumes compared to the saturated profiles. Up to 92% of the final applied rainfall volume converted into surface runoff. Furthermore, as higher rainfall intensities were applied, the profiles neared saturation, and the difference between measured runoff and rainfall volumes decreased substantially. The reader can notice the gap between the applied rainfall and the resultant runoff series decrease as higher rainfall intensities were applied. This signifies that with higher rainfall intensities the profiles were closer to saturation.

Upon comparing the water balance components of equal applied rainfall intensities from saturated and unsaturated profiles, higher infiltration cumulative volumes are evident in the unsaturated profiles. The higher infiltration volumes can be attributed to both storage capacity and higher infiltration rate discussed in the next chapter. Upon comparing the runoff response of unsaturated profiles based on different rainfall intensities, the increase in rainfall intensity prompted an increase in the overall runoff percentages A detailed discussion of the results of cumulative runoff volumes as a percentage of applied rainfall for each profile is described in depth in Section 5.3.5.

In short, the cumulative runoff volumes exhibit the following characteristics in the low permeability profiles:

1. The incremental increase in rainfall volume with time generates a proportional increase in runoff volume with time in saturated profiles.

2. A brief period of no runoff in unsaturated profiles after rainfall was applied can be observed.

3. After runoff is generated in the unsaturated profiles, an incremental increase in rainfall volume with time produces a proportional increase in runoff volume with time.

4. Naturally, longer duration of rainfall in unsaturated profiles brought profiles to saturation.

5. Higher rainfall intensities brought profiles to saturation more rapidly compared to low rainfall intensities, as one would intuitively conclude.

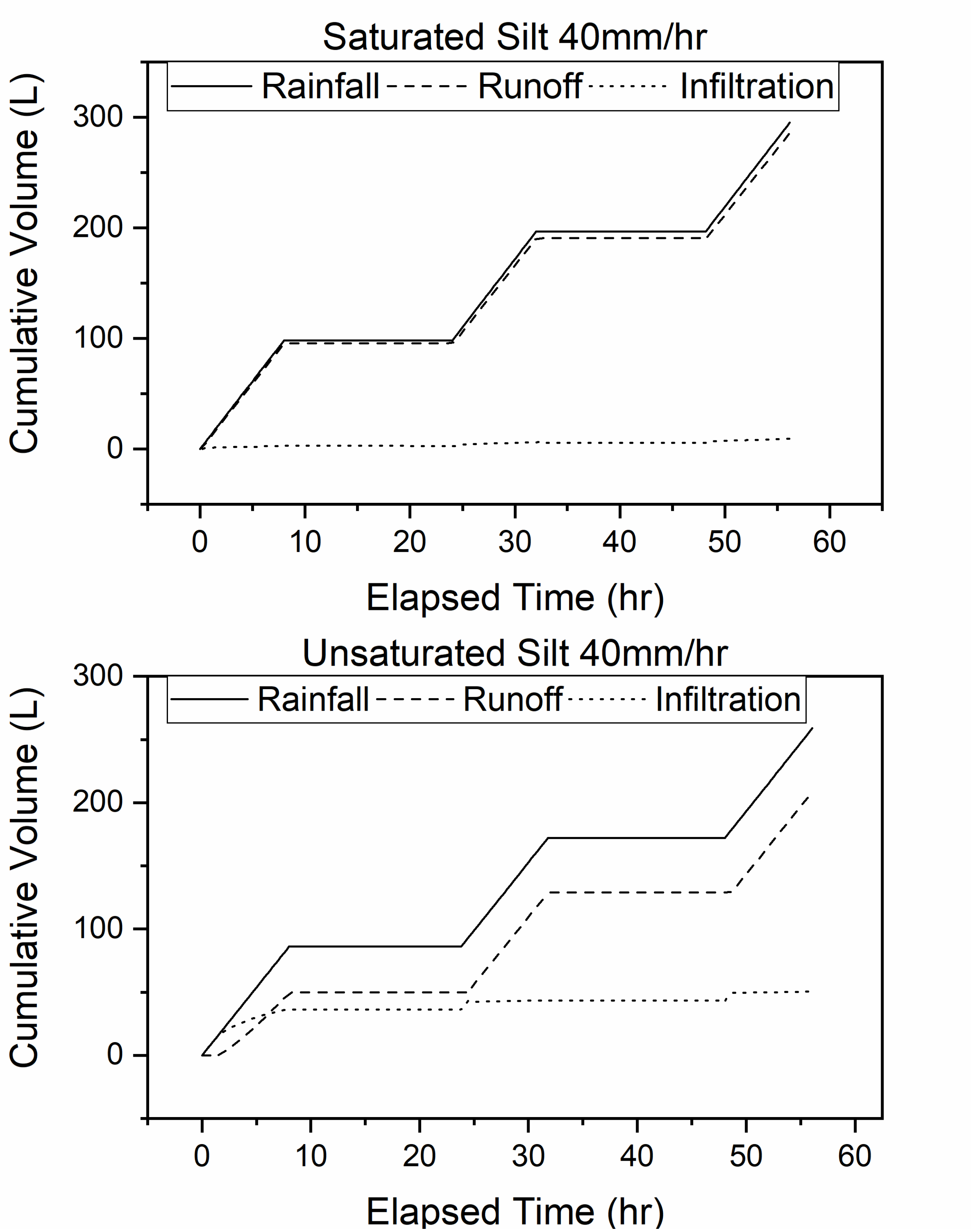

Figure 5.6 Measured cumulative volumes of water balance components for saturated (top) and unsaturated (bottom) silt profiles at 40 mm/hr applied rainfall intensity.

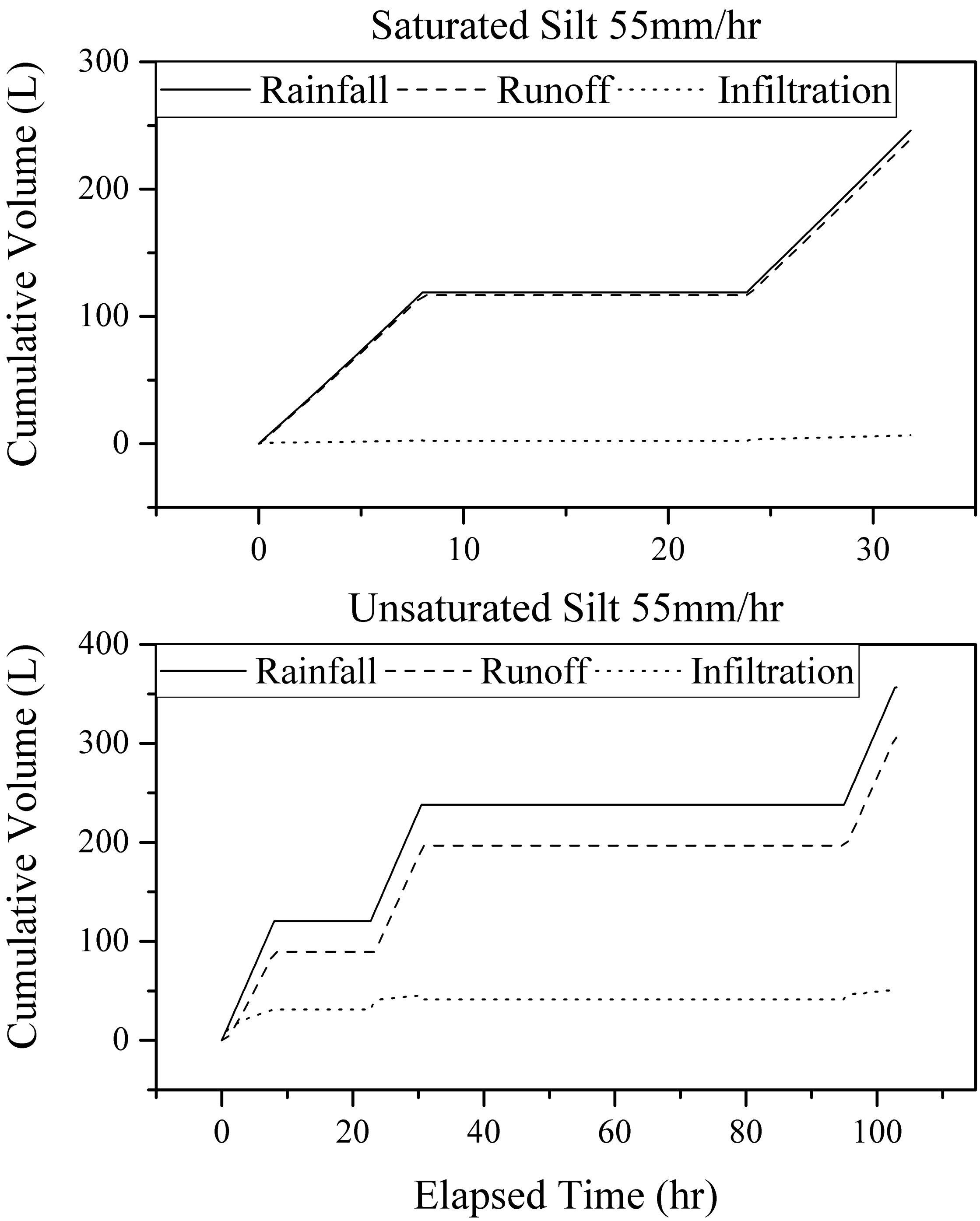

Figure 5.7 Measured cumulative volumes of water balance components for saturated (top) and unsaturated (bottom) silt profiles at 55 mm/hr applied rainfall intensity.

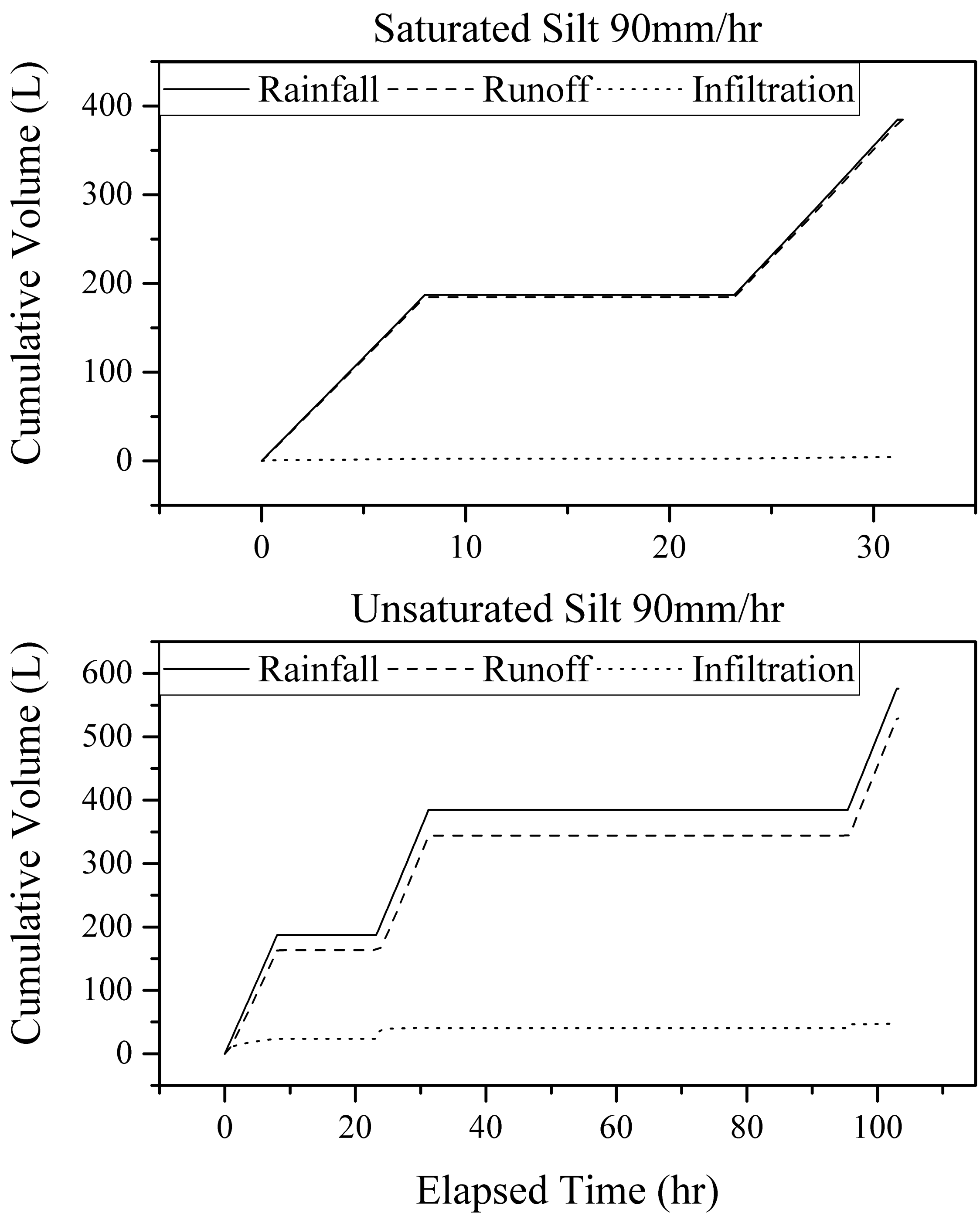

Figure 5.8 Measured cumulative volumes of water balance components for saturated (top) and unsaturated (bottom) silt profiles at 90 mm/hr applied rainfall intensity.

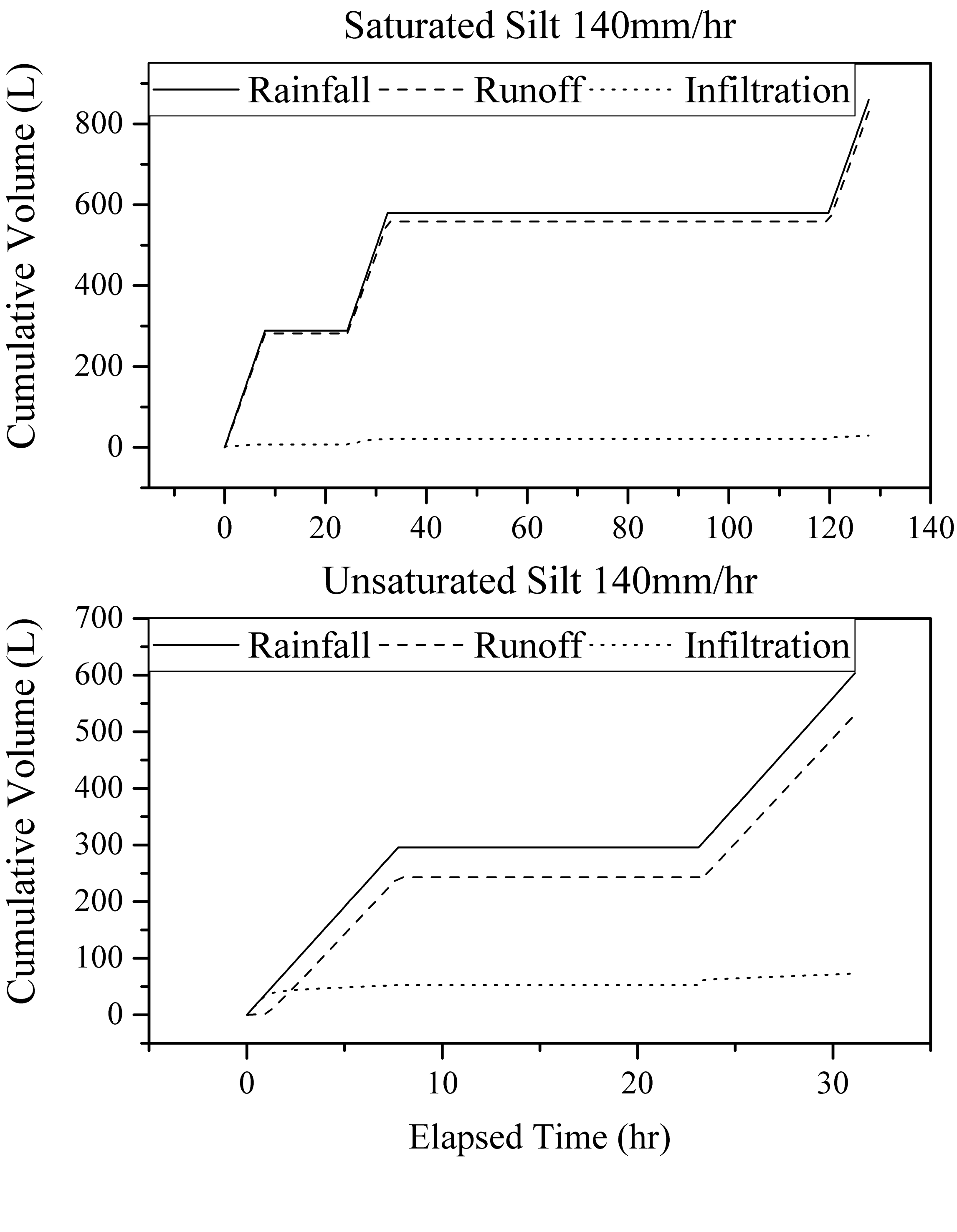

Figure 5.9 Measured cumulative volumes of water balance components for saturated (top) and unsaturated (bottom) silt profiles at 140 mm/hr applied rainfall intensity.

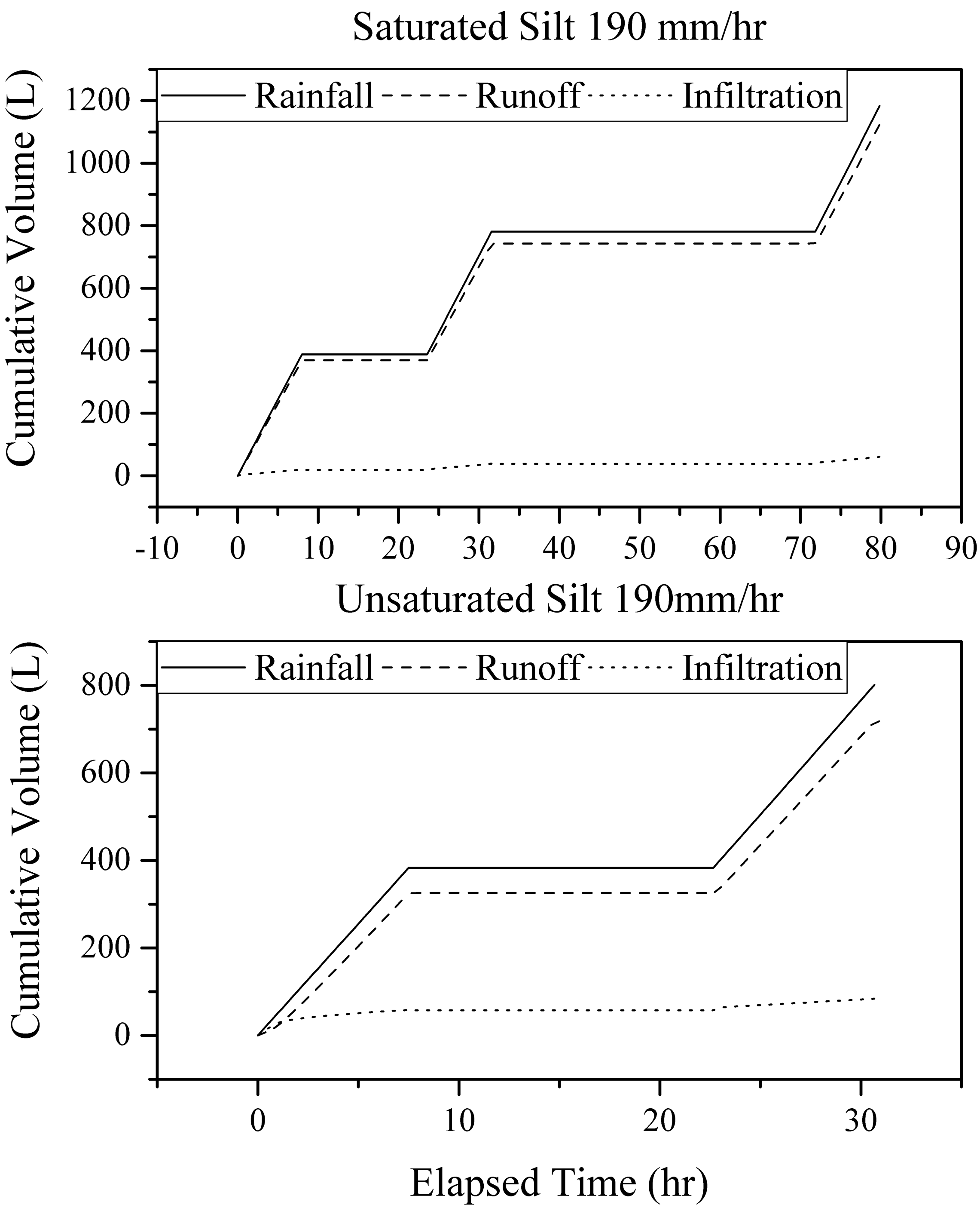

Figure 5.10 Measured cumulative volumes of water balance components for saturated (top) and unsaturated (bottom) silt profiles at 190 mm/hr applied rainfall intensity.

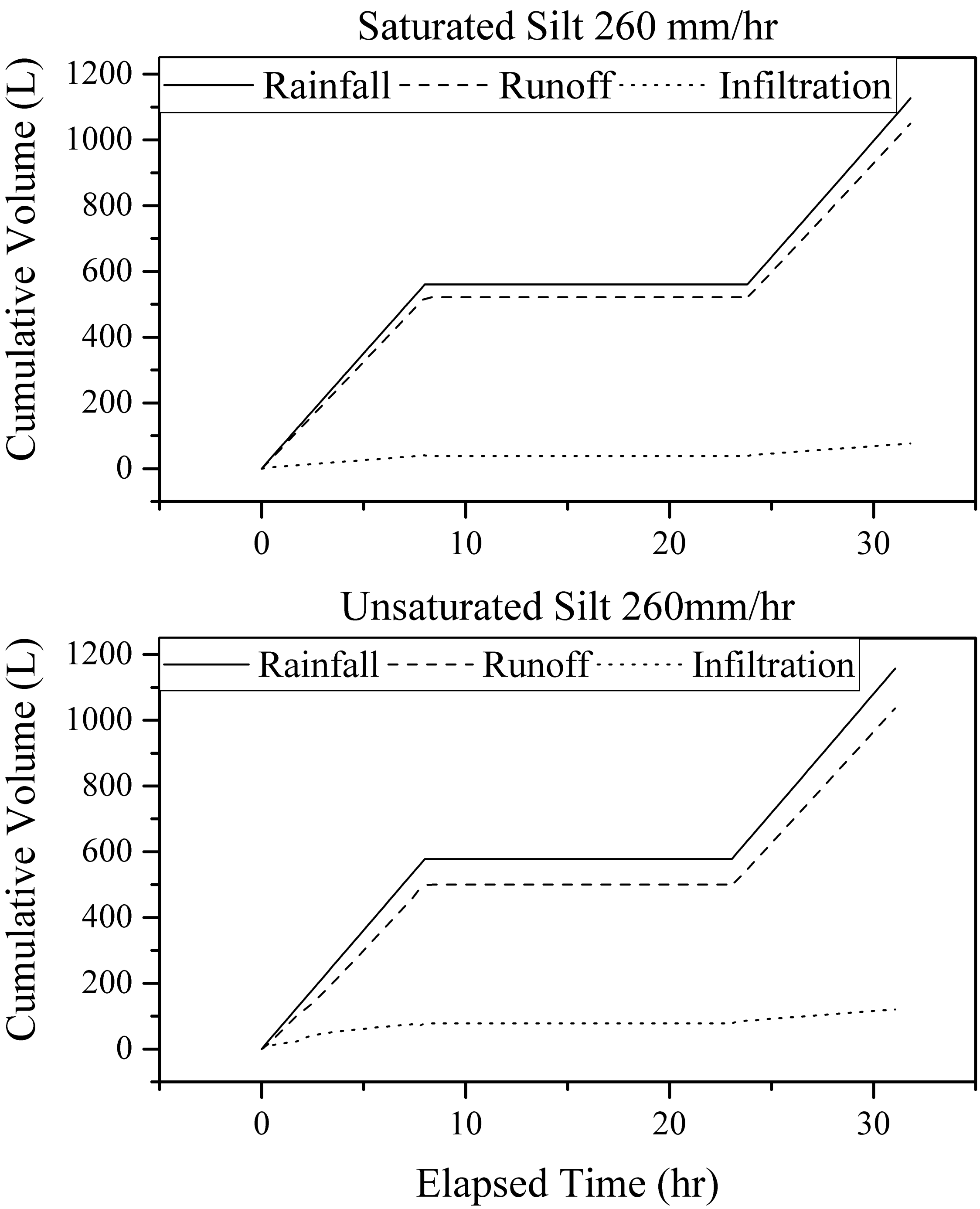

Figure 5.11 Measured cumulative volumes of water balance components for saturated (top) and unsaturated (bottom) silt profiles at 260 mm/hr applied rainfall intensity.

5.3.1.2. Rates

The rates of water balance components with time are presented for the first 8 hours of testing to highlight the subtle changes in data. Variation in the rate of precipitation and runoff with time were recorded every 15 minutes for each scenario. Infiltration rates were determined based on the infiltration volume and time increment. Results for the saturated and unsaturated silt profiles contrasted on the same figure are presented in Figures 5.12 through 5.17.

Results of the saturated silt profiles show that infiltration rate remained fundamentally unaffected as time progressed during each test. This observation remains valid regardless of the applied rainfall intensity. This implies that a certain soil property is controlling the infiltration rate in the saturated profiles – suggestively, the saturated hydraulic conductivity of the soil as per Darcy's law.

The saturated hydraulic conductivity of the silt determined via the falling head tests for Devon silt was in the order of 10^{-8} m/s and varied within half an order of magnitude depending on the dry density of the sample. The constant discharge was measured at the toe of the flume averaging 10^{-7} m^3/s (i.e., $4x10^{-7}$ m/s) roughly matching the saturated hydraulic conductivity of the soil. The small discrepancy can be justified by the density of the profile. Variation in the bulk dry density of the soil can cause up to an order of magnitude difference in measured hydraulic conductivity (Andrade 1971 and Osunbitan et al. 2005).

Like the infiltration rate, the runoff rate remained relatively constant throughout each test. Nonetheless, higher applied rainfall intensities increased the runoff rate accordingly. Hence, it can be inferred that the runoff rates in saturated profiles are primarily governed by both the applied rainfall intensity and the saturated hydraulic conductivity of the soil.

In the case of unsaturated silt profiles, initially, the entire amount of precipitation infiltrated into the soil profile with zero runoff. As time progressed, runoff was initiated; the rate of runoff increased, and the rate of infiltration decreased non-linearly with time. The time until runoff was generated decreased as higher rainfall intensities were applied.

The observed infiltration trends were consistent with the notion of infiltration capacity function first introduced by Horton (1939), and summarized by Stone et al. (1996) as follows:

1. After a rainfall begins, infiltration capacity is at its maximum, and the potential infiltration rate is greater than the rainfall rate.

2. However, the actual infiltration rate is equal to rainfall rate, since the water can only enter the soil at the application rate.

3. At a certain point in time referred to as *the time to ponding*, the water begins to pond, and the excess water overflows accordingly.

This pattern was observed in all cases regardless of the applied rainfall intensity with one exception. A malfunction in the runoff measurement regime in the case of rainfall intensity of 260 mm/hr caused two anomalies in the corresponding infiltration trend as seen in Figure 5.17. As the applied rainfall intensity increased, the rate of runoff followed suit. This collectively suggests that the runoff rate in the unsaturated profiles is primarily governed by the rainfall intensity and the infiltration capacity of the soil.

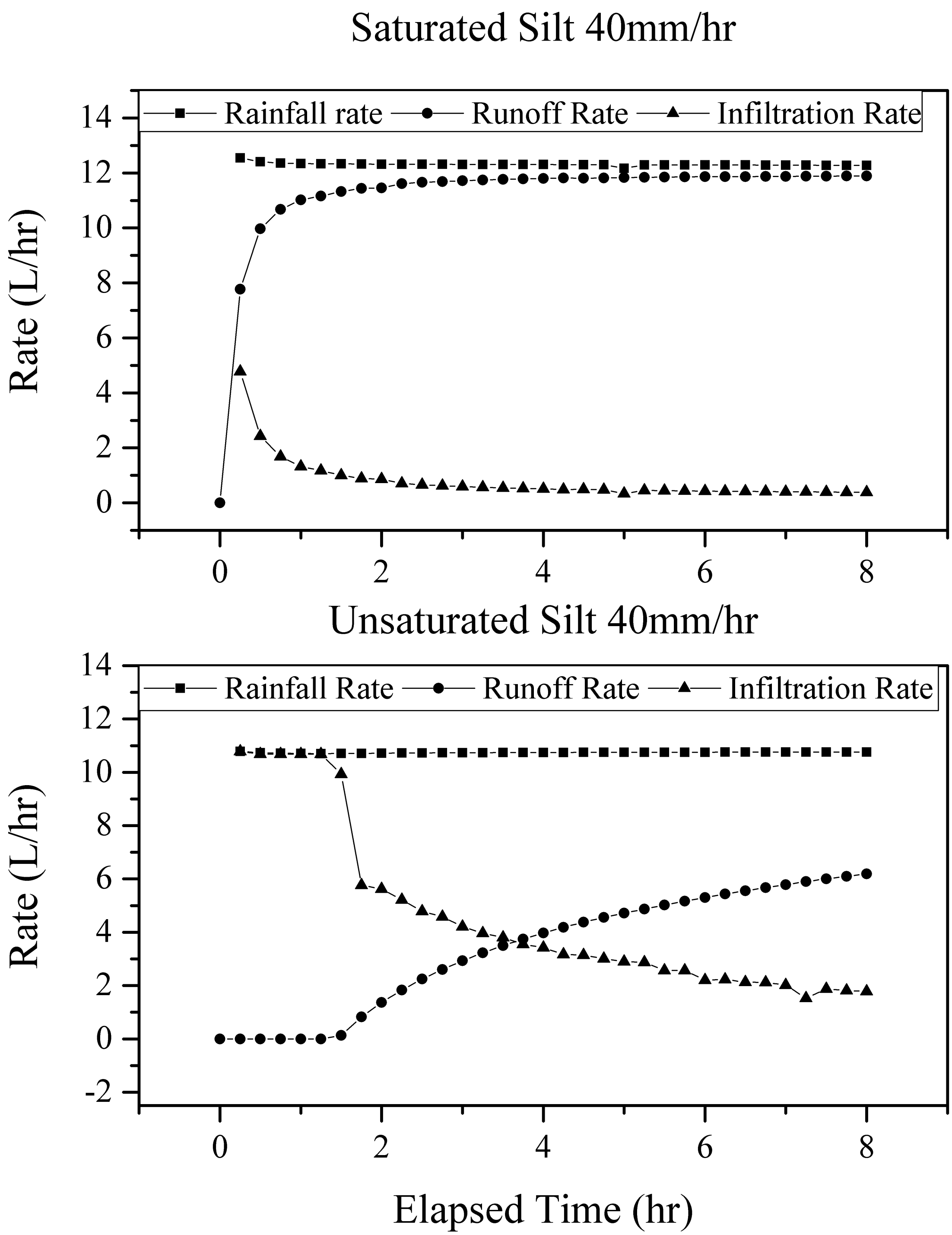

Figure 5.12 Measured rates of water balance components for saturated (top) and unsaturated (bottom) silt profiles at 40 mm/hr applied rainfall intensity.

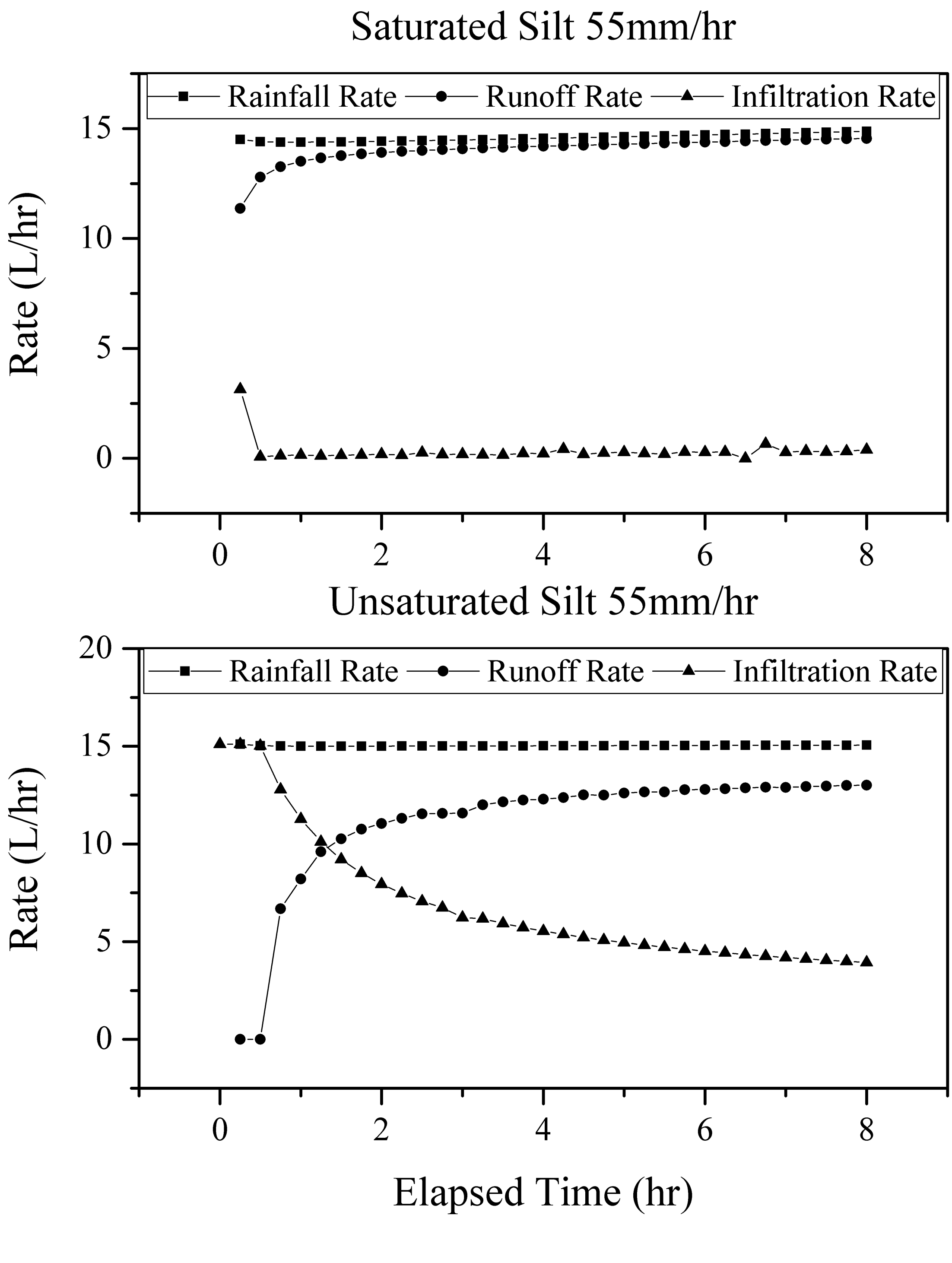

Figure 5.13 Measured rates of water balance components for saturated (top) and unsaturated (bottom) silt profiles at 55 mm/hr applied rainfall intensity.

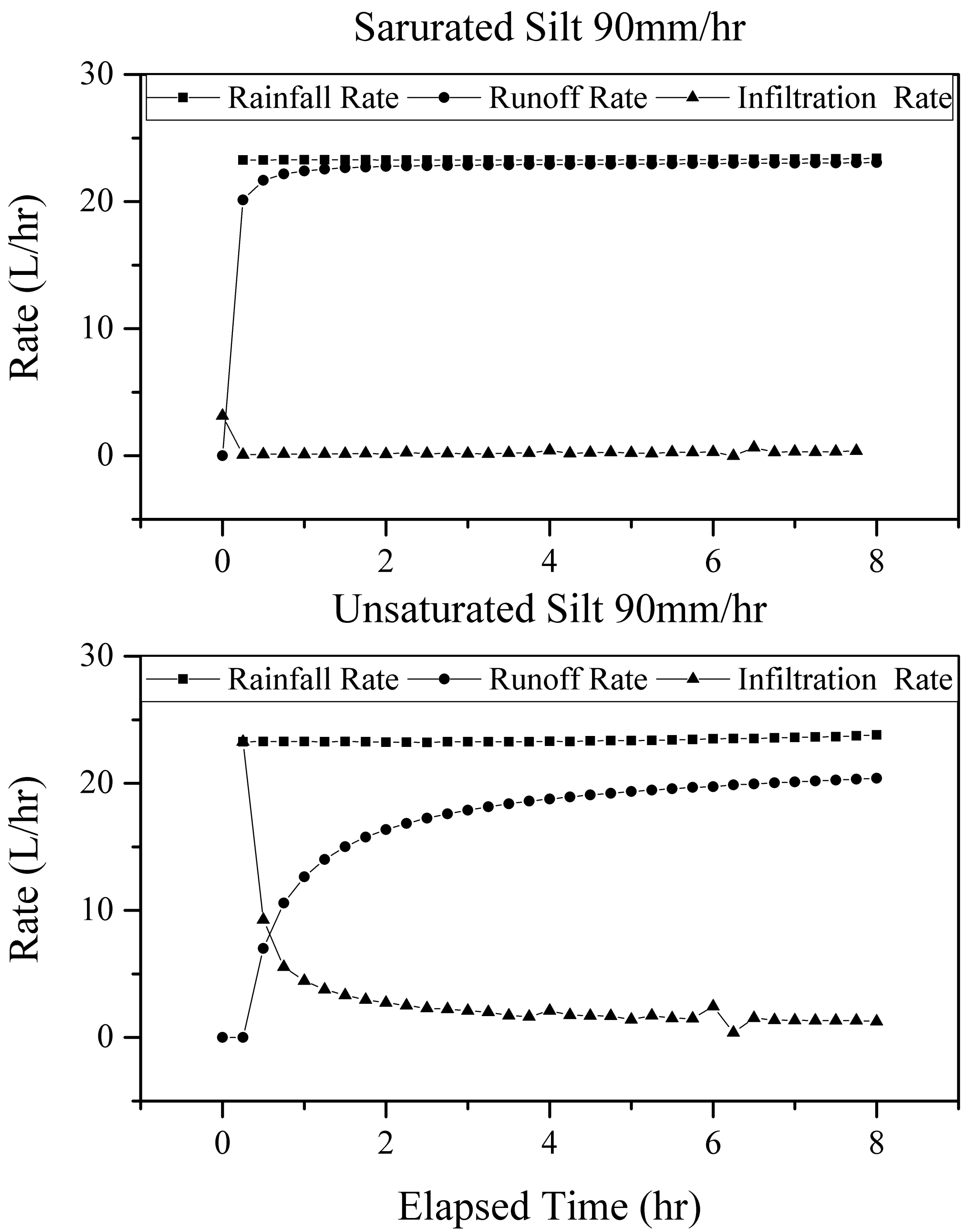

Figure 5.14 Measured rates of water balance components for saturated (top) and unsaturated (bottom) silt profiles at 90 mm/hr applied rainfall intensity.

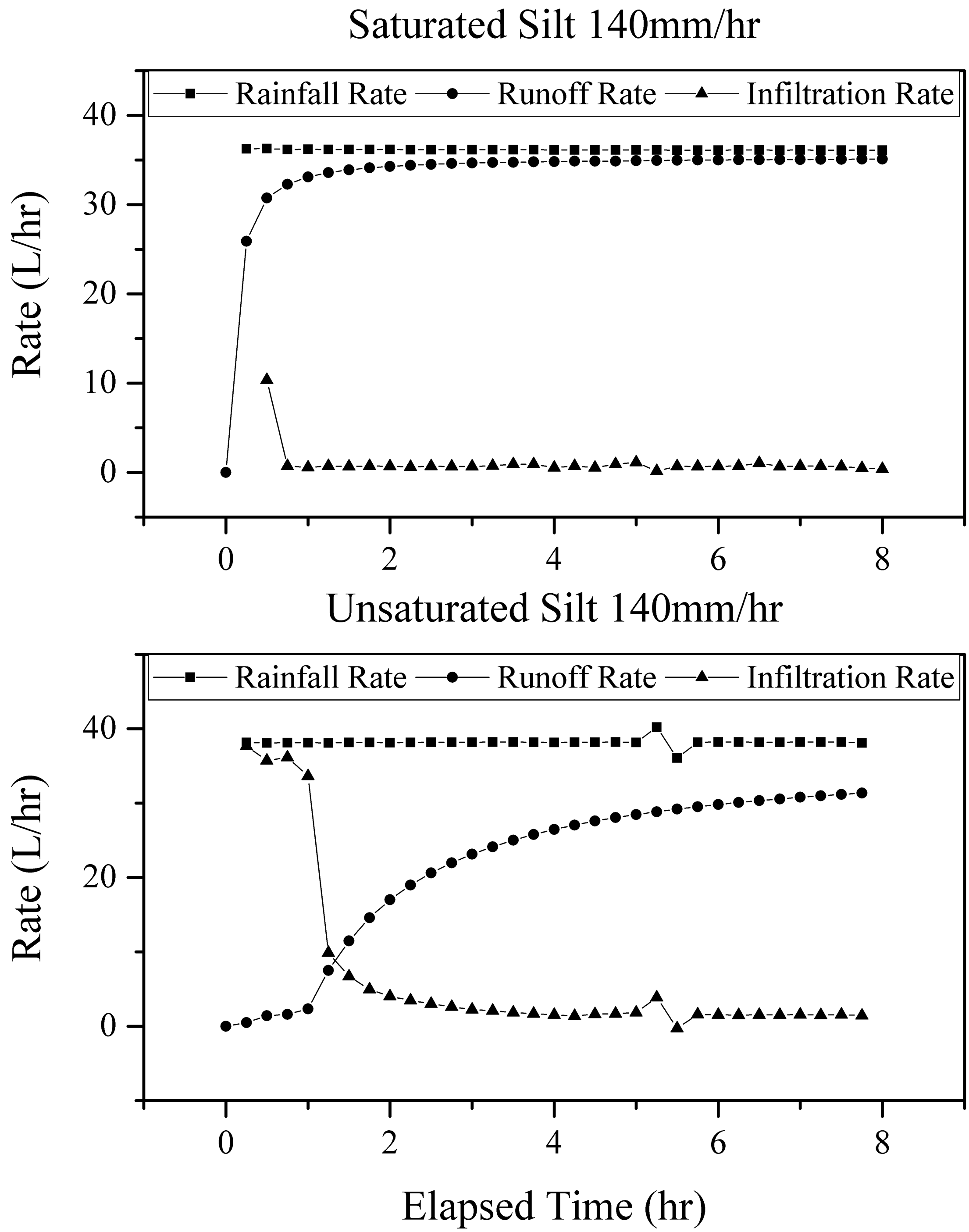

Figure 5.15 Measured rates of water balance components for saturated (top) and unsaturated (bottom) silt profiles at 140 mm/hr applied rainfall intensity.

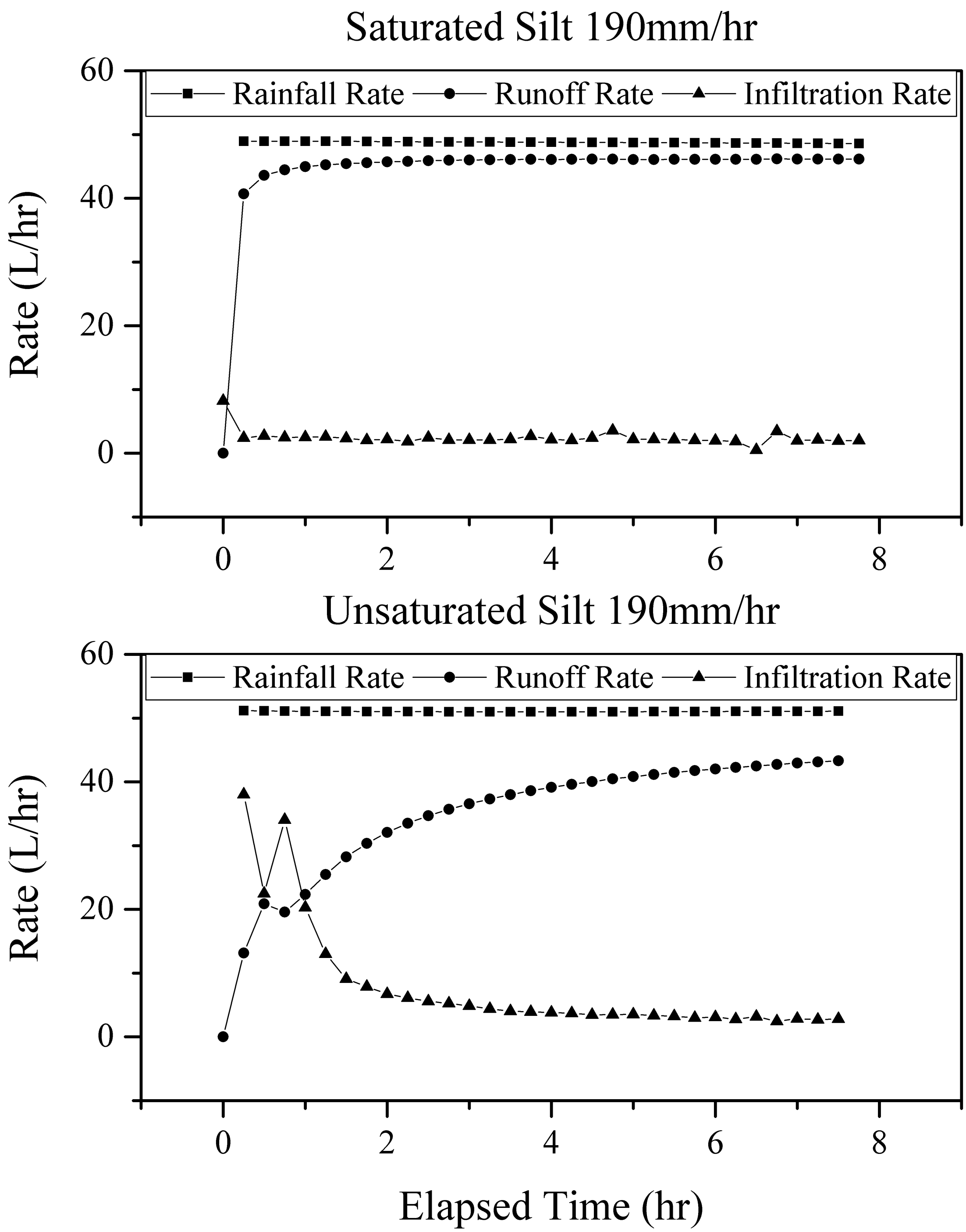

Figure 5.16 Measured rates of water balance components for saturated (top) and unsaturated (bottom) silt profiles at 190 mm/hr applied rainfall intensity.

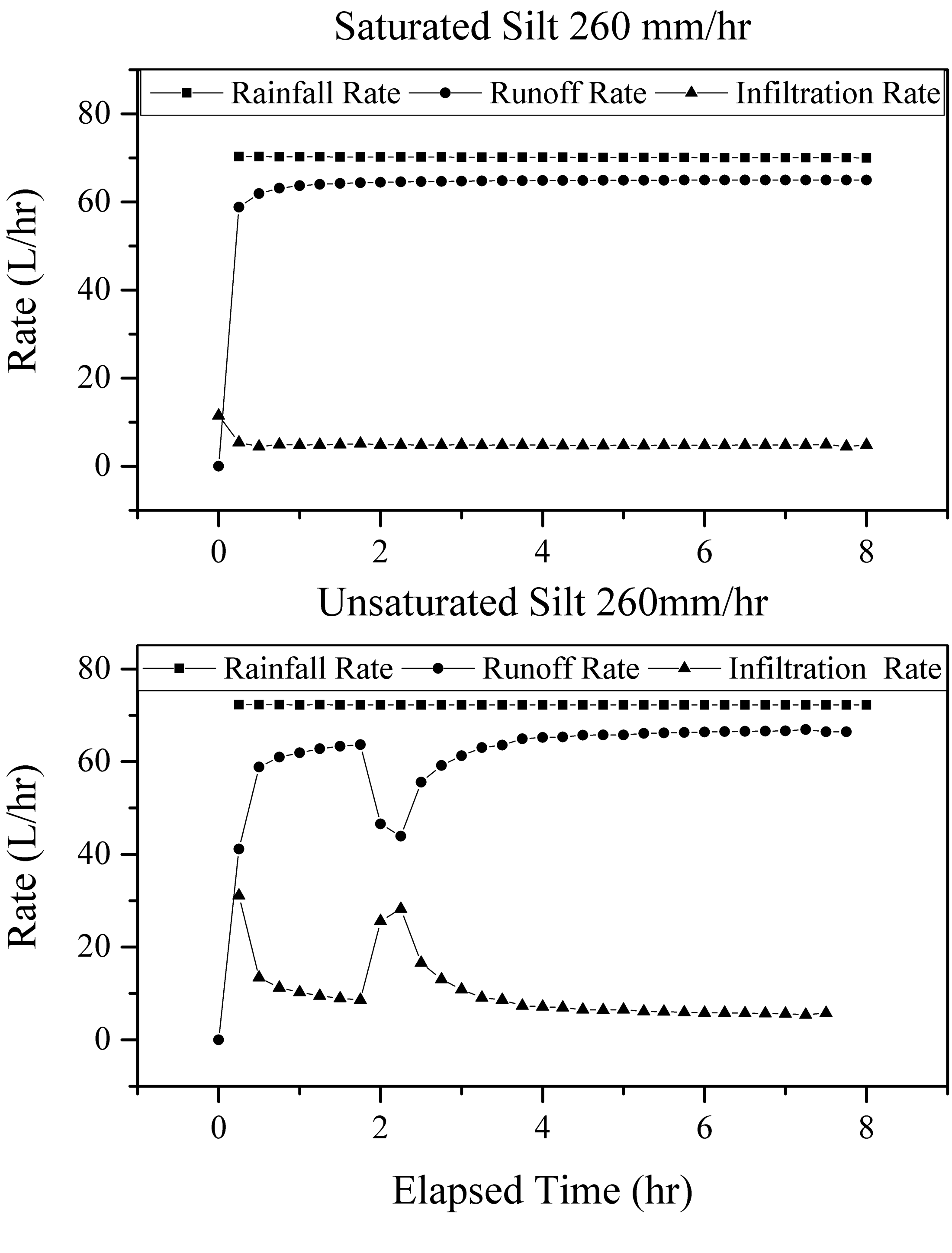

Figure 5.17Measured rates of water balance components for saturated (top) and unsaturated (bottom) silt profiles at 260 mm/hr applied rainfall intensity.

5.3.1.3. Volumetric Water Content

Twelve Time Domain Reflectometry (TDR) probes were installed at two elevations within the silt profiles: the top TDR group was located at a depth of 75 mm from the surface, and the bottom TDR group was located at a depth of 225 mm from the surface as described in 4.2.5. The typically measured changes in the volumetric water content in unsaturated silt profiles are shown in Figure 5.18. The following zones can be identified relative to the change in applied rainfall:

- Zone 1 exhibits an increase in volumetric water content corresponding to rainfall application.
- Zone 2 shows a period of unchanged volumetric water content; no testing took place overnight.
- Zone 3 exhibits a further increase in volumetric water content as rainfall is applied to the surface.
- Zone 4 exhibits no change in volumetric water content, and no rainfall is applied.
- Zone 5 exhibits a decrease in volumetric water content due to desaturation at the top of the profile.
- Zone 6 no further change in volumetric water content is evident. No rainfall was applied.
- Zone 7 exhibits an increase in volumetric water content. Rainfall was applied.
- Zone 8 exhibits no change in volumetric water content despite rainfall application.

Overall, the results suggest that for the unsaturated silt profiles, TDR probes, embedded at the same elevation, obtained water content readings approximately at the same time for each test regardless of the applied rainfall intensity. This observation confirmed the uniform rate of water flow through each profile.

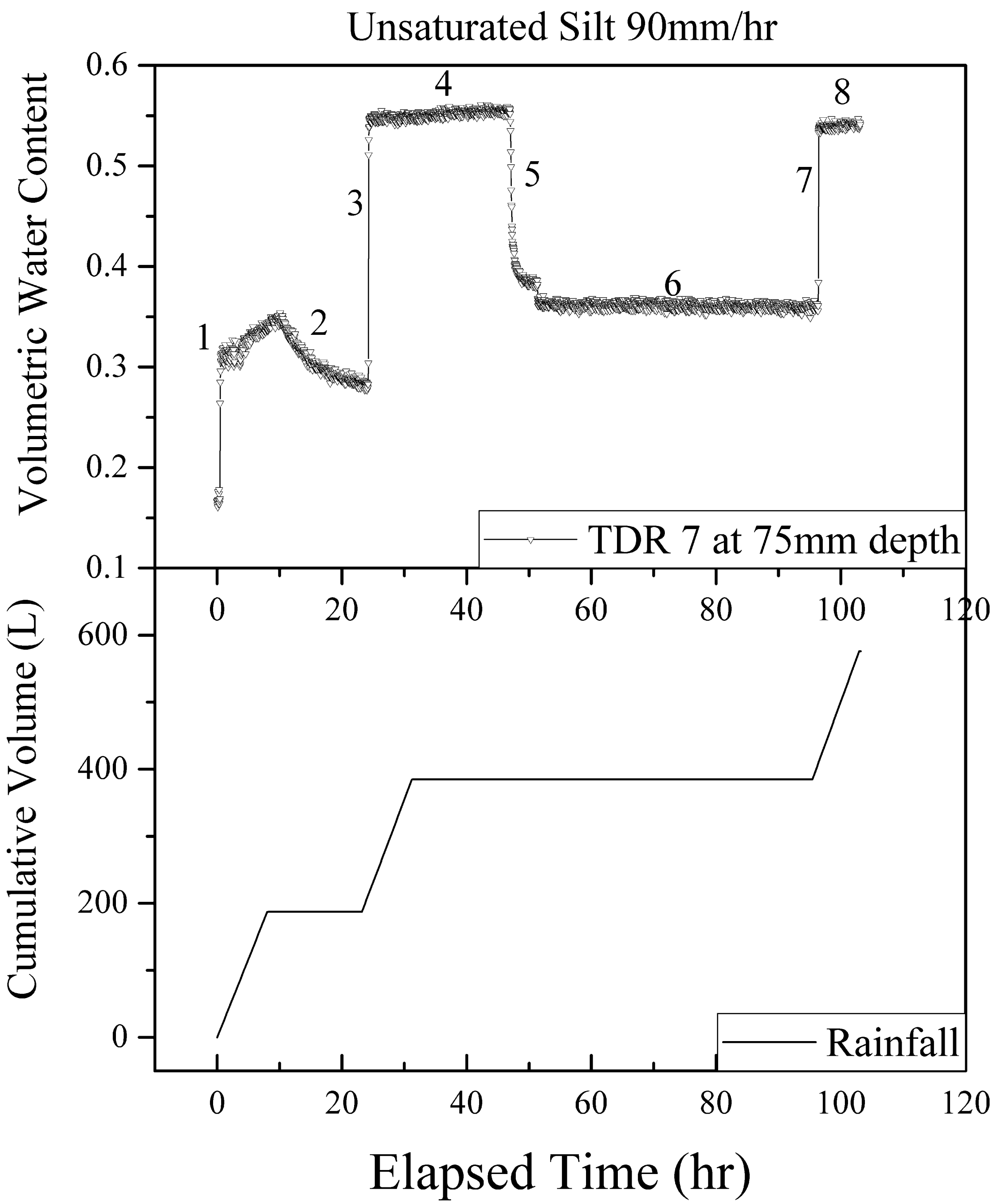

Figure 5.18 Typical variation in volumetric water content profiles in the unsaturated silt profile at 90 mm/hr intensity (top) and corresponding applied rainfall volumes (bottom).

5.3.1.4. Matric Suction

Four tensiometers were installed at two elevations within the soil profiles as described in Section 4.2.5. The top tensiometers were embedded 75 mm deep, and the bottom tensiometers were embedded 225 mm deep. The typically measured changes in the matric suction values with time in unsaturated silt profiles are shown in Figure 5.19. The results exhibit the following:

- All tensiometers start at matric suction around 80-85 kPa corresponding to dry profiles.

- A sharp decrease in matric suction is noticed as soon as the waterfront reaches the tensiometer instrument.

- On average, the time elapsed until the upper tensiometer (i.e., tensiometers located at z = 75 mm deep) started reading a decrease in (u_a-u_w) around two hours after the test commenced.

- The time elapsed until the upper tensiometer (i.e., tensiometers located at z = 225mm deep) started reading a decrease in (u_a-u_w) around four hours after the test commenced.

Overall, tensiometers readings were consistent for each profile regardless of applied rainfall intensity. The instantaneous change in matric suction was recorded as soon as waterfront reached the instruments as seen from time-lapse photography discussed in Section 5.3.4 in more details.

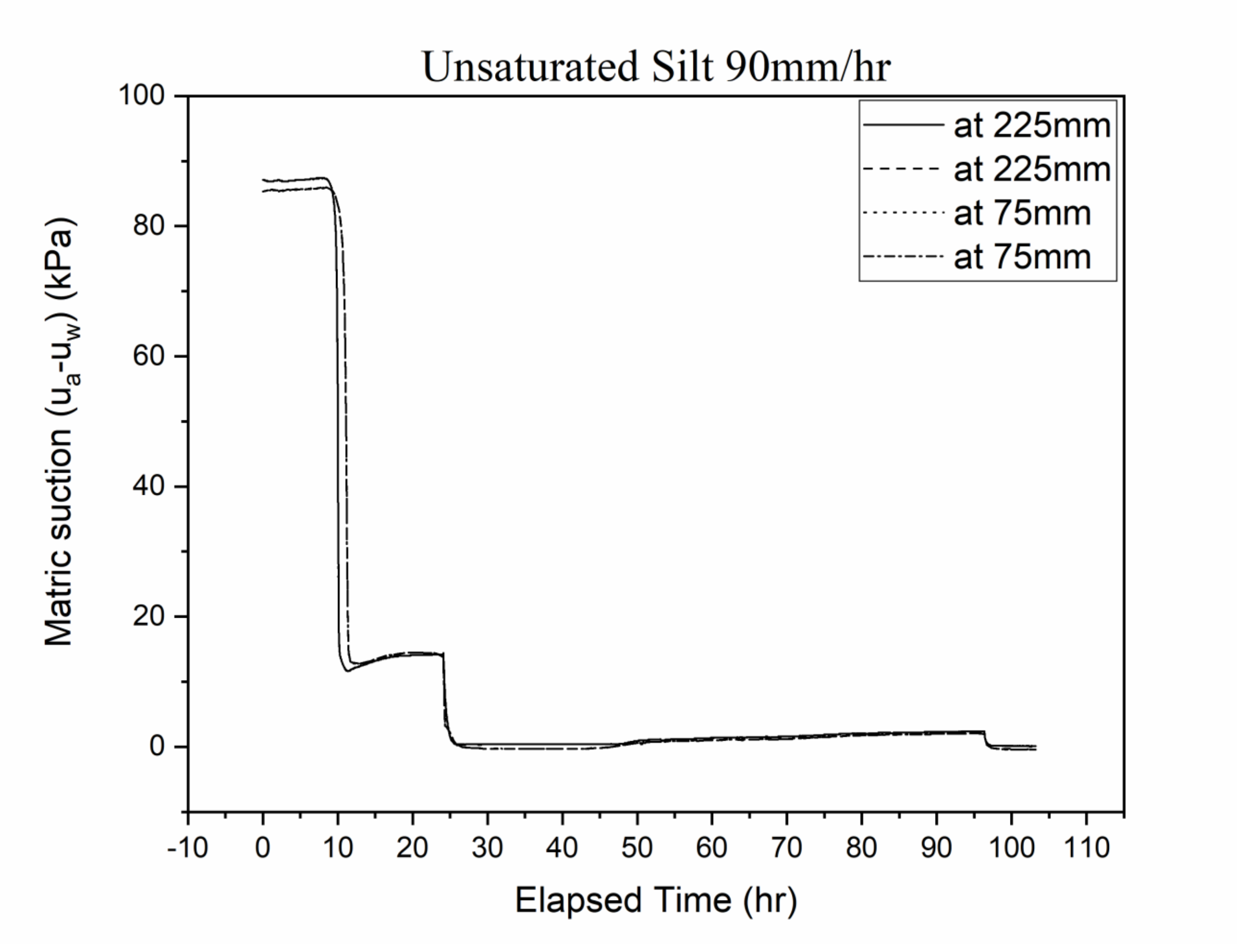

Figure 5.19 Typical variation in matric suction with time in the unsaturated silt profiles.

5.3.2. Capillary Barrier Profiles

A multi-layer profile of Devon silt overlaying tailings beach sand represented the capillary barrier profiles. Each profile comprised each soil of approximately equal thickness as seen in Figure 5.20. For unsaturated capillary barrier profiles, the soils were deposited in an oven-dried state, as described in Section 4.4. Saturated capillary barrier profiles were derived from unsaturated profiles and were allowed to saturate fully and reach equilibrium prior to testing.

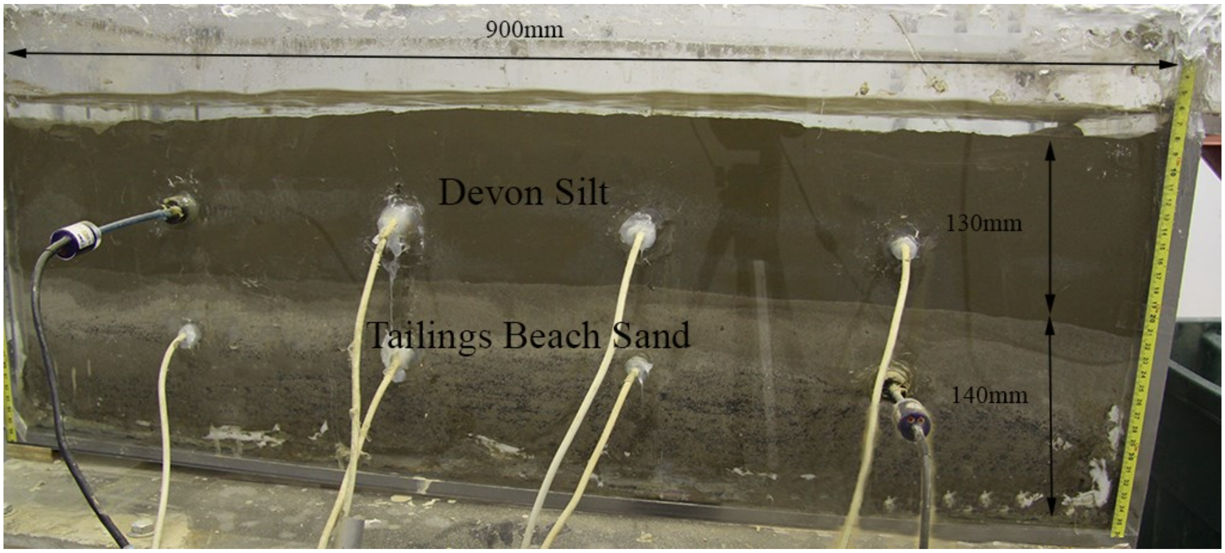

Figure 5.20 Typical dimensions of the capillary barrier profiles.

5.3.2.1. Volumes

Cumulative volumes of water balance components (i.e., rainfall, runoff, and infiltration) were plotted with time for each experiment, and are presented in Figures 5.21 through 5.26. Rainfall volumes measurements were obtained from the flowmeter mounted on the spraying system. Runoff volumes measurements were collected from the flume's runoff spout and continuously measured using an electronic scale. Infiltration volumes were determined by conducting a water balance as described in Section 4.5.

In all cases, about 85% to 96% of the entire applied rainfall volume eventually converted into runoff in the saturated capillary barrier profiles. The cumulative runoff volume increased with time in accord with the applied rainfall cumulative volume. An increase in the applied rainfall intensities produced a corresponding increase in both rainfall and runoff volumes; yet, infiltration volumes remained unaffected.

In contrast to the unsaturated silt profiles, higher percentages of runoff and, subsequently, less infiltration were observed in the unsaturated capillary barrier profiles when subjected to the same applied rainfall intensity. The unsaturated capillary barrier profiles permitted significantly less rainwater to infiltrate into the profile, especially at lower rainfall intensities.

Presentation of Results

As observed in the unsaturated silt profiles, infiltration overlapped with rainfall at the beginning of the tests when the entire amount of applied rain infiltrated into the profiles. The patterns observed in the first two hours of testing are provided in Appendix II. The following sequence of events was observed in each rainfall intensity scenario:

1. At the beginning of each test, no runoff was generated, and the entire applied rainfall volume infiltrated into the profile.

2. At a certain point in time referred to as *the time to ponding/time to runoff*, the water began to pond, and the excess water overflow in the form of surface runoff.

3. The time required until runoff was generated decreased as the applied rainfall intensity increased, as has been observed in the unsaturated silt profiles.

4. Compared to unsaturated silt profiles, unsaturated capillary barrier profile required less time until runoff was generated except for the profile corresponding to 40 mm/hr intensity where longer time to runoff was detected compared to unsaturated silt profile at the same intensity.

5. The time until runoff onset for each profile is discussed in further details in Section 5.3.3.

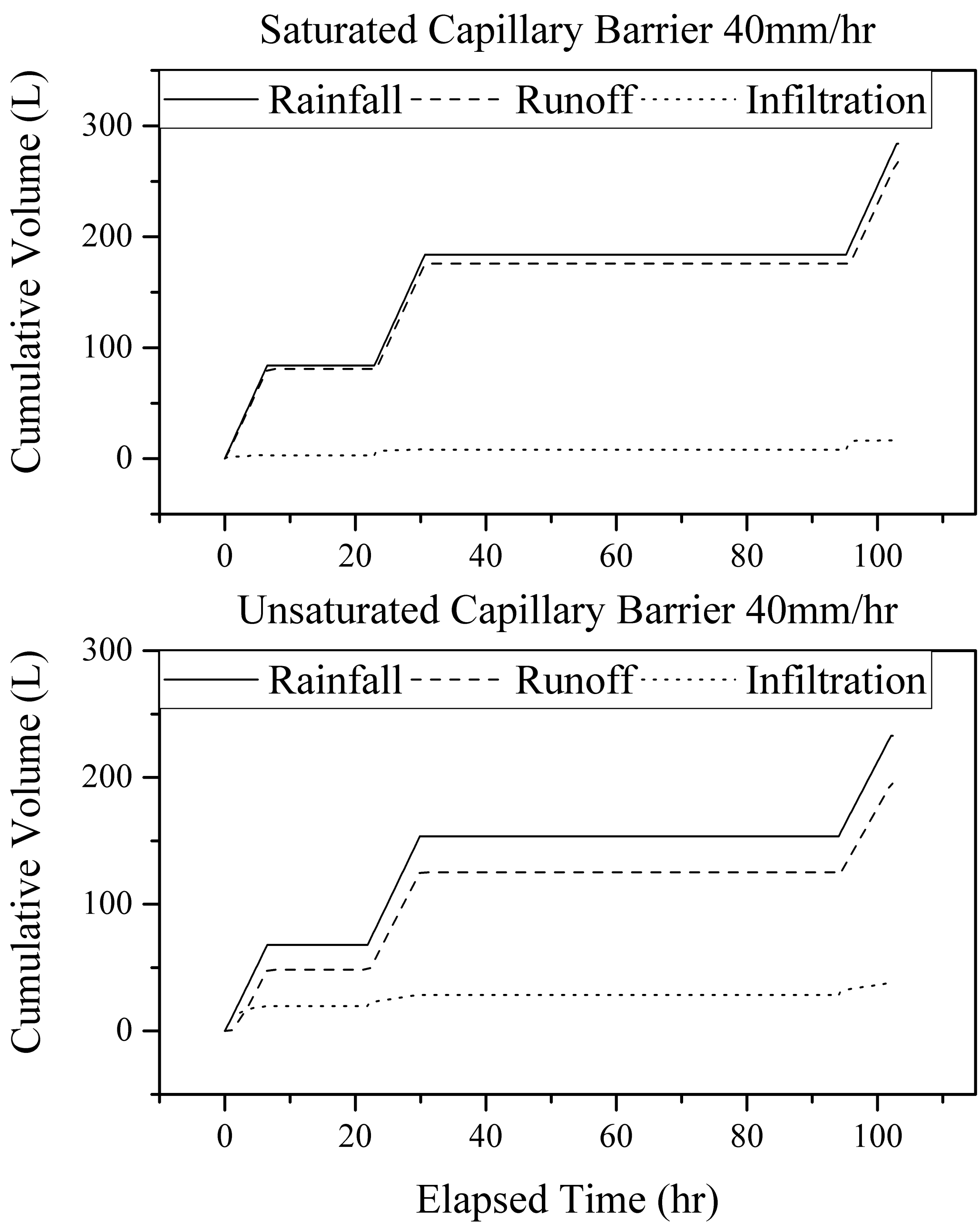

Figure 5.21 Measured cumulative volumes of water balance components for saturated (top) and unsaturated (bottom) capillary barrier profiles at 40 mm/hr applied rainfall intensity.

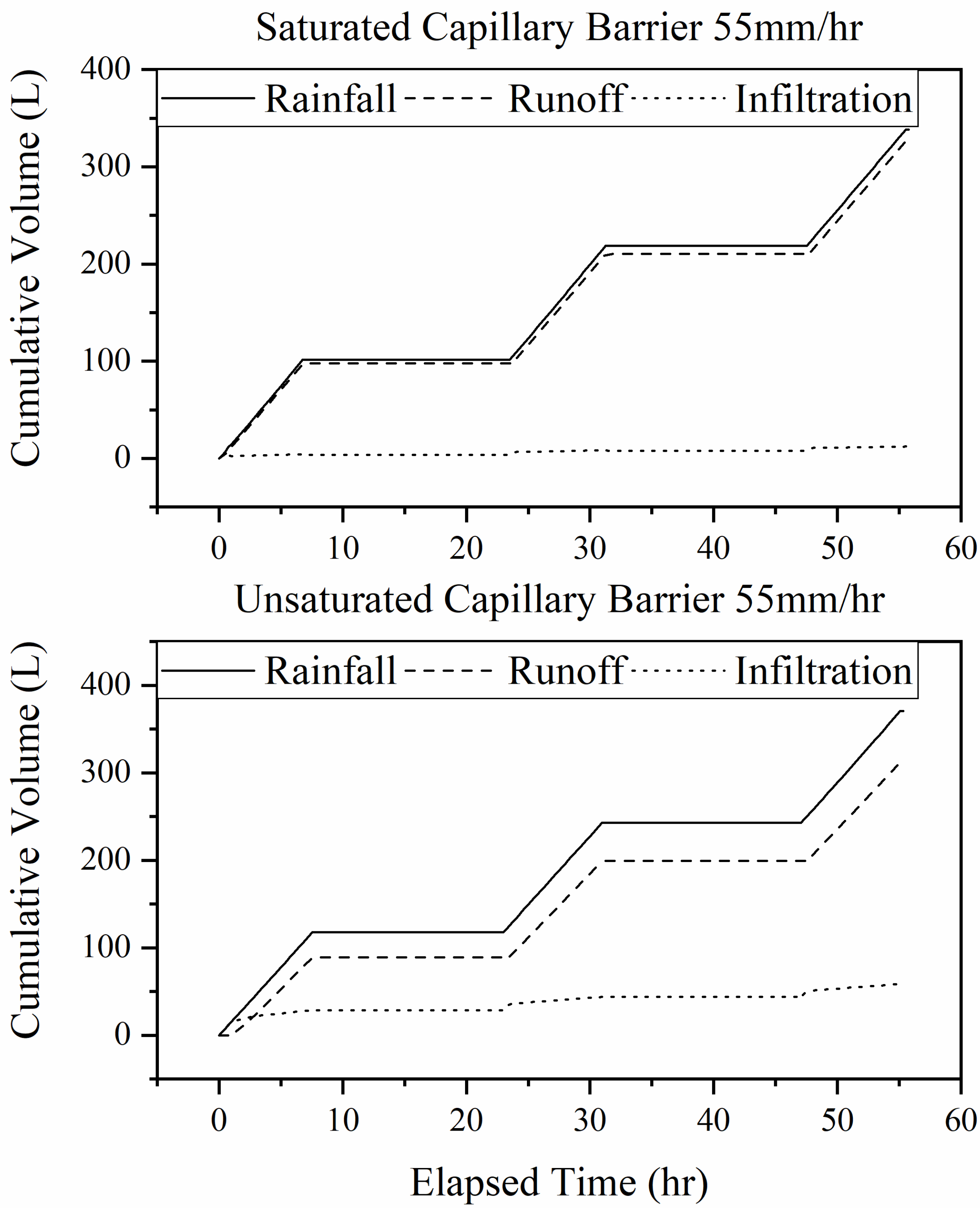

Figure 5.22 Measured cumulative volumes of water balance components for saturated (top) and unsaturated (bottom) capillary barrier profiles at 55 mm/hr applied rainfall intensity.

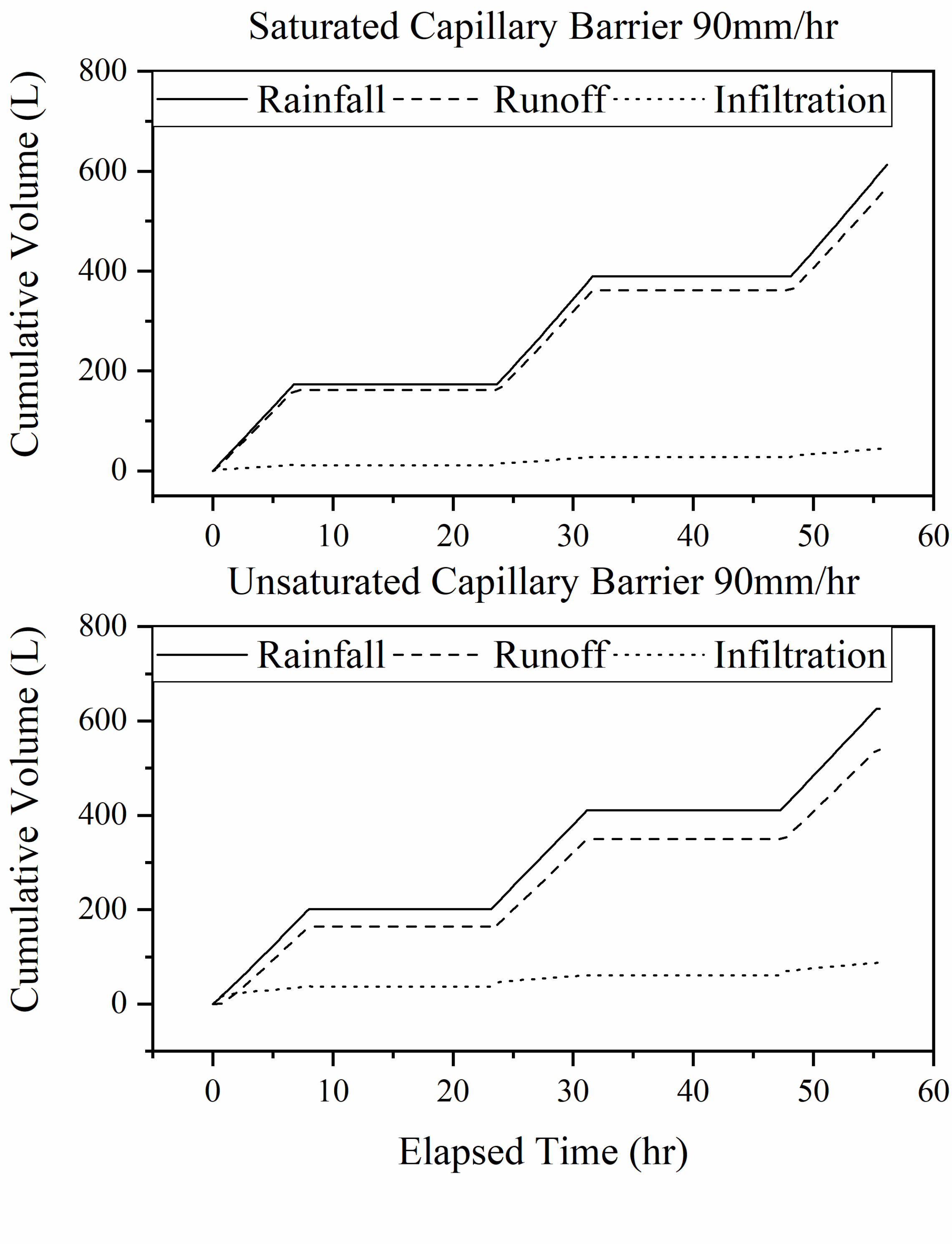

Figure 5.23 Measured cumulative volumes of water balance components for saturated (top) and unsaturated (bottom) capillary barrier profiles at 90 mm/hr applied rainfall intensity.

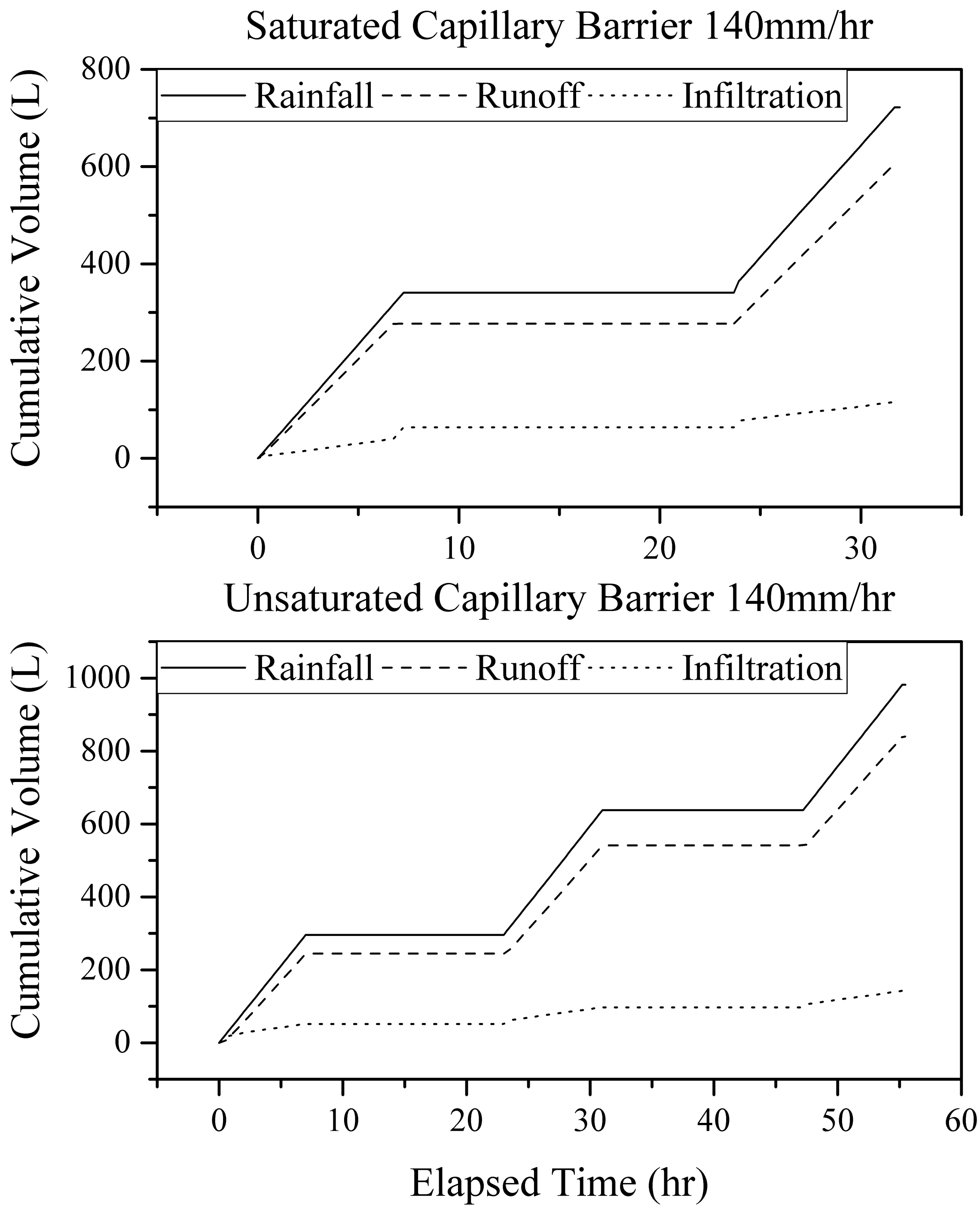

Figure 5.24 Measured cumulative volumes of water balance components for saturated (top) and unsaturated (bottom) capillary barrier profiles at 140 mm/hr applied rainfall intensity.

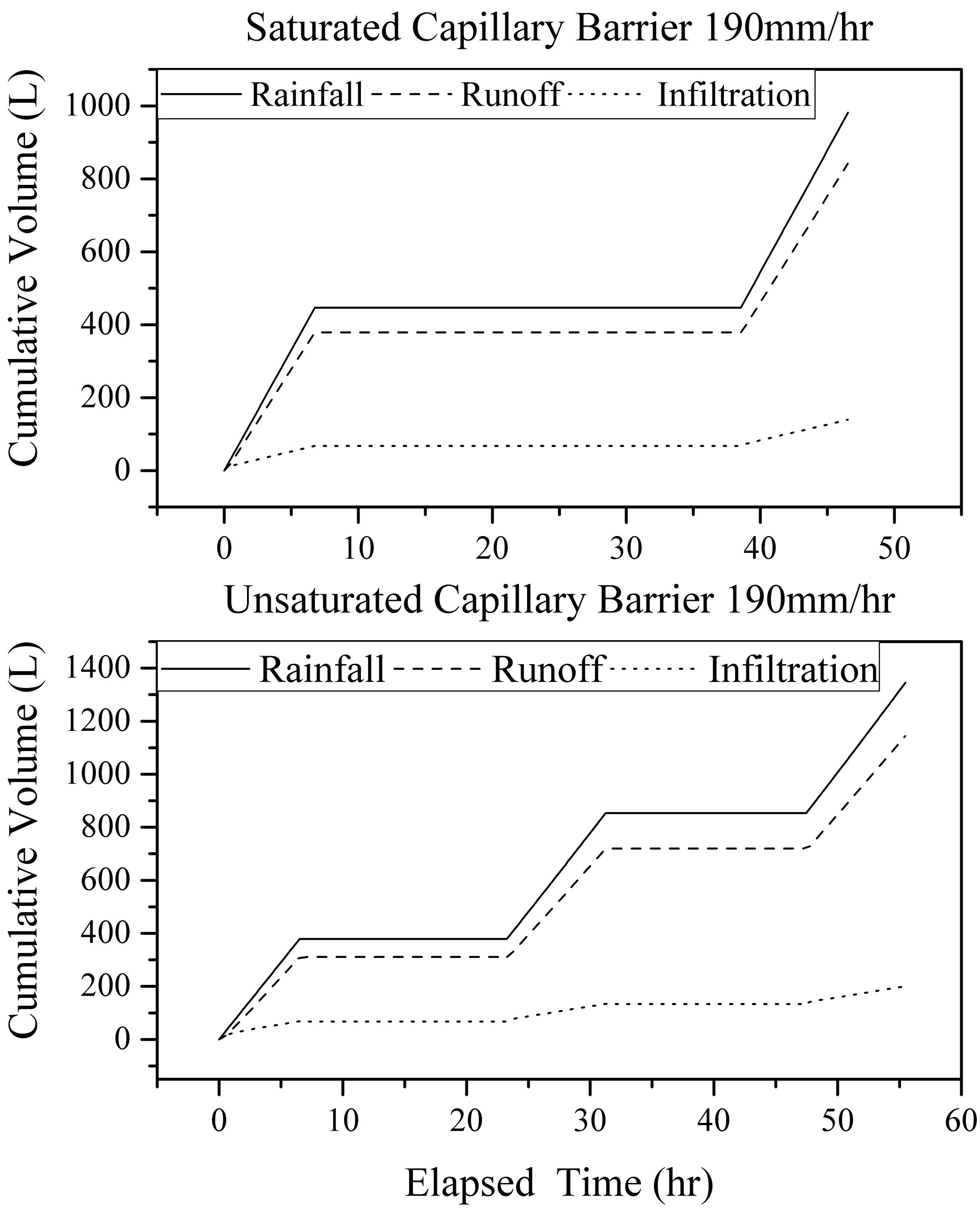

Figure 5.25 Measured cumulative volumes of water balance components for saturated (top) and unsaturated (bottom) capillary barrier profiles at 190 mm/hr applied rainfall intensity.

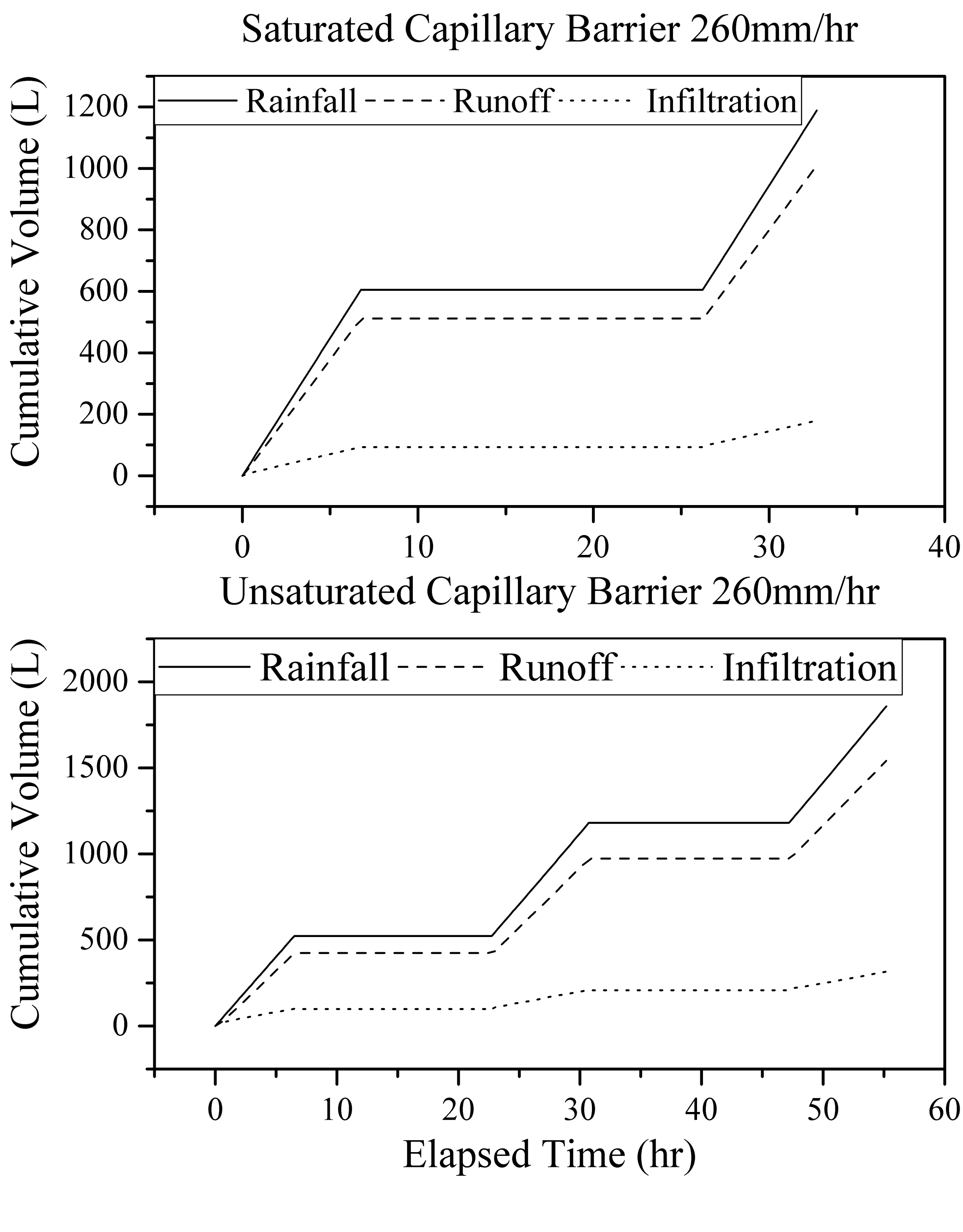

Figure 5.26 Measured cumulative volumes of water balance components for saturated (top) and unsaturated (bottom) capillary barrier profiles at 260 mm/hr applied rainfall intensity.

5.3.2.2. Rates

Changes in measured rates of rainfall, runoff, and infiltration with time for different applied rainfall intensities in the saturated capillary barrier profiles compared to the unsaturated counterparts are presented in Figures 5.27 through 5.32. The results show that both runoff and infiltration rates remained constant throughout each test in the saturated profiles regardless of the applied rainfall intensity.

Variations in the rate of water balance constituents with time for the unsaturated capillary barrier profiles exhibited the following characteristics:

1) Initially, the entire amount of precipitation infiltrates into the soil. Once runoff is generated, the rate of runoff increases and rate of infiltration decreases non-linearly with time to a constant value.

2) The unsaturated capillary barrier profiles approach a constant infiltration rate earlier compared to unsaturated silt profiles.

3) Lower infiltration rates observed in unsaturated capillary barrier profiles were more distinct when lower rainfall intensity was applied.

4) Infiltration was impeded at the layer interface between the sand and silt layers creating a capillary break as theorized in Section 3.3. The infiltration impedance was detected by time-lapse photography and discussed in full details in Section 5.3.4.3.

5) At higher applied rainfall intensities, slightly elevated infiltration rates were observed. This resulted from an improper filling of the profile causing water ponding at the top of the profile. The excess rainwater seemed to pond, and, therefore, impacted the apparent infiltration volumes and rates as discussed in more details in Section 6.2.2.

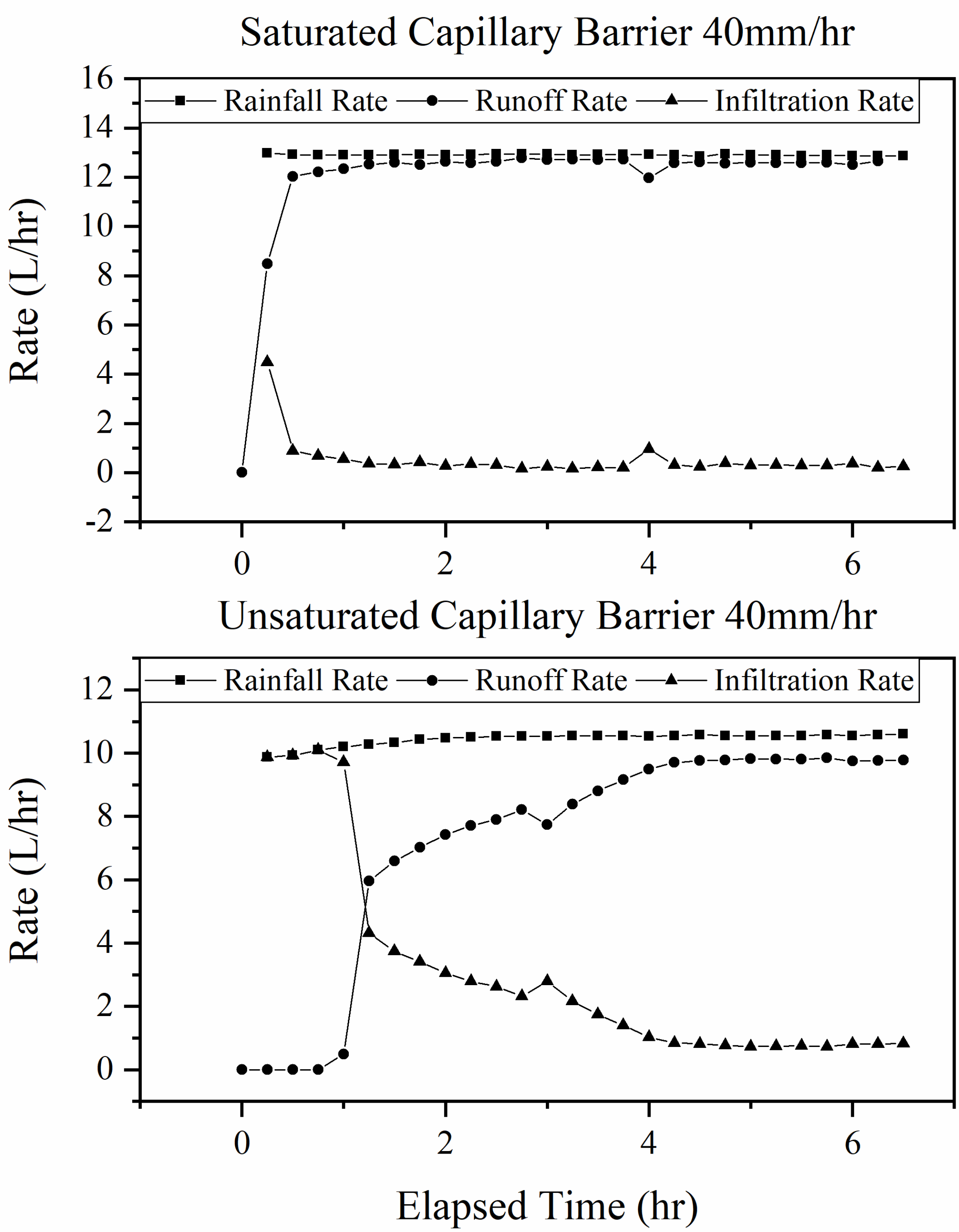

Figure 5.27 Measured rates of water balance components for saturated (top) and unsaturated (bottom) capillary barrier profiles at 40 mm/hr applied rainfall intensity.

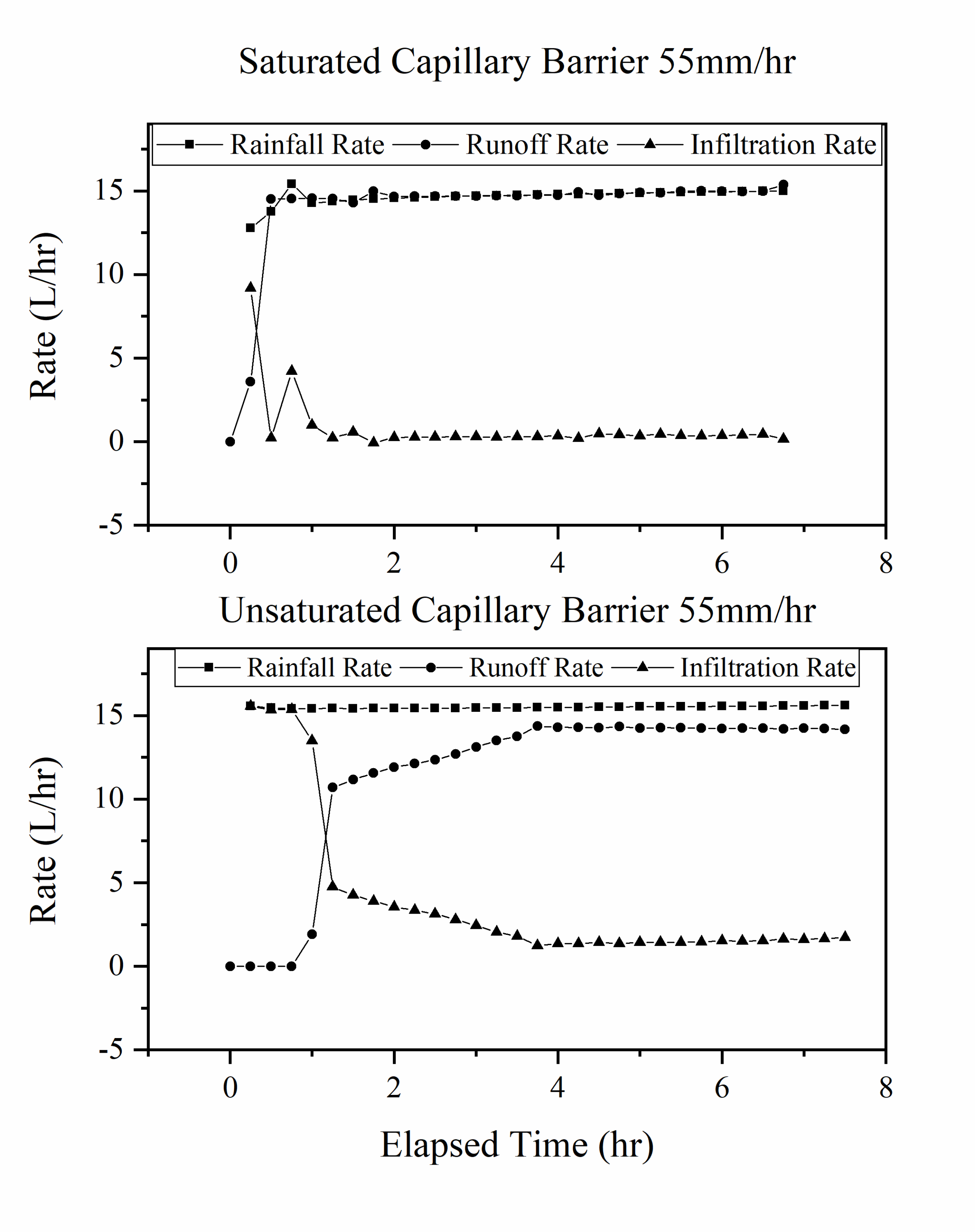

Figure 5.28 Measured rates of water balance components for saturated (top) and unsaturated (bottom) capillary barrier profiles at 55 mm/hr applied rainfall intensity.

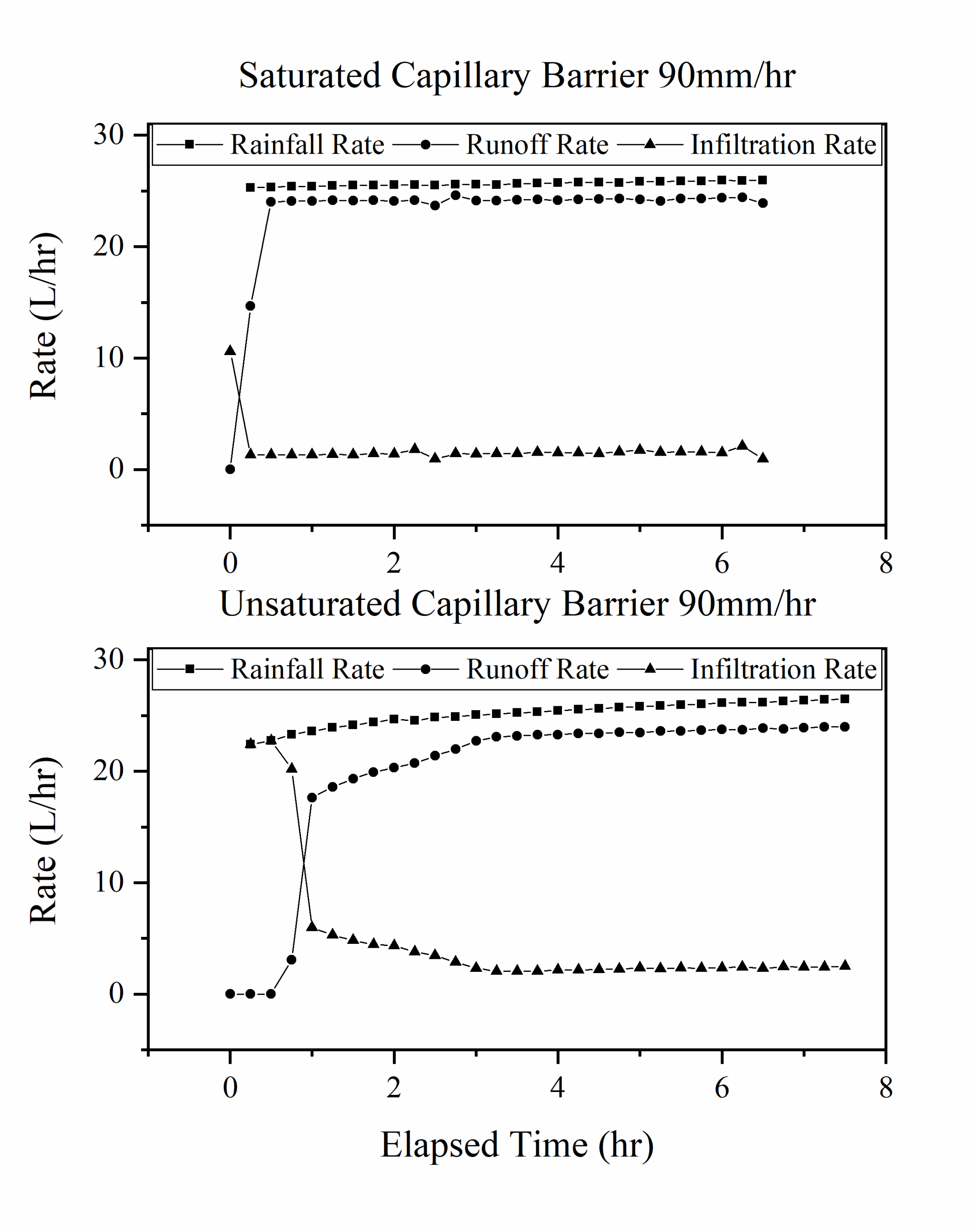

Figure 5.29 Measured rates of water balance components for saturated (top) and unsaturated (bottom) capillary barrier profiles at 90 mm/hr applied rainfall intensity.

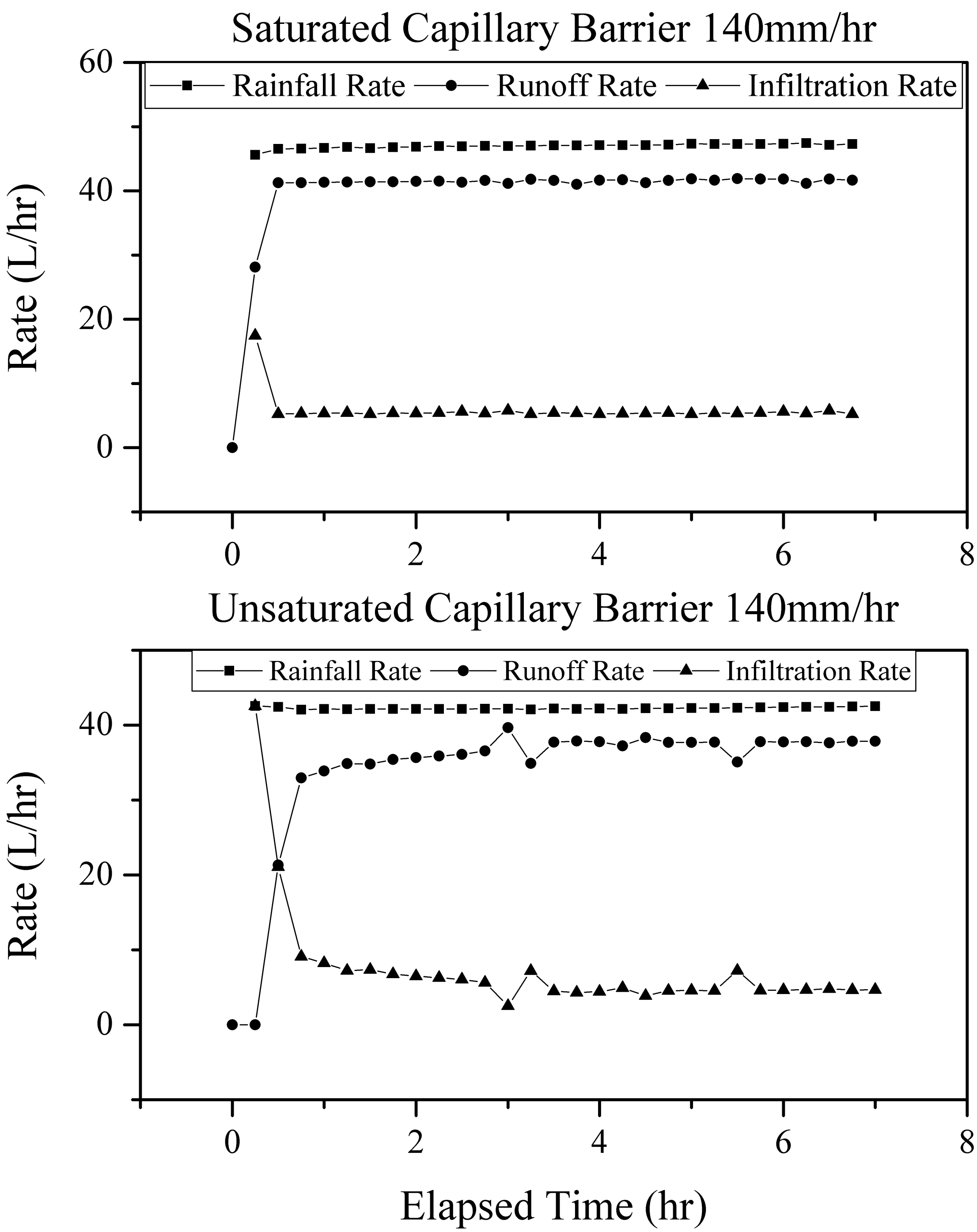

Figure 5.30 Measured rates of water balance components for saturated (top) and unsaturated (bottom) capillary barrier profiles at 140 mm/hr applied rainfall intensity.

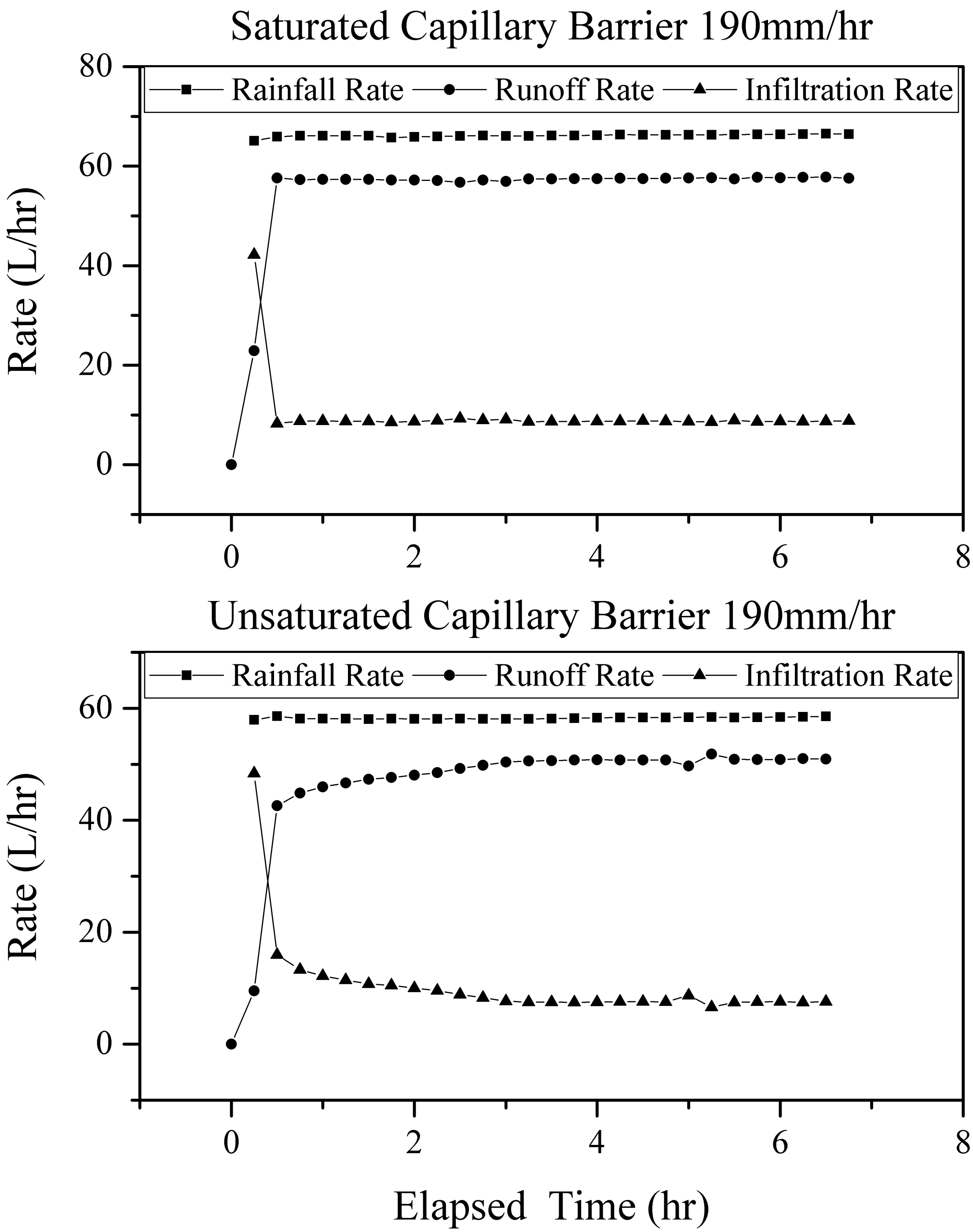

Figure 5.31 Measured rates of water balance components for saturated (top) and unsaturated (bottom) capillary barrier profiles at 190 mm/hr applied rainfall intensity.

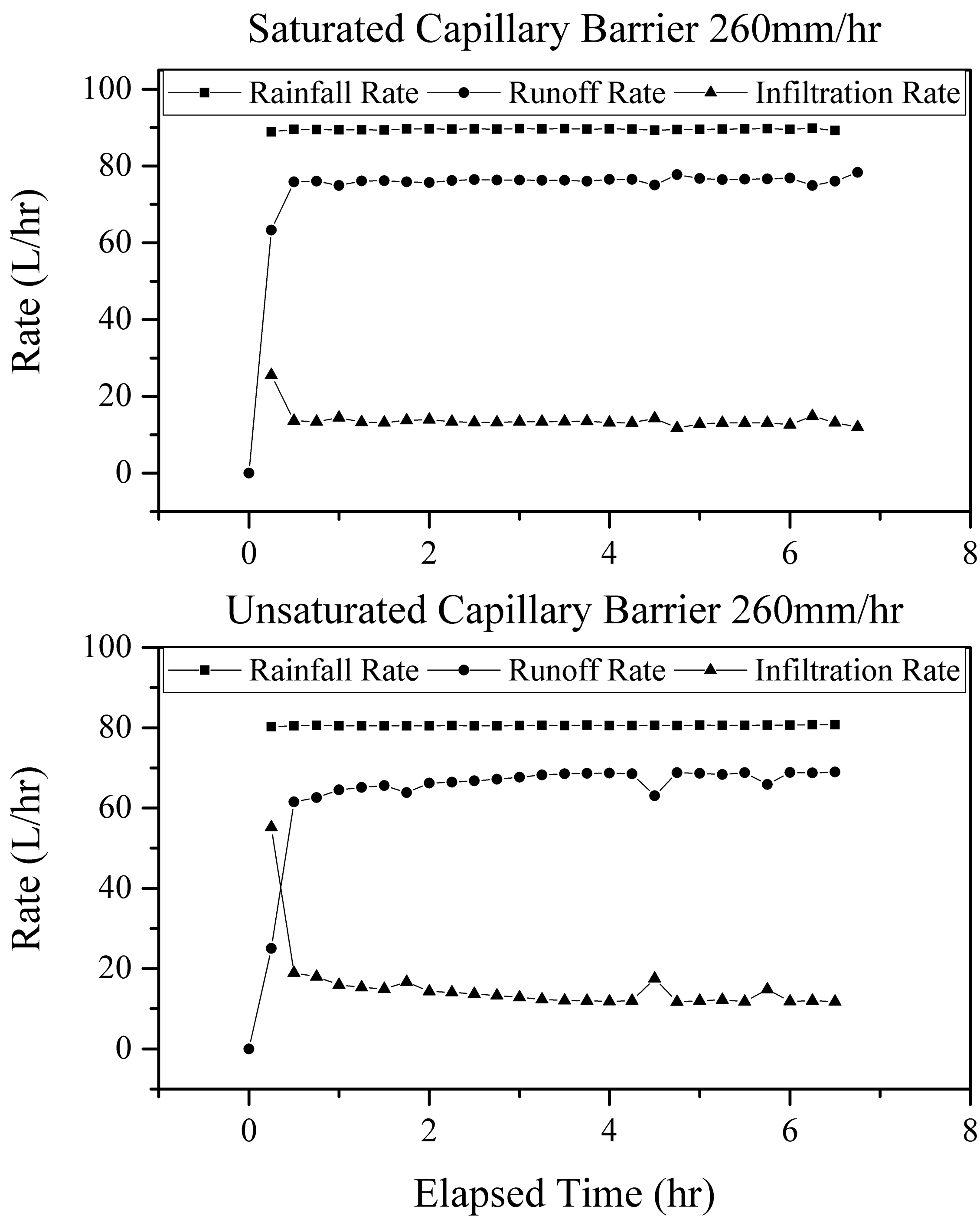

Figure 5.32 Measured rates of water balance components for saturated (top) and unsaturated (bottom) capillary barrier profiles at 260 mm/hr applied rainfall intensity.

5.3.2.3. Volumetric Water Content

Twelve TDR probes were installed at two elevations within the profiles as described in 4.2.5. TDR probes were distributed at two elevations within the capillary barrier profiles. The TDRs in the top layer (i.e., silt) were located at z = 75 mm from the surface. Similarly, TDRs in the sand layer were positioned at z = 225 mm from the surface. A typically measured change in volumetric water content with time is illustrated in Figure 5.33. Appendix III provides measured volumetric water content with time for all unsaturated silt and unsaturated capillary barrier profiles.

The changes in volumetric water content in the unsaturated capillary barrier profiles demonstrated the following features:

1. The time required for TDRs embedded in the sand layer to obtain water was approximately three times longer in unsaturated capillary barrier profiles compared to the unsaturated silt profiles subjected to the same applied rainfall intensity.

2. Lower saturated volumetric water content (vwc_{sat}) in the sand layer compared to the silt layer was noticed.

3. Reduced total water storage in the sand layer was observed in the capillary barrier profiles, comparable to that of silt profiles at the same elevation and rainfall intensity.

4. The capillary barrier profiles exhibited hydraulic impedance at the interface due to the contrast in hydraulic properties between the fine and coarse materials, thereby, limiting downward infiltration into the coarse layer as described in Section 3.3. This was further illustrated by tensiometers data discussed in section 5.3.3.2; time-lapse photographs are discussed in Section 5.3.3.3.

5. Phases observed in vwc changed with time in unsaturated silt profiles and were suppressed in the unsaturated capillary barrier profiles.

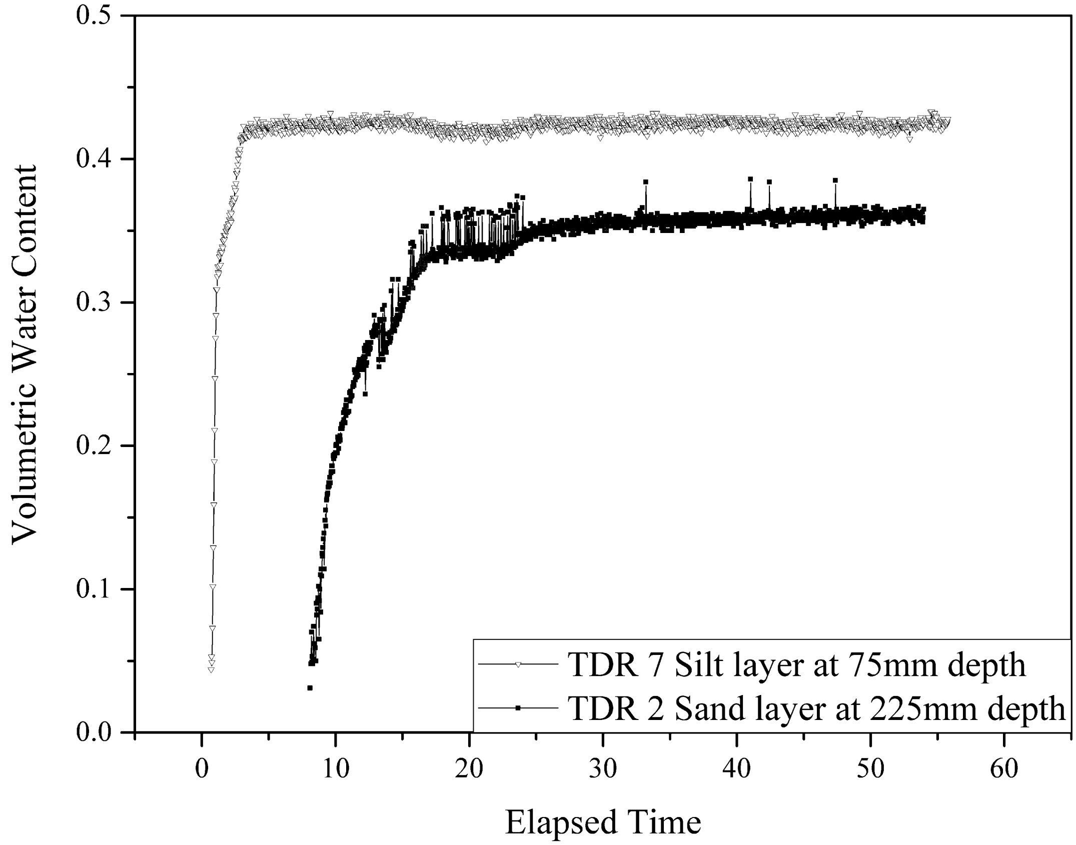

Figure 5.33 Typical variation in volumetric water content profiles in the unsaturated capillary barrier profiles.

5.3.2.4. Matric Suction

Four tensiometers were installed at two elevations within the capillary barrier profiles as described in Section 4.2.5. The typical variation in matric suction with time during the testing of the unsaturated capillary barrier profiles is shown in Figure 5.34. Appendix IV provides measured matric suction with time for all unsaturated silt and unsaturated capillary barrier profiles

The general trend of matric suction variation with time in the silt layer, and was comparable to the observed behaviour in unsaturated silt profiles. Nevertheless, tensiometers embedded in the sand layer displayed the capillary barrier effect very distinctly through the following characteristics:

1. The time required for the waterfront to propagate into the lower tensiometers was approximately half an order of magnitude longer in unsaturated capillary barrier profiles compared to the unsaturated silt profiles subjected to the same applied rainfall intensity. This remarkable time delay signifying the capillary break effect was systematically observed in all the capillary barrier profiles.

2. The matric suction profiles with time in the unsaturated capillary barrier profiles clearly reflect the time delay discussed above. The tensiometers embedded in the sand layer displayed a decrease in matric suction reading (i.e., waterfront reached the tensiometer) 25 hours into the test.

3. This time delay was less pronounced at higher applied rainfall intensities, implying that the effectiveness of capillary barrier profiles may be limited at high rainfall intensities.

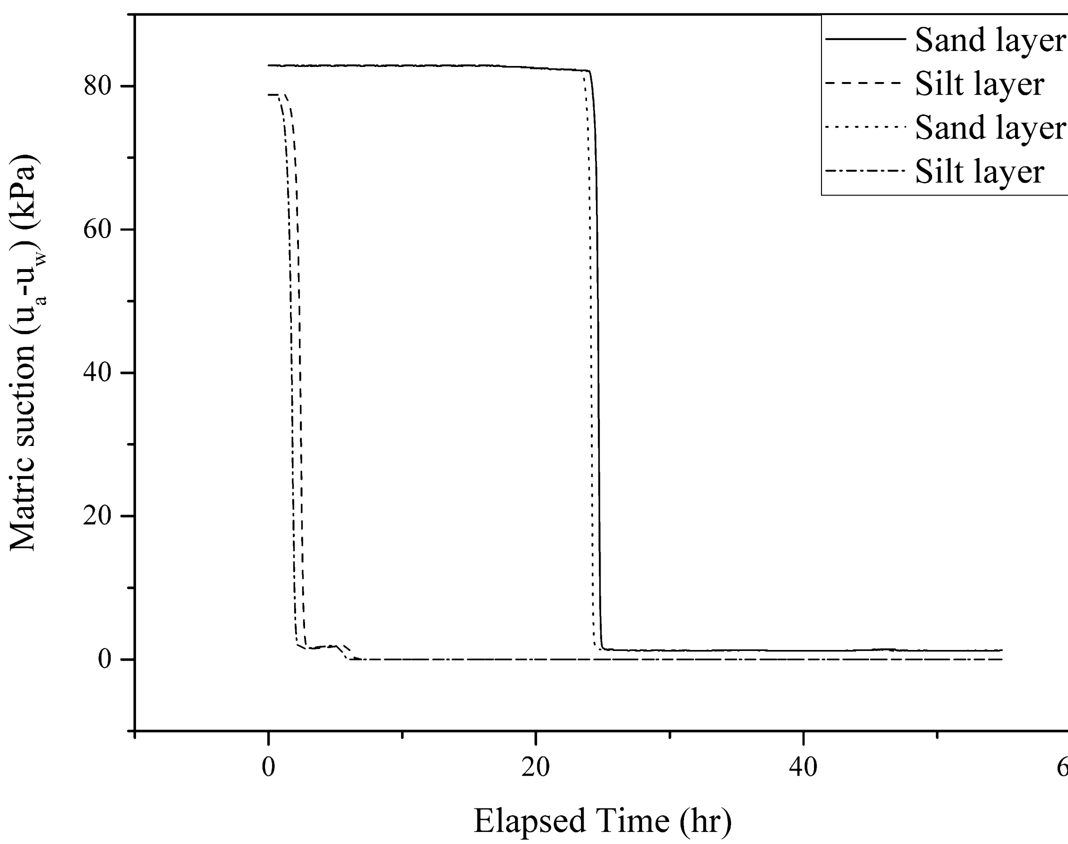

Figure 5.34 Typical variation in matric suction with time in the unsaturated capillary barrier profiles.

5.3.3. Time to Runoff

The time required to generate runoff decreased as the rainfall intensity increased for both unsaturated silt and unsaturated capillary barrier profiles. Unsaturated capillary barrier profiles generally required less time to generate runoff compared to unsaturated silt profiles. Figure 5.35 compares the time to runoff between unsaturated silt and unsaturated capillary barrier profiles at the same applied rainfall intensity. Earlier runoff onset in profiles with higher applied rainfall intensity is consistent with the deduction that as higher rainfall intensities were applied, these profiles achieved saturation sooner.

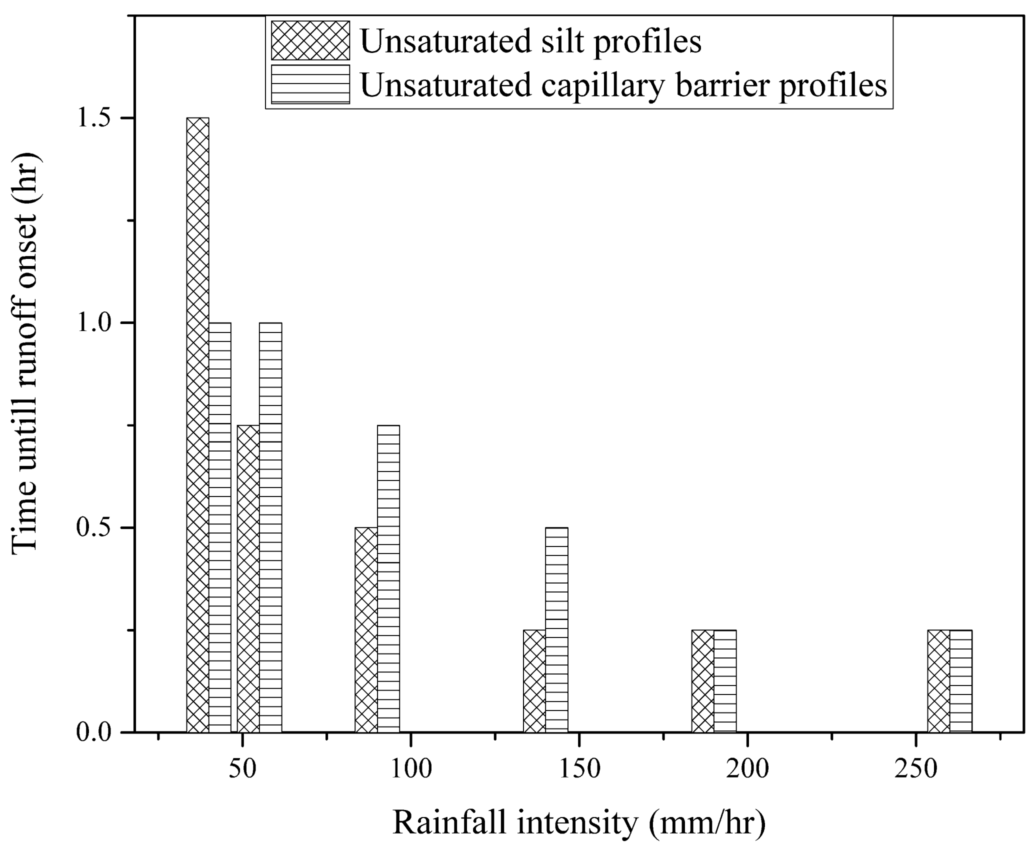

Figure 5.35 Time until the onset of runoff for unsaturated silt and unsaturated capillary barrier profiles at corresponding rainfall intensity.

5.3.4. Comparison between Unsaturated Silt and Unsaturated Capillary Barrier Profiles

Measured changes in the volumetric water content and matric suction profiles as a function of time in the unsaturated silt and unsaturated capillary barrier profiles exhibited the capillary break phenomenon.

Further to those measurements, particular attention was given to observing the propagation of wetting fronts for each unsaturated profile. Wetting fronts were monitored at a 15-minute interval for each unsaturated profile. Photographs confirm that the wetting front in unsaturated silt profiles propagated at a similar rate as was observed in the infiltration capacity tests.

However, the wetting front propagation in the unsaturated capillary barrier profiles exhibited the hallmark of capillary barrier phenomenon where downward infiltration was hindered at the layer interface. Figure 5.36 shows the response of unsaturated silt and unsaturated capillary barrier profiles at the same rainfall intensity. The following aspects can be noticed:

- Identical propagation of the wetting front within the silt layer in both unsaturated silt and unsaturated capillary barrier profiles. At t=1 hour, the wetting front was 80 mm deep within both profiles.

- The waterfront in the unsaturated silt profiles exhibited a uniform surface throughout the profile.

- The layer interface hindered the wetting front propagation in the unsaturated capillary barrier profiles compared to unsaturated silt profiles. At t=8 hours, the wetting front was 225 mm deep, whereas it reached only up to 160 mm in depth in the unsaturated capillary barrier profile.

- The waterfront in the unsaturated capillary barrier profile exhibited narrow fringes outspreading from the wetting front beyond the inter-layer boundary.

- A reduced time delay in wetting front propagation between unsaturated silt and unsaturated capillary barrier profiles was evident when higher rainfall intensities were applied.

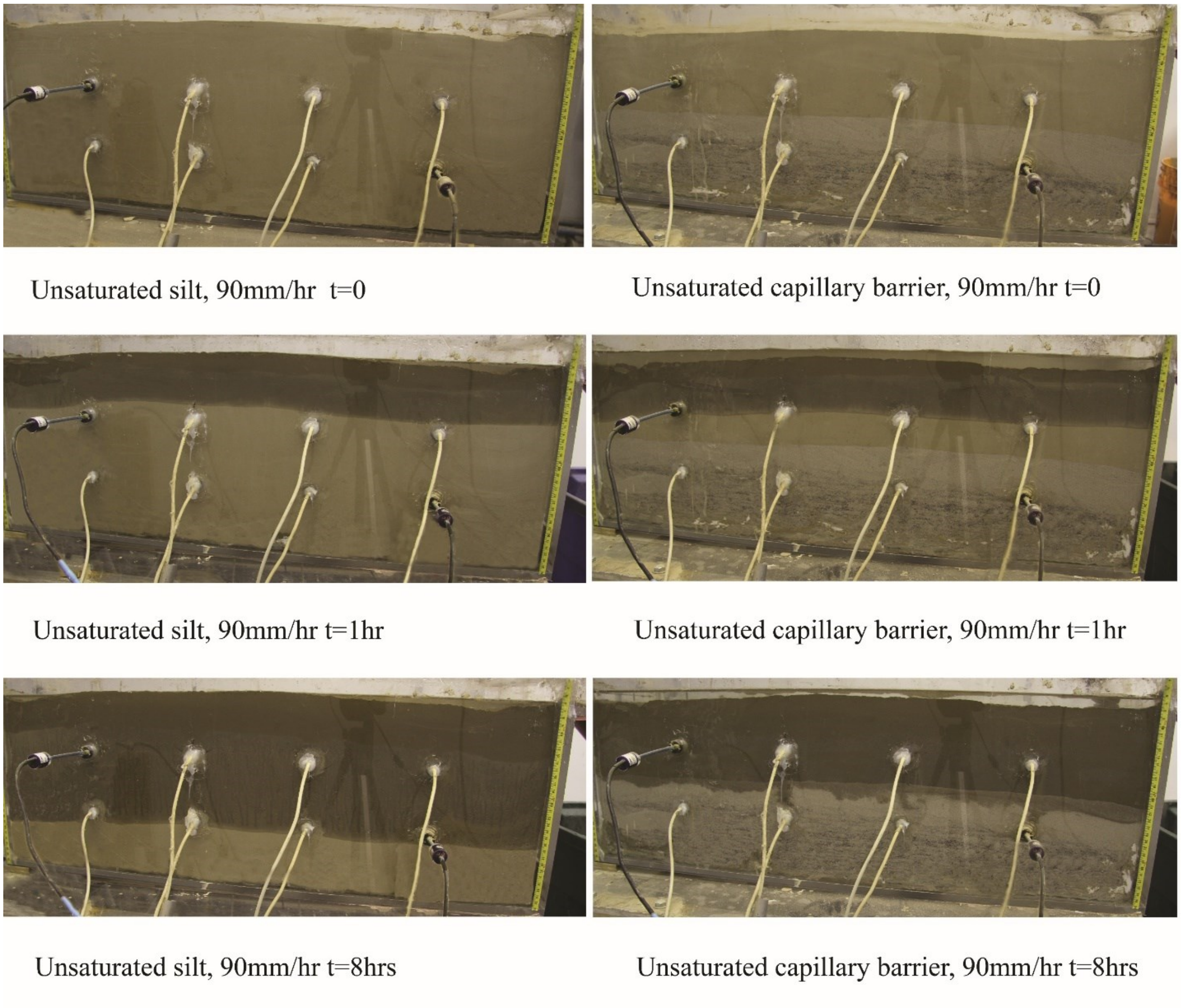

Figure 5.36 The wetting front propagation in the unsaturated silt (left) and unsaturated capillary barrier profiles (right) at the same rainfall intensity (90 mm/hr for this photo).

5.4. Numerical Simulation of the Laboratory Experiments

Numerical predictions of runoff and infiltration for twenty-four laboratory-simulated scenarios at six different rainfall intensities were conducted. The numerical predictions of both low permeability and capillary barrier profiles examined during the laboratory investigations as described in Section 4.6 were modelled. The predictions encompassed saturated and unsaturated initial state of each profile. One-dimensional (1D) and three-dimensional (3D) analyses were conducted as discussed in detail in Section 4.6. The following sections summarize the typical results from 1D and 3D analyses.

5.4.1. One-Dimensional Analyses

One-dimensional (1D) analyses are commonly used to predict water fluxes in soil cover systems since water flow in soil cover systems occurs predominantly in the vertical direction. More specific insight into the numerical performance of 1D versus 3D models is discussed in the following sections through comparisons with controlled laboratory results.

5.4.1.1. Saturated Profiles

Table 5.1 presents a comparison between measured and 1D predicted final cumulative runoff volumes for each rainfall intensity indicated by the profile type. The accuracy in the saturated profiles was within a 6% difference for low applied rainfall intensities, whereas up to 19% difference was found in capillary barrier profiles that were subjected to higher rainfall intensities.

The variation of water balance components with time for experimental versus 1D predictions for the saturated silt and capillary barrier profiles are shown in Figures 5.37 through 5.42. At a glance, one can see that the prediction of infiltration and runoff in the saturated silt profiles produced a precise match with measured values. This is a result of the profiles being fully saturated and solely controlled by the saturated hydraulic conductivity of the profile. Furthermore, laboratory profiles comprised a uniform layer of homogeneous silt. Therefore, no temporal or spatial variability was involved in the results. Likewise, saturated capillary barrier profile results were in good agreement with the measured response. However, at higher rainfall intensity the quality of predictions was not maintained in the capillary barrier profiles.

Table 5.1 Measured and 1D predicted final cumulative runoff volumes for saturated silt and saturated capillary barrier profiles at the corresponding applied rainfall intensity.

Intensity (mm/hr)	Measured final cumulative volume (L)		1D final cumulative Predicted volume (L)		Percent difference between measured and predicted final cumulative volumes (%)	
	Saturated silt	Saturated capillary barrier	Saturated silt	Saturated capillary barrier	Saturated silt	Saturated capillary barrier
40	286	268	284	261	1	2%
55	240	326	249	322	-4[*]	1%
90	385	568	382	563	1	1%
140	830	585	840	699	-1	-19%
190	1122	842	1162	969	-4	-15%
260	1051	1009	1118	1154	-6	-14%

[*]Negative values in percent difference indicate that models overpredicted runoff volumes (i.e., predicted values are more than measured values).

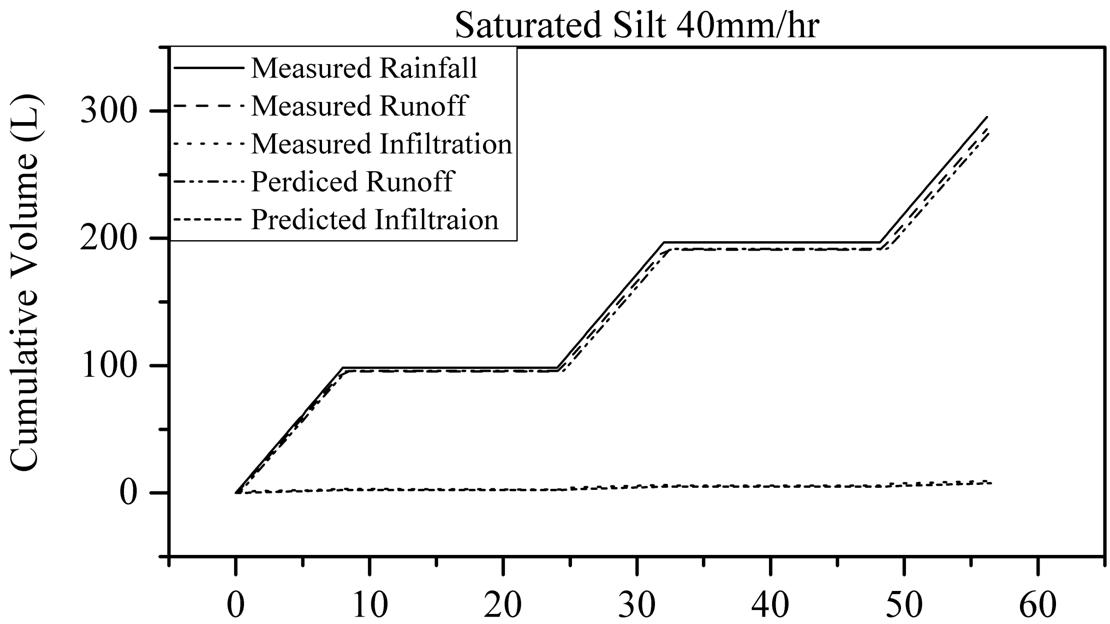

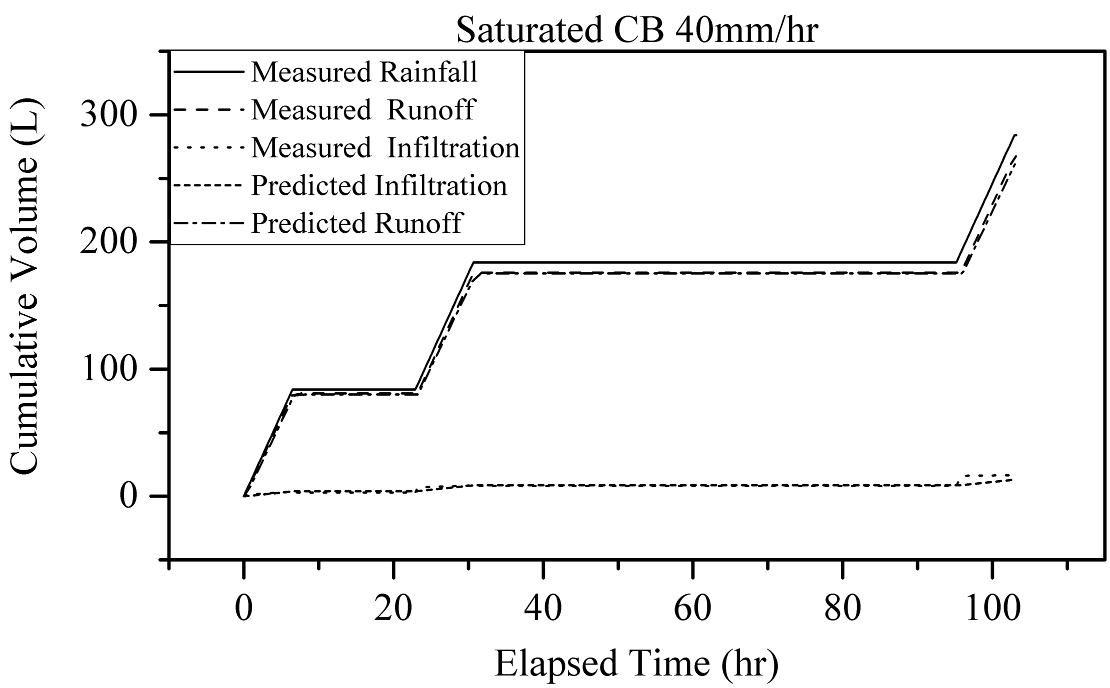

Figure 5.37 Measured versus 1D predicted water balance components for saturated silt (top) and saturated capillary barrier (bottom) profiles at a rainfall intensity of 40 mm/hr.

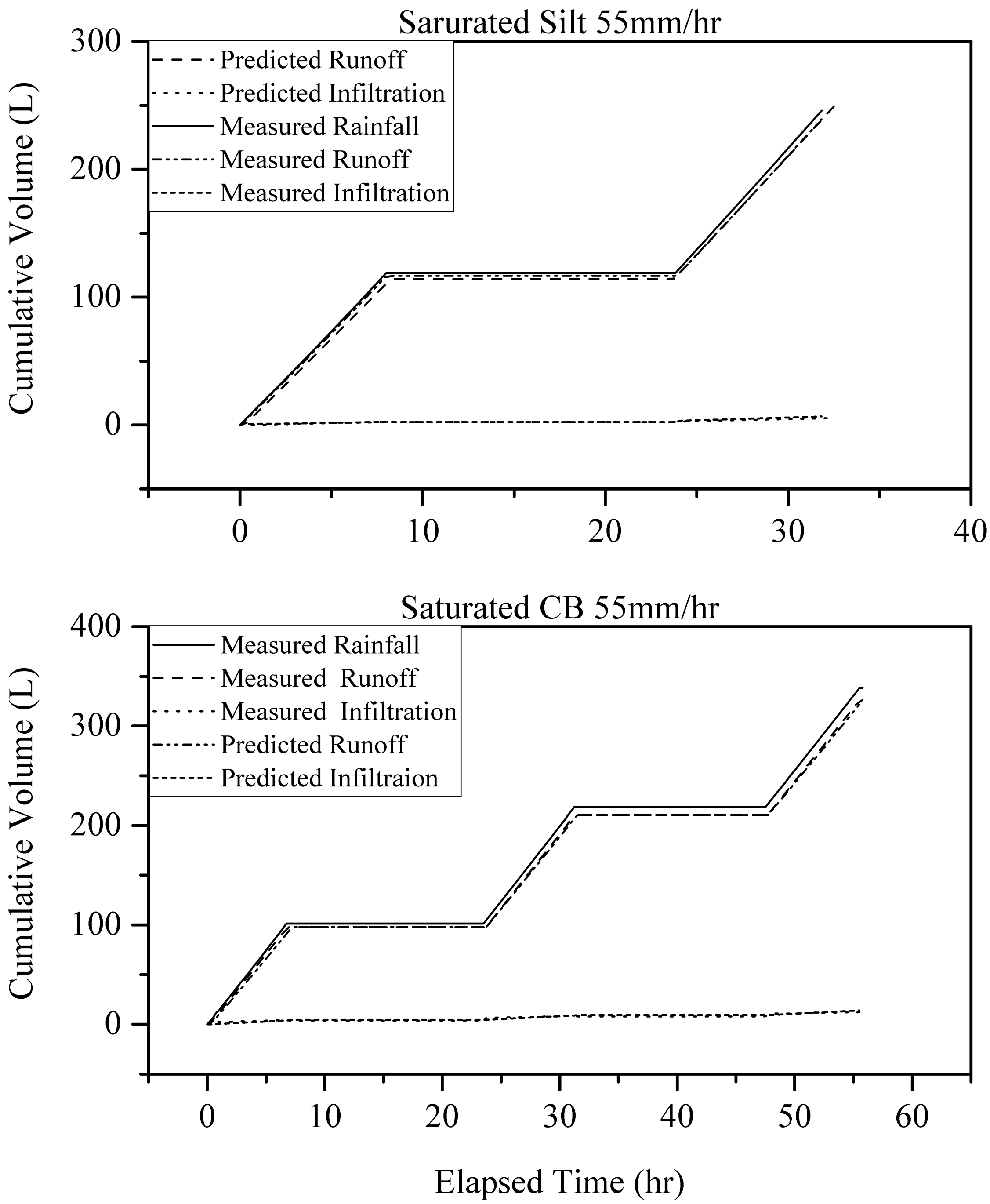

Figure 5.38 Measured versus 1D predicted water balance components for saturated silt (top) and saturated capillary barrier (bottom) profiles at a rainfall intensity of 55 mm/hr.

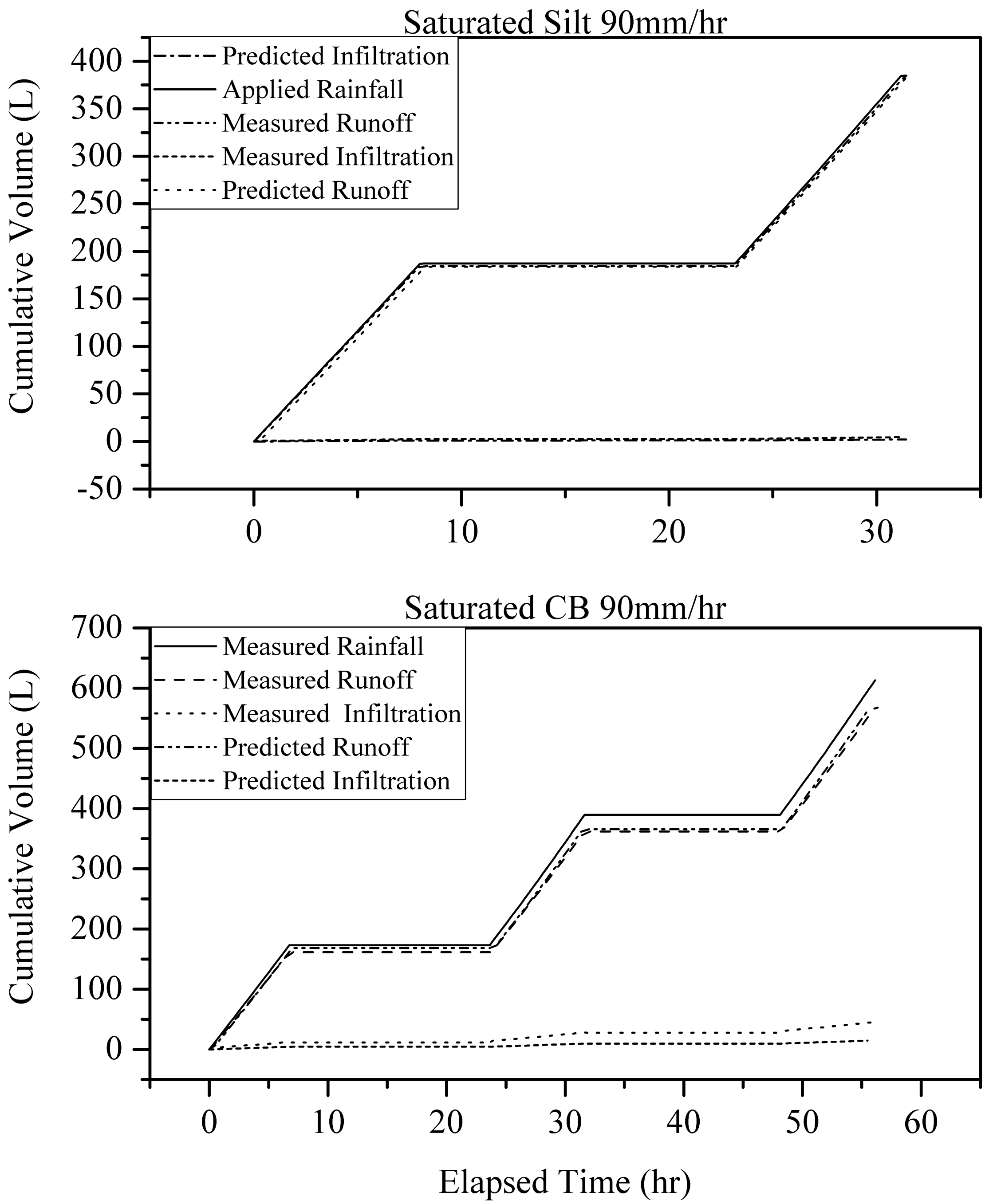

Figure 5.39 Measured versus 1D predicted water balance components for saturated silt (top) and saturated capillary barrier (bottom) profiles at a rainfall intensity of 90 mm/hr.

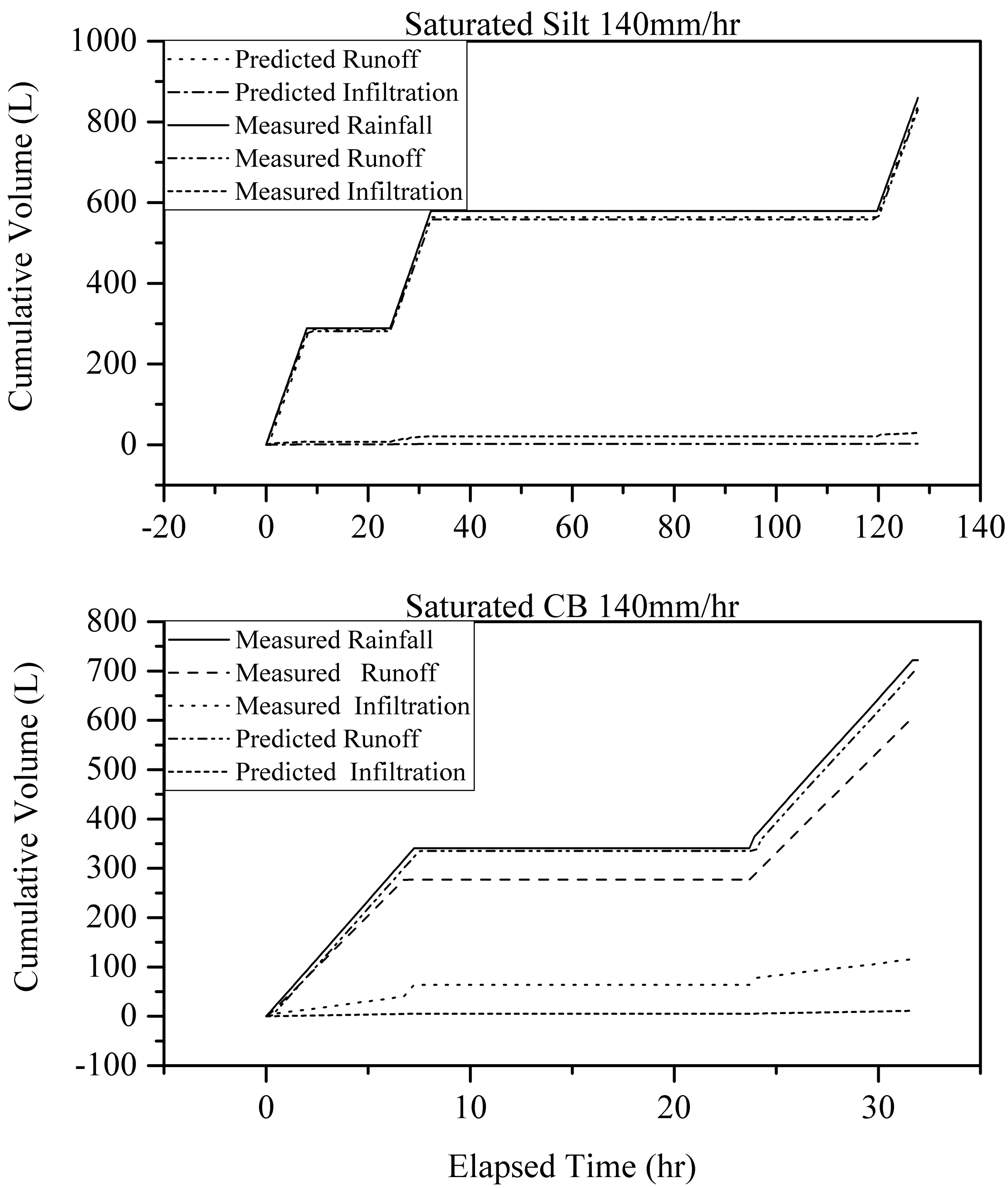

Figure 5.40 Measured versus 1D predicted water balance components for saturated silt (top) and saturated capillary barrier (bottom) profiles at a rainfall intensity of 140 mm/hr.

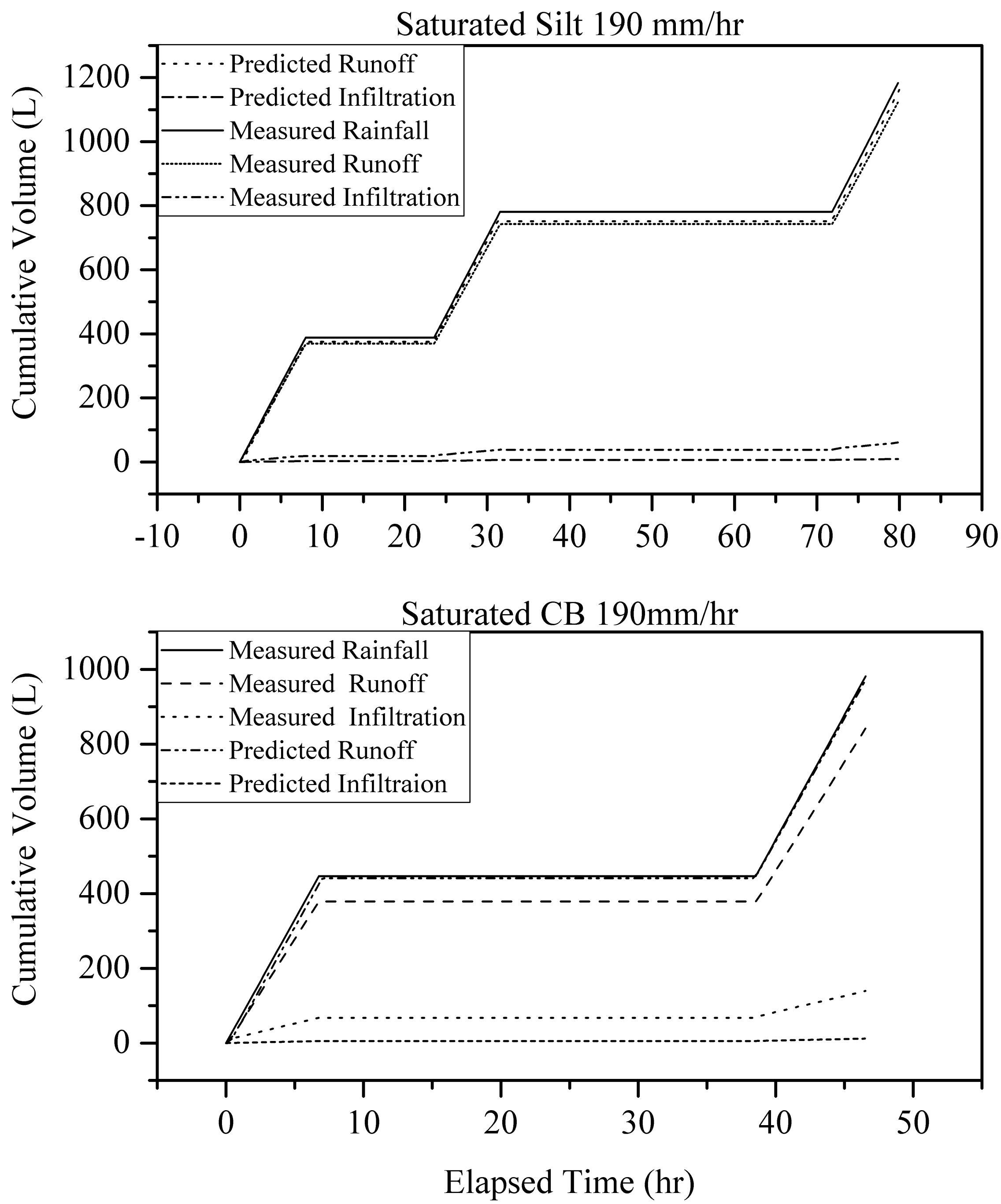

Figure 5.41 Measured versus 1D predicted water balance components for saturated silt (top) and saturated capillary barrier (bottom) profiles at a rainfall intensity of 190 mm/hr.

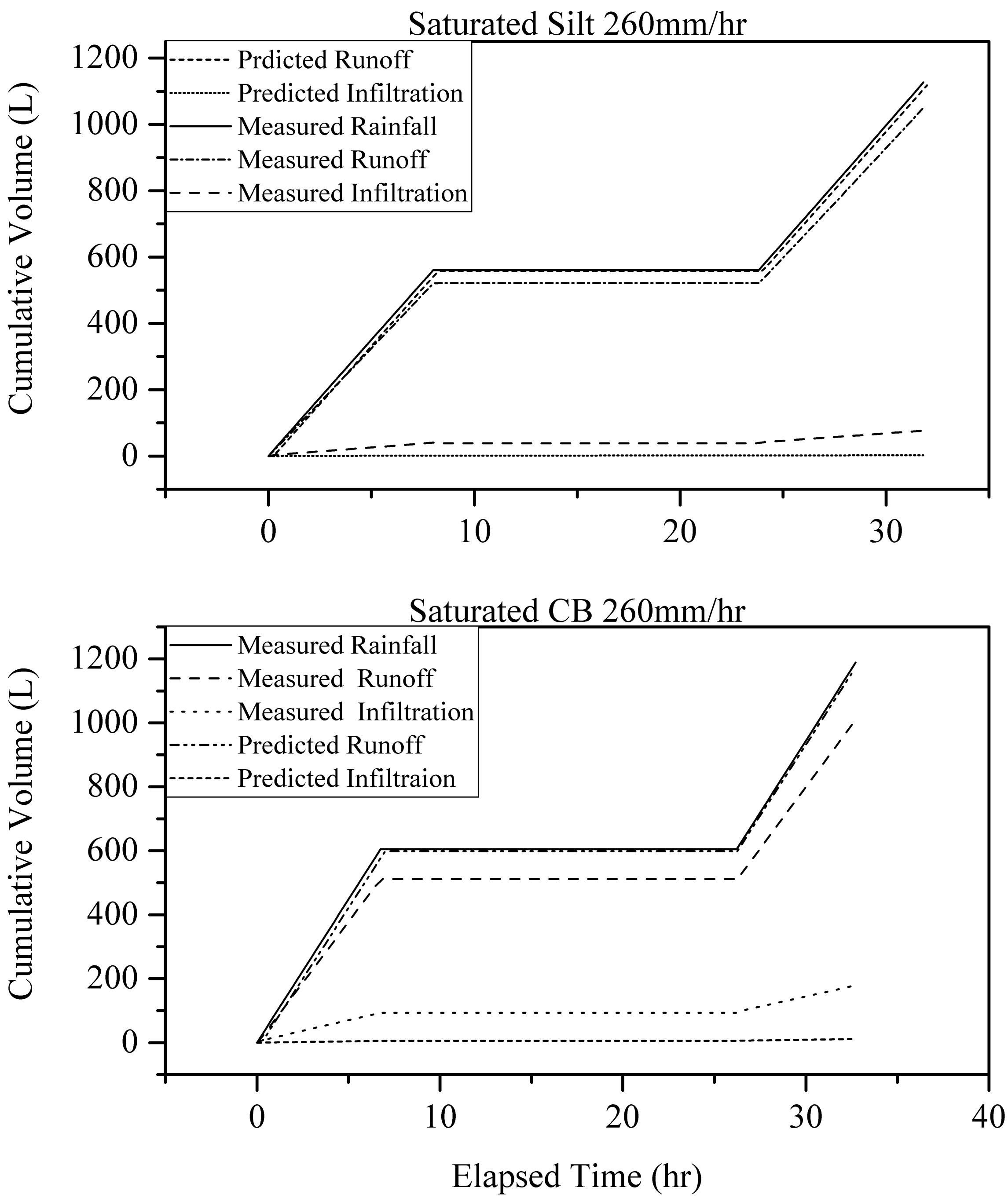

Figure 5.42 Measured versus 1D predicted water balance components for saturated silt (top) and saturated capillary barrier (bottom) profiles at a rainfall intensity of 260 mm/hr.

5.4.1.2. Unsaturated Profiles

The difference between measured and 1D predicted final cumulative runoff volumes in unsaturated silt and capillary barrier profiles are presented in Table 5.2 for each applied rainfall intensity. Overall, the predictions for single-layer profiles were within a 6% difference, whereas the predictions for capillary barrier varied up to a 32% difference. The corresponding variations in water balance components with time are illustrated in Figures 5.43 through 5.48.

There is a stark difference in the quality of predictions between saturated and unsaturated profiles. Numerical predictions of runoff and infiltration matched the experimental data trends. However, in terms of precision, numerical predictions overestimated infiltration and underestimated runoff in most scenarios. The reason may be due to limited options to characterize the boundary at the layer interface between the silt and sand layer in the case of capillary barrier profiles.

Table 5.2 Measured and 1D predicted final cumulative runoff volumes for unsaturated silt and unsaturated capillary barrier profiles at the corresponding applied rainfall intensity.

Intensity (mm/hr)	Measured final cumulative volume (L)		1D final cumulative Predicted volume (L)		Percent difference between measured and predicted final cumulative volumes (%)	
	unsaturated silt	unsaturated capillary barrier	unsaturated silt	unsaturated capillary barrier	unsaturated silt	unsaturated capillary barrier
40	208	195	240	158	-15%	19%
55	306	312	300	291	2%	7%
90	529	539	528	534	0%	1%
140	530	839	557	890	-5%	-6%
190	718	1144	731	1234	-2%	-8%
260	1037	1542	1073	1734	-3%	-13%

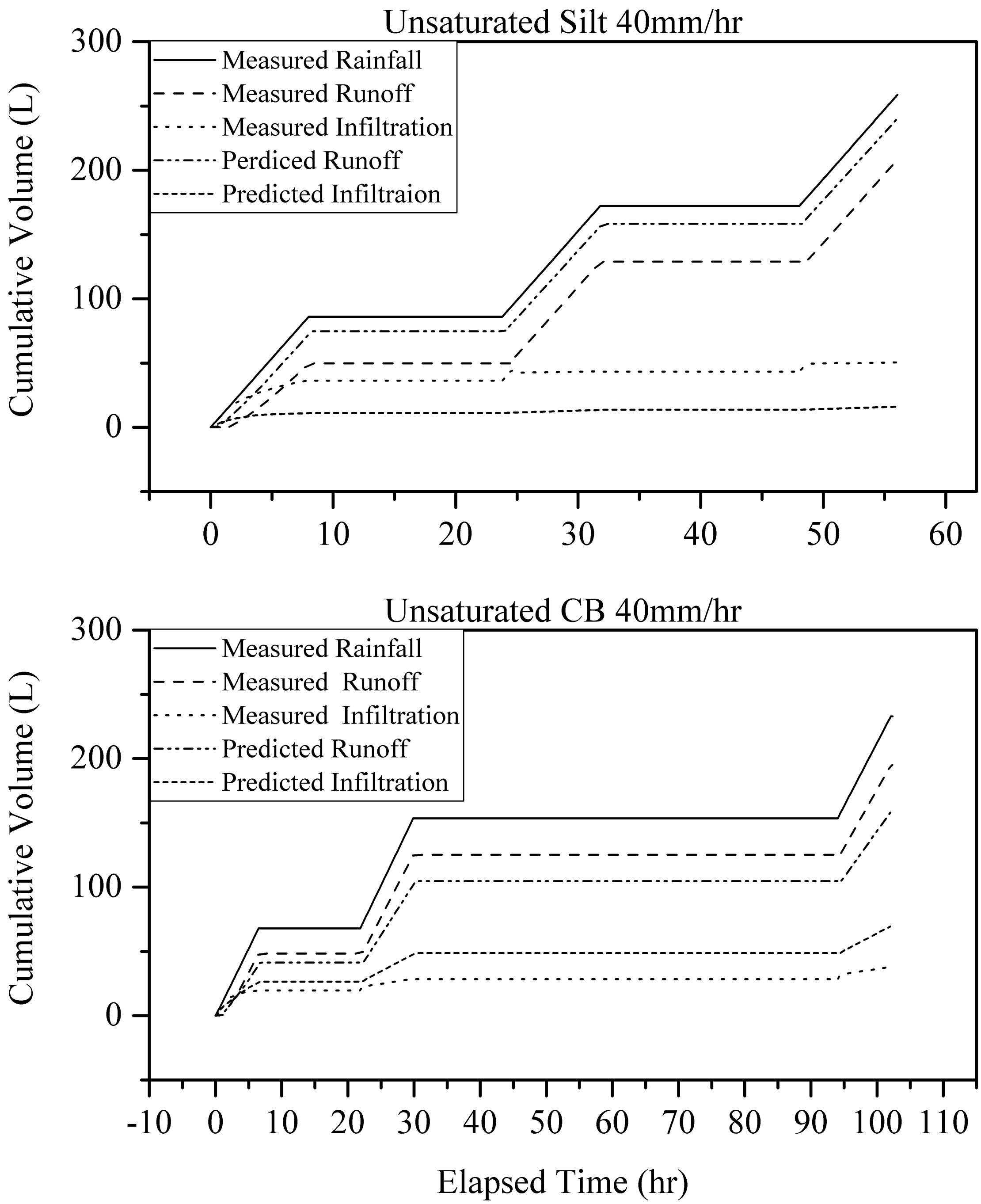

Figure 5.43 Measured versus 1D predicted water balance components for unsaturated silt (top) and unsaturated capillary barrier (bottom) profiles at a rainfall intensity of 40 mm/hr.

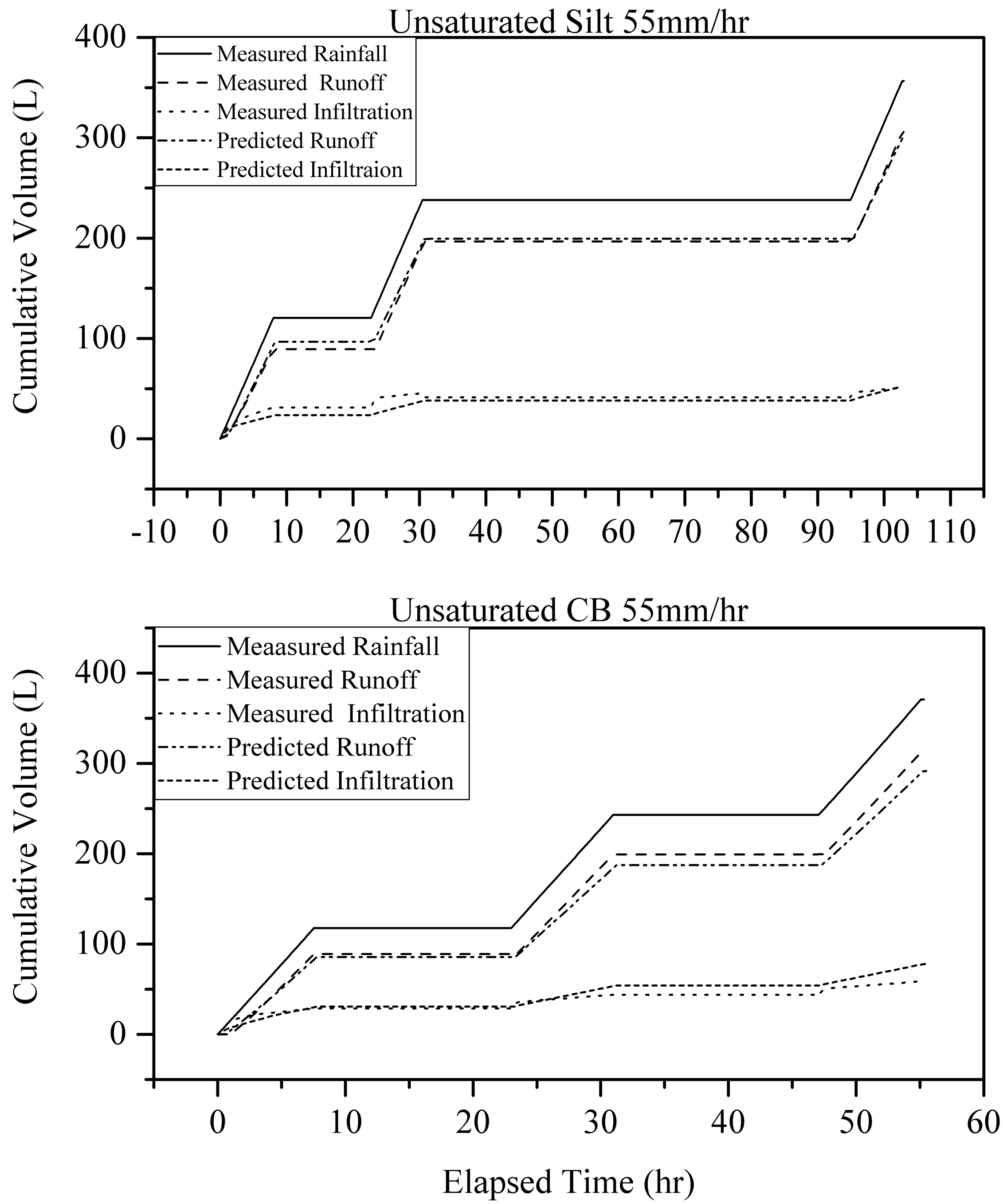

Figure 5.44 Measured versus 1D predicted water balance components for unsaturated silt (top) and unsaturated capillary barrier (bottom) profiles at a rainfall intensity of 55 mm/hr.

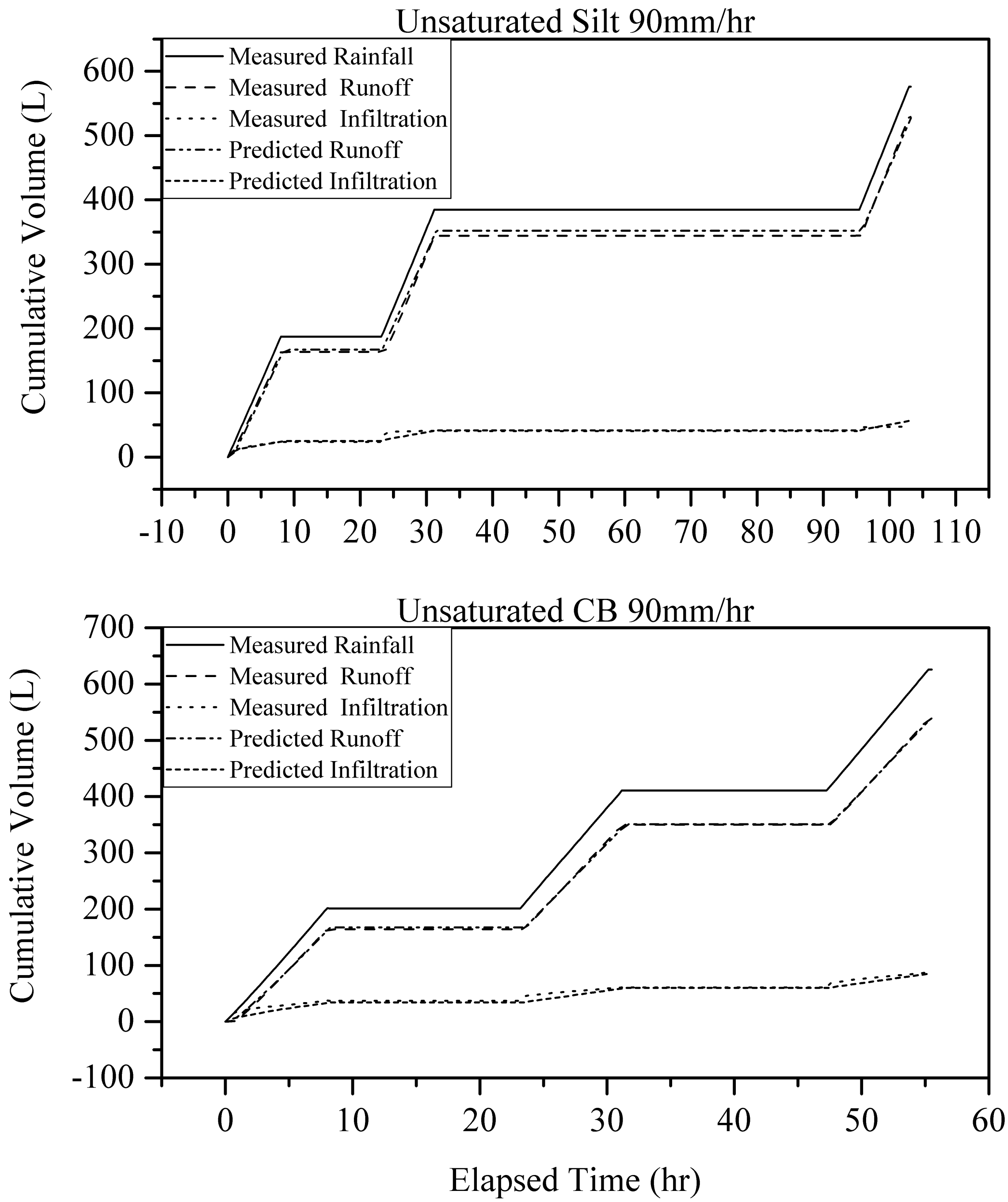

Figure 5.45 Measured versus 1D predicted water balance components for unsaturated silt (top) and unsaturated capillary barrier (bottom) profiles at a rainfall intensity of 90 mm/hr.

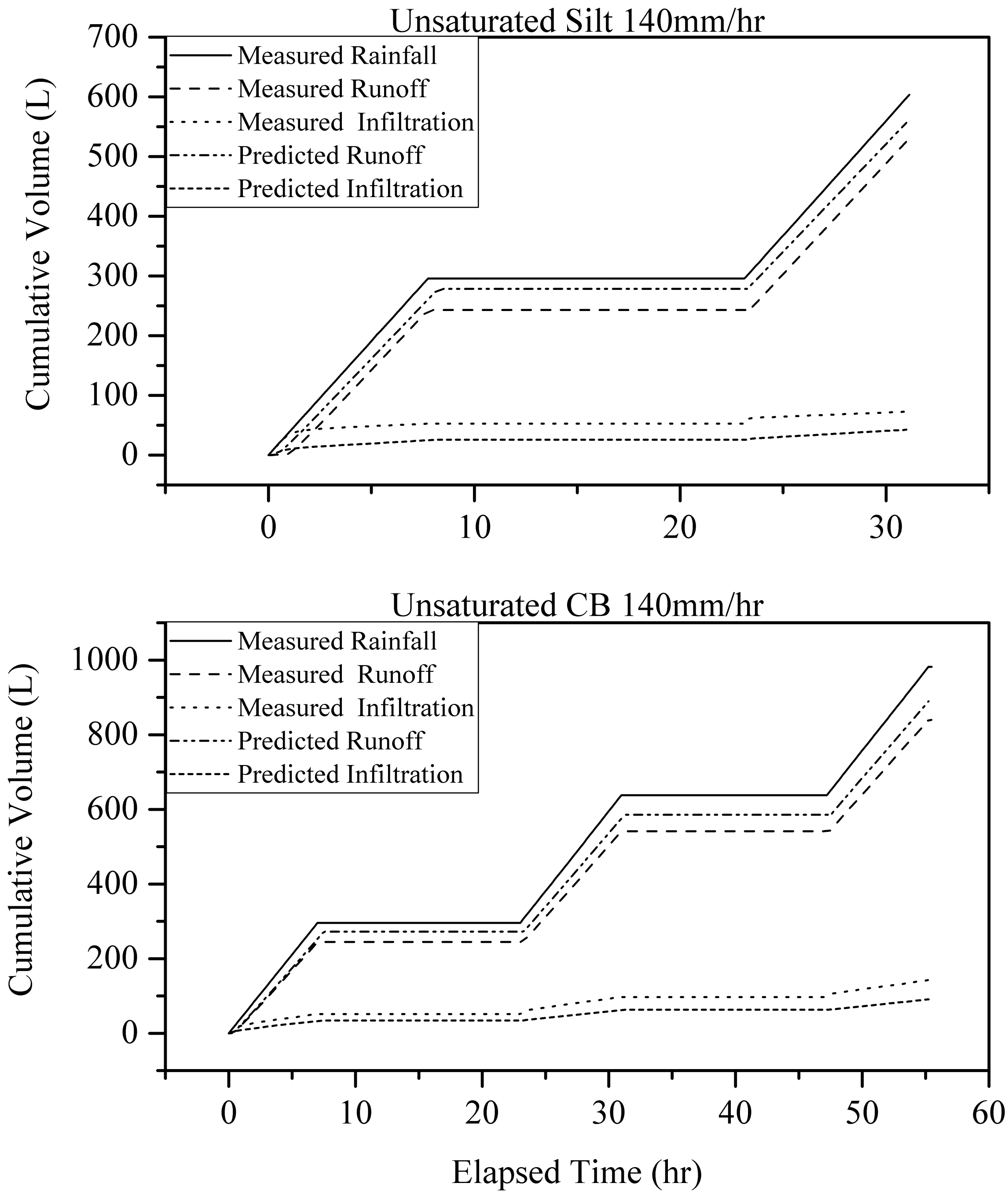

Figure 5.46 Measured versus 1D predicted water balance components for unsaturated silt (top) and unsaturated capillary barrier (bottom) profiles at a rainfall intensity of 140 mm/hr.

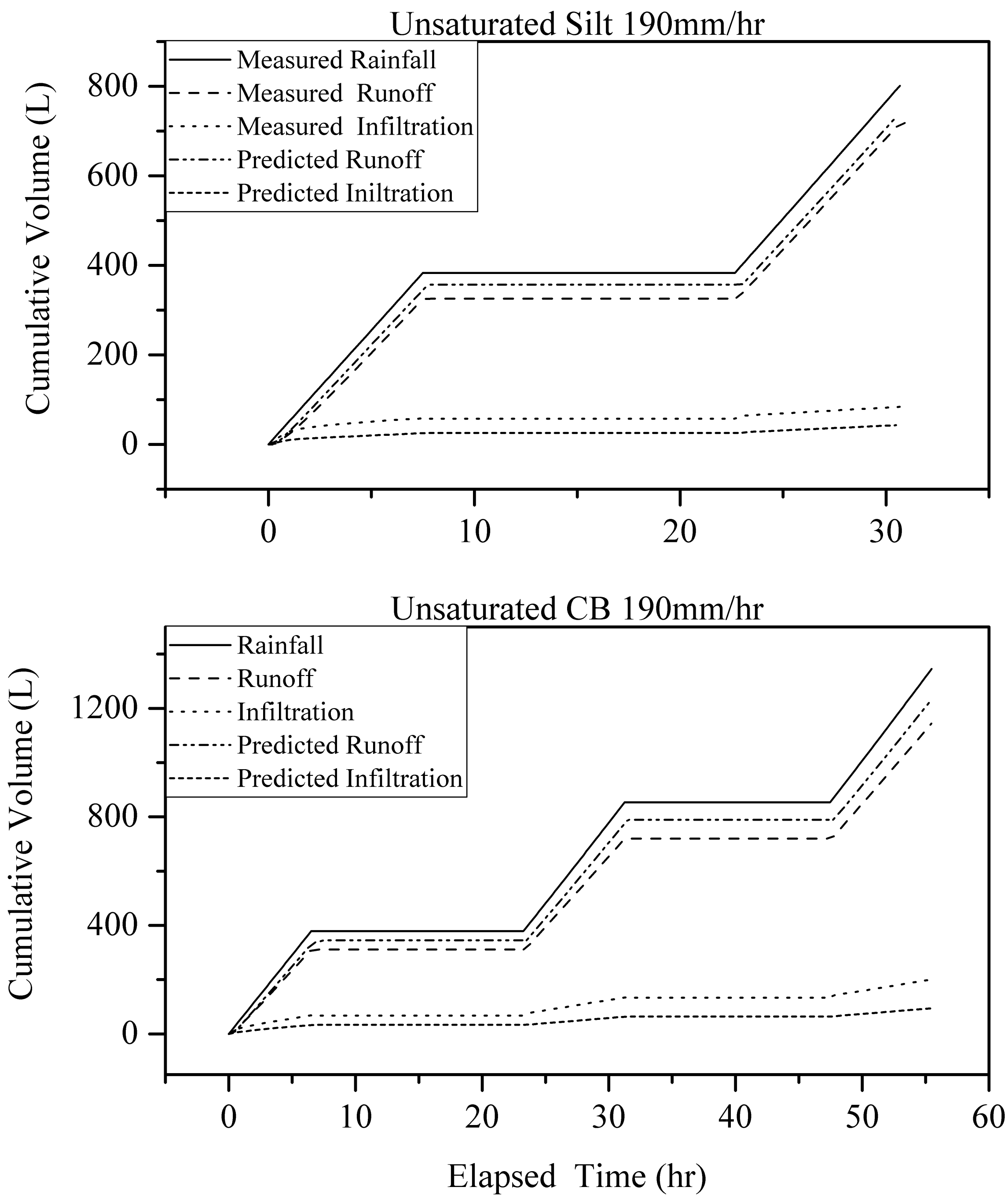

Figure 5.47 Measured versus 1D predicted water balance components for unsaturated silt (top) and unsaturated capillary barrier (bottom) profiles at a rainfall intensity of 190 mm/hr.

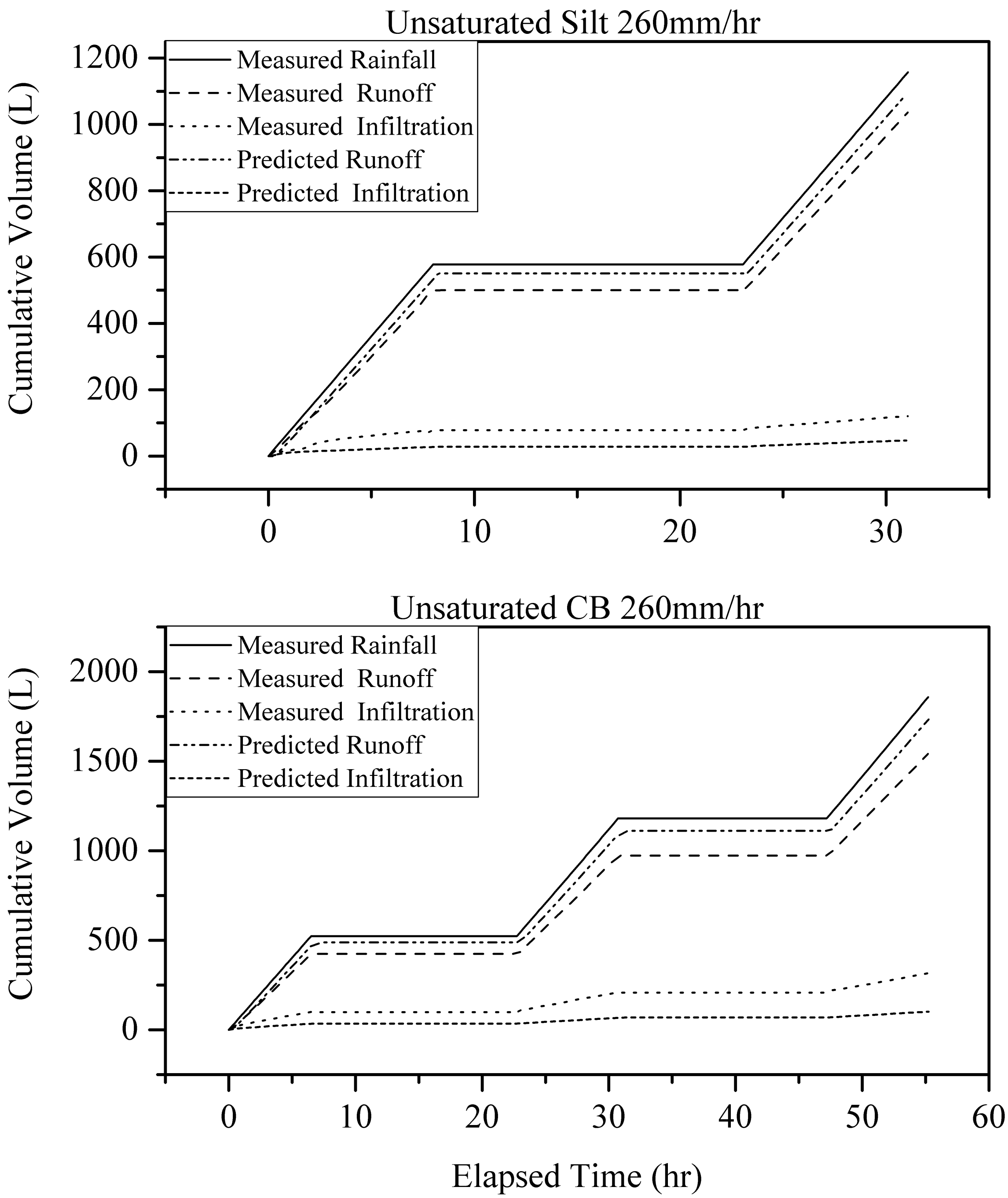

Figure 5.48 Measured versus 1D predicted water balance components for unsaturated silt (top) and unsaturated capillary barrier (bottom) profiles at a rainfall intensity of 260 mm/hr.

5.4.2. Three-Dimensional Analyses

Soil covers systems are structures of large horizontal continuity with water transfer occurring mainly in the vertical dimension. Therefore, 1D analyses have long been accepted as an appropriate tool for water flux assessment. Nevertheless, the potential advantage of 3D models was a notion worth exploring, especially with the available results of laboratory-controlled data.

5.4.2.1. Saturated Profiles

Comparisons between laboratory-measured and 3D predicted final cumulative runoff volumes for saturated silt and capillary barrier profiles at each rainfall intensity are presented in Table 5.3. The corresponding variations of water balance components with time are presented in Figures 5.49 through 5.54. In short, only a minor improvement in the results of 3D predictions over 1D predictions is evident.

Table 5.3 Measured and 3D predicted final cumulative runoff volumes for saturated silt and saturated capillary barrier profiles at the corresponding applied rainfall intensity.

Intensity (mm/hr)	Measured final cumulative volume (L)		3D final cumulative Predicted volume (L)		Percent difference between measured and predicted final cumulative volumes (%)	
	Saturated silt	Saturated CB	Saturated silt	Saturated CB	Saturated silt	Saturated CB
40	286	268	279	259	2%	3%
55	240	326	246	319	-3%	2%
90	385	568	373	571	3%	-1%
140	830	585	844	702	-2%	-20%
190	1122	842	1155	972	-3%	-15%
260	1051	1009	1104	1158	-5%	-15%

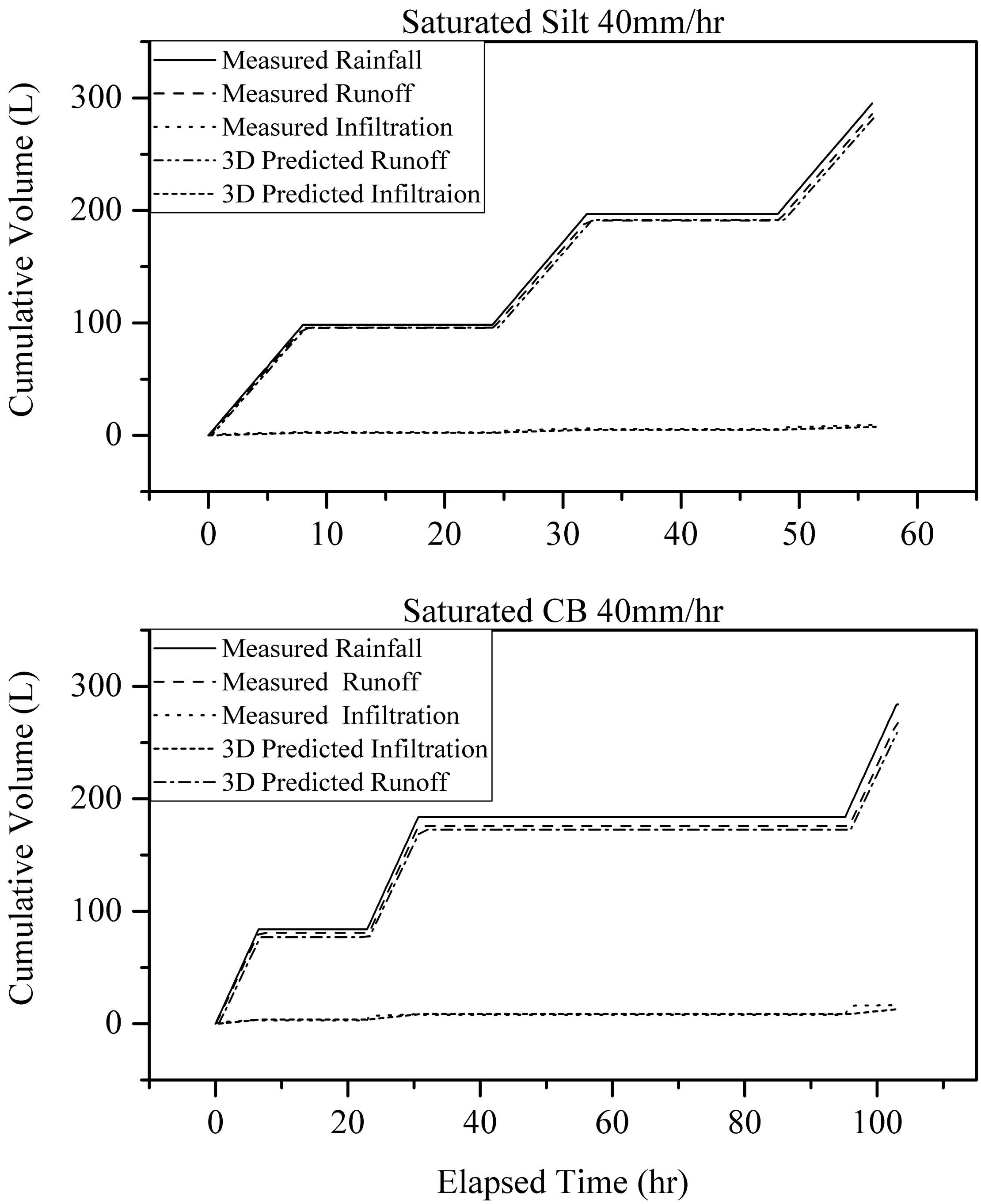

Figure 5.49 Measured versus 3D predicted water balance components for saturated silt (top) and saturated capillary barrier (bottom) profiles at a rainfall intensity of 40 mm/hr.

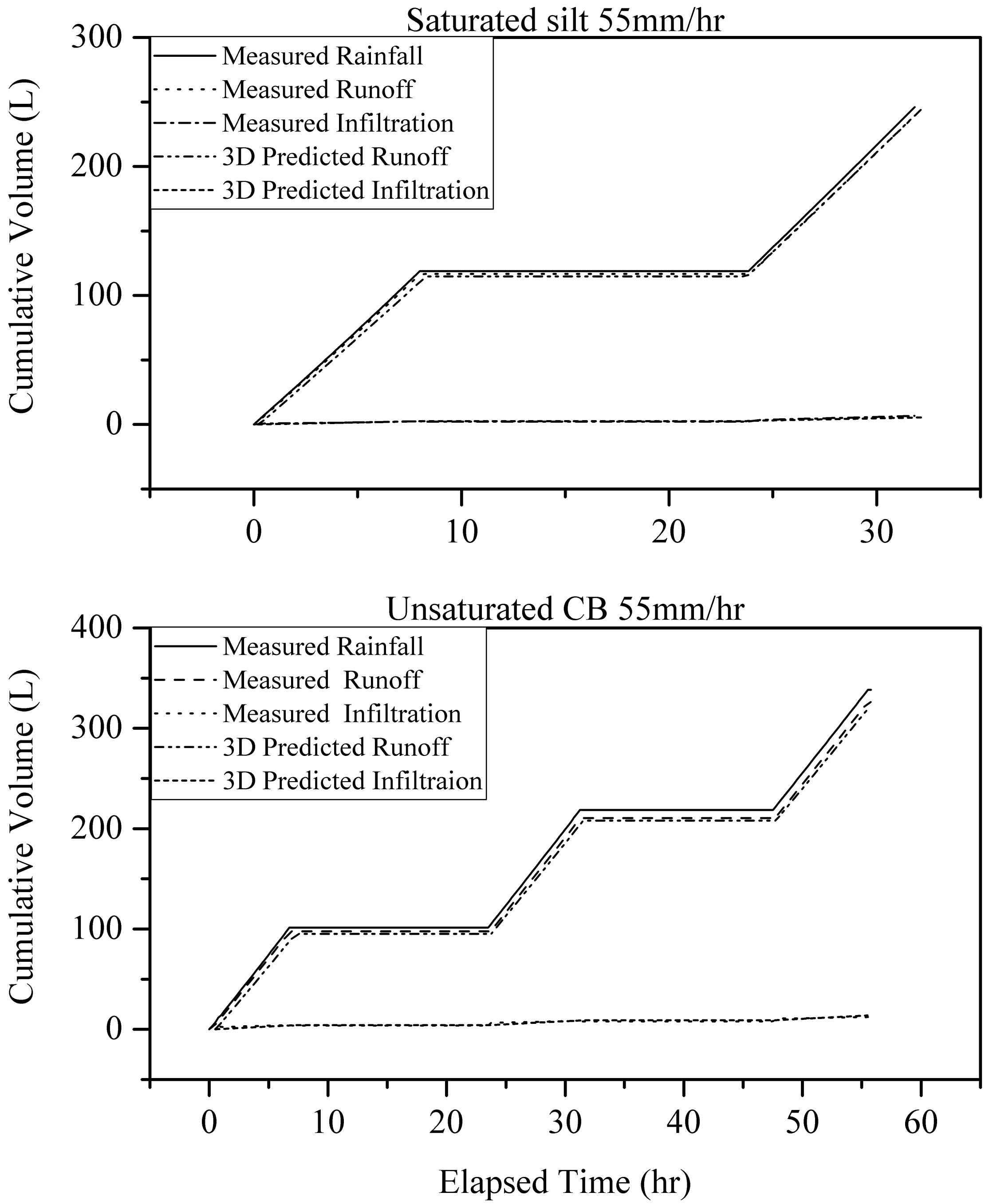

Figure 5.50 Measured versus 3D predicted water balance components for saturated silt (top) and saturated capillary barrier (bottom) profiles at a rainfall intensity of 55 mm/hr.

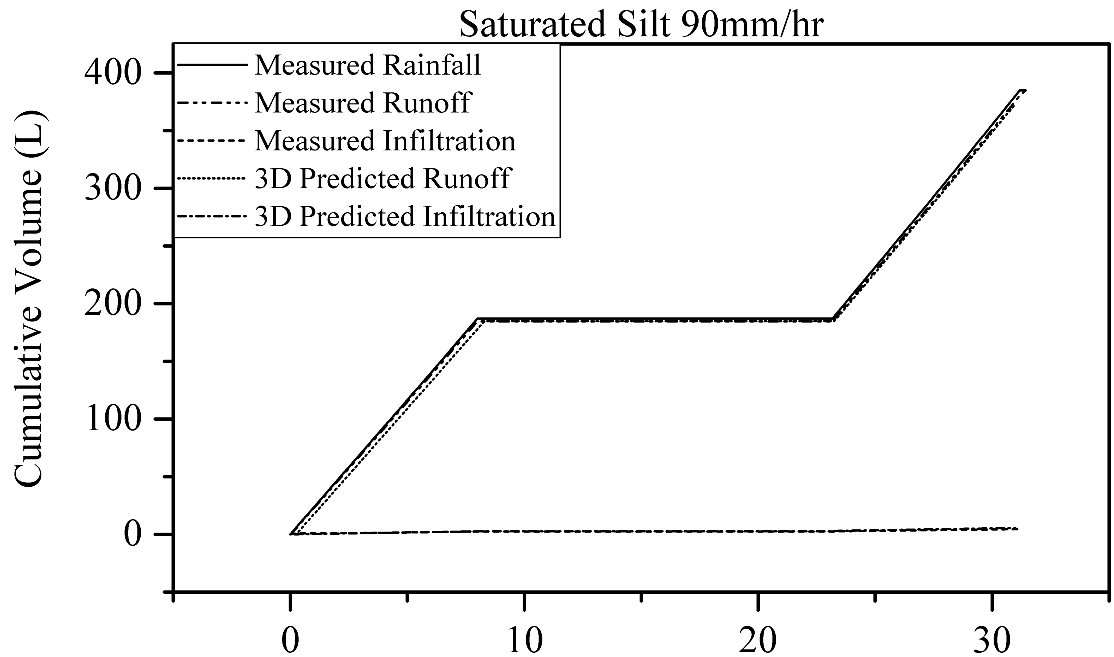

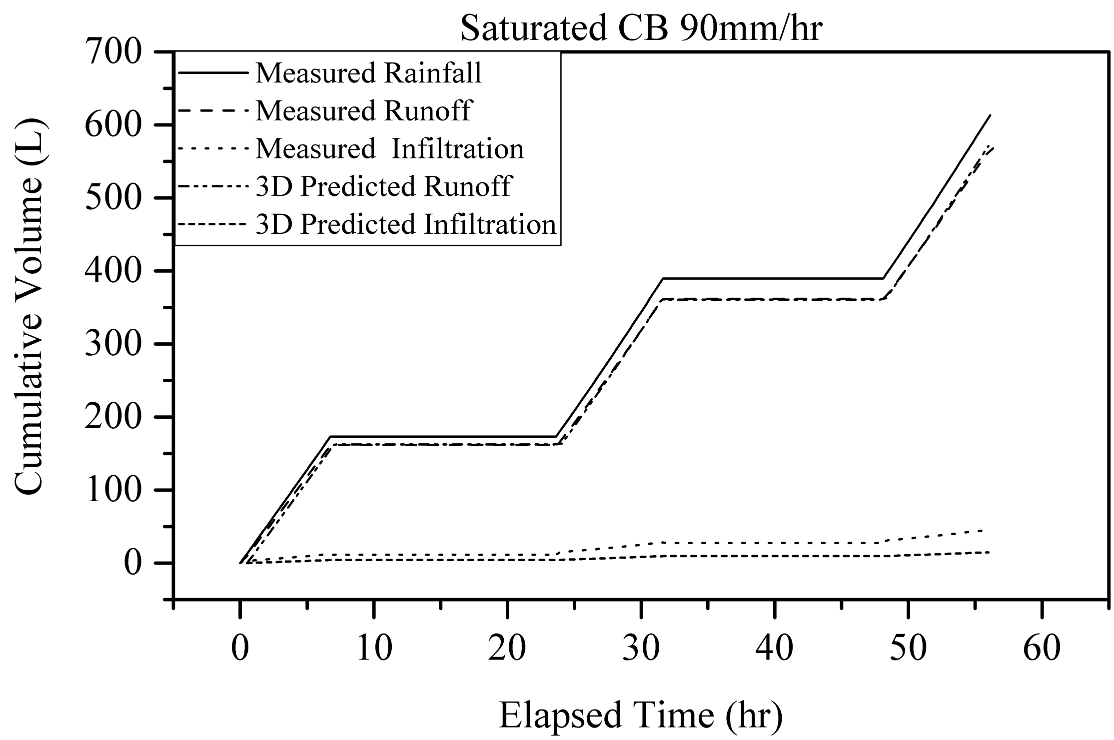

Figure 5.51 Measured versus 3D predicted water balance components for saturated silt (top) and saturated capillary barrier (bottom) profiles at a rainfall intensity of 90 mm/hr.

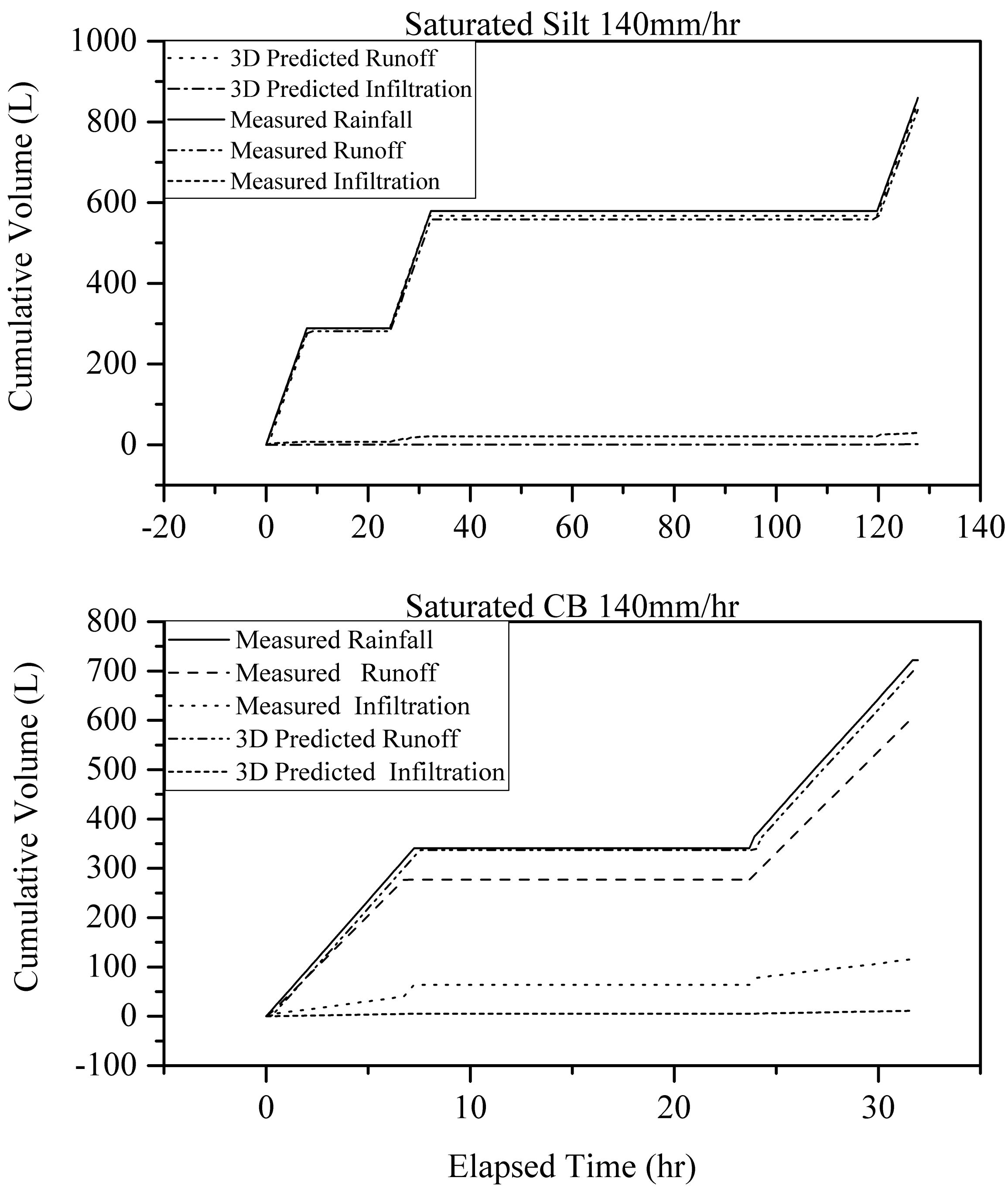

Figure 5.52 Measured versus 3D predicted water balance components for saturated silt (top) and saturated capillary barrier (bottom) profiles at a rainfall intensity of 140 mm/hr.

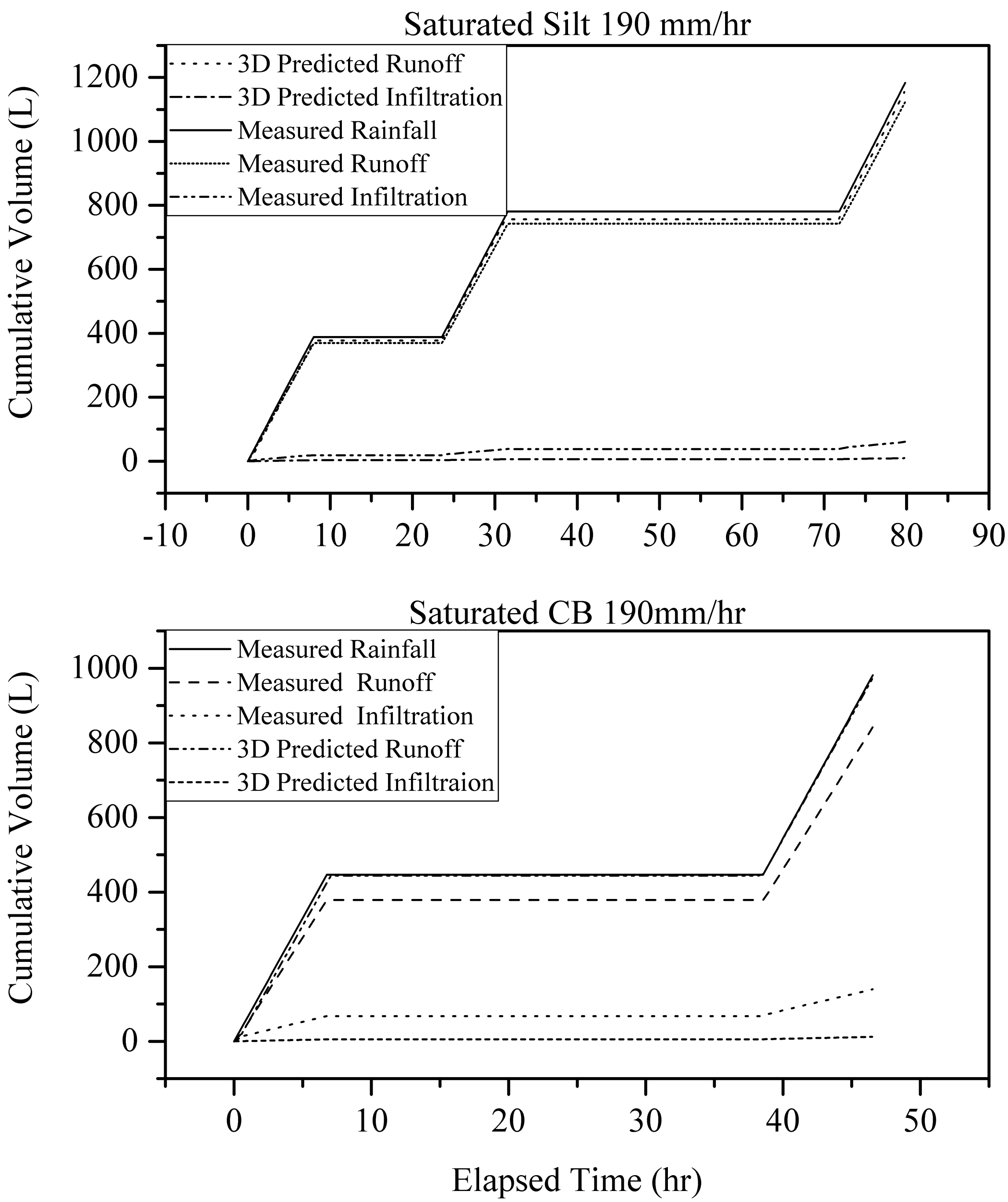

Figure 5.53 Measured versus 3D predicted water balance components for saturated silt (top) and saturated capillary barrier (bottom) profiles at a rainfall intensity of 190 mm/hr.

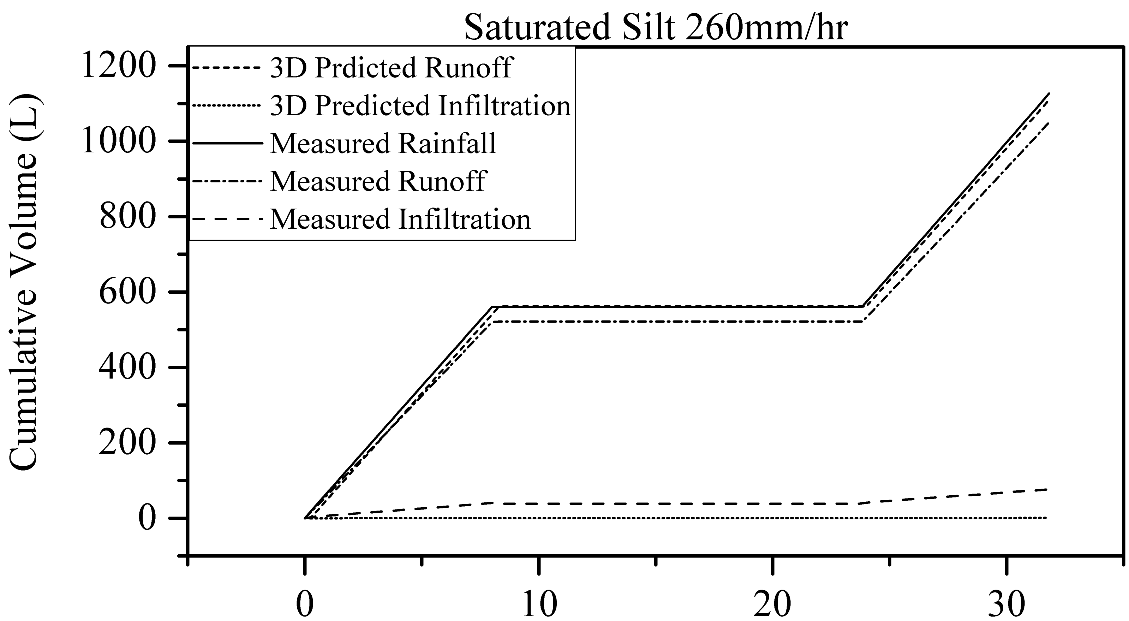

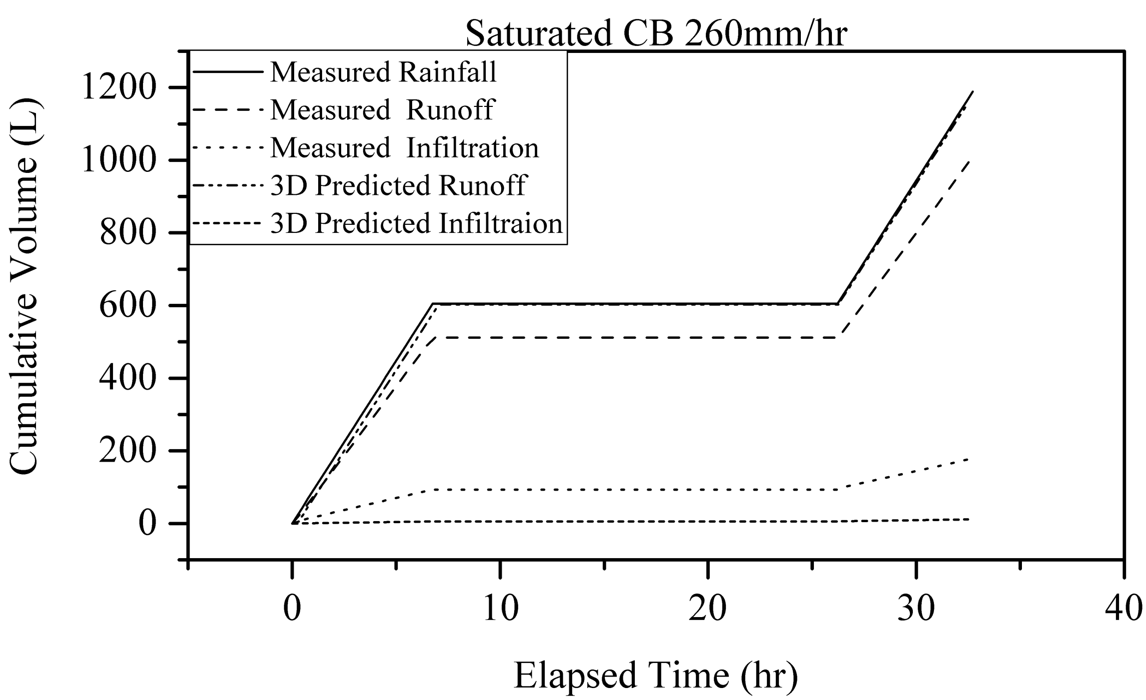

Figure 5.54 Measured versus 3D predicted water balance components for saturated silt (top) and saturated capillary barrier (bottom) profiles at a rainfall intensity of 260 mm/hr.

5.4.2.2. Unsaturated Profiles

Table 5.4 summarizes the percentage difference between laboratory-measured and 3D-predicted final cumulative runoff volumes. Putting aside the unsaturated silt profile at 40 mm/hr where using 3D models improved accuracy from 15% to 3%, there was a minor difference in the results when 3D models were utilized. This suggests that for this class of problems, i.e., single-layer profiles, 1D analyses can be adequate as long as the profiles have gentle slopes as was the case in the laboratory study.

Figure 5.55 through 5.60 illustrate comparisons of water balance components of 3D-predicted values versus experimental data for rainfall intensity ranging between 40 mm/hr and 260 mm/hr for 3D models. Minor improvement over 1D predictions is evident.

Table 5.4 Measured and 3D predicted final cumulative runoff volumes for unsaturated silt and unsaturated capillary barrier profiles at the corresponding applied rainfall intensity.

Intensity (mm/hr)	Measured final cumulative volume (L)		3D final cumulative predicted volume (L)		Percentage difference between measured and predicted final cumulative volumes (%)	
	unsaturated silt	unsaturated CB	unsaturated silt	unsaturated CB	unsaturated silt	unsaturated CB
40	208	158	203	132	3%	32%
55	306	291	298	257	3%	18%
90	529	534	526	503	1%	7%
140	530	890	555	848	-5%	-1%
190	718	1234	730	1201	-2%	-5%
260	1037	1734	1090	1700	-5%	-10%

In summary, 1D models provided a reasonably good representation of the laboratory flume results when single-layer profiles were considered. The results suggest that water flow through saturated and unsaturated single-layer profiles is well represented by numerical models.

Multilayered profiles, on the other hand, produced more variability in results relative to the applied rainfall intensity. This may be an artifact of the limited capacity of the model to replicate the physical hydraulic condition at the layer interface. Moreover, dependency on rainfall intensity may be a result of the model not being able to accommodate the high flux applied at the top boundary, which is well exceeding the saturated hydraulic conductivity of the top layer at high rainfall intensity. However, this has not been proven to pose an issue for single-layer profiles.

Upon comparing low permeability and capillary barrier profiles, the discrepancy between measured and predicted values was higher in the latter in both 1D and 3D analyses. This may indicate that a certain physical process in capillary barrier profiles is not well captured by numerical models. Lastly, transient water flow through an unsaturated 3D layered system required long computation time, especially for capillary barrier profiles even when the finite element formulation was simplified.

Observing the overall results, one concludes that for single-layer soil covers, reliable results can be attained using numerical models. Nevertheless, the numerical models' ability to simulate the actual physical state of the water flow declines when multilayer systems are examined. Section 6.3 further discusses the comparisons between 1D and 3D analyses for various profile types.

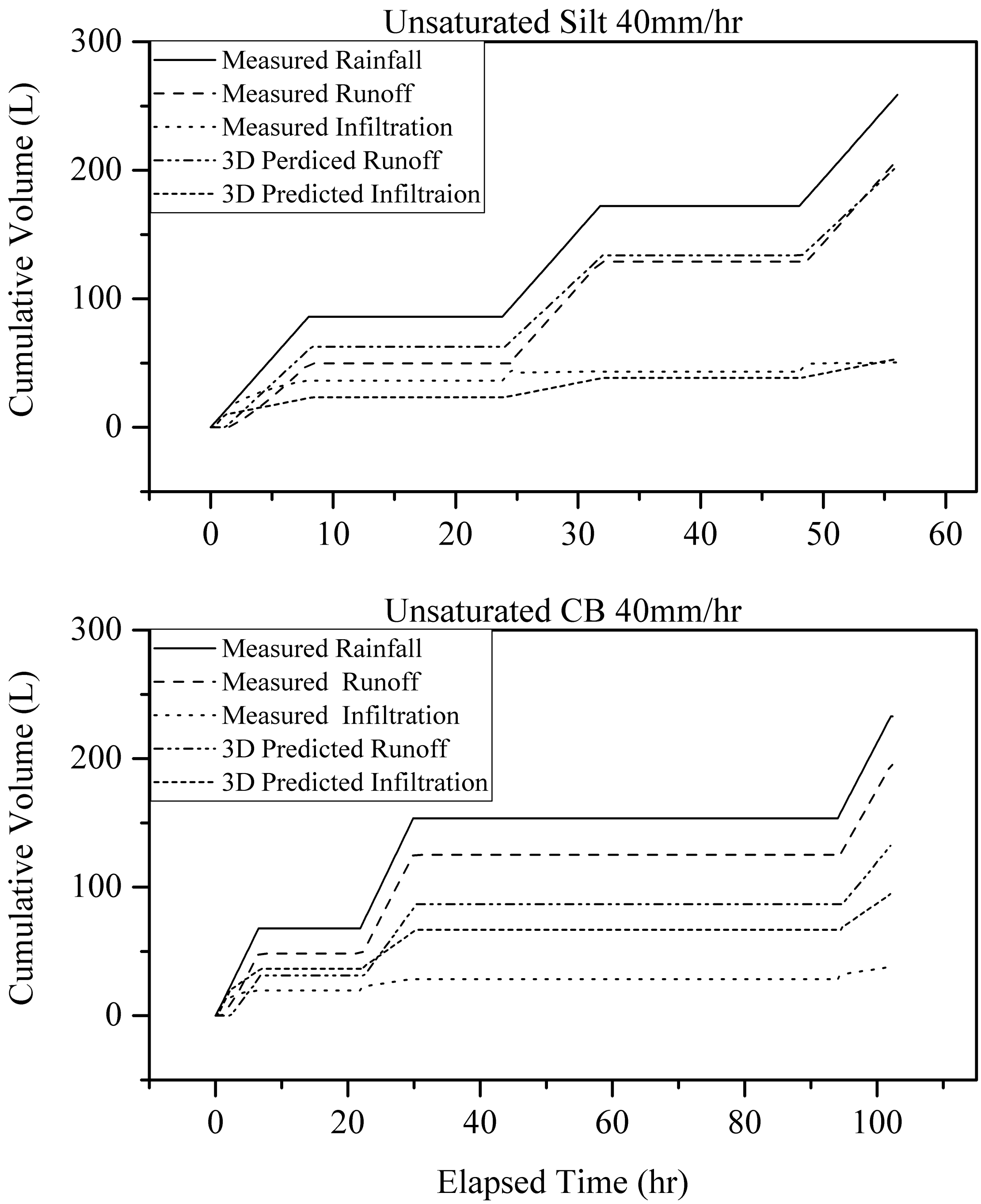

Figure 5.55 Measured versus 3D predicted water balance components for unsaturated silt (top) and unsaturated capillary barrier (bottom) profiles at a rainfall intensity of 40 mm/hr.

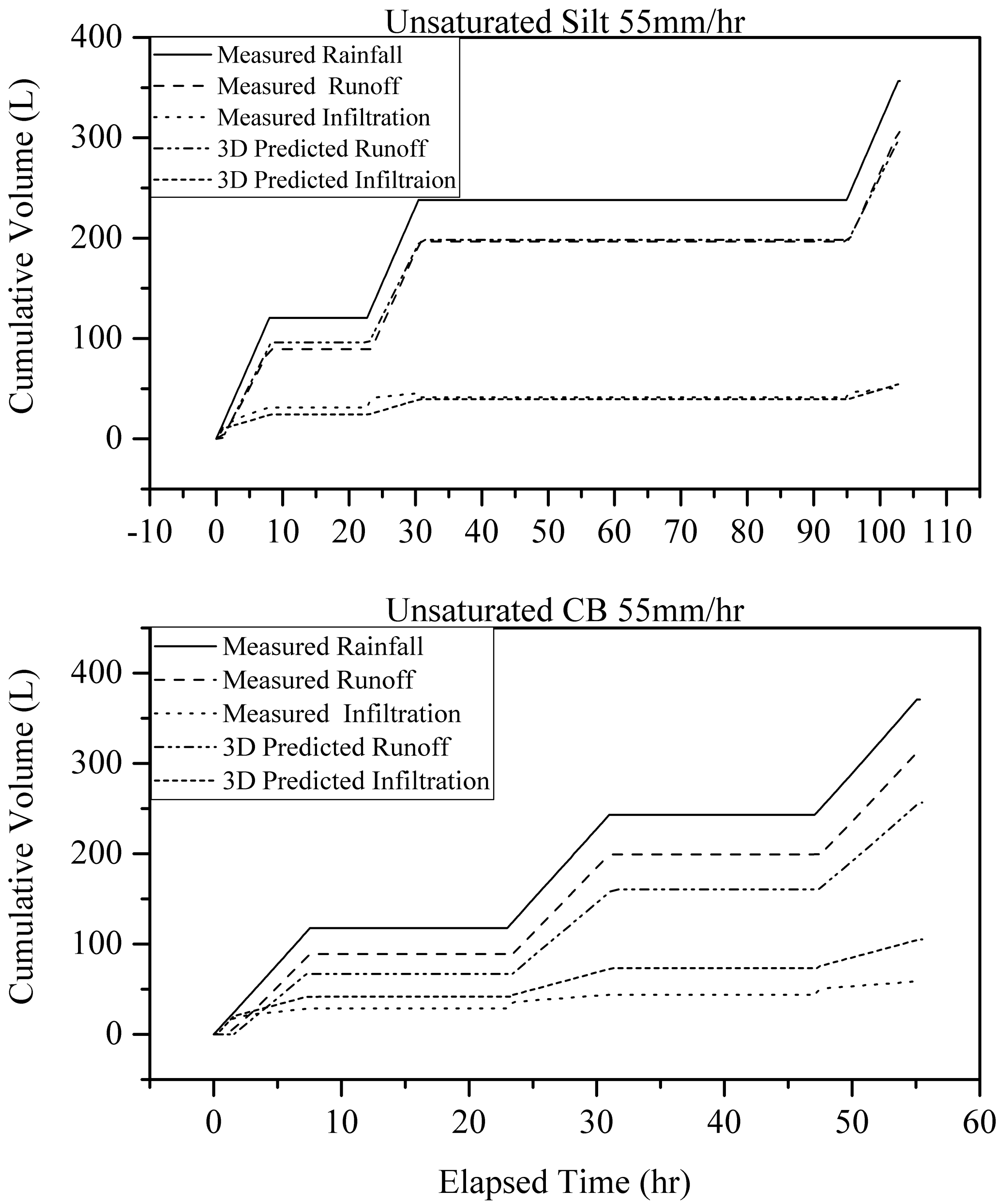

Figure 5.56 Measured versus 3D predicted water balance components for unsaturated silt (top) and unsaturated capillary barrier (bottom) profiles at a rainfall intensity of 55 mm/hr.

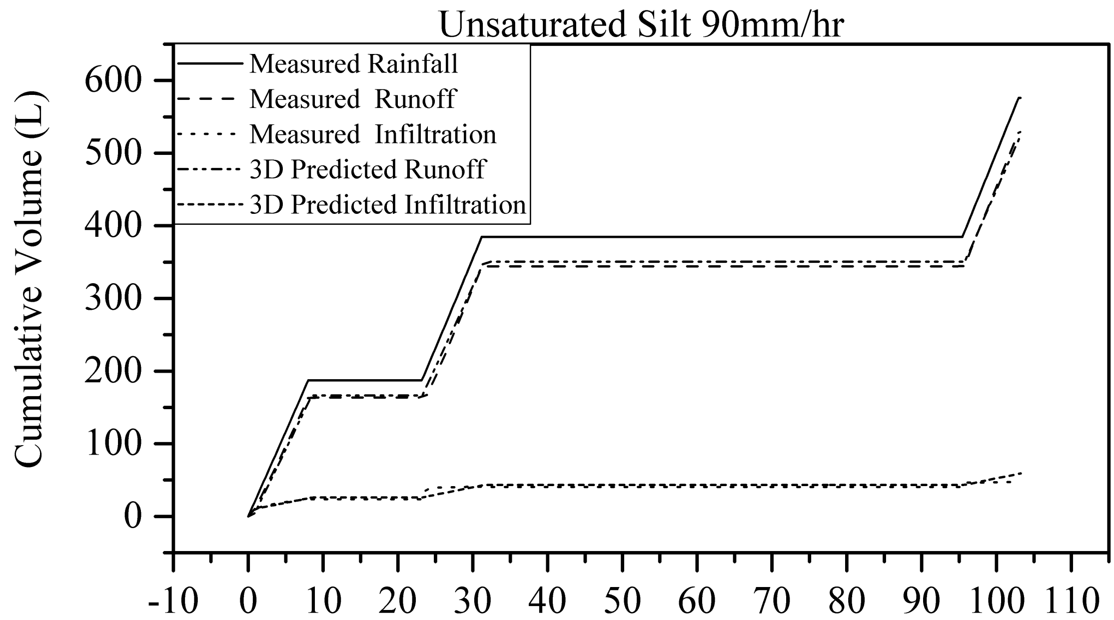

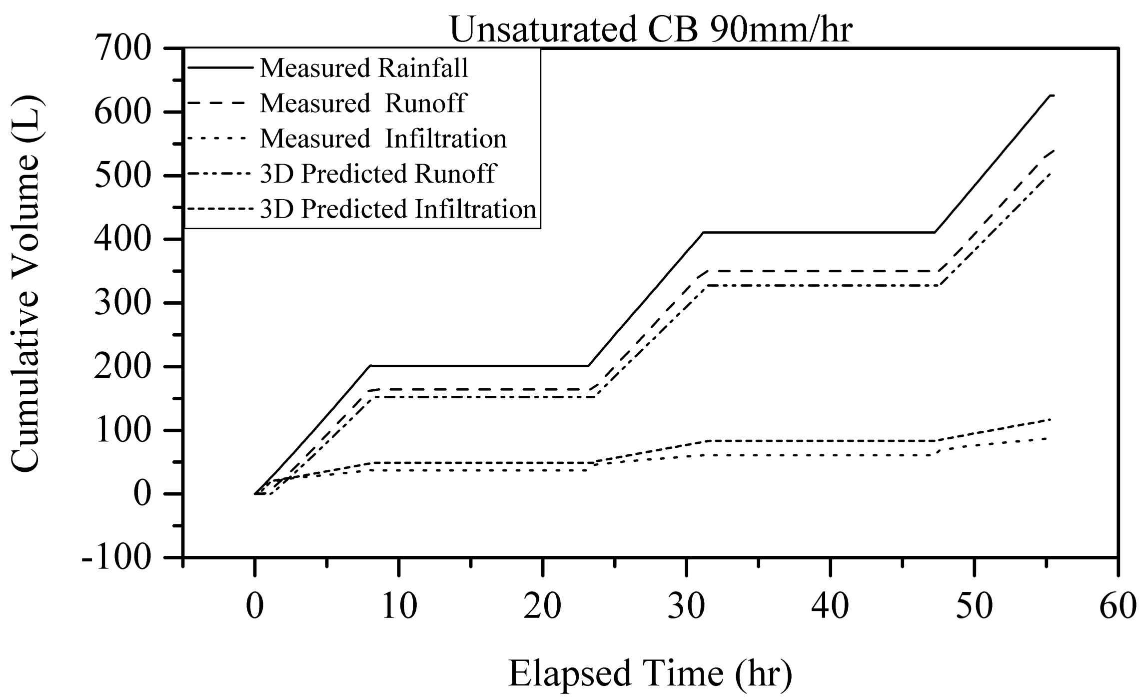

Figure 5.57 Measured versus 3D predicted water balance components for unsaturated silt (top) and unsaturated capillary barrier (bottom) profiles at a rainfall intensity of 90 mm/hr.

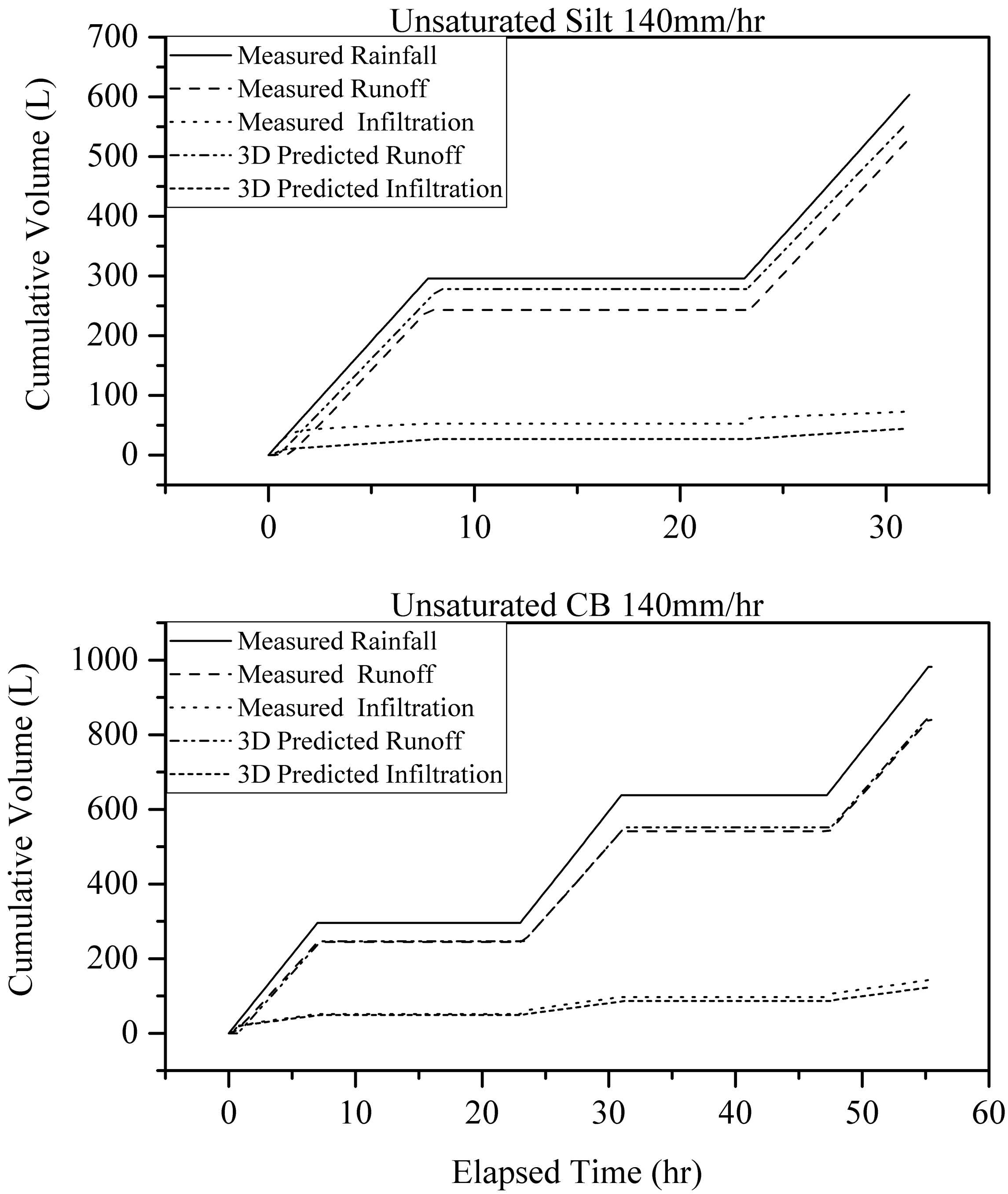

Figure 5.58 Measured versus 3D predicted water balance components for unsaturated silt (top) and unsaturated capillary barrier (bottom) profiles at a rainfall intensity of 140 mm/hr.

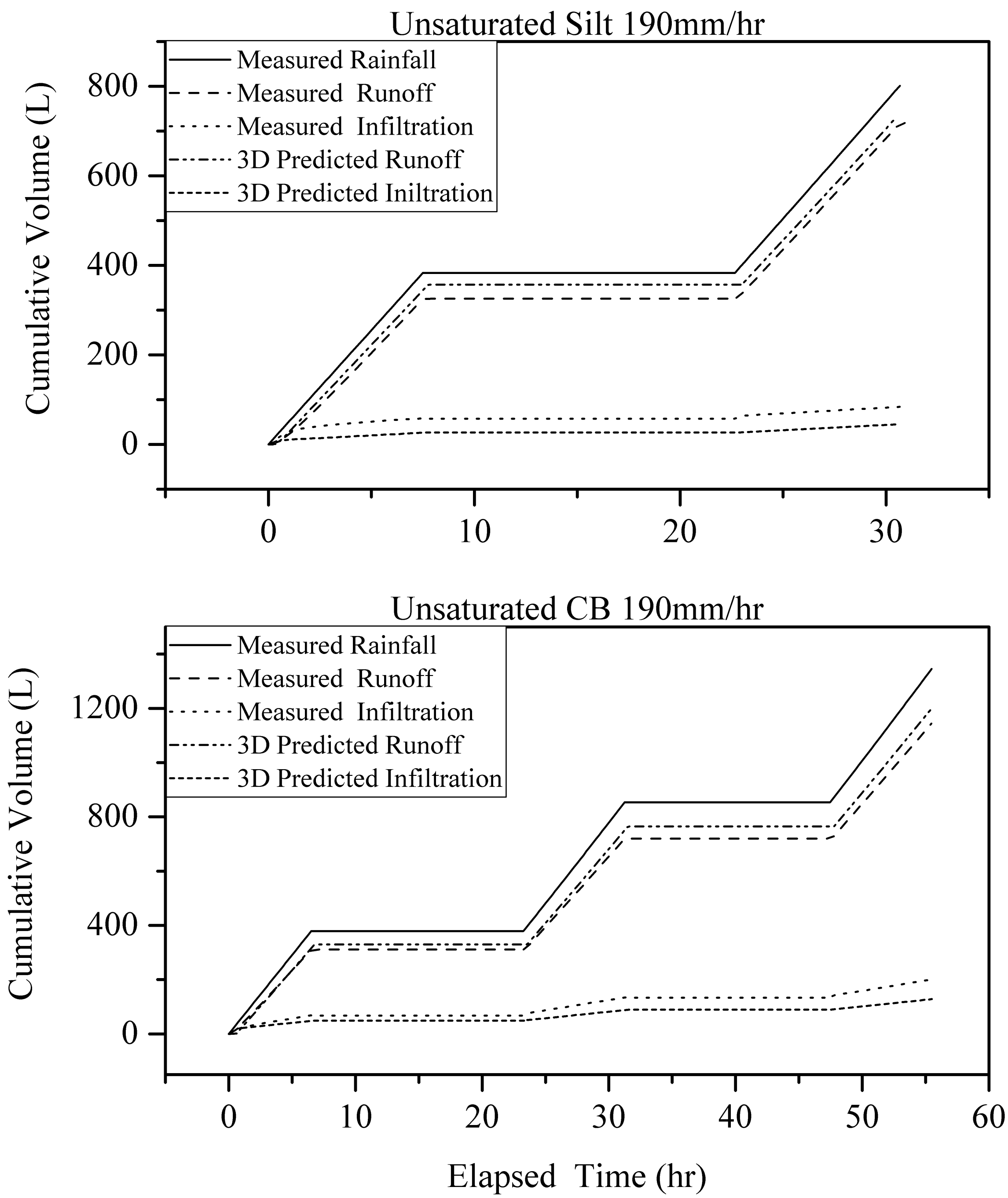

Figure 5.59 Measured versus 3D predicted water balance components for unsaturated silt (top) and unsaturated capillary barrier (bottom) profiles at a rainfall intensity of 190 mm/hr.

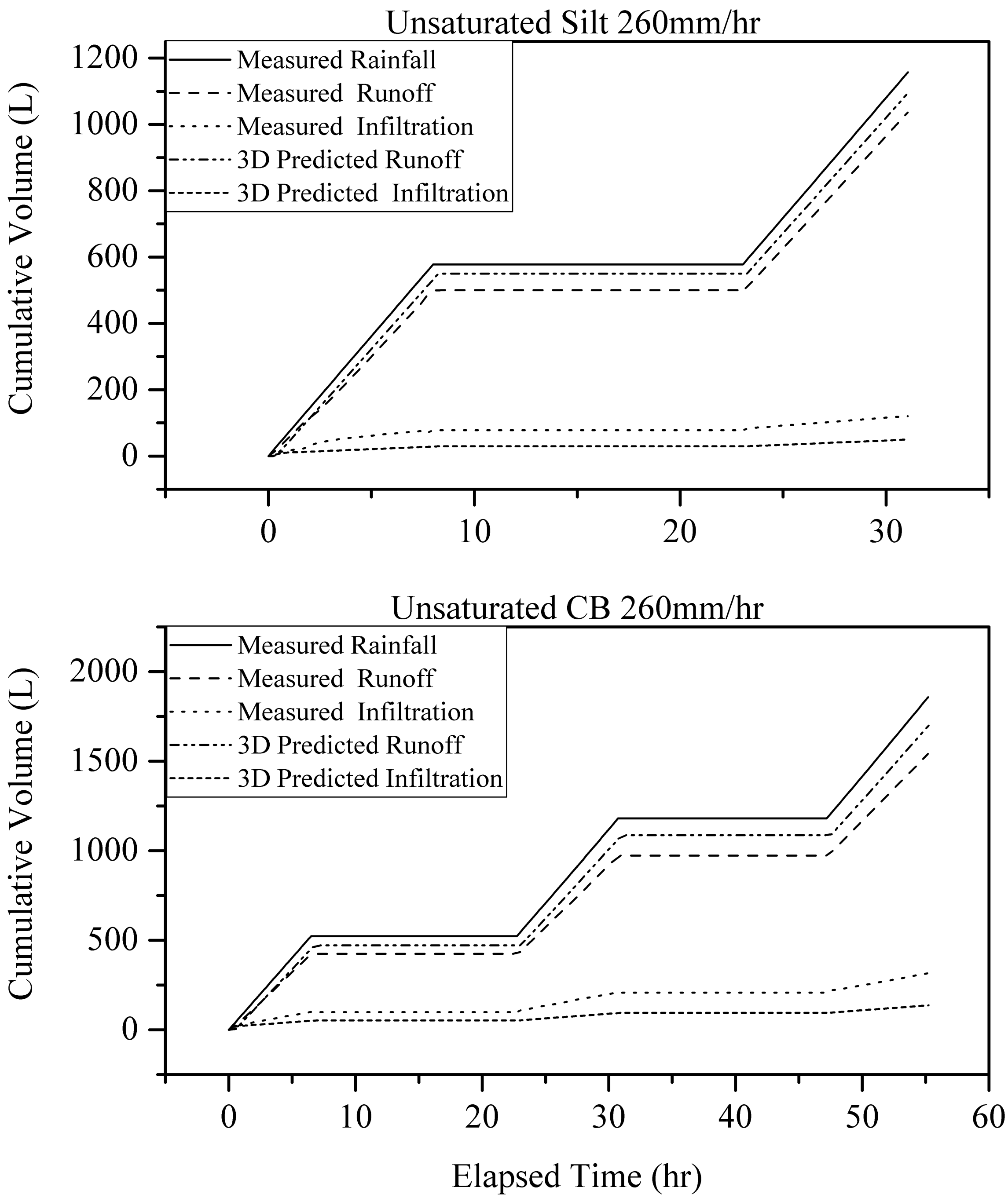

Figure 5.60 Measured versus 3D predicted water balance components for unsaturated silt (top) and unsaturated capillary barrier (bottom) profiles at a rainfall intensity of 260 mm/hr.

5.5. Case Study Results

Rainfall-runoff predictions on a field scale were investigated using the numerical model, SVFlux. A case study of the Savage River mine was investigated. Two locations in the mine were examined namely, the B-Dump and the Old Tailings Dam (OTD). Site descriptions and climate settings were described in Section 4.7.1. Material properties of both locations were presented in Section 4.7.2. Model input parameters and theoretical principals were provided in Section 4.7.4. Sensitivity analyses of runoff predictions were assessed in terms of the resolution of rainfall intensity input, and the variation in hydraulic conductivity – details can be found in Section 4.7.5.

5.5.1. Results of the B-Dump

Percentage differences between final predicted and measured cumulative runoff volumes summarized in Table 5.5 reveal that SVFlux results follow a trend comparable to the measured values. Still, a noticeable difference in actual numbers is evident. Comparisons of the predicted SVFlux volumes to the field measured cumulative runoff volumes are illustrated in Figure 5.61 and Figure 5.62 for B-Dump Catchment 1 and 2, respectively.

For ease of assessment, measured rainfall and runoff volumes are seen in blue and red series, respectively. Predicted runoff using the lowest, average, and highest measured K_{sat} are shown in green, orange, and purple series, respectively. Furthermore, rainfall resolution inputs of 15 minutes, event-averaged, and 24 hours are denoted by solid, dashed and dotted line styles, respectively.

B-Dump results indicate that the predicted runoff volumes are highly sensitive to both the hydraulic conductivity input and the resolution of rainfall input. The difference in K_{sat} did not exceed half an order of magnitude. Still, this relatively slight change in K_{sat} values produced significantly different runoff predictions. Similarly, the resolution of rainfall input had a distinct influence on the subsequent runoff volumes. Overall, SVFlux seemed to underestimate runoff in Catchment 1.

The measured runoff for the B-Dump Catchment 2 was best represented by SVFlux when the highest measured K_{sat} was input. This contrast between results of Catchment 1 and Catchment 2, despite consisting similar soils, can be traced back to the raw measured runoff data of both catchments. The percentage of precipitation that converted to runoff in Catchment 1 and Catchment 2 was about 97% and 33%, respectively, which can be attributed to more gentle slopes on Catchment 2.

The slope of the cover surface is a crucial factor influencing the onset of both runoff and infiltration. For covers made of the same materials, sloped surfaces can promote runoff, while flat surfaces promote ponding and, thus, infiltration. One-dimensional models do not consider the slope of cover systems. However, slope effect can be captured by inputting higher permeability, as is the case in Catchment 2, to better predict volumes of rainfall runoff.

Overall, the best runoff prediction for Catchment 1 was attained by using the lowest measured hydraulic conductivity K_{sat} for each material, and the highest resolution of rainfall intensity. Conversely, the best runoff prediction for Catchment 2 was using the highest measured hydraulic conductivity even when lower rainfall intensity resolution is used. This strongly suggests that a notion of the expected runoff may be necessary to calibrate input parameters for optimum numerical predictions results.

Table 5.5 Percentage difference between predicted and measured final cumulative runoff volumes for B-Dump catchments for sensitivity analyses cases.

Ksat \ Intensity	15-minute	Event-averaged	24-hour
Catchment 1			
Lowest measured	-4[4]	-13	-22
Average measured	-30	-41	-52
Highest measured	-51	-59	-66
Catchment 2			
Lowest measured	108	91	73
Average measured	58	33	10
Highest measured	14	-2	-22

[4] Negative values in percentage difference indicate that models underpredicted runoff volumes (i.e., predicted values are less than measured values).

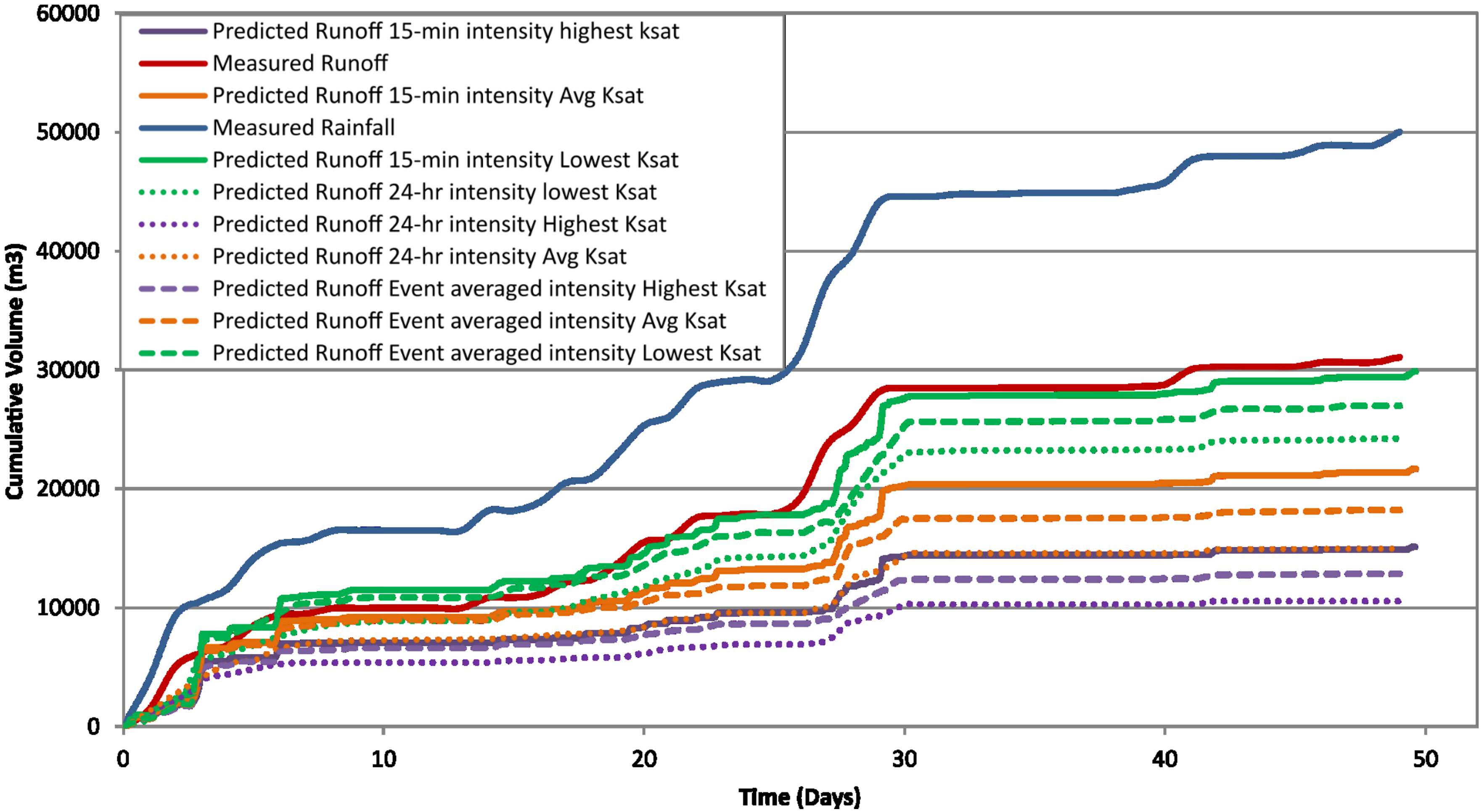

Figure 5.61 Comparison of measured versus predicted runoff cumulative volumes for B-Dump Catchment 1 using SVFLux.

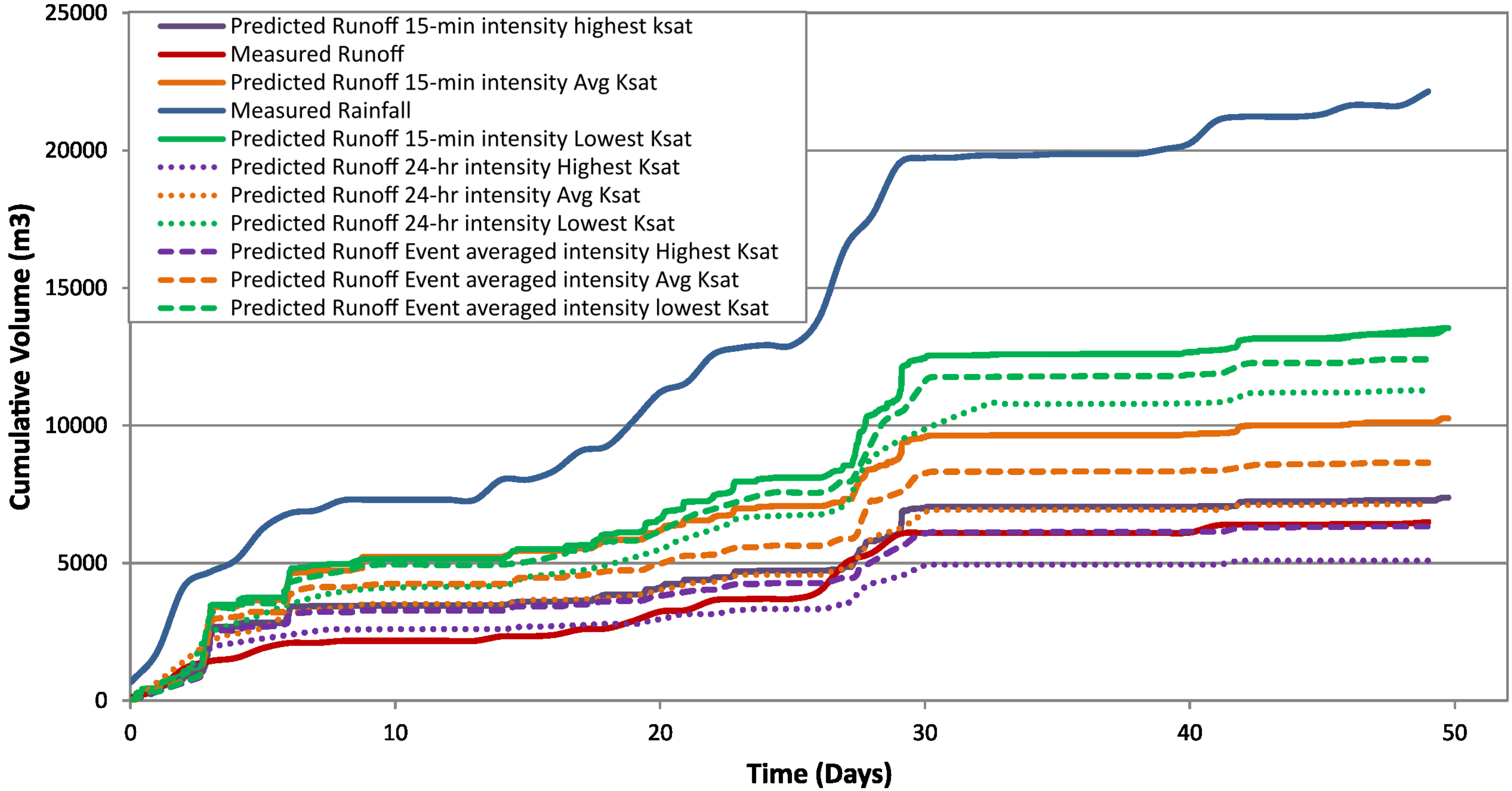

Figure 5.62 Comparison of measured versus predicted runoff cumulative volumes for B-Dump Catchment 2 using SVFlux.

5.5.2. Results of the Old Tailings Dam (OTD)

High-resolution runoff measurements were not available for the OTD. Therefore, the rainfall data available from B-Dump was used. The predicted runoff volumes are presented as a percentage of measured rainfall and are shown in Table 5.6. Predicted cumulative volumes of runoff for different input scenarios for the OTD Catchment A using SVFlux model are presented in Figure 5.63.

For the ease of assessment, measured rainfall is shown in blue series. Predicted runoff cumulative volumes using lowest, average, and highest measured K_{sat} are shown in green, orange, and purple series, respectively. Moreover, rainfall resolution input of 15 minutes, event-averaged, and 24 hours are denoted by solid, dashed, and dotted line styles, respectively.

As anticipated, runoff predictions using SVFlux were highly dependent upon both the saturated hydraulic conductivity and the resolution of rainfall. Only a minor change in K_{sat} input induced a significant variation in results.

OTD Catchment A has a slope similar to the B-Dump Catchment 2. Since no runoff measurements were available for OTD, similar logic of the rainfall resolution and slope/K_{sat} interdependency observed in the B-Dump analysis results should be considered when selecting an appropriate runoff estimate for OTD Catchment A. Therefore, a reasonable runoff volume for OTD Catchment A would be attained by using the highest K_{sat} and the highest rainfall resolution amounting to 11% of the measured rainfall.

Table 5.6 Predicted final cumulative runoff volumes as a percentage of measured final cumulative rainfall volumes for OTD Cathement A.

K_{sat} \ Intensity	15-minute	Event-averaged	24-hour
Lowest measured	29	23	16
Average measured	20	12	6
Highest measured	11	6	2

The following observations can summarize the major findings of the numerical modelling case study:

1. Numerical predictions of rainfall runoff are highly sensitive even to the slightest changes in the saturated hydraulic conductivity (K_{sat}).

2. Predictions of runoff varied up to 100% difference within half an order of magnitude difference in K_{sat}.

3. Predictions of rainfall runoff are sensitive to the resolution of rainfall data, though to a lesser extent compared to K_{sat}.

4. High-resolution rainfall input may result in higher computation times.

5. One dimensional predictions of rainfall runoff can be representative in soil covers modelling when field conditions and topography are properly understood.

6. An estimate of expected runoff volumes should exist to ensure a proper soil property selection and a correct interpretation of numerical modelling results.

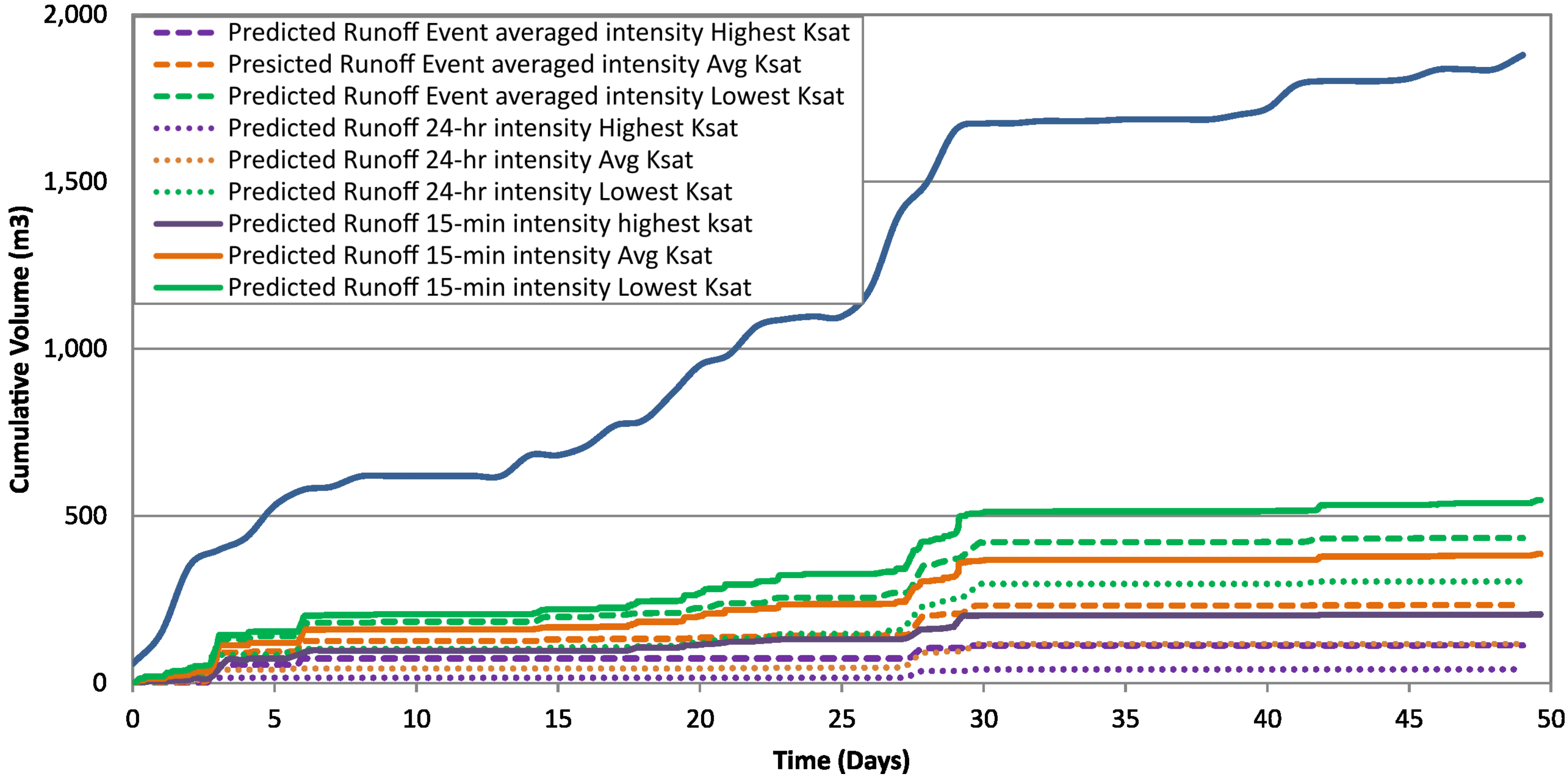

Figure 5.63 Comparison of measured rainfall versus predicted runoff cumulative volumes for OTD Catchment A using SVFLux.

5.6. Summary

Chapter 5 offered the results of soil properties investigation for each type of soil used in the laboratory component. These include particle size distributions, saturated hydraulic conductivities, infiltration capacity functions and soil water characteristics curves.

Furthermore, detailed results of the laboratory rainfall runoff experiments on low permeability and capillary barrier profiles were presented. Laboratory results were categorized in terms of cumulative volumes, rates, volumetric water content and matric suction measurements. Results were presented for saturated and unsaturated profiles individually.

Moreover, the results of one- and three-dimensional numerical predictions of laboratory experiments were offered. Predictions for saturated and unsaturated initial state for each profile type were discussed. Percent differences between laboratory-measured and numerically-predicted values were presented.

Finally, sensitivity assessment results for the Savage River Mine case study were discussed. Results for the water shedding cover, the B-Dump, and the Old Tailings Dam were presented, separately. Percent differences between field-measured and numerically-predicted volumes were compared. Results demonstrated that saturated hydraulic conductivity input and the resolution of rainfall input both profoundly influenced numerically-predicted volumes.

CHAPTER 6. Discussion of Major Findings

6.1. Introduction

The primary objective of this study was to examine the process of rainfall runoff in soil cover systems. A theoretical context was provided in Chapter 3. Chapter 4 described three tiers of methodology, including laboratory tests, numerical modelling of laboratory tests, and a field case study. Results were presented in Chapter 5. The major results are interpreted and analyzed herein.

6.2. Laboratory Results

Rainfall-runoff responses in low permeability and capillary barrier profiles were investigated in a specially designed rainfall simulator apparatus under different rainfall intensities and initial conditions. Section 5.3 presented the results individually for each initial soil and cover type.

6.2.1. Empirical Relationship between Applied Rainfall and Runoff Response

A positive linear correlation between the applied rainfall volumes and the subsequent runoff volumes was evident in both types of profiles regardless of initial saturation. The direct increase in the volume of applied rainfall-induced a proportional increase in the volume of subsequent runoff regardless of the applied rainfall intensity for both types of soil profiles as seen in Figure 6.1 and Figure 6.2. The correlation can be expressed as follows:

$$R = a.\ P + b \tag{6.1}$$

where

R	=	Cumulative volume of runoff
P	=	Cumulative volume of rainfall
a	=	Empirical coefficient function of the type of profile

b = Empirical coefficient function of the data-fitting technique

Parameter a, indicative of the type of profile, is represented by the slope of the correlation function. For single layer profiles, a slope of 0.9 for both saturated and unsaturated profiles was observed. For capillary barrier profiles, the slope was around 0.8. Parameter b represents the intercept of the correlation function. The intercept has no physical or intrinsic denotation, it purely eliminates bias in the linear regression residuals, and is, therefore an artifact of the data-fitting scheme. Table 6.1 summarizes the empirical correlation parameters obtained for each type of profile under saturated and unsaturated conditions.

Table 6.1 Summary of empirical correlation parameters obtained for each type of profile.

Parameter	a	b	R^2
Saturated silt profiles	0.942	4.278	0.999
Unsaturated silt profiles	0.900	-14.527	0.997
Saturated capillary barrier	0.841	10.154	0.997
Unsaturated capillary barrier	0.839	-4.192	0.999

This empirical correlation can be used for covers of comparable materials when rainfall volumes, or rainfall intensity and storm duration, are available. This method is suitable to estimate potential volumes of runoff. The availability of such estimate can help serve as a measure for numerical prediction since rarely do we have runoff measurements. Attention should be given when implementing this correlation for sloping profiles as the correlation was made for a gentle slope of 1%. Higher runoff may result in profiles with significant slopes as discussed in Section 5.5.1.

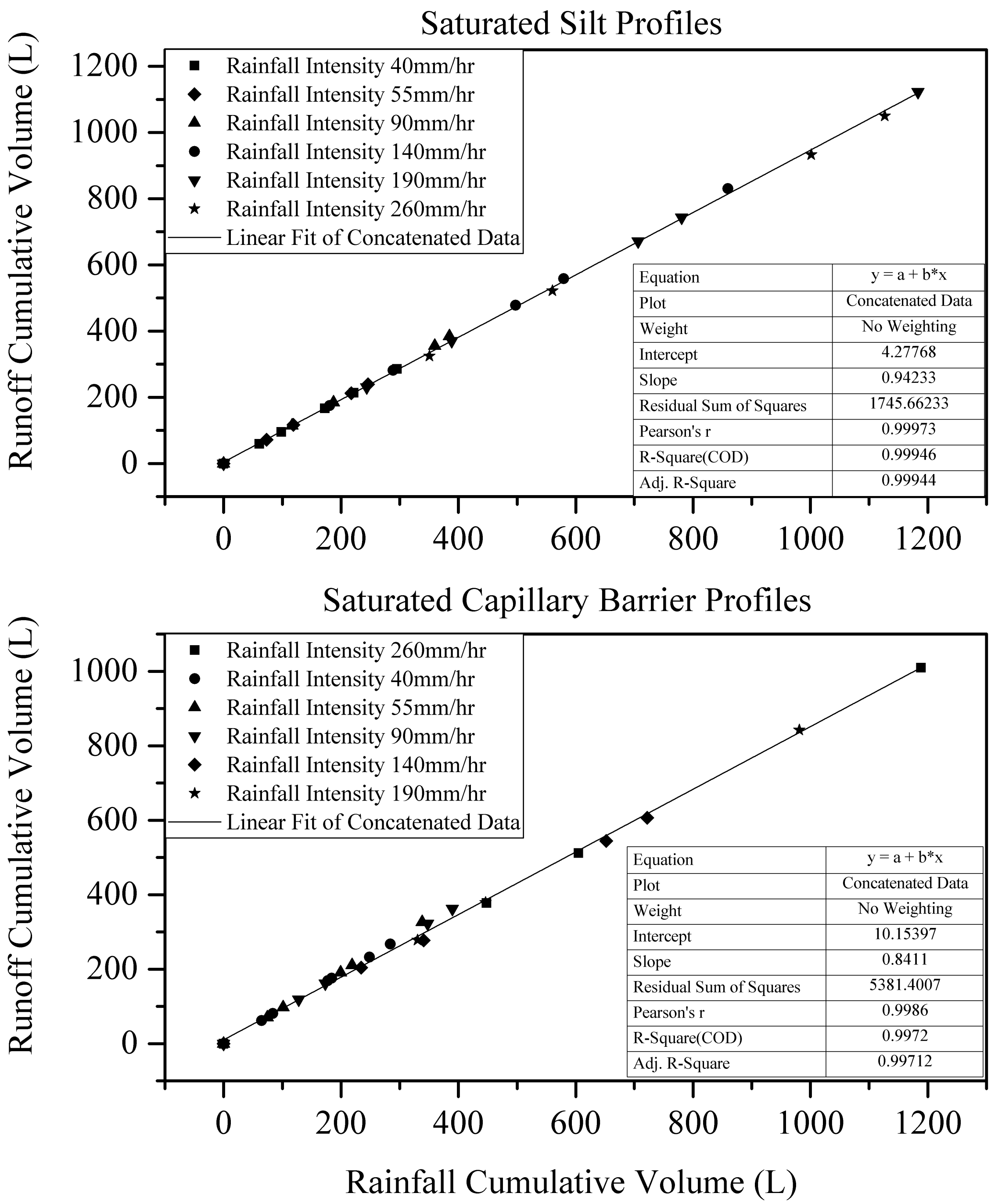

Figure 6.1 Relationship between applied rainfall volumes and resulting runoff volumes in saturated silt (top) and saturated capillary barrier profiles (bottom).

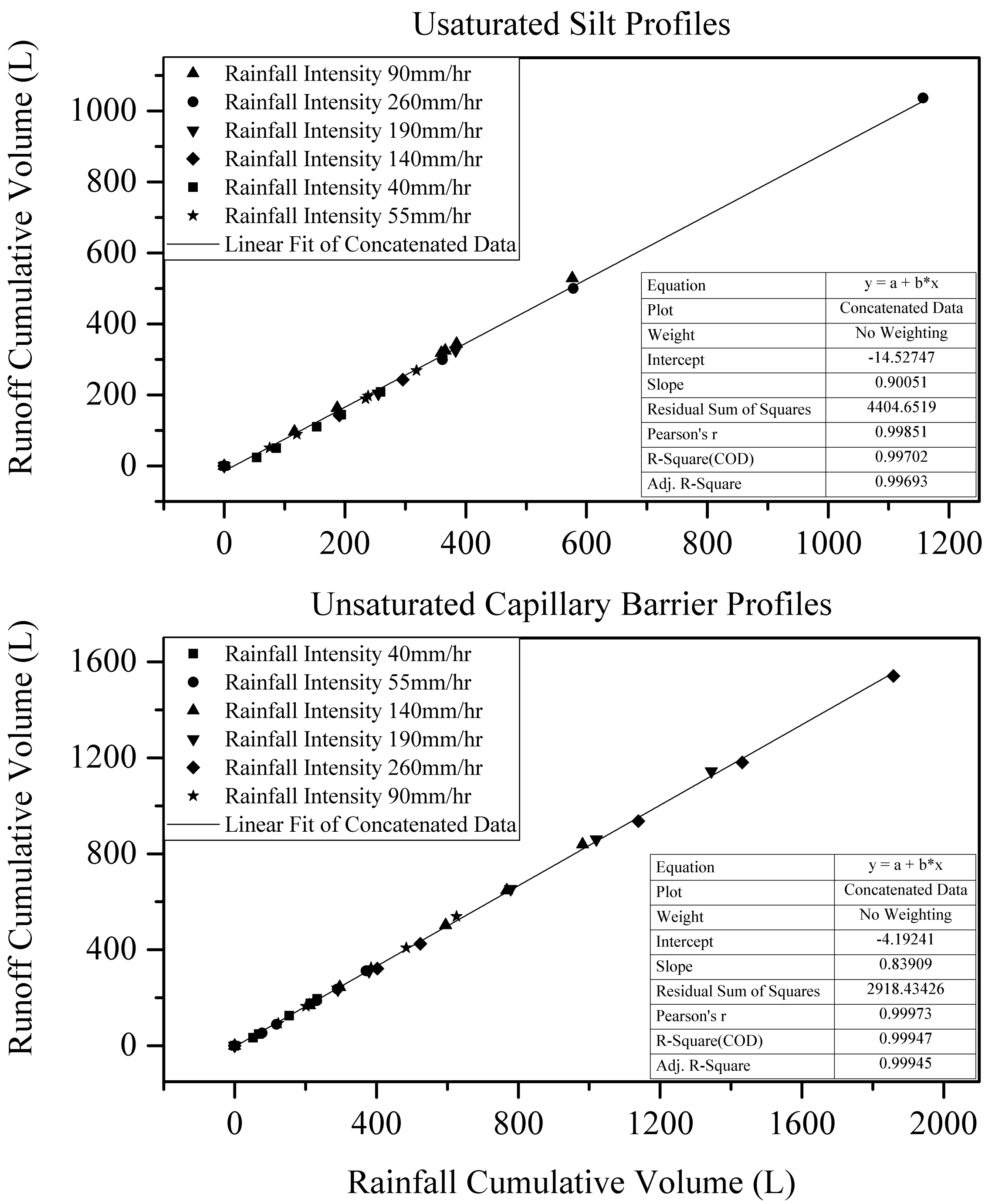

Figure 6.2 Relationship between applied rainfall volumes and resulting runoff volumes in unsaturated silt (top) and unsaturated capillary barrier profiles (bottom).

6.2.2. Runoff as a Percentage of Applied Rainfall

Final cumulative runoff volumes as a percentage of the final cumulative rainfall volumes applied to each profile type and initial state are summarized in Table 6.2. The results of saturated silt profiles show that up to 98% of applied rainfall converts to runoff. Such response was anticipated since the profiles were at full saturation. The minute difference in percentage can be expected due to a change in density. However, low percentages of runoff at rainfall intensities exceeding 90 mm/hr was an interesting feature to investigate.

Further examination of percentage trends of runoff related to applied rainfall was conducted. Figure 6.3 illustrates a plot of runoff as a percentage of applied rainfall volumes with respect to applied rainfall intensity. The figure reveals a general decrease in runoff percentage; the decrease becomes especially sharp for saturated capillary barrier profiles when applied rainfall intensity exceeds 90 mm/hr. Time-lapse photographs were analyzed to investigate this seemingly illogical trend. The photographs revealed that in some of these scenarios the flume was not filled completely. This caused water to be entrapped within the flume as a ponding depth as shown in Figure 6.4. Because of how infiltration volumes were determined, this top ponding depth was included in the calculated infiltration creating an inaccurate representation of infiltration.

The volume of the entrapped water was determined using AutoCAD by obtaining the area within the black perimeter shown in Figure 6.4. Percentages were then corrected for the entrapped water volume. Corrections were made by adding the volume of entrapped water to the final cumulative runoff volume and then concluding the corrected percentage of runoff. However, the trends remained predominantly unchanged as shown in Figure 6.5.

Table 6.2 Summary of final cumulative runoff volume as a percentage of final cumulative applied rainfall volume.

Profile type	Final cumulative runoff volumes as a percentage of final cumulative rainfall volumes (%)			
	Saturated profiles		Unsaturated profiles	
Rainfall intensity (mm/hr)	silt	capillary barrier	silt	capillary barrier
40	97	94	80	84
55	97	96	86	84
90	99	92	92	86
140	97	84	88	85
190	95	86	89	85
260	93	85	89	83

Due to the way infiltration was determined, these entrapped water volumes erroneously counted as infiltration. Therefore, the final cumulative infiltration volume was corrected similarly to runoff volumes corrections. Table 6.3 summarizes the corrected final cumulative infiltration volumes as a percentage of the final cumulative rainfall volumes for each profile. Similarly, Figure 6.5 illustrates the percentages as a function of applied rainfall intensities. Parallel trends of increasing infiltration percentage are evident in the saturated silt, unsaturated silt, and unsaturated capillary barrier profiles in rainfall intensity exceeding 90 mm/hr.

Statistically, the mean and (standard deviation) for final cumulative infiltration volume in saturated silt, saturated capillary barrier, unsaturated silt and unsaturated capillary barrier profiles are 3% (2%), 9% (6%), 11% (3%) and 14% (1%), respectively. In terms of rates, the mean and (standard deviation) rate of infiltration as a percentage of applied rainfall rate are 5% (2%) and 9% (6%) for saturated silt and saturated capillary barrier profiles, respectively.

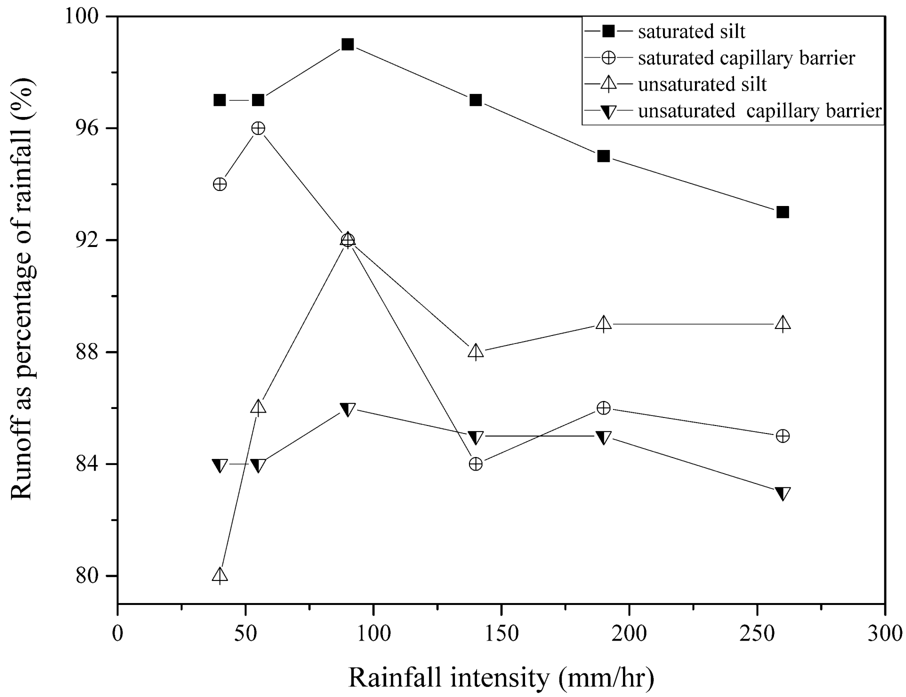

Figure 6.3 Trends of final cumulative runoff as a percentage of final cumulative applied rainfall with respect to applied rainfall intensity as measured.

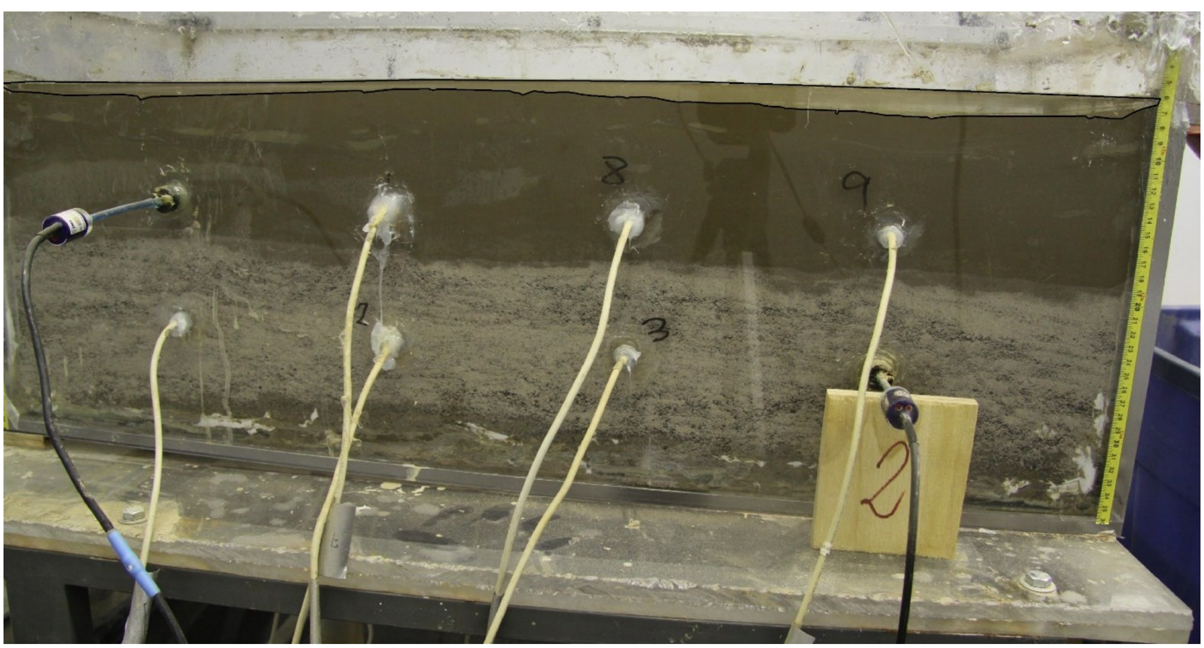

Figure 6.4 A sample of water ponding on top of unsaturated capillary barrier profiles (rainfall intensity in this photograph is 40 mm/hr).

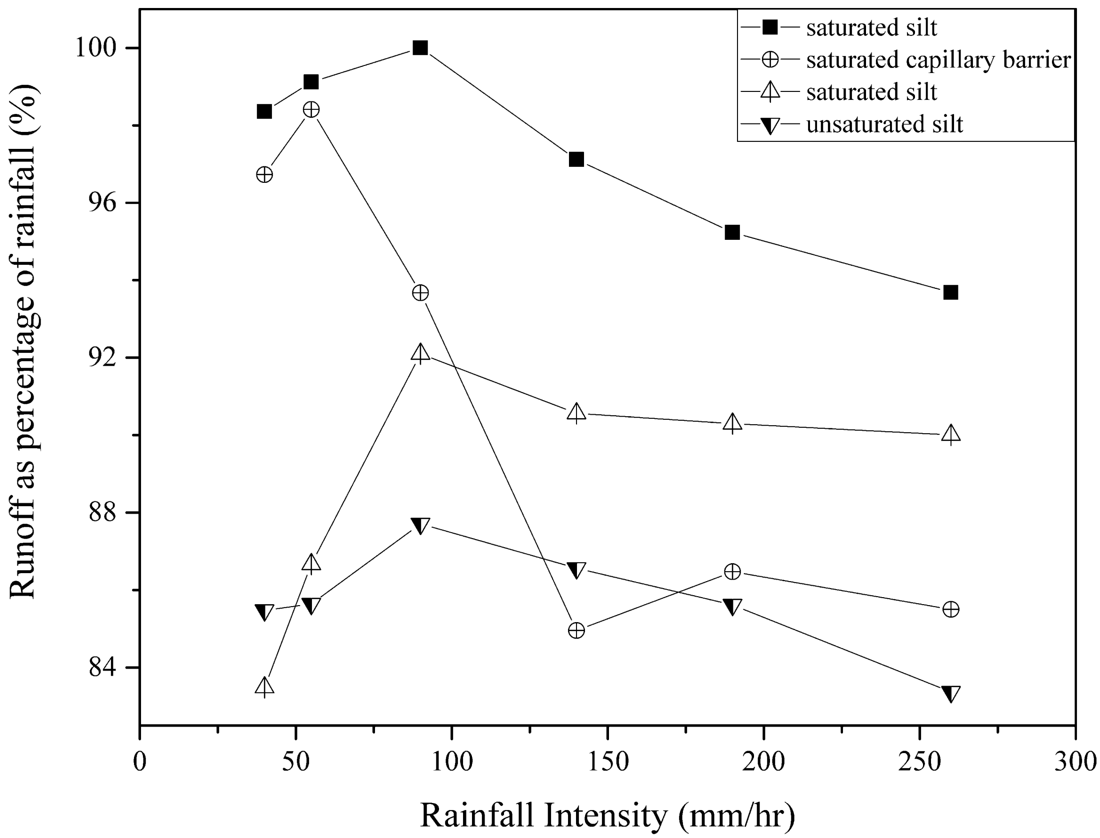

Figure 6.5 Trends of final cumulative runoff as a percentage of final cumulative applied rainfall with respect to applied rainfall intensity as corrected by ponding water volume.

The most plausible explanation for the sharp decrease in runoff percentage trends in the saturated capillary barrier profiles may, perhaps, be as follows: the capillary barrier profiles thickness is made up of 50% tailings beach sand. The sand has a saturated hydraulic conductivity five orders of magnitude higher than that of the overlying silt. As both layers become saturated, the capillary barrier break no longer limits infiltration as seen in unsaturated profiles. On the contrary, higher infiltration is allowed into the profile, and, subsequently, lower runoff. This conclusion means that when capillary barrier profiles are designed for high rainfall climates, the design must ensure proper desaturation – otherwise, the profile is rendered inept.

Table 6.3 Summary of infiltration rates as a percentage of applied rainfall rate.

	Final cumulative volumes of infiltration as a percentage of final cumulative volumes of applied rainfall (%).			
Profile	Saturated		Unsaturated	
Intensity (mm/hr)	silt	capillary barrier	silt	capillary barrier
40	2	3	17	15
55	1	2	13	14
90	0	6	8	12
140	3	15	9	13
190	5	14	10	14
260	6	14	10	16

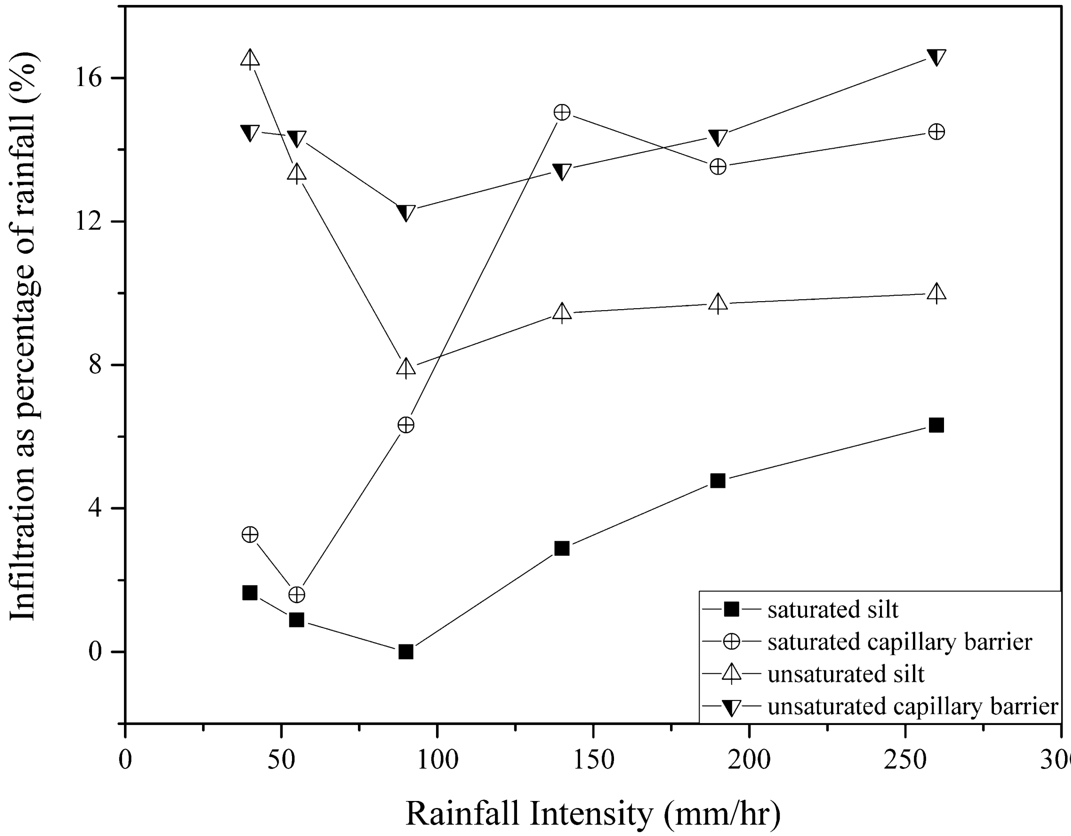

Figure 6.6 Final cumulative volumes of infiltration as a percentage of final cumulative volumes of applied rainfall.

6.2.3. Parameters Controlling Rainfall-Runoff

Results from the laboratory experiments indicate that for saturated profiles, the saturated hydraulic conductivity, along with rainfall intensity, control runoff volumes. Similarly, for unsaturated profiles, the infiltration capacity function, along with rainfall intensity, control runoff volumes. Let us examine the potential of using these two easily measured parameters to predict surface runoff.

6.2.3.1. Saturated Profiles

Jubinville (2013) proposed a simple analytical solution for single layer saturated soil covers based on Wilson (2006). Figure 6.6 illustrates the general premise of the solution summarized as follows: when the rainfall intensity does not exceed the saturated hydraulic conductivity of the profile K_{sat}, then no runoff is generated, and rainfall infiltrates the soil profile at the rate of K_{sat} or rainfall intensity, whichever is smaller. When the rainfall intensity exceeds K_{sat}, then runoff rate can be calculated as the arithmetic difference between the rainfall intensity and the material saturated hydraulic conductivity $K_{sat.}$ Rainfall intensity function can take on any shape, the normal distribution in Figure 6.6 is for illustration only.

In the laboratory study, the rainfall intensity was constant throughout each test. Therefore, the runoff volumes can be predicted using simple 1D arithmetic for each profile as follows:

$$R = (i - k_{sat})\ t\ A \qquad (6.2)$$

where,

R = runoff volume [L^3]

i = rainfall intensity [L/T]

k_{sat} = saturated hydraulic conductivity of the soil [L/T]

t = duration of rainfall

A = profile area [L^2]

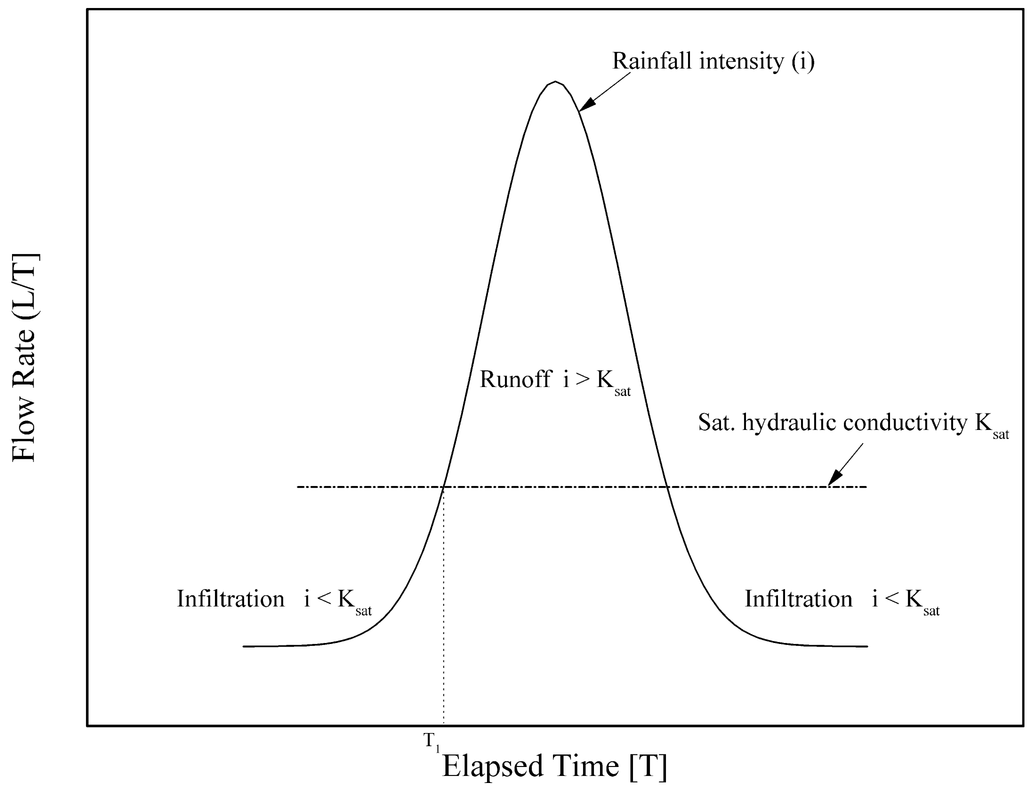

Figure 6.7 A simplified schematic representation of the parameters controlling runoff generation in saturated soils (Wilson, 2006: after Jubinville, 2013).

The results of the analytical calculations of runoff volumes using Equation 6.2 are summarized in Table 6.4. Cumulative volumes of runoff are compared using the percentage difference between laboratory-measured and calculated values. Detailed calculations of rainfall volumes are provided for each profile at the corresponding rainfall intensity in Appendix V. Runoff calculations were limited to the first eight hours of testing where continuous application of rainfall occurred. Results can be easily extended to a full period of testing by cumulatively adding runoff volumes at each duration.

In conclusion, the results indicate that for saturated silt profiles, percentage difference results ranged between an exact match and up to 21%. For saturated capillary barrier profiles, a very good agreement was obtained at low rainfall intensities, whereas greater discrepancies arose at high rainfall intensities. The limit between low and high intensities, in this case, is the rainfall intensity of 90 mm/hr.

Table 6.4 Comparison between measured and predicted runoff values using the infiltration capacity function in the saturated profiles.

Profile type	Rainfall Intensity (mm/hr)	Calculated Final Cumulative Runoff Volume (L)	Measured Final Cumulative Runoff Volume (L)	Percentage difference between measured and calculated volumes (%)
saturated silt profiles	40	97.7	95.5	-2%
	55	115.9	116.4	0%
	90	185.6	184.5	-1%
	140	288.4	280.9	-8%
	190	377.3	369.0	-8%
	260	542.8	521.5	-21%
Saturated capillary barrier profiles	40	80.1	81.0	1%
	55	98.3	97.6	-1%
	90	166.1	161.7	-4%
	140	304.8	276.9	-28%
	190	445.8	379.0	-67%
	260	511.0	511.6	1%

6.2.3.2. Unsaturated Profiles

Using K_{sat} to estimate runoff in unsaturated profiles with the assumption that the immediate soil surface should be saturated for runoff to occur (Smith 2002), is fundamentally flawed. There can be a significant amount of runoff across the ground surface even when the profile is unsaturated as seen in the laboratory results. Failure to include the substantial runoff that can occur in the unsaturated zone may lead to unrealistic predictions.

So, the question becomes: how can we predict rainfall runoff without overlooking the period when the profile is unsaturated? What is the equivalent unsaturated soil property that can characterize rainfall runoff and can be simply measured? The answer is quite simple: it is the infiltration capacity function. The infiltration capacity function can be considered the controlling parameter to quantify water flow through unsaturated media. Surface runoff would be a function of both the applied rainfall intensity and the soil infiltration capacity function as shown in the laboratory experiments on the unsaturated profiles. Field infiltration capacity functions can be simply obtained using a field infiltrometer or a column test in the laboratory. The test is both time- and cost-effective. Rather simple test steps were described in Section 4.3.2.2, and the calculations sheet is presented in Appendix VI.

The notion of calculating runoff in unsaturated profiles based on infiltration capacity functions follows the logic illustrated in Figure 6.7, and is summarized as follows: when the rainfall intensity does not exceed the infiltration capacity of the profile (I_c), then no runoff is generated, and rainfall infiltrates the soil profile at the rate of I_c or rainfall intensity, whichever is smaller. When the rainfall intensity exceeds the I_c, then runoff rate can be calculated as the integration of the arithmetic difference between the rainfall intensity and the infiltration capacity function.

For the laboratory results of this study, runoff volumes can be predicted for each profile using Equation 6.3.

$$R = \int_0^t (i - I_c) \ \ t \ \ A \tag{6.3}$$

where,

R	=	runoff volume [L^3]
i	=	rainfall intensity [L/T]
I_c	=	infiltration capacity of the soil [L/T]
t	=	duration of rainfall
A	=	profile area [L^2]
$\int_0^t (i - I_c) \ \ t$	=	area between the two curves shown in Figure 6.8

The results of the analytical calculations of runoff volumes based on the infiltration capacity function are summarized in Table 6.5. Cumulative volumes of runoff are compared using the percentage difference between laboratory measured and calculated values.

Calculations of the runoff rate were conducted via the software Origin. The area between the applied rainfall intensity and the infiltration capacity function was determined. This area was then multiplied by the area of the profile creating runoff volumes. Calculations for each unsaturated profile at each rainfall intensity are provided in Appendix VI.

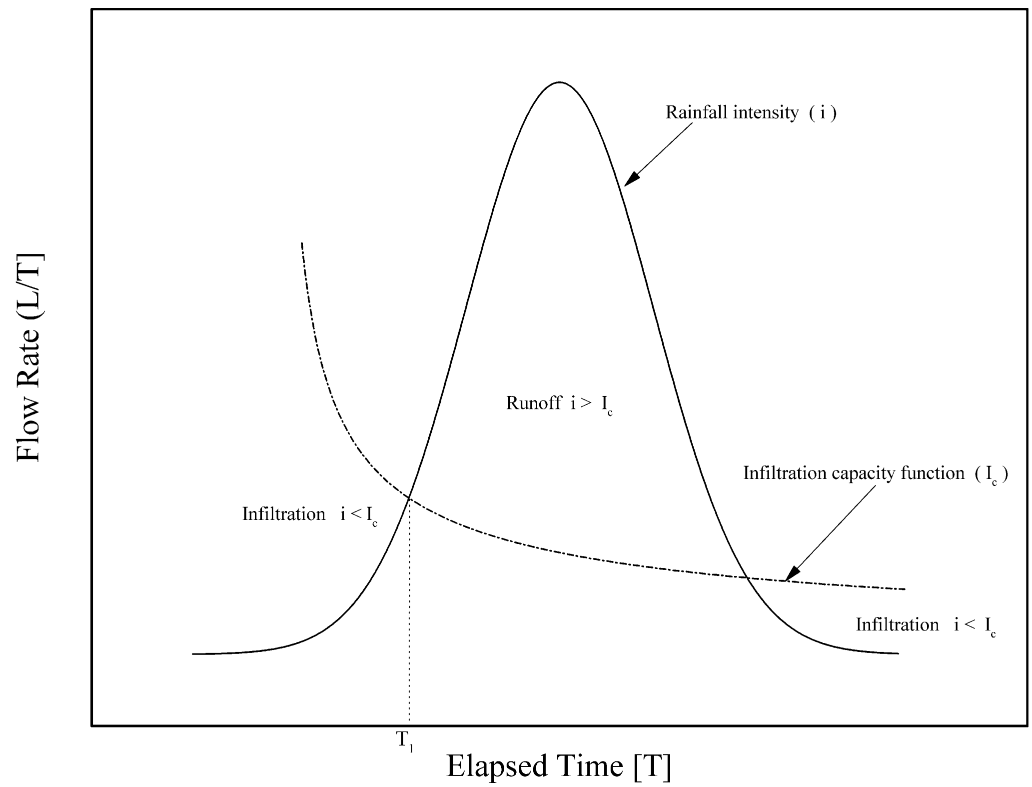

Figure 6.8 A simplified schematic representation of the parameters controlling runoff generation in unsaturated soils.

An important point to emphasize is that the normal distribution of the rainfall rate shown in Figure 6.8 is for illustration purposes only. Rainfall events can take on any distribution of rate variation with time. During the laboratory experiments, rainfall intensities were applied at a constant rate throughout each scenario. Nevertheless, the infiltration capacity function shown in Figure 6.8 is the general trend for the infiltration to occur. Infiltration capacity functions for both Devon silt and tailings beach sand during the soil characterization (discussed in Section 5.2.4) exhibited the same trend with a different magnitude. Furthermore, the actual measured infiltration rates within the flume during the laboratory experiments exhibited similar general trends.

Table 6.5 Comparison between measured and predicted runoff values using the infiltration capacity function in the unsaturated profiles.

Profile type	Rainfall Intensity (mm/hr)	Calculated Final Cumulative Runoff Volume (L)	Measured Final Cumulative Runoff Volume (L)	Percentage Difference between Measured and Calculated Volumes (%)
unsaturated silt profiles	40	46.0	49.8	4%
	55	102.0	89.1	-13%
	90	173.6	163.2	-10%
	140	273.3	243.24	-30%
	190	365.3	325.7	-40%
	260	504.4	499.1	-5%
unsaturated capillary barrier profiles	40	60.5	48.2	-12%
	55	105.1	88.9	-16%
	90	178.6	164.0	-15%
	140	272.8	244.5	-28%
	190	347.6	311.1	-36%
	260	494.0	424.7	-69%

A statistical summary of the analytical solution for both saturated and unsaturated profiles is shown in Figure 6.9. Overall, analytical predictions provide a reasonably good first estimate of runoff volumes, especially at or below rainfall intensities 90 mm/hr.

Attaining satisfactory results from one-dimensional analytical solution based solely on rainfall intensity and saturated hydraulic conductivity (K_{sat}) in saturated soils, and rainfall intensity and infiltration capacity (I_c) in unsaturated soils, can be considered significant. Unlike tests, such as the SWCC that are time- and cost-intensive, the soil parameters K_{sat} and Ic can be measured easily in the laboratory. This solution can have a substantial practical value in field applications since runoff measurements are rarely available to help guide, calibrate, and address the sensitivity of runoff numerical predictions.

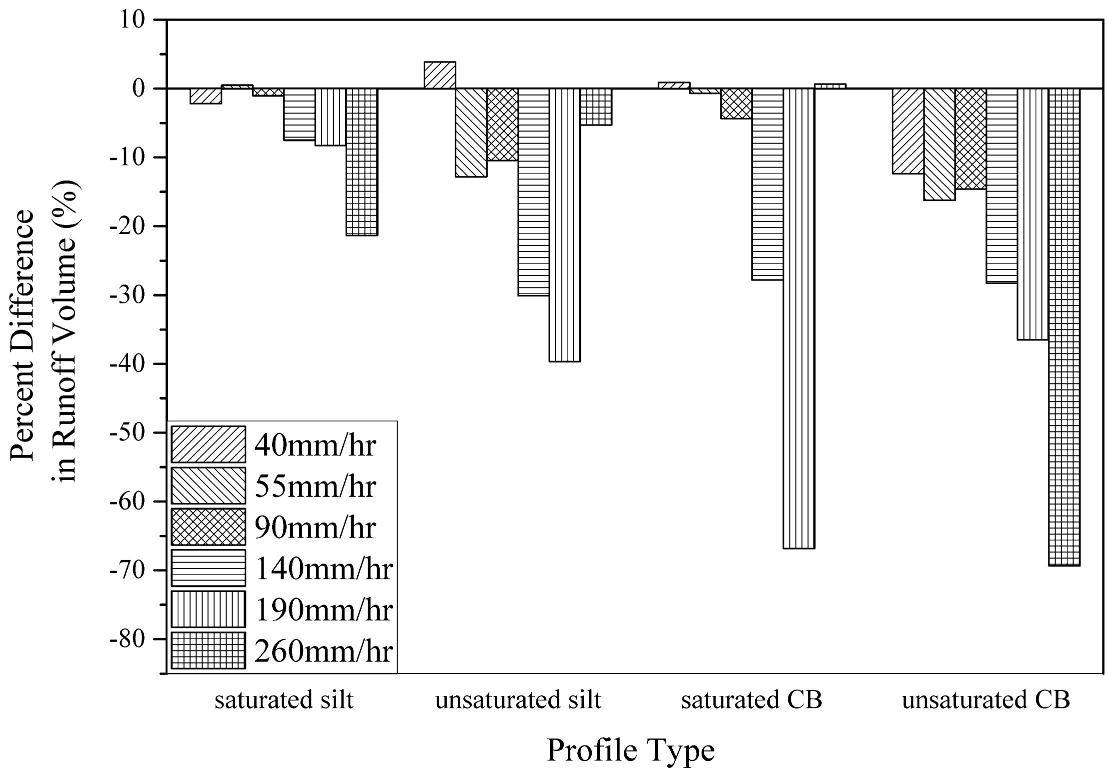

Figure 6.9 Percentage difference between the laboratory-measured and analytical solution of final cumulative runoff volumes denoted by profile type and the applied rainfall intensity.

6.3. Numerical Modelling of Laboratory Experiments

Numerical predictions of runoff volumes that were measured during the laboratory program at six different rainfall intensities were conducted using SVFlux. The numerical results of both low permeability and capillary barrier profiles examined during the laboratory investigation were described in Section 5.4. The predictions encompassed saturated and unsaturated initial state of both profiles using one-dimensional (1D) and three-dimensional (3D) analyses. The following sections discuss a detailed comparison of the accuracy of each prediction.

6.3.1. Comparison between 1D and 3D Predictions

The histograms shown in Figure 6.10 illustrate the comparisons between the one-dimensional and three-dimensional numerical predictions of runoff for low permeability and capillary barrier profiles. The graph clearly shows that the predictions for low permeability profiles have better accuracy than capillary barrier profiles with respect to the percentage difference in final cumulative runoff volumes between measured and predicted values. The higher percentage difference is observed in capillary barrier profiles in general, even more conspicuous in unsaturated capillary barrier profiles.

In terms of rainfall intensity, both 1D and 3D models systematically underpredicted runoff for high rainfall intensity regardless of cover type. This point is better illustrated in Figure 6.11 where results are grouped based on applied rainfall intensity. Both 1D and 3D predictions for rainfall intensities exceeding 90 mm/hr were negative (i.e., predicted volumes were lower than measured volumes). The opposite is true, however, for rainfall intensity equal to or less than 90 mm/hr (i.e., both 1D and 3D models overpredicted runoff volumes). In terms of quality of the predictions, no clear consistent effect of rainfall intensity on prediction accuracy can be made.

Discussion of Major Findings

Prediction results are slightly improved in the 3D simulations of single-layer profiles. The same, however, cannot be said for multi-layer systems (i.e., capillary barrier profiles). However, unlike 1D models, 3D models are time-consuming to create and characterize. Moreover, longer times were required for both computing the models and analyzing them.

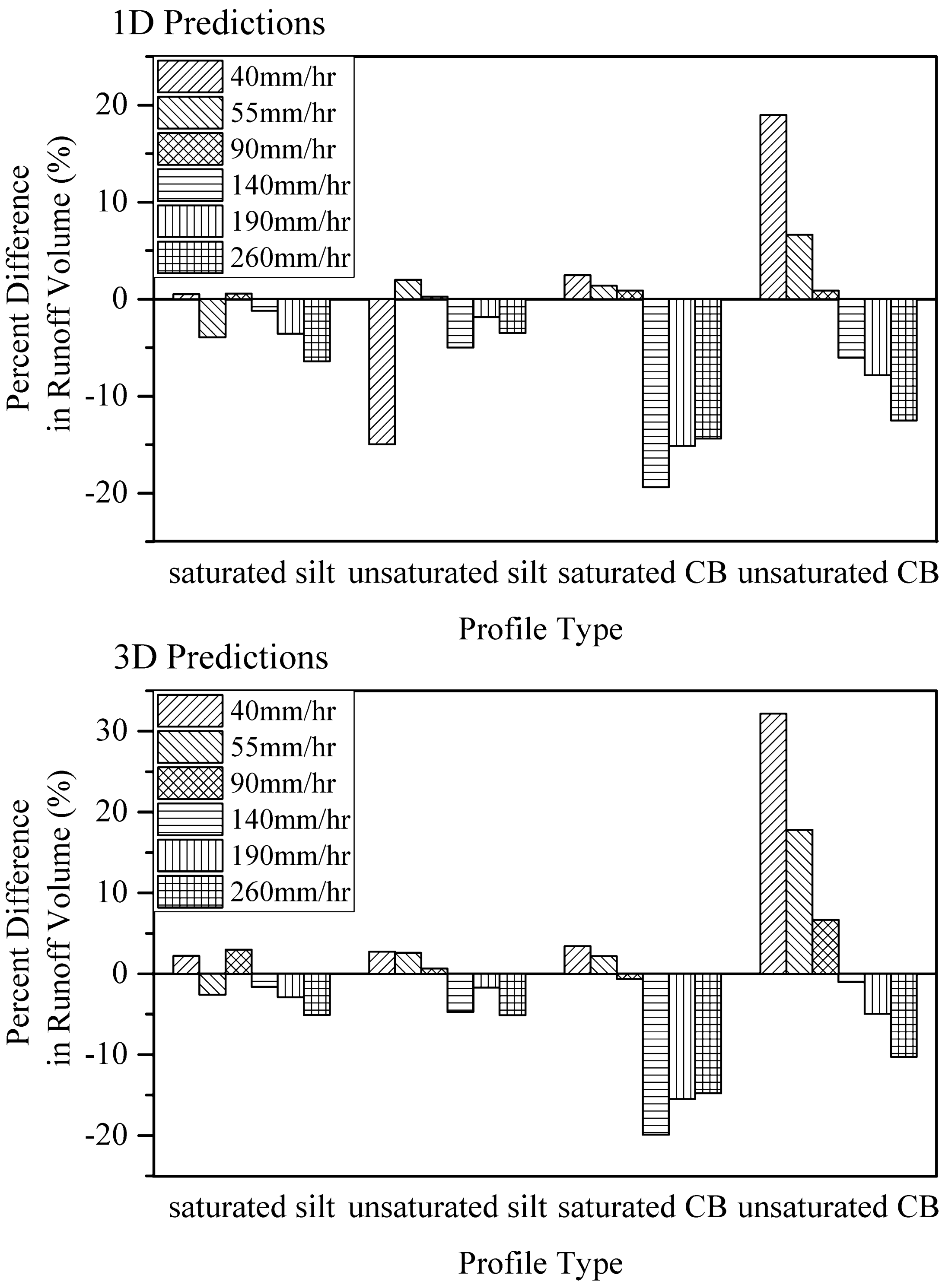

Figure 6.10 Percentage difference between laboratory-measured and 1D predicted (top), and 3D predicted (bottom) final cumulative runoff volumes denoted by profile type and initial saturation relative to the applied rainfall intensity grouped by the profile type.

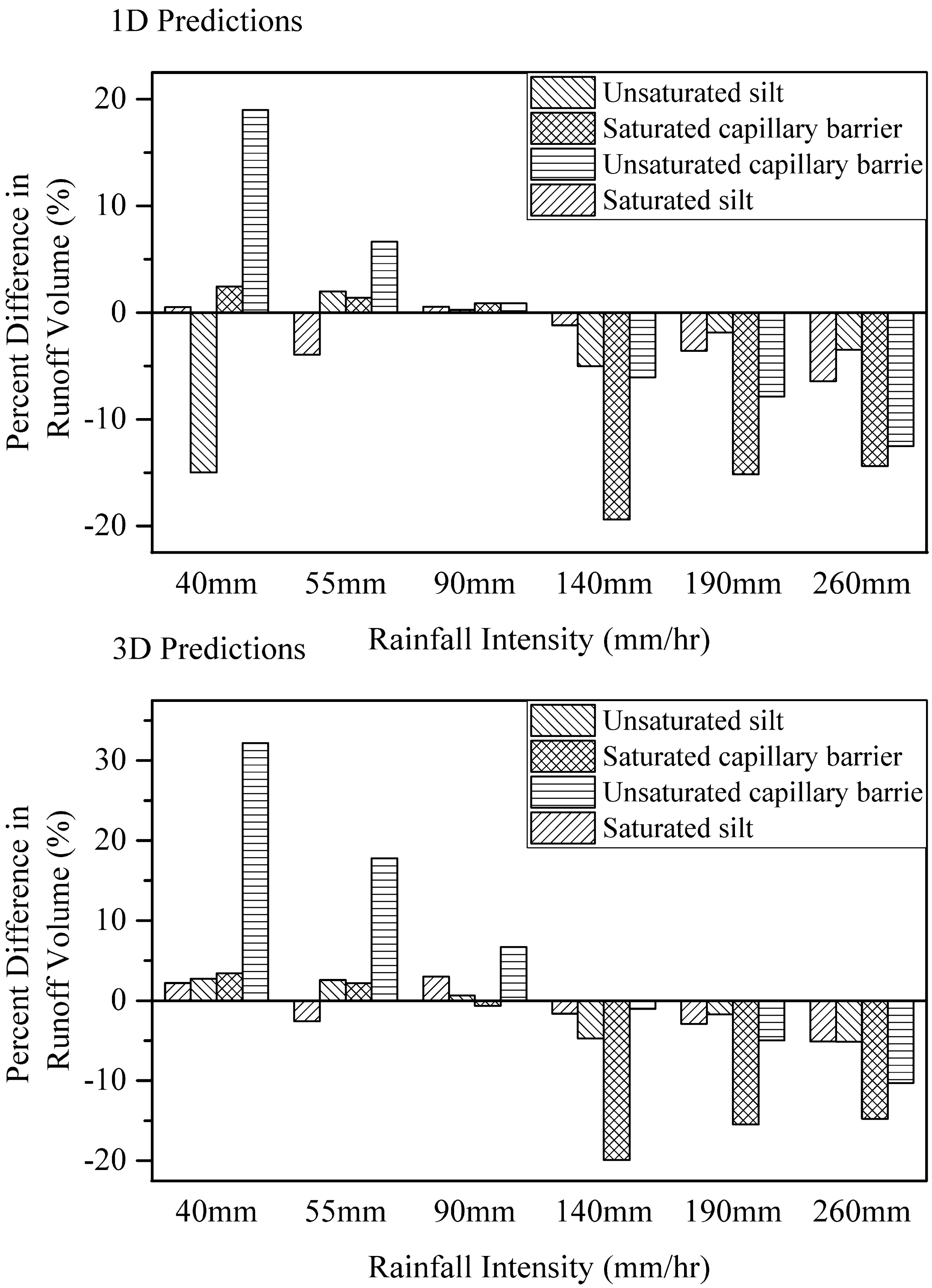

Figure 6.11 Percentage difference between laboratory-measured and 1D predicted (top), and 3D predicted (bottom) final cumulative runoff volumes denoted by profile type and initial saturation relative to the applied rainfall intensity grouped by the applied rainfall intensity.

A crucial point to highlight is that the lack of improvement in the results' quality when 3D predictions were employed may be case specific. The laboratory profiles had a gentle slope of 1%, which means that water flow was primarily happening in the vertical direction. Runoff was generated when the downward water flow was limited by either the saturated hydraulic conductivity in the saturated profiles or the infiltration capacity in the unsaturated profiles. In other words, the essence of the problem was one-dimensional, as is often the case in soil cover systems. For runoff predictions in scenarios that have a significantly sloping surfaces, three-dimensional analyses may account for a substantial portion of water flow.

6.3.2. The Challenge of Unsaturated Soils

The reality of unsaturated soils in a field setting is an added challenge for numerical modelling pathway of estimating runoff fluxes. How does the soil desaturate after periods of rainfall? The premise was examined in the laboratory context by allowing the profile to desaturate fully. As expected, during prolonged dry periods, the profile is exposed to extensive drying and desiccation. This is especially of significance when cover systems are constructed from fine-grained soils: drying by evaporation creates significant cracks at the surface extending to various depths such as those illustrated in Figure 6.12. The hydraulic response of this type of desiccated profile is important to investigate since it constitutes a better representation of actual conditions in the field. Not only would the saturated hydraulic conductivity be altered significantly, but also those cracks would create preferential flow paths for rainwater, perhaps, ultimately rendering the cover system compromised.

In previous papers, and indeed throughout literature, the author has shown how extremely sensitive the numerical predictions are to the saturated hydraulic conductivity. Figure 6.12 implies a powerful perception of the true bearings of soil cover systems and provokes key questions about the merit of using them and the means by which we assess them.

Figure 6.12 A view of a desiccated capillary barrier profile in the laboratory flume.

Undeniably, this issue is more of a problem for capillary barrier profiles. If the climate regime allows for extreme drying of the top layer of the cover system, and the cracks run deep enough, then the capillary barrier mechanism may be entirely undermined. This may become an issue of growing significance with current trends of record heat observed around the globe. If this is so, what is implied for the relevance of numerical models in such settings?

How practicing geotechnical professionals can reconcile this knowledge with current design and long-term performance checks is something to be addressed in the future. Nature is not obliged to conform to what is considered plausible or reasonable. And again, if those systems do not comply with design tenets, what is implied for numerically based design? What do we really want from numerical models? Many aspects of the debate remain unsolved. Despite many limitations, numerical models remain indispensable tools that require physical field tests to sculpt and fine-tune their results.

Theoretically, the contrast in hydraulic conductivity between the silt and sand material in the region of matric suction where the silt layer is saturated, but the sand layer is not, creates the impedance to infiltration at the layer interface. This limits downward infiltration and diverts water laterally up to a point where matric suction exceeds the air entry value of the coarse layer, which is required for a breakthrough to occur. The numerical representation of this physical phenomenon is challenging, especially when the unsaturated hydraulic conductivity of the coarse material is steep. This creates a numerical instability and causes long computation times even for one-dimensional estimations.

The notion proposed in this thesis suggests performing simple laboratory tests to identify the saturated hydraulic conductivity and infiltration capacity functions. Identifying these soil parameters, along with simple real-time calculation, provides a good first estimate of the actual physical performance of a prospect cover system. In doing so, confidence in the accompanying numerical modelling may be improved.

6.4. Numerical Modelling at the Field Scale

Results of the finite element predictions of rainfall runoff at the field scale were presented in Section 5.5. A case study of the Savage River mine was described. The study evaluated the sensitivity of runoff predictions to rainfall resolution and hydraulic conductivity input. The numerical model, SVFlux, was utilized to assess two locations in the mine, the B-Dump and the Old Tailings Dam (OTD). Figures 6.13 and 6.14 illustrate the statistical representation of model sensitivity in the B-Dump and the OTD, respectively.

The histograms seen in Figures 6.13 and 6.14 clearly demonstrate the model sensitivity to both changes in rainfall resolution and hydraulic conductivity input, though, to a varying extent. Higher sensitivity to the input of saturated hydraulic conductivity is evident; the resolution of rainfall input does have an effect, though not as crucial. No more than half an order of magnitude difference in the saturated hydraulic conductivity input instigated substantial variation in results.

Discussion of Major Findings

The underlying effects of temporal and spatial variability of both soil properties and rainfall events are indirectly embedded in the case study analyses. The logic behind this can be understood as follows: The B-Dump Catchments 1 and 2 were originally designed as a single layer water-shedding cover. One would consider that the results of the B-Dump echo the low permeability profiles investigated in the laboratory in a field setting. Comparison between the prediction accuracy trends of a uniform laboratory profile and a field cover system helps to highlight the spatial and temporal effects. Despite the difference in soil types and rainfall events, the effect of spatial variability is still palpable when comparing the predictions' accuracy in the B-Dump to predictions' accuracy in uniform profiles in the laboratory study.

Literature suggests that spatial and temporal variations can have profound implications for runoff predictions. This point is clearly seen when comparing the results of uniform laboratory profiles under controlled conditions to a field cover system under real-time conditions. Addressing the spatial and temporal variations is an added challenge in predicting surface runoff using numerical models.

Furthermore, although the best runoff predictions were attained using the highest rainfall intensity input, one should remain cognizant that high rainfall resolution measurements are not available in most cases. Most weather stations employ tipping bucket rain gauges to daily measure the precipitation to create a monthly record of daily precipitation. That also mounts to an added challenge, unless weather stations are strategically located onsite.

Overall, rainfall runoff is a four-dimensional process highly dependent on the space and time during which rainfall occurs. Therefore, achieving numerical runoff predictions within 4% of measured runoff from one-dimensional simulations is noteworthy. A close understanding of field conditions can be a keystone to overcome spatial variability successfully. By the same token, the sensitivity to hydraulic conductivity can be incorporated into the analyses by a proper judgement of field condition.

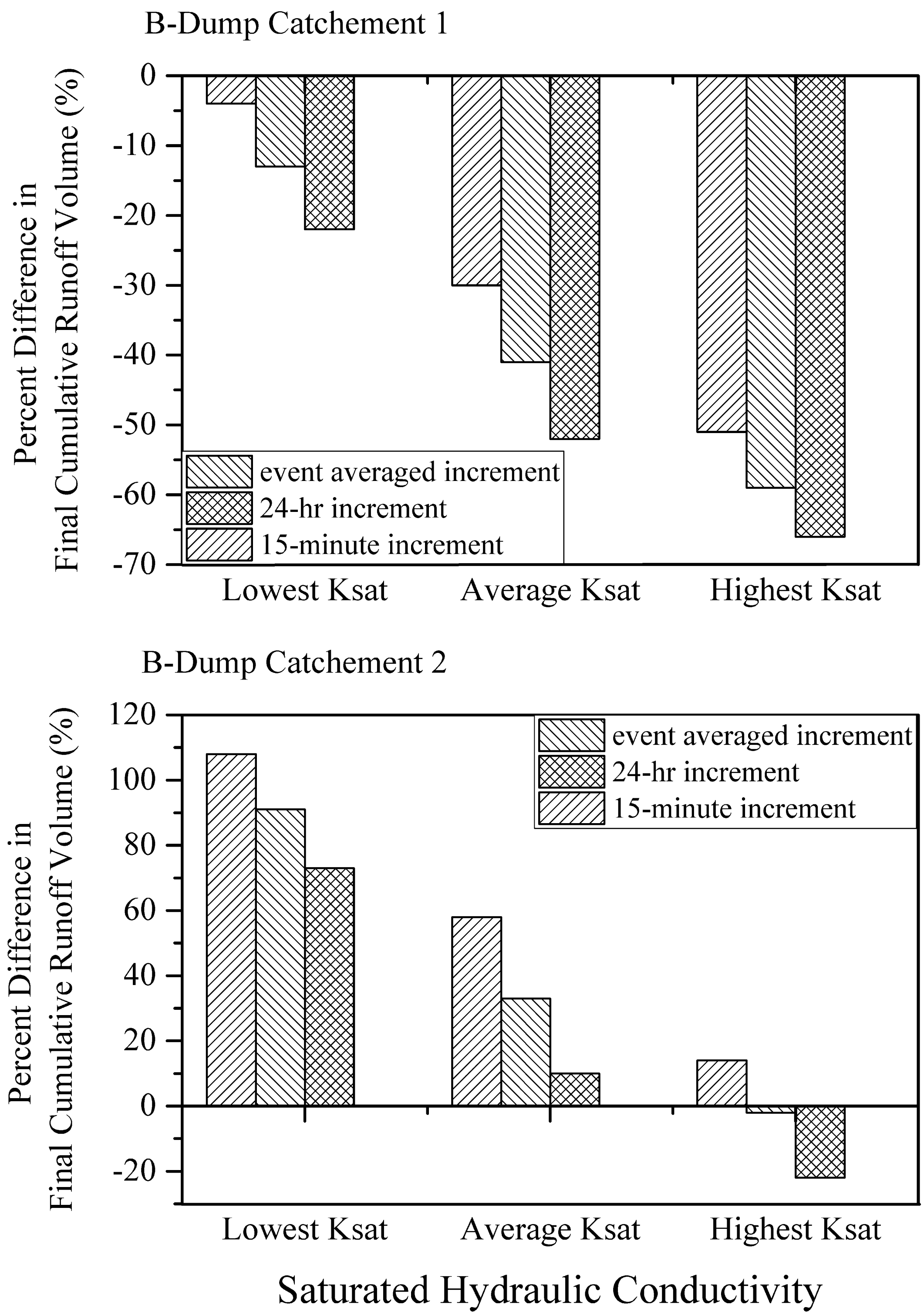

Figure 6.13 Percentage difference between predicted and measured final cumulative runoff volumes for B-Dump Catchment 1 (top) and Catchment 2 (bottom).

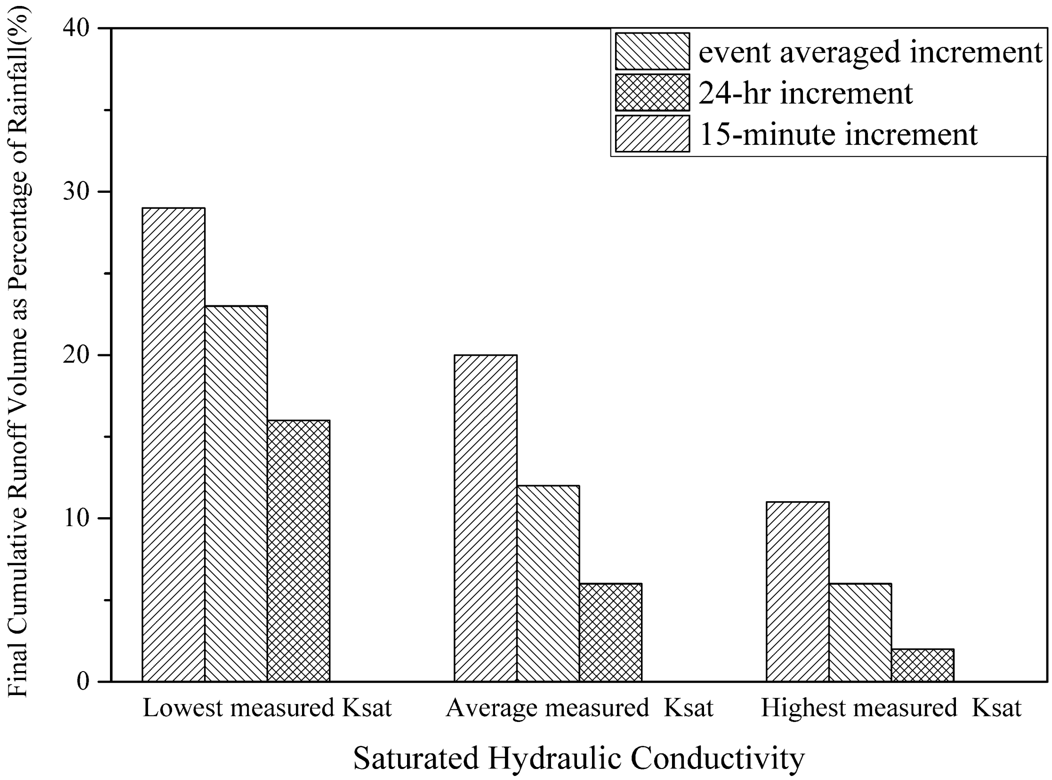

Figure 6.14 Predicted final cumulative runoff volumes for OTD Catchment A as a percentage of measured final cumulative rainfall.

6.5. Summary

A linear correlation between the applied rainfall and the measured runoff was developed as a result of the laboratory program. Chapter 6 discussed the empirical correlation proposed for each type of profile in saturated and unsaturated initial state.

Furthermore, a simple procedure to predict rainfall runoff based on simple, measurable parameters is recommended based on the initial condition of a soil profile. Results revealed that runoff fluxes are controlled by saturated hydraulic conductivity and rainfall intensity in saturated profiles, and infiltration capacity function and rainfall intensity in unsaturated profiles.

Discussion of Major Findings

Comparisons between one- and three-dimensional numerical analyses of the laboratory results were discussed. Results indicated a higher level of certainty in numerical predictions in a single layer profiles regardless of saturation condition compared to capillary barrier profiles.

Numerical prediction of runoff fluxes at the field scale proved to be challenging due to a high degree of sensitivity to input parameters. For instance, less than half an order of magnitude variation in the saturated hydraulic conductivity produced up to 100% difference in predicted runoff volumes. Moreover, runoff predictions proved sensitive to the resolution of rainfall intensity input in the analyses. Results indicated that perception of anticipated runoff is a necessity to reconcile the sensitivity to parameters as mentioned earlier. The proposed first estimate of runoff facilitates judgement when selecting the appropriate runoff predictions.

CHAPTER 7. Summary, Conclusions and Recommendations

7.1. Summary

The primary objective of this research was to examine the process of rainfall runoff in soil covers systems. The following specific goals were emphasized:

1. Identify physical processes operating at and below the ground surface when rainfall occurs.

2. Identify appropriate soil parameters that control rainfall runoff in different saturation conditions.

3. Formulate a theoretical framework for predicting rainfall runoff in soil profiles at different saturation conditions.

4. Carry out laboratory tests that investigate the theoretical approach regarding different initial conditions and profile types exposed to controlled and variable rainfall intensities.

5. Conduct numerical simulations to investigate how accurate numerical prediction is compared to the laboratory results.

6. Demonstrate the practical significance of the current research in a field case study.

The collective results of this research framework indicate that the research objectives have been progressively achieved. The physical processes and generation mechanisms associated with the rainfall-runoff phenomenon were introduced in Chapter 2 through a comprehensive literature review. This included a survey of available prediction models of surface runoff and a complete evaluation of the factors influencing rainfall runoff. A theoretical framework for water flow through saturated and unsaturated soil including soil properties estimation was introduced in Chapter 3. Details of capillary barrier profiles and a physical cause for the phenomenon were also discussed. Chapter 4 described the details of the laboratory program and the numerical modelling framework. The results of the laboratory program and the numerical simulations were presented in Chapter 5 and analyzed in Chapter 6. In addition to comparisons between laboratory and numerical results, Chapter 6 proposed a simple procedure to predict surface runoff for saturated and unsaturated soils based on simple, measurable soil properties. Furthermore, runoff numerical prediction for a practical field case study was presented and discussed.

7.2. Conclusions

Surface runoff can be the most critical component of the water cycle that directly influences infiltration into soil covers systems, thus, controlling their design. In this research, the rainfall-runoff phenomenon was studied in a laboratory program, conducted separately on saturated and unsaturated soil profiles. Six different precipitation rates were applied on both low hydraulic conductivity and capillary barrier profiles. The data obtained in the laboratory program were found to be both consistent and adherent to saturated and unsaturated soil behaviour. Furthermore, a linear correlation between the applied precipitation volume and the subsequent runoff volume was evident. The specific conclusions of the research program are as follows:

1. The physical processes operating at and below the ground surface when rainfall occurs were identified for two different types of profiles at saturated and unsaturated initial states. The physical partitioning of rainfall into infiltration and runoff in unsaturated profiles can be understood as follows: After a rainfall begins, infiltration capacity is at its maximum, and the potential infiltration rate is greater than the rainfall rate. However, the actual infiltration rate is equal to rainfall rate, since the water can only enter the soil at the application rate. At a certain point in time referred to as the time to ponding, the water begins to pond, and the excess water overflows accordingly. The physical partitioning of rainfall into infiltration and runoff in saturated profiles is simpler where infiltration occurs at a constant rate.

2. The appropriate soil parameters that control runoff is understood as follows:

a. Laboratory experiments on saturated silt profiles showed that up to 98% of the entire applied rainfall volume converted into runoff by the end of each test. The rates at which runoff occurred were found to remain constant with time throughout each test. However, as the precipitation rate increased from one test to the other, the runoff rate increased accordingly. Overall, runoff rates and volumes were primarily governed by precipitation rate and the saturated hydraulic conductivity of the soil in the saturated silt profiles.

b. Laboratory experiments on unsaturated silt profiles showed that between 60 and 80% of the applied rainfall eventually converted into runoff. Runoff rates increased nonlinearly with time during each test, proportional to the applied precipitation rate. The measured infiltration rates decreased nonlinearly with time and were consistent with the soil infiltration-capacity functions. Overall, in unsaturated silt profiles, runoff rates were chiefly governed by the precipitation rate and the infiltration capacity of the soil.

c. Unsaturated capillary barrier profiles resulted in higher runoff total volumes, and less infiltration compared to the unsaturated silt counterparts at the same conditions. About 70% to 80% of the overall applied rainfall converted to runoff. Moreover, the rate of runoff was found to be higher than that in the silt profiles. Runoff rates increased non-linearly with time in each test, though at higher rates compared to those in the corresponding unsaturated silt profiles.

3. The theoretical framework for predicting rainfall runoff in soil profiles at different saturation conditions is presented in chapter 6 with underlying theories introduced in chapter 3.

4. Laboratory tests were carried out to investigate runoff based on different initial conditions and profile types exposed to controlled and variable rainfall intensities. As a result, a simple analytical solution suitable as a first estimate of rainfall runoff for both saturated and unsaturated profiles is proposed. The proposed solution requires only a minimal input comprised simple, measurable soil properties and rainfall intensity. The corresponding equations are as follows:

   Saturated profiles:

$$R = (i - k_{sat})\ t\ A \tag{7.1}$$

   Unsaturated profiles:

$$R = \int_0^t (i - I_c)\ t\ A \tag{7.2}$$

   where

R	=	runoff volume [L^3]
i	=	rainfall intensity [L/T]
k_{sat}	=	saturated hydraulic conductivity of the soil [L/T]
t	=	duration of rainfall
A	=	profile area [L^2]
I_c	=	infiltration capacity of the soil [L/T]

5. One- and three-dimensional numerical simulations of the laboratory experiments on low permeability and capillary barrier profiles were investigated. Both saturated and unsaturated responses of each profile were studied. The results from 1D simulations matched reasonably well with laboratory measurements for

single-layer saturated profiles. The percentage difference of the final cumulative runoff volume was mostly within 6% accuracy. For capillary barrier profiles, more variable results were observed. The percentage difference between measured and predicted cumulative volumes produced up to a 32% difference. The discrepancy in results was more pronounced at high rainfall intensities. The reason for that may potentially be related to the capacity of the model to accommodate high fluxes at the layer interface relative to the saturated hydraulic conductivity. To explain this point further, when the soil is unsaturated then the unsaturated hydraulic conductivity functions seen in chapter 3 are steep nonlinear function of the matric suction of the profile. This fact is very difficult to represent in numerical models, it creates model instability especially when t the rainfall applied at the top boundary condition is much higher than K_{unsat}. Three-dimensional predictions slightly improved in single-layer profiles. These two sets of simulations demonstrate that, even in the absence of spatial and temporal variability, numerical modelling has limitations in representing the physical and hydraulic processes in multilayered systems. The 3D analyses in multilayer profiles required longer computation times.

6. A case study of numerical predictions of rainfall runoff at the field scale was presented. The study evaluated the sensitivity of runoff predictions to rainfall resolution and hydraulic conductivity input. The finite element model, SVFlux, was utilized to predict runoff volumes. Runoff predictions were found highly sensitive to change in both hydraulic conductivity and rainfall resolution input in the model. The best runoff predictions were achieved using a combination of the highest resolution of rainfall data and the selection of K_{sat} to incorporate the surface slope into a one-dimensional analysis. Comparisons of predicted cumulative runoff volumes made by each model were found congruent in trends, but the numbers varied noticeably. The best SVFlux prediction was within 4% accuracy if good judgment is used when selecting the hydraulic conductivity to incorporate slope. Overall, runoff generation is a four-dimensional phenomenon, so achieving reasonably good runoff predictions within 4% of measured runoff from one-dimensional simulations can be considered significant. This success

can be incorporated into cover systems design. Nevertheless, obtaining high-resolution rainfall data and remaining cognizant of the actual field conditions is paramount.

7. Lastly, the study underlines the challenges associated with numerical modelling of soil cover systems. In addition to classic challenges, such as spatial and temporal variability, the study reflects on the physics of unsaturated desiccated profiles. It scrutinizes the merit of the cover systems and the means by which we analyze them considering how the profiles desaturate and desiccate. Further research should be carried out to account for such behaviour fully. Knowing that we are storing reactive acid-generating waste in these repositories, knowing how the covers dry up and desiccate, where does prudence lie?

7.3. Future Research

The main objective of the study was to characterize the rainfall-runoff phenomenon for soil cover systems and propose a simple procedure to obtain runoff fluxes based on simple easily measured soil properties. Even though this purpose has been fulfilled, there remain aspects requiring further exploration for a comprehensive methodology for engineering practice. Some of the most relevant elements as an extension of this study are listed below:

1. The laboratory profiles investigated in this thesis had a gentle slope of 1%. Further investigation into the rainfall-runoff response on profiles with varying slopes could be conducted. The slope of the profile plays a key role in the overall runoff/infiltration partitioning. Variation of the profile slope gives rise to insights about the three-dimensional aspects of runoff generation. The same profiles made of the same material properties and exposed to the same rainfall intensity could be studied to measure the resulting runoff corresponding to varying profile slopes. The slopes can simply be varied by utilizing a hydraulic lifting tool fixed at one end of the profiles. The correlation between an increasing slope of the profiles and infiltration/runoff percentages can be established. Instrumentation could be distributed at different depths to track wetting profiles with depth. Time-lapse photography can also be utilized.

2. The capillary barrier profiles investigated during the laboratory program comprised Devon silt overlaying tailings beach sand with equal thickness. Further investigations into the effects of variation of appropriate capillary barrier materials and relative thickness could be conducted. Prospect research can investigate the correlation between the relative thickness of each layer of the capillary barrier and runoff volumes. Furthermore, inspecting the response time delay at the interface as a function of different combinations of fine/coarse soils would provide insight into the minimum limiting requirements and their effect on surface runoff. Moreover, the effects of layers' thickness and material types on lateral diversion at the layer interface of a capillary barrier system can be examined. Instrumentation could be focused on the layer interface to track changes in matric suction and volumetric water content as breakthrough occurs in the capillary barrier profiles.

3. The laboratory program focused on quantifying the water balance components particularly relevant to soil cover systems. Another important application of the laboratory framework developed in the thesis is the realm of rainfall-induced slope instability. Further examination of the correlation between surface runoff and kinematics of slope stability could be investigated in controlled laboratory

settings. Instruments, including slope inclinometers and piezometers, can be employed to establish whether a correlation exists between the flow of water at the soil atmosphere boundary and any instability incurred by flow in addition to the strength loss of residual soils due to rainfall.

4. Attention was paid during the design of the laboratory investigations to select rainfall nozzles that would ensure that the raindrop size would not cause profile erosion as this was beyond our scope. However, erosion is a crucial element to address during the estimation of surface runoff, especially in the context of land reclamation. Soil particles may be carried with runoff depending on the size and kinematic energy of the raindrops. This can be examined in a controlled laboratory setting such as the one described in this thesis. Nozzles selection can be made to adjust the rainfall pattern and size. The velocities and kinetic energy of raindrops and their effect on the erosion process during periods of runoff can be studied. A rainfall simulator can be designed to evaluate the relationship between rainfall intensity and surface runoff to determine the effects of overland flow on sediment transport. Furthermore, techniques to limit the erosion process and sediment transfer can be examined within the same conditions, and the effectiveness of different stabilizing methods appropriate for different rainfall intensity scenarios can be compared.

5. Another potential extension of this study would be the verification of the proposed runoff estimation method in a field setting. An appropriate site should be selected to carry out field rainfall simulations. A field rainfall simulator can be designed, similar to the one designed in this thesis regarding the spraying system and measuring devices. Runoff can be collected using in-situ weirs. Field infiltrometers can be employed to determine the in-situ infiltration capacity functions. Steps described in Section 4.3.2.2 can be carried out, along with calculations presented in Appendix VI. Unlike the current study where the rainfall-runoff tests were conducted in a controlled laboratory setting where no evaporation was allowed, the field study would encompass in-situ evaporation. Several challenges associated with field simulators, including uncertainty of

weather conditions, and high winds interfering with applied rainfall, should be addressed.

6. The flume boundary conditions during the rainfall-runoff experiments in this study allowed drainage only at the toe of the flume. Parallel experiments allowing infiltration through the entire area at the bottom of the flume may potentially be conducted. Investigation of the influence of different boundary conditions on rainfall runoff and infiltration may be of value. This could be easily done by adding a mesh at the bottom with a layer of geotextile to prevent soil particles' migration by creating a permeable layer at the bottom of the profiles. Matching bench-scale column experiments may be prepared to determine infiltration capacity functions, such as the ones described in Section 4.3.2. The analytical solution proposed in Section 6.2.3 can then be verified for the new boundary conditions scenario.

7. The most challenging adjunction to this study is, perhaps, the investigation of the response of unsaturated profiles exhibiting desiccation upon drying in a controlled laboratory environment. Such trials of drying followed by rainfall would be time-consuming. However, the fundamental understanding of change in infiltration capacity and hydraulic properties in desiccated soil matrix has very significant practical implications for the future of soil cover systems and their efficiency. Climate is a key player accentuating such instances by prolonged periods of drought. Given the current climate trends, this might be a crucial point of interest. Given the way covers desaturate, geotechnical professionals are obligated to answer the following question: where does prudence lie? A survey of soil cover systems functioning as intended might help answer this question.

The work completed in this thesis contributes to the fundamental understanding of the rainfall-runoff response supported by laboratory evidence. Further work may be developed based on this underpinning knowledge, which can be extended to numerous applications in geotechnical engineering practice.

Many practical applications can utilize the proposed runoff prediction based on simple easily measurable properties. Quantifying the water flux at the soil atmosphere boundary condition is vital for several problems encountered by practicing engineers and researchers in geotechnical engineering. The true bearing of unsaturated soil behaviour on engineering structures is continuously evolving in practice. Having this work as a simple foundation, which further work may benefit from is valuable. This research forms a cornerstone for future research concerning the ability to predict water migration and water balances, which are vital in many engineering structures. Examples include but not limited to earth dams, slope stability, soil cover systems design, long-term performance assessment, and the like.

BIBLIOGRAPHY

Abbott, M. B and Refsgaard, J. C. 1996. Distributed hydrological modelling. Kluwer Academic, Dordrecht; Boston.

Abdulnabi, A. 2015 A Comprehensive Literature Review for Soil Covers and the Role of Rainfall Runoff in Soil Atmospheric Modelling. Meng. Report University of Alberta, Canada.

Abdulnabi, A. and Wilson, G. W. 2015 Laboratory Testing Program for the Prediction of Rainfall Runoff from Soil Cover Systems. In Proceedings of the 68 Canadian Geotechnical Conference Quebec City, Canada. September 20-23, 2015 pp. 222-231.

Abdulnabi, A. Jubinville, S. K. and Wilson, G. W. 2016 A Case Study of Numerical Prediction of Rainfall Runoff for Soil Cover Systems. In Proceedings of the 69 Canadian Geotechnical Conference Vancouver, Canada. October 2nd - 5th 2016.

Abdulnabi, A. and Wilson, G. W. 2017 Rainfall Runoff in Cover Systems Design: Are Numerical Predictions and Observational Science Reconcilable? In Proceedings of the 7 Canadian Geotechnical Conference Ottawa, Canada. October 1-4 20-23, 2015 pp. 222-231

ABM. 2006. SRRP B-dump water shedding cover construction report. Australian Bulk Minerals, Tasmania, AUS.

Abudi, I., Carmi, G., and Berliner, P. (2012). "Rainfall simulator for field runoff studies." Journal of Hydrology, 454–455(0), 76-81.

Albright, W. H., Apiwantragoon, P., Shackelford, C. D., Benson, C. H., Bohnhoff, G. L., and Ogorzalek, A. S. (2008). "Field Data and Model Predictions for a Monolithic Alternative Cover." American Society of Civil Engineers, 1-16.

Albright, W., Benson, C., and Apiwantragoon, P. (2013). "Field Hydrology of Landfill Final Covers with Composite Barrier Layers." J. Geotech. Geoenviron. Eng., 139(1), 1-12.

Albright, W., Benson, C., Gee, G., Abichou, T., McDonald, E., Tyler, S., and Rock, S. (2006). "Field Performance of a Compacted Clay Landfill Final Cover at a Humid Site." J. Geotech. Geoenviron. Eng., 132(11), 1393-1403.

Al-Qurashi, A., McIntyre, N., Wheater, H., and Unkrich, C. (2008). "Application of the Kineros2 rainfall–runoff model to an arid catchment in Oman." Journal of Hydrology, 355(1–4), 91-105.

Amerman, C. R. (1965). "The use of unit-Source watershed data for runoff prediction Water Resources Research." 1(4), 499–507.

Andrade, R. B., 1971 . "The Influence of Bulk Density on the Hydraulic Conductivity and Water Content-Matric Suction Relation of Two Soils" MSc. Thesis Utah State University. United States.

Anctil, F., Lauzon, N., Andréassian, V., Oudin, L., and Perrin, C. (2006). "Improvement of rainfall runoff forecasts through mean areal rainfall optimization." Journal of Hydrology, 328(3–4), 717-725.

Asadi, S., Shahrabi, J., Abbaszadeh, P., and Tabanmehr, S. (2013). "A new hybrid artificial neural networks for rainfall–runoff process modeling." Neurocomputing, 121(0), 470-480.

ASTM D6913-04 2009 e1 Standard Test Methods for Particle-Size Distribution (Gradation) of Soils Using Sieve Analysis, ASTM International, West Conshohocken, PA, 2009, https://doi.org/10.1520/D6913-04R09E01

ASTM D4221-11 Standard Test Method for Dispersive Characteristics of Clay Soil by Double Hydrometer, ASTM International, West Conshohocken, PA, 2011, https://doi.org/10.1520/D4221-11

ASTM D2434-68 2006 (Withdrawn Version) Standard Test Method for Permeability of Granular Soils (Constant Head) Withdrawn 2015 DOI: 10.1520/D2434-68R06

ASTM D6836-16 Standard Test Methods for Determination of the Soil Water Characteristic Curve for Desorption Using Hanging Column, Pressure Extractor, Chilled Mirror Hygrometer, or Centrifuge, ASTM International, West Conshohocken, PA, 2016, https://doi.org/10.1520/D6836-16

ASTM D3385-09 Standard Test Method for Infiltration Rate of Soils in Field Using Double-Ring Infiltrometer, ASTM International, West Conshohocken, PA, 2009, https://doi.org/10.1520/D3385-09.

Benson, C. (2010). "Prediction in Geoenvironmental Engineering: Recommendations for Reliable Predictive Modeling." American Society of Civil Engineers, 1-13.32

Benson, C.H., Sawangsuriya, A., Trzebiatowski, B., and Albright, W.H. 2007. Postconstruction changes in the hydraulic properties of water balance cover soils, Journal of Geotechnical and Geoenvironmental Engineering, 133(4): 349-359.

Beven, K. (2001). "How far can we go in distributed hydrological modelling?" Hydrology and Earth System Sciences, 5 1-12.

Beven, K., J. 2012. Rainfall runoff modelling: The primer. Jon Wiley & Sons Ltd., Oxford, UK.

Birkel, C., Tetzlaff, D., Dunn, S. M., and Soulsby, C. (2011). "Using lumped conceptual rainfall–runoff models to simulate daily isotope variability with fractionation in a nested mesoscale catchment." Adv.Water Resour., 34(3), 383-394.

Bohnhoff, G., Ogorzalek, A., Benson, C., Shackelford, C., and Apiwantragoon, P. (2009). "Field Data and Water-Balance Predictions for a Monolithic Cover in a Semiarid Climate." J.Geotech.Geoenviron.Eng., 135(3), 333-348.

Boughton, W. C. (2007). "Effect of data length on rainfall–runoff modelling." Environmental Modelling & Software, 22(3), 406-413.

Brett, D., and Hutchison, B. (2001). Design and Performance of a 'Flow - Through' Spillway at Broderick Creek Waste Rock Dump - Savage River mine. Institution of Engineers, Australia, Barton, A.C.T.

Brett, D.,. (2006). "Strategic planning for ARD remediation." Brett, D. 2006. Strategic Planning for ARD Remediation. Proceedings of 7th ICARD Conference (March 26-30, 2006), St. Louis, MO., .

Bronstert, A., and Plate, E. J. 1997 . "Modelling of runoff generation and soil moisture dynamics for hillslopes and micro-catchments." Journal of Hydrology, 198(1–4), 177-195.

Bronstert, A. and Bardossy, A. 2003. Uncertainty of runoff modelling at the hillslope scale due to temporal variations of rainfall intensity, Physics and Chemistry of the Earth, 28: 283-288.

Brooks, J.P., Adeli, A., Read, J.J., McLaughlin, M.R., 2009. Rainfall simulation in greenhouse microcosms to assess bacterial-associated runoff from land-applied poultry litter. J. Environ. Qual. 38 (1), 218–229.

Bruce, S. L., Noller, B. N., Grigg, A. H., Mullen, B. F., Mulligan, D. R., Ritchie, P. J., Currey, N., and Ng, J. C. (2003). "A field study conducted at Kidston Gold Mine, to evaluate the impact of arsenic and zinc from mine tailing to grazing cattle." Toxicol.Lett., 137(1–2), 23-34.

Calver, A., and Cammeraat, L. H. (1993). "Testing a physically-based runoff model against field observations on a Luxembourg hillslope." Catena, 20(3), 273-288.

Campbell G. S. 1974 A simple method for determining unsaturated conductivity from moisture retention data. Soil Sci. 117 311-314.

Cerdà, A., Ibáñez, S., and Calvo, A. (1997). "Design and operation of a small and portable rainfall simulator for rugged terrain." Soil Technol., 11(2), 163-170.

Chen, J., and Adams, B. J. (2007). "Development of analytical models for estimation of urban stormwater runoff." Journal of Hydrology, 336(3–4), 458-469.

Commonwealth of Australia, Bureau of Meteorology (BOM). 2012. Climate data online - Savage River mine [online]. Available from http://www.bom.gov.au/climate/data/index.shtml [cited 07/17 2012].

Connolly, R. D., Silburn, D. M., Ciesiolka, C. A. A., and Foley, J. L. 1991 . "Modelling hydrology of agricultural catchments using parameters derived from rainfall simulator data." Soil Tillage Res., 20(1), 33-44.

Dawdy, D. R., R. W. Lichty, and J. M. Bergmann, 1972. A rainfall runoff simulation model for estimation of flood peaks for small drainage basins, U.S. Geol. Surv. Prof Pap. 506-B, 28 pp.

de Lima, J. L. M. P., and Singh, V. P. (2003). "Laboratory experiments on the influence of storm movement on overland flow." Physics and Chemistry of the Earth, Parts A/B/C, 28(6–7), 277-282.

de Lima, J. L. M. P., Tavares, P., Singh, V. P., and de Lima, M. I. P. (2009). "Investigating the nonlinear response of soil loss to storm direction using a circular soil flume." Geoderma, 152(1–2), 9-15.

Du, Jun. Shi, Chang-xing Zhang, Chen-di Modeling and analysis of effects of precipitation and vegetation coverage on runoff and sediment yield in Jinsha River Basin, Water Science and Engineering, Volume 6, Issue 1, 2013, Pages 44-58, ISSN 1674-2370, http://dx.doi.org/10.3882/j.issn.1674-2370.2013.01.004.

Drnevich, V., Zambrano, C., Huang, P., and Jung, S. (2007). "TDR Technologies for Soil Identification and Properties." American Society of Civil Engineers, 1-11.

Dunkerley, D. (2011). "Effects of rainfall intensity fluctuations on infiltration and runoff: rainfall simulation on dryland soils, Fowlers Gap, Australia." Hydrological Processes, 26(15), 2211 - 2224.

Elwell, H. A., and Stocking, M. A. (1974). "Rainfall parameters and a cover model to predict runoff and soil loss from grazing trials in the Rhodesian sandveld." Proceedings of the Annual Congresses of the Grassland Society of Southern Africa, 9(1), 157-164.

Fayer, M.J., Rockhold, M.L., and Campbell, M.D. 1992. Hydrologic modeling of protective barriers: Comparison of field data and simulation results, Soil Science Society of America Journal, 56(3): 690-700.

Fernandez, I., and Bouraoui, P., F. (1999). "Study of the rainfall runoff process in the Andes region using a continuous distributed model." Journal of Hydrology, 216(3–4), 155-171.

Fox, D. M., Le Bissonnais, Y., and Bruand, A. (1998). "The effect of ponding depth on infiltration in a crusted surface depression." Catena, 32(2), 87-100.

Fredlund, D.G. and Rahardjo, H. 1993. Soil mechanics for unsaturated soils. John Wiley & Sons Inc., USA.

Fredlund, D.G. Fredlund. M. D. and Rahardjo, H. 2012. Unsaturated Soil Mechanics in Engineering Practice. John Wiley & Sons Inc., USA.

Freeze, R. A. (2010). "A stochastic-conceptual analysis of rainfall runoff processes on a hillslope." Freeze, R. A. (1980), A Stochastic-Conceptual Analysis of Rainfall runoff Processes on a Hillslope, Water Resour. Res., 16(2), 391–408, Doi:10.1029/WR016i002p00391., Volume 16(Issue 2), pages 391–408.

Freeze, R. A., and Banner, J. (1970). "The mechanism of natural ground-water recharge and discharge: 2. Laboratory column experiments and field measurements." Water Resources Research, 6 138 - 55.

Gasmo, J. M., Rahardjo, H., and Leong, E. C. (2000). "Infiltration effects on stability of a residual soil slope." Comput. Geotech., 26(2), 145-165.35

GHD. 2009. Report for B-dump cap: Report on flow monitoring. Rev 1, January 2009, Australian Bulk Minerals, Hobart, AUS.

Gitirana, G., Jr., Fredlund, M. D., and Fredlund, D. G. (2005). "Infiltration-Runoff Bundary Conditions in Seepage Analysis." 516-523.

Grange Resources. 2012a. Savage river – location [online]. Available from http://www.grangeresources.com.au/php/page.php?grangeS+11 [cited 07 2013].

Grange Resources. 2012b. Savage river - environment [online]. Available from http://www.grangeresources.com.au/php/page.php?grangeS+14 [cited 07 2013].

Grange Resources. 2012c. ASX release. 29 February 2012, Grange Resources Limited, Australia.

Green WH, Ampt G. 1911. Studies on soil physics, 1. The flow of air and water through soils. The Journal of Agricultural Science 4: 1–24.

Grierson, I. T., and Oades, J. M. (1977). "A rainfall simulator for field studies of run-off and soil erosion." J.Agric.Eng.Res., 22(1), 37-44.

Gumbo, B., Munyamba, N., Sithole, G., and Savenije, H. H. G. (2002). "Coupling of digital elevation model and rainfall runoff model in storm drainage network design." Physics and Chemistry of the Earth, Parts A/B/C, 27(11–22), 755-764.

Hamed, Y., Albergel, J., Pépin, Y., Asseline, J., Nasri, S., Zante, P., Berndtsson, R., El-Niazy, M., and Balah, M. (2002). "Comparison between rainfall simulator erosion and observed reservoir sedimentation in an erosion-sensitive semiarid catchment." Catena, 50(1), 1-16.

Hernandez, Mariano and Miller, ScottN. and Goodrich, DavidC., Goff, B., Kepner, W., Edmonds, C., and Jones, K. B. (2000). "Modeling Runoff Response to Land Cover and Rainfall Spatial Variability in Semi-Arid Watersheds." Environmental Monitoring and Assessment}, 64 285-298.

Hopp, L., McDonnell, J. J., and Condon, P. (2011). "Lateral Subsurface Flow in a Soil Cover over Waste Rock in a Humid Temperate Environment." Vadose Zone Journal, 10(1), 332.

Horton, R. (1935). Surface Runoff Phenomena. Horton Hydrologic Laboratory Publication, USA. 36

Houston, W. N., and Houston, S. L.,. (1995). "Infiltration Studies for Unsaturated Soils." 869-884.

Huang, J., Zhao, X., and Wu, P. (2013). "Surface runoff volumes from vegetated slopes during simulated rainfall events." Journal of Soil and Water Conservation, 68(4), 283-295.

Indrawan, I. G. B., Rahardjo, H., and Leong, E. (2007). "Drying and wetting characteristics of a two-layer soil column." Canadian Geotechnical Journal, 44 20-32.

Jacobs Jennifer M., Myers David A., Whitfield Brent M. "IMPROVED RAINFALL/RUNOFF ESTIMATES USING REMOTELY SENSED SOIL MOISTURE." 39(2), 313–324.

Jain, M. K., and Singh, V. P. (2005). "DEM-based modelling of surface runoff using diffusion wave equation." Journal of Hydrology, 302(1–4), 107-126.

Jain, M. K., Kothyari, U. C., and Ranga Raju, K. G. (2004). "A GIS based distributed rainfall–runoff model." Journal of Hydrology, 299(1–2), 107-135.

Jubinville, S. K. 2013. Prediction of Rainfall Runoff for Soil Cover Modelling. M.Sc., University of Alberta, Canada.

Karssenberg, D. (2006). "Upscaling of saturated conductivity for Hortonian runoff modelling." Adv.Water Resour., 29(5), 735-759.

Kasiviswanathan, K. S., Cibin, R., Sudheer, K. P., and Chaubey, I. (2013). "Constructing prediction interval for artificial neural network rainfall runoff models based on ensemble simulations." Journal of Hydrology, 499(0), 275-288. 37

Kato, H., Onda, Y., Tanaka, Y., and Asano, M. (2009). "Field measurement of infiltration rate using an oscillating nozzle rainfall simulator in the cold, semiarid grassland of Mongolia." Catena, 76(3), 173-181.

Krumbein, W. C. and Graybill, F. A. 1965 An introduction to statistical models in geology. New York, McGraw-Hill book co., 475p.

Langhans, C., Govers, G., Diels, J., Leys, A., Clymans, W., Putte, A. V. d., and Valckx, J. (2011). "Experimental rainfall–runoff data: Reconsidering the concept of infiltration capacity." Journal of Hydrology, 399(3–4), 255-262.

Lee, H. Zehe, E. and Sivapalan M. (2007). Lee, H. Zehe, E. and Sivapalan M. 2007 Predictions of Rainfall runoff Response and Soil Moisture Dynamics in a Microscale Catchment using the CREW Model Hydrol. Earth Syst. Sci., 11, 819-849, 819-849.

Lin, C., Chung, C., Tang, S., and Lin, C. (2007). "Some Innovative Developments of TDR Technology for Geotechnical Monitoring." American Society of Civil Engineers, 1-12.

Liu, Q. Q., Chen, L., Li, J. C., and Singh, V. P. (2004). "Two-dimensional kinematic wave model of overland-flow." Journal of Hydrology, 291(1–2), 28-41.

Liu, Z., and Todini, E. "Towards a comprehensive physically-based rainfall runoff model." Liu, Z. and Todini, E.: Towards a Comprehensive Physically-Based Rainfall runoff Model, Hydrol. Earth Syst. Sci., 6, 859-881, Doi:10.5194/hess-6-859-2002, 2002., .

Loos, M., and Elsenbeer, H. (2011). "Topographic controls on overland flow generation in a forest – An ensemble tree approach." Journal of Hydrology, 409(1–2), 94-103.

Mao, L. L., Lei, T. W., Li, X., Liu, H., Huang, X. F., and Zhang, Y. N. (2008). "A linear source method for soil infiltrability measurement and model representations." Journal of Hydrology, 353(1–2), 49-58.

Maurer, E. P., Brekke, L. D., and Pruitt, T. (2010). "Contrasting Lumped and Distributed Hydrology Models for Estimating Climate Change Impacts on California Watersheds." JAWRA Journal of the American Water Resources Association, 46(5), 1024 - 1035.

McDonnell, J. J. (2003). "Where does water go when it rains? Moving beyond the variable source area concept of rainfall runoff response." Hydrological Processes, 17(9), 1869 - 1875. 38

Mein, R.G. and Larson, C.L. 1973. Modeling infiltration during a steady rain, Water Resources Research, 9(2): 384-394.

Miller, W. P. 1987. A solenoid–operated, variable intensity rainfall simulator. Soil Science Society of America J. 51(3): 832–834.

Molina, A., Govers, G., Vanacker, V., Poesen, J., Zeelmaekers, E., and Cisneros, F. (2007). "Runoff generation in a degraded Andean ecosystem: Interaction of vegetation cover and land use." Catena, 71(2), 357-370.

Moody, J. A., Shakesby, R. A., Robichaud, P. R., Cannon, S. H., and Martin, D. A. (2013). "Current research issues related to post-wildfire runoff and erosion processes." Earth-Sci.Rev., 122(0), 10-37.

Navas, A., Alberto, F., Machín, J., and Galán, A. 1990 . "Design and operation of a rainfall simulator for field studies of runoff and soil erosion." Soil Technol., 3(4), 385-397.

Nandakumar, N., and Mein, R. G. (1997). "Uncertainty in rainfall—runoff model simulations and the implications for predicting the hydrologic effects of land-use change." Journal of Hydrology, 192(1–4), 211-232.

Navas, A., Alberto, F., Machín, J., and Galán, A. (1990). "Design and operation of a rainfall simulator for field studies of runoff and soil erosion." Soil Technol., 3(4), 385-397.

Nearing, M. A., Jetten, V., Baffaut, C., Cerdan, O., Couturier, A., Hernandez, M., Le Bissonnais, Y., Nichols, M. H., Nunes, J. P., Renschler, C. S., Souchère, V., and van Oost, K. (2005). "Modeling response of soil erosion and runoff to changes in precipitation and cover." Catena, 61(2–3), 131-154.

O'Connor, K. (2007). "Geotechnical Alarm Systems Based on TDR Technology." American Society of Civil Engineers, 1-12.

O'Kane, M., and Wels, C. 2003. "Mine Waste Cover System Design – Linking Predicted Performance to Groundwater and Surface Water Impacts." 341-350.

Osunbitan, J. A. Oyedele, D.J. Adekalu, K.O. 2005 Tillage effects on bulk density, hydraulic conductivity and strength of a loamy sand soil in southwestern Nigeria, Soil and Tillage Research, Volume 82, Issue 1, , Pages 57-64, ISSN 0167-1987,http://dx.doi.org/10.1016/j.still.2004.05.007.(http://www.sciencedirect.com/science/article/pii/S0167198704001515)

Oudin, L., Michel, C., and Anctil, F. 2005 . "Which potential evapotranspiration input for a lumped rainfall runoff model?: Part 1—Can rainfall runoff models effectively handle detailed potential evapotranspiration inputs?" Journal of Hydrology, 303(1–4), 275-289.

Overton, D.E., and M.E. Meadows. 1976. Stormwater Modeling. Academic Press, New York.

Paige, GB, Stone, JJ, Smith, JR, Kennedy, JR, 2003.The walnut gulch rainfall simulator: a computer-controlled variable intensity rainfall simulator. Appl. Eng. Agric. 20, 25–31.

Panday, S., and Huyakorn, P. S. (2004). "A fully coupled physically-based spatially-distributed model for evaluating surface/subsurface flow." Adv.Water Resour., 27(4), 361-382.

Pappas, E. A., Smith, D. R., Huang, C., Shuster, W. D., and Bonta, J. V. (2008). "Impervious surface impacts to runoff and sediment discharge under laboratory rainfall simulation." Catena, 72(1), 146-152.

Paydar, Z., and Cresswell, H. p. (1996). "Water retention in Australian soils. II. Prediction using particle size, bulk density, and other properties." Aust. J. Soil Res., 34 679-93.

Piman, T., and Babel, M. (2013). "Prediction of Rainfall runoff in an Ungauged Basin: Case Study in the Mountainous Region of Northern Thailand." J.Hydrol.Eng., 18(2), 285-296.

Penman, H.L. 1948 Natural evaporation from open water, bare soil and grass. Proc. Roy. Soc. London A(194), S. 120-145.

Philip, J.R. 1957. The theory of infiltration: 1. the infiltration equation and its solution. Soil Science, 83: 345-357.

Post, D. A., and Jakeman, A. J. 1999 . "Predicting the daily streamflow of ungauged catchments in S.E. Australia by regionalising the parameters of a lumped conceptual rainfall runoff model." Ecol.Model., 123(2–3), 91-104.

Rahardjo, H., Lee, T. T., Leong, E. C., and Rezaur, R. B., 2005, "Response of a residual soil slope to rainfall," Canadian Geotechnical Journal, Vol. 42, pp. 340 - 351.

Rahardjo, H., Santoso, V., Leong, E., Ng, Y., and Hua, C. (2012). "Performance of an Instrumented Slope Covered by a Capillary Barrier System." J.Geotech.Geoenviron.Eng., 138(4), 481-490.

Rahimi, A., Rahardjo, H., and Leong, E. (2011). "Effect of Antecedent Rainfall Patterns on Rainfall-Induced Slope Failure." J.Geotech.Geoenviron.Eng., 137(5), 483-491.

Roesler, A.C., Benson, C.H., and Albright, W.H. 2002. Field hydrology and model predictions for final covers in the alternative assessment program. Geo Engineering Report No. 02-08, University of Wisconsin-Madison, USA.

Römkens, M. J. M., Glenn, L. F., Nelson, D. W., and Roth, C. B. "A Laboratory Rainfall Simulator for Infiltration and Soil Detachment Studies." 39 39: 158–160.

Rousseau, M., Cerdan, O., Ern, A., Le Maître, O., and Sochala, P. (2012). "Study of overland flow with uncertain infiltration using stochastic tools." Adv.Water Resour., 38(0), 1-12.

Sajid, A. H. (2009). "Investigation of rainfall runoff process in relation to soil physical and hydraulic properties". Ph.D. University of Guelph (Canada), Canada.

Sajjan, AK, Gyasi-Agyei, Y & Sharma, RH 2012, 'Continuous rainfall runoff modelling of railway embankment steep slopes', in G Smith (ed), 2012 Hydrology and Water Resources Symposium, Engineers Australia, Canberra, Australia."

Scanlon, B.R., Christman, M., Reedy, R.C., Porro, I., Simunek, J., and Flerchinger, G.N. 2002. Intercode comparisons for simulating water balance of surficial sediments in semiarid regions, Water Resources Research, 38(12):1323-1339.

Scherrer, S., Naef, F., Faeh, A. O., and Cordery, I. (2007). "Formation of runoff at the hillslope scale during intense precipitation." Hydrology and Earth System Sciences, 11 907 - 922.

Schmocker-Fackel, P. and Naef, F. and Scherrer, S. 2007. "Identifying runoff processes on the plot and catchment scale." Hydrology and Earth System Sciences, 11 891- 906.

Seeger, M. (2007). "Uncertainty of factors determining runoff and erosion processes as quantified by rainfall simulations." Catena, 71(1), 56-67.

Seyoum, M., van Andel, S. J., Xuan, Y., and Amare, K. (2013). "Precipitation forecasts for rainfall runoff predictions. A case study in poorly gauged Ribb and Gumara catchments, upper Blue Nile, Ethiopia." Physics and Chemistry of the Earth, Parts A/B/C, 61–62(0), 43-51.

Sheridan, G. J., Noske, P. J., Lane, P. N. J., and Sherwin, C. B. (2008). "Using rainfall simulation and site measurements to predict annual interrill erodibility and phosphorus generation rates from unsealed forest roads: Validation against in-situ erosion measurements." Catena, 73(1), 49-62.

Shelton, C. H., R. D. von Bernuth, and S. P. Rajbhandari. 1985. A continuous–application rainfall simulator. Transactions of the ASAE 28(4): 1115–1119.

Shuster, W., Pappas, E., and Zhang, Y. (2008). "Laboratory -Scale Simulation of Runoff Response from Pervious-Impervious Systems." J.Hydrol.Eng., 13(9), 886-893.

Smith, R.E. 2002. Infiltration theory for hydrologic applications. American Geophysical Union, Washington, DC.

Stone, J.J., Paige, G.B., and Hawkins, R.H. 2008. "Rainfall intensity-dependent infiltration rates on rangeland rainfall simulator plots." Transactions of the ASABE, 51(1): 45-53, 51(1)

Suarez, D. L., Wood, J. D., and Lesch, S. M. 2006 . "Effect of SAR on water infiltration under a sequential rain–irrigation management system." Agric.Water Manage., 86(1–2), 150-164.

Swanson, D. A., Barbour, S. L., Wilson, G. W., and O'Kane, M. (1995). "Modelling the Performance of Engineered Soil Covers for Acid Generating Mine Waste." Conference on Mining and the Environment, 861.

Tami, D 2004 Mechanisms of Sloping Capillary Barrier under High Rainfall Conditions. PhD thesis. Nanyang Technological University. p243.

Tami, D., Rahardjo, H., Leong, E., and Fredlund, D. G. 2004. "Design and laboratory verification of a physical model of sloping capillary barrier." Canadian Geotechnical Journal, 41 814-830.

The International Network for Acid Prevention (INAP). 2009. Global acid rock drainage guide (GARD guide) [online]. Available from http://www.gardguide.com/ [cited 02 2015].

Ulrich, U., Dietrich, A., and Fohrer, N. 2013 . "Herbicide transport via surface runoff during intermittent artificial rainfall: A laboratory plot scale study." Catena, 101(0), 38-49.

Van den Putte, A., Govers, G., Leys, A., Langhans, C., Clymans, W., and Diels, J. (2013). "Estimating the parameters of the Green–Ampt infiltration equation from rainfall simulation data: Why simpler is better." Journal of Hydrology, 476(0), 332-344.

Wallach, R., Grigorin, G., and (Byk), J. R. (1997). "The errors in surface runoff prediction by neglecting the relationship between infiltration rate and overland flow depth." Journal of Hydrology, 200(1–4), 243-259.

Westra, S. Brown, C. Lall, U. Koch, I. Sharma A. 2010 Interpreting variability in global SST data using independent component analysis and principal component analysis Int. J. Climatol. http://dx.doi.org/10.1002/joc.1888

Weyman, D. R. 1975 . Run off processes and streamflow modelling, 52 pages, 90p ISBN 0–19–874038-7 Oxford University Press Series.

Wilson, G. W., Wickland, B., and Fines, P. 2002. Concepts for co-mixing waste rock and tailings. Symposium on Mining and the Environment: Challenges and Prospects. Rouyn-Noranda, Quebec. 3-5 November 2002.

Wilson, G. W., Fredlund, D.G., and Barbour, S.L. 1994. Coupled soil-atmosphere modelling for soil evaporation. Canadian Geotechnical Journal, 31(2): 151– 161. doi:10.1139/t94-021.

Wilson, G. W. 2006. The application of cover systems for mine closure - are we doing it right? In First International Seminar on Mine Closure, Perth, Australia, pp.17.045631-42.

Wainwright, J. and Parsons, A.J. 2002. The effect of temporal variations in rainfall on scale dependency in runoff coefficients, Water Resources Research, 38(12): 1271-1281.

Won, C. H., Choi, Y. H., Shin, M. H., Lim, K. J., and Choi, J. D. (2012). "Effects of rice straw mats on runoff and sediment discharge in a laboratory rainfall simulation." Geoderma, 189–190(0), 164-169.

Wu, C. L., and Chau, K. W. (2011). "Rainfall–runoff modeling using artificial neural network coupled with singular spectrum analysis." Journal of Hydrology, 399(3–4), 394-409.

Yang, H., Rahardjo, H., Leong, E. C., and Fredlund, D. G. 2004 . "A study of infiltration on three sand capillary barriers." Canadian Geotechnical Journal, 41 629-643.

Yamamuro, J. A. and Wood, F. M. 2004 Effect of depositional method on the undrained behavior and microstructure of sand with silt, Soil Dynamics and Earthquake Engineering, Volume 24, Issues 9–10, Pages 751-760, ISSN 0267-7261, http://dx.doi.org/10.1016/j.soildyn.2004.06.004

Yeasmin, D., and Pasha, M. (2008). "Runoff Prediction by GIS Using Optimal Number of Rain Gauges." American Society of Civil Engineers, 1-9.

Young, A. R. (2006). "Stream flow simulation within UK ungauged catchments using a daily rainfall runoff model." Journal of Hydrology, 320(1–2), 155-172.

Yu, P., Yang, T., and Chen, S. (2001). "Comparison of uncertainty analysis methods for a distributed rainfall–runoff model." Journal of Hydrology, 244(1–2), 43-59.

Zhan, T. L., Ng, C. W., and Fredlund, D. G. (2007). "Field study of rainfall infiltration into a grassed unsaturated expansive soil slope." Canadian Geotechnical Journal, 44 392-408.

APPENDIX I

Infiltration Capacity and Void Ratio

Infiltration capacity samples for Devon silt

Sample	Dry Density(g/cm^3)	Infiltration Capacity[5] (m/s)
S3	1.6	2.4E-08
S1	1.54	3.2E-08
S4	1.5	4.8E-08
S2	1.46	1.0E-07

[5] Indicates the value at which the infiltration capacity function levelled off.

Infiltration capacity functions for Devon silt samples at different density.

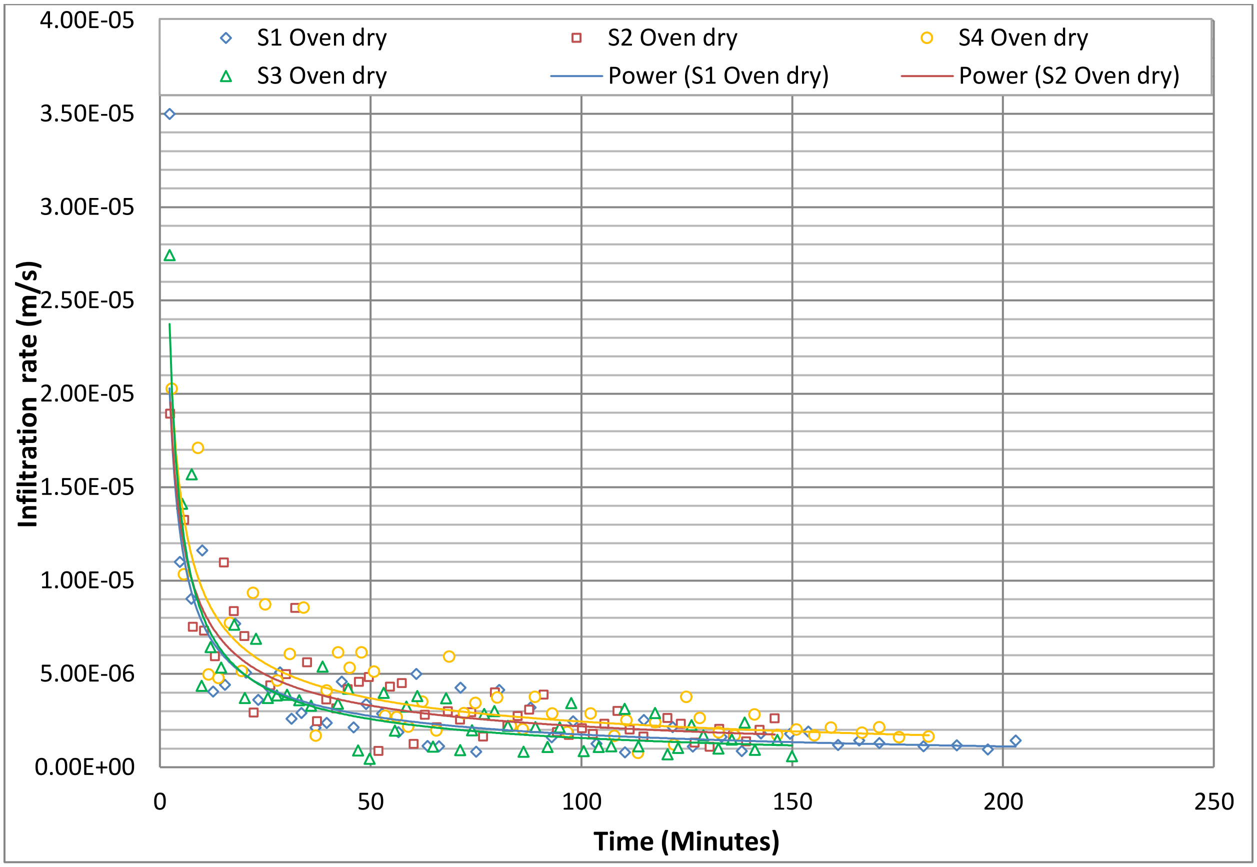

A close up to the part where infiltration capacity functions for Devon silt samples equilibrate.

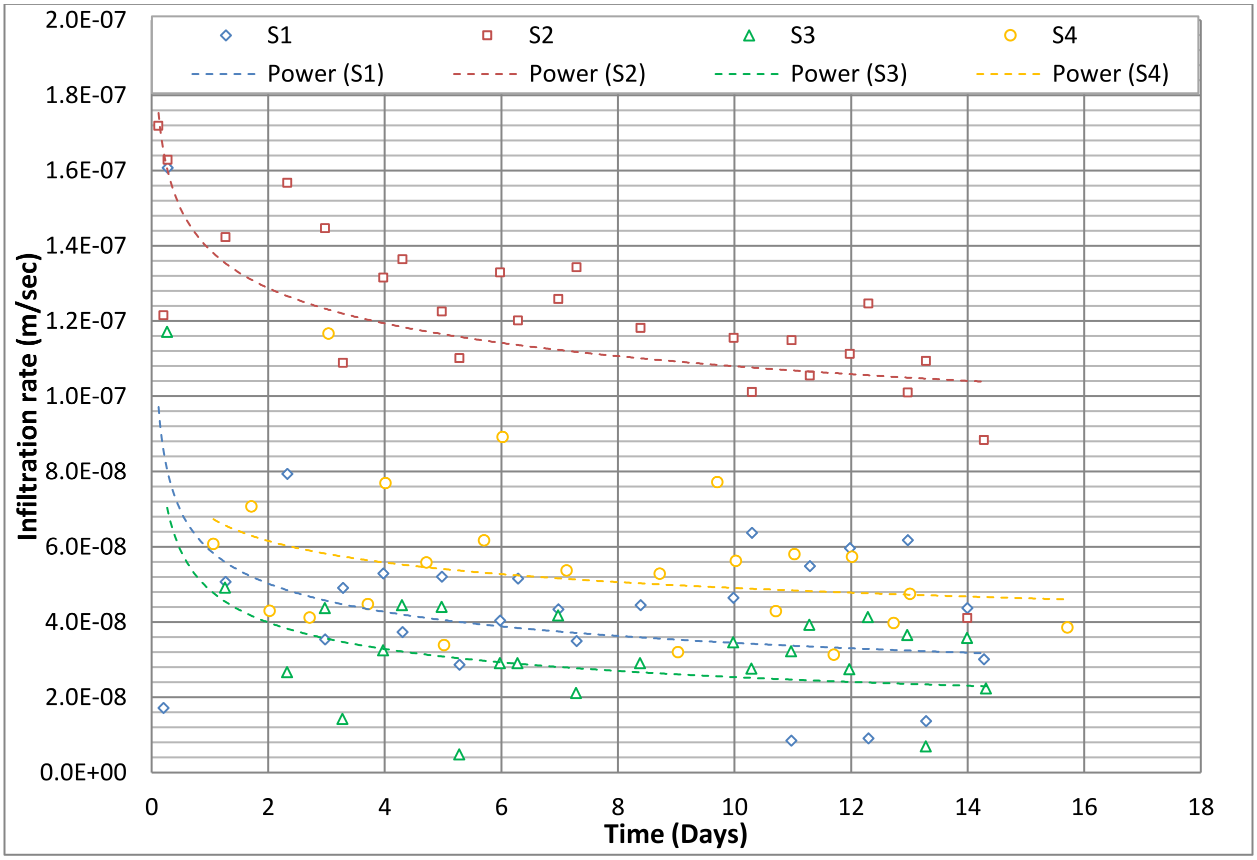

Tailings Beach Sand Samples

Sample	Dry Density(g/cm^3)	Infiltration Capacity (m/s)
S1	1.6	1.81E-04
S3	1.54	1.90E-04
S4	1.5	1.95E-04
S2	1.46	2.00E-04

A close up to the part where infiltration capacity functions for tailings beach sand samples equilibrate.

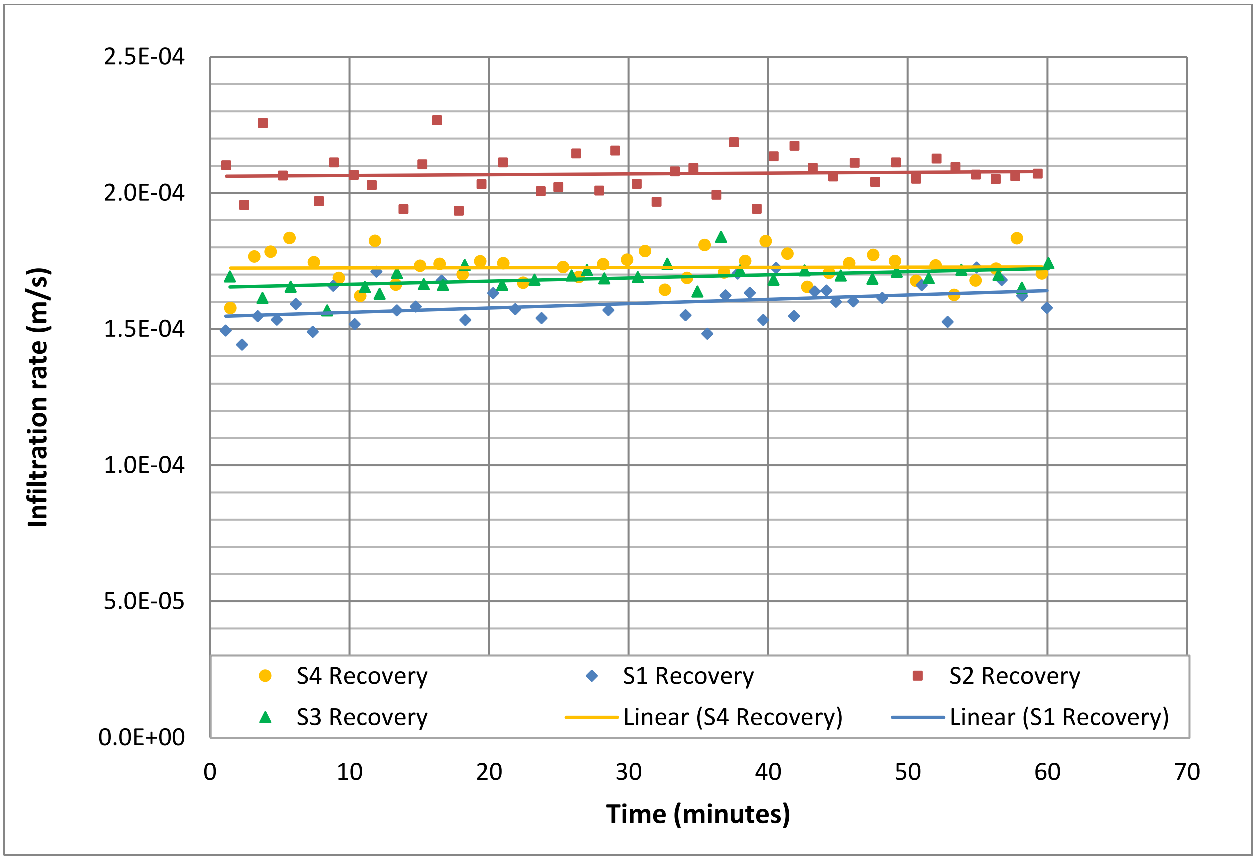

Calibration curves for measuring devices

Flowmeter Calibration

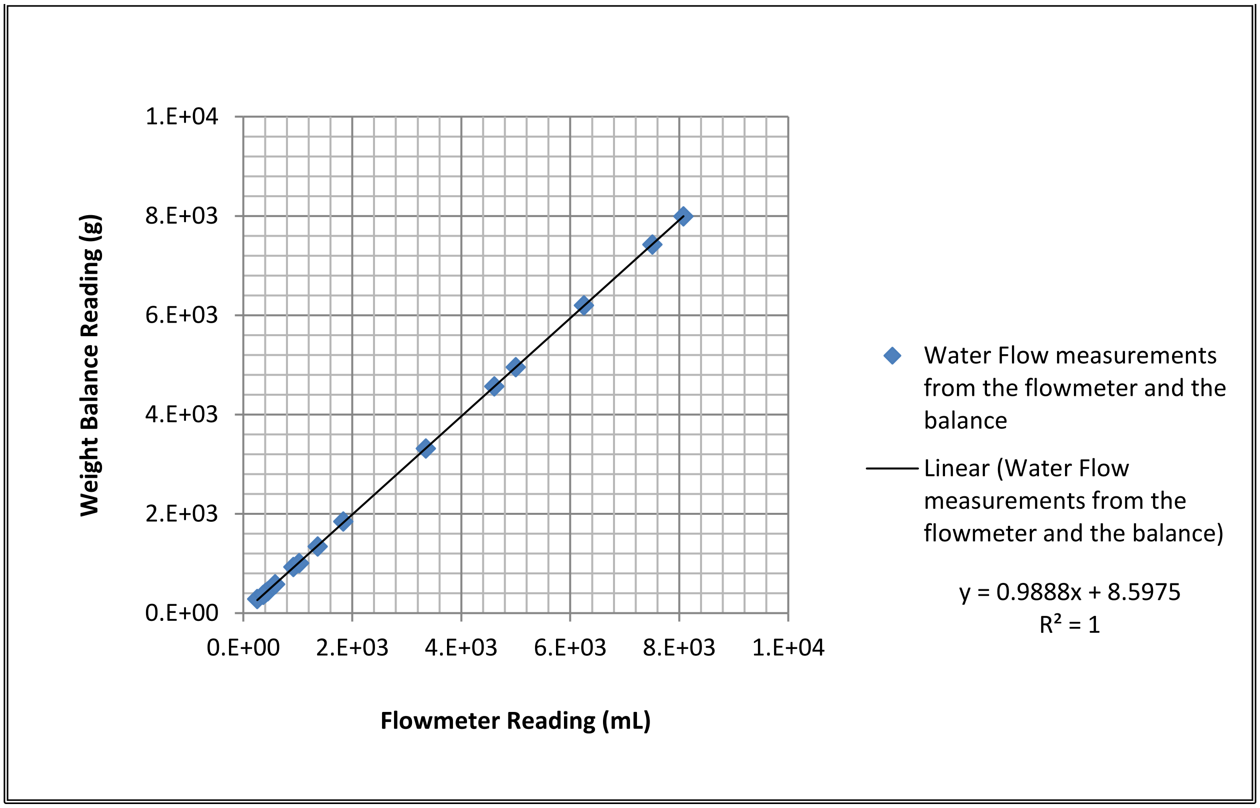

Pressure Gauge Calibration

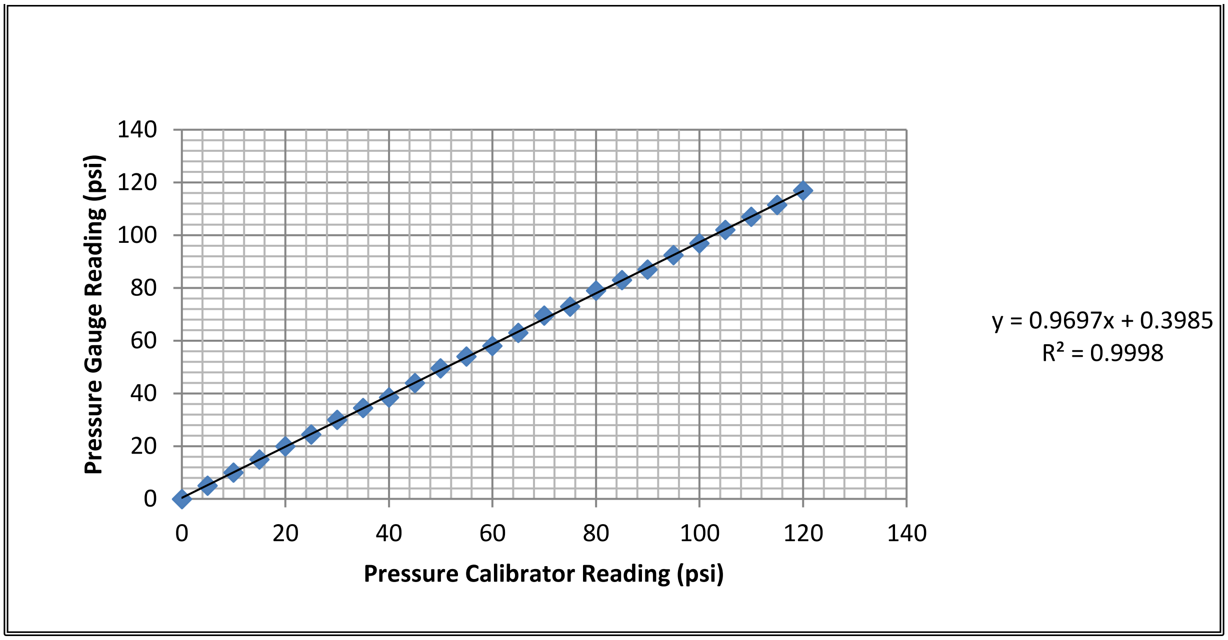

TDR Probes Calibration

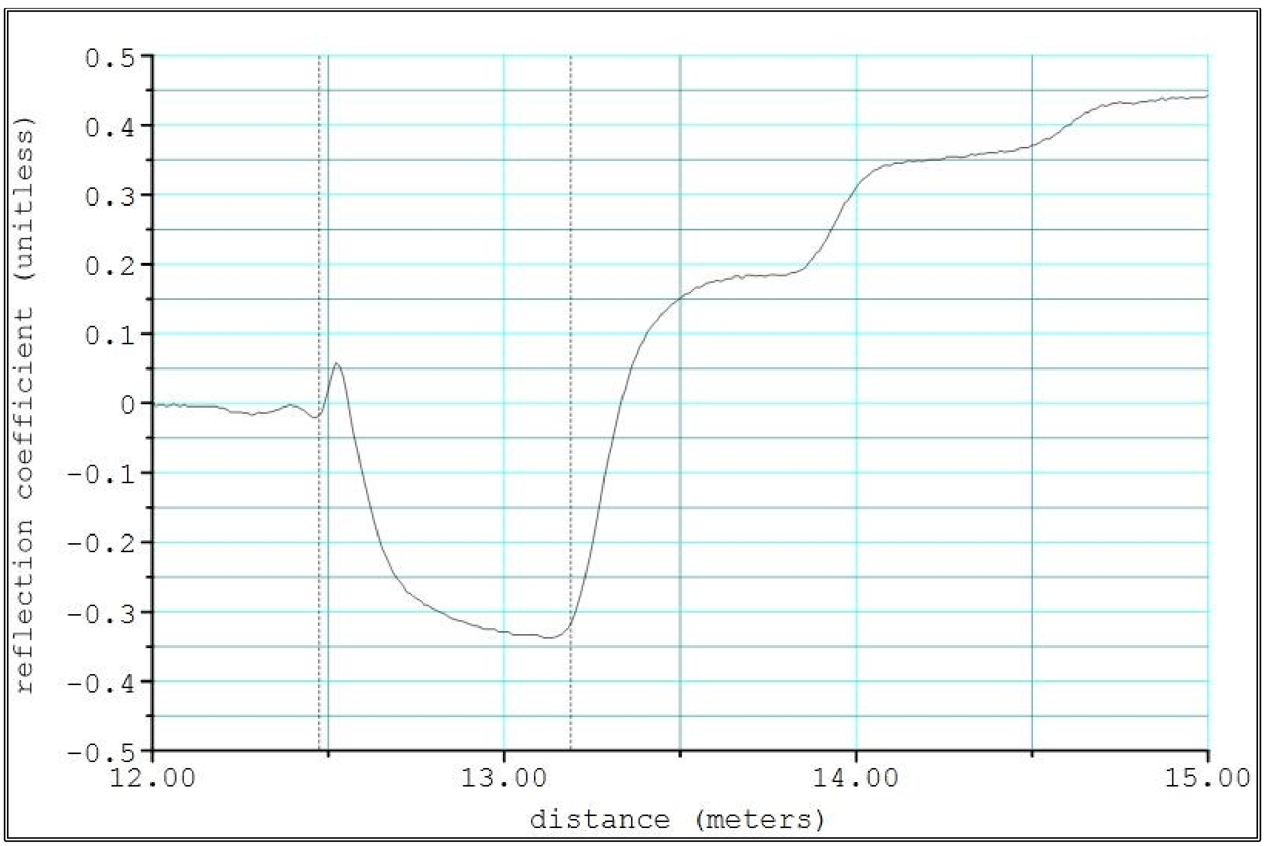

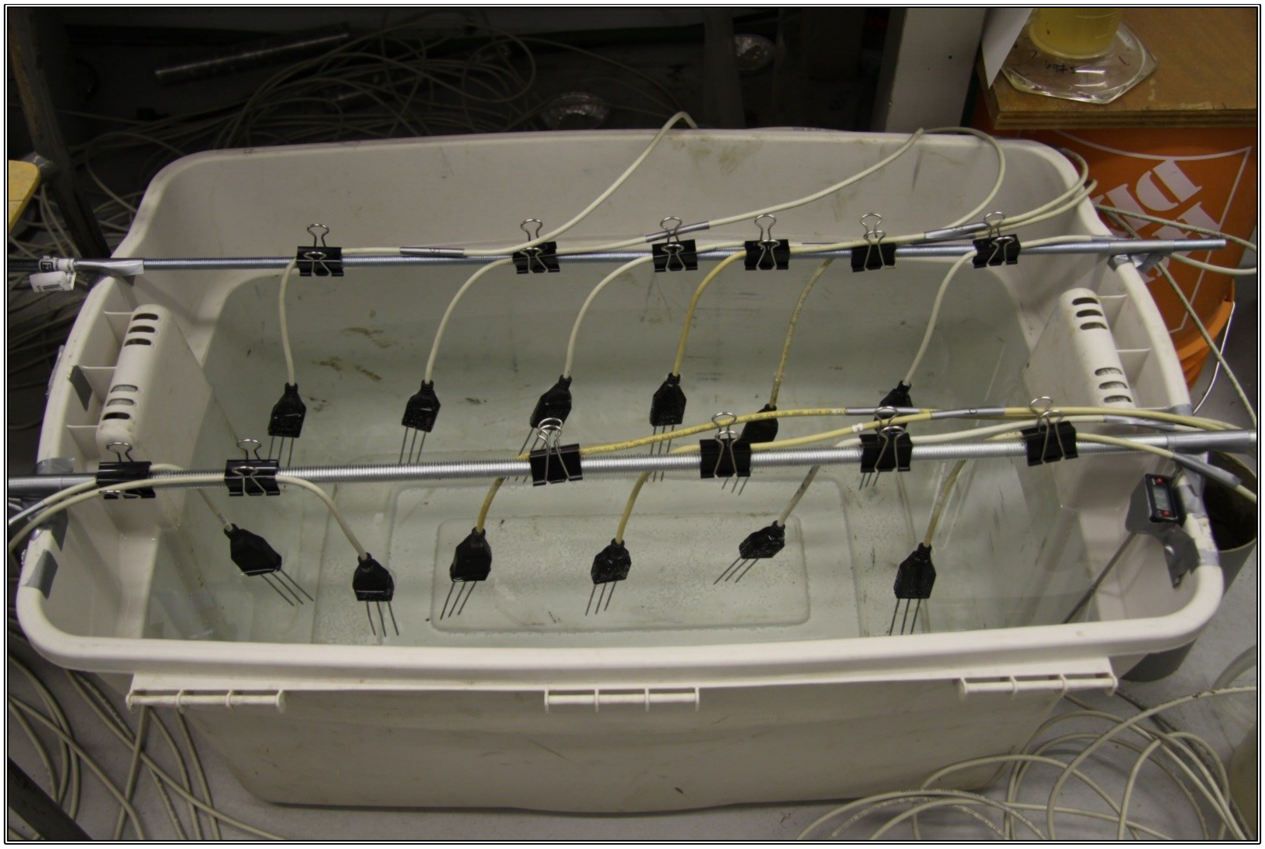

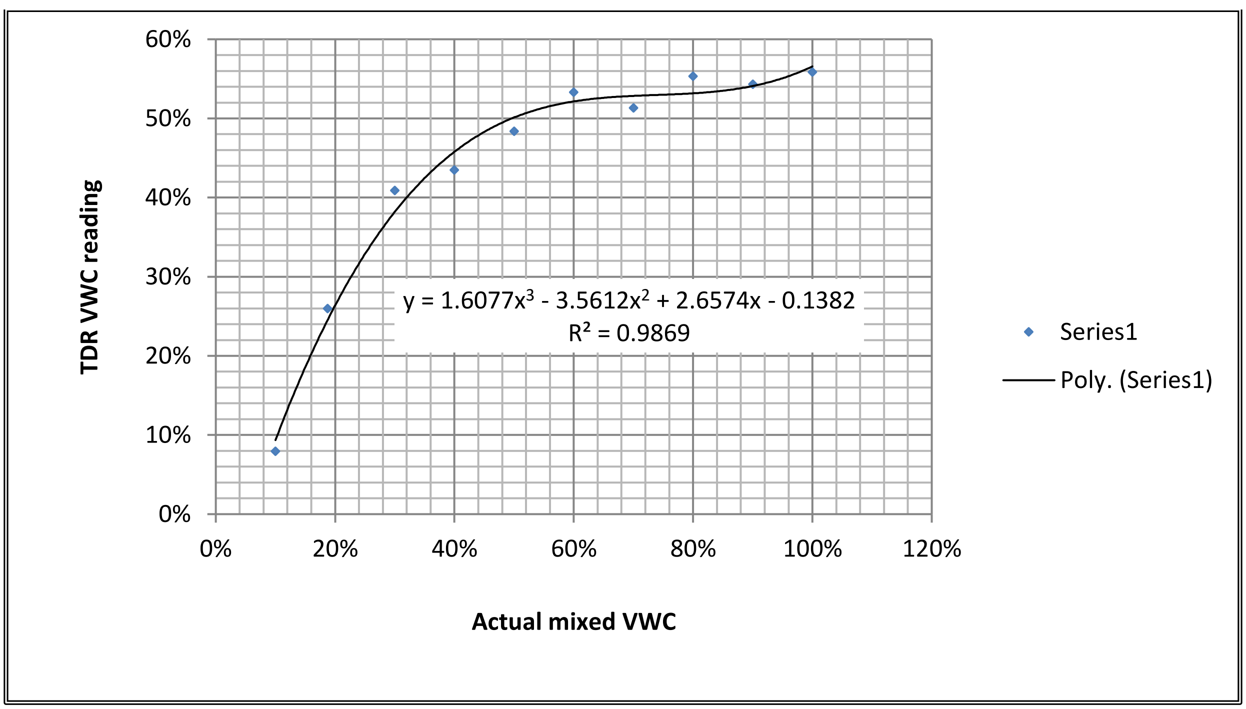

60%
50%
40%
30%
20%
10%
0%
TDR VWC reading
y = 1.6077x³ - 3.5612x² + 2.6574x - 0.1382
R² = 0.9869
0%
20%
40%
60%
80%
100%
120%
Actual mixed VWC
Series1
Poly. (Series1)

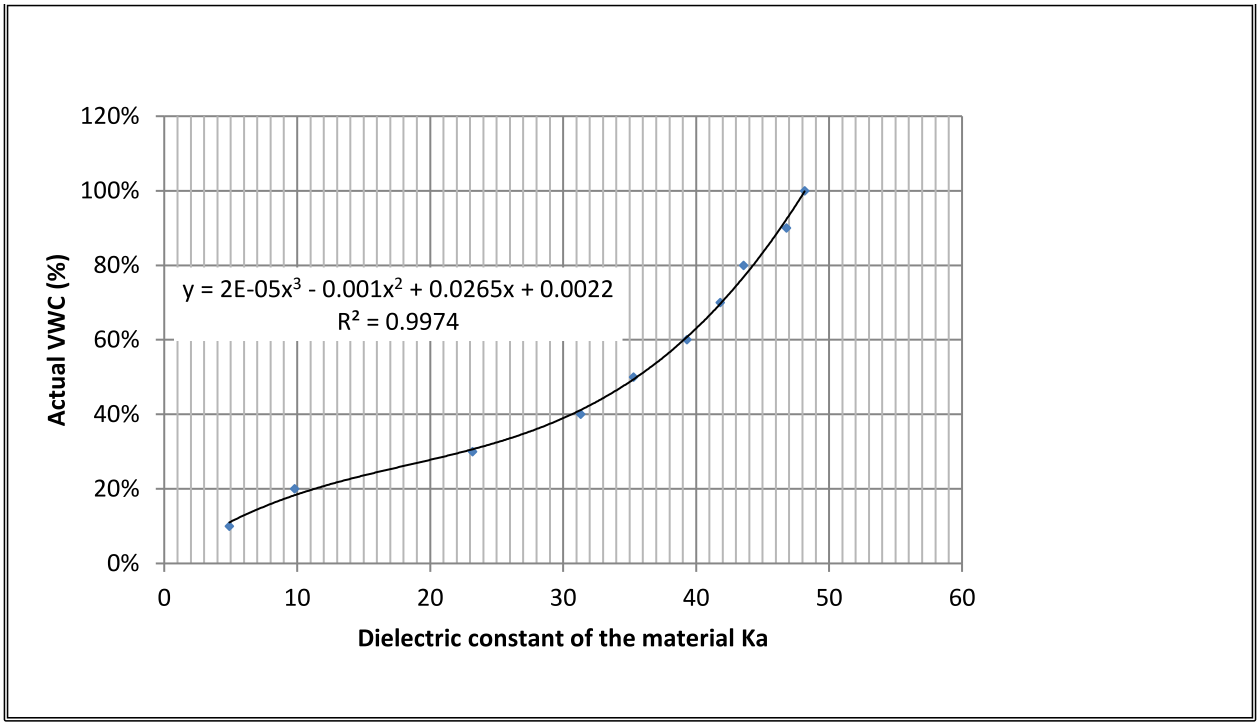

y = 2E-05x³ - 0.001x² + 0.0265x + 0.0022
R² = 0.9974
120%
100%
80%
60%
40%
20%
0%
Actual VWC (%)
0
10
20
30
40
50
60
Dielectric constant of the material Ka

APPENDIX II

Time to runoff in unsaturated silt profiles

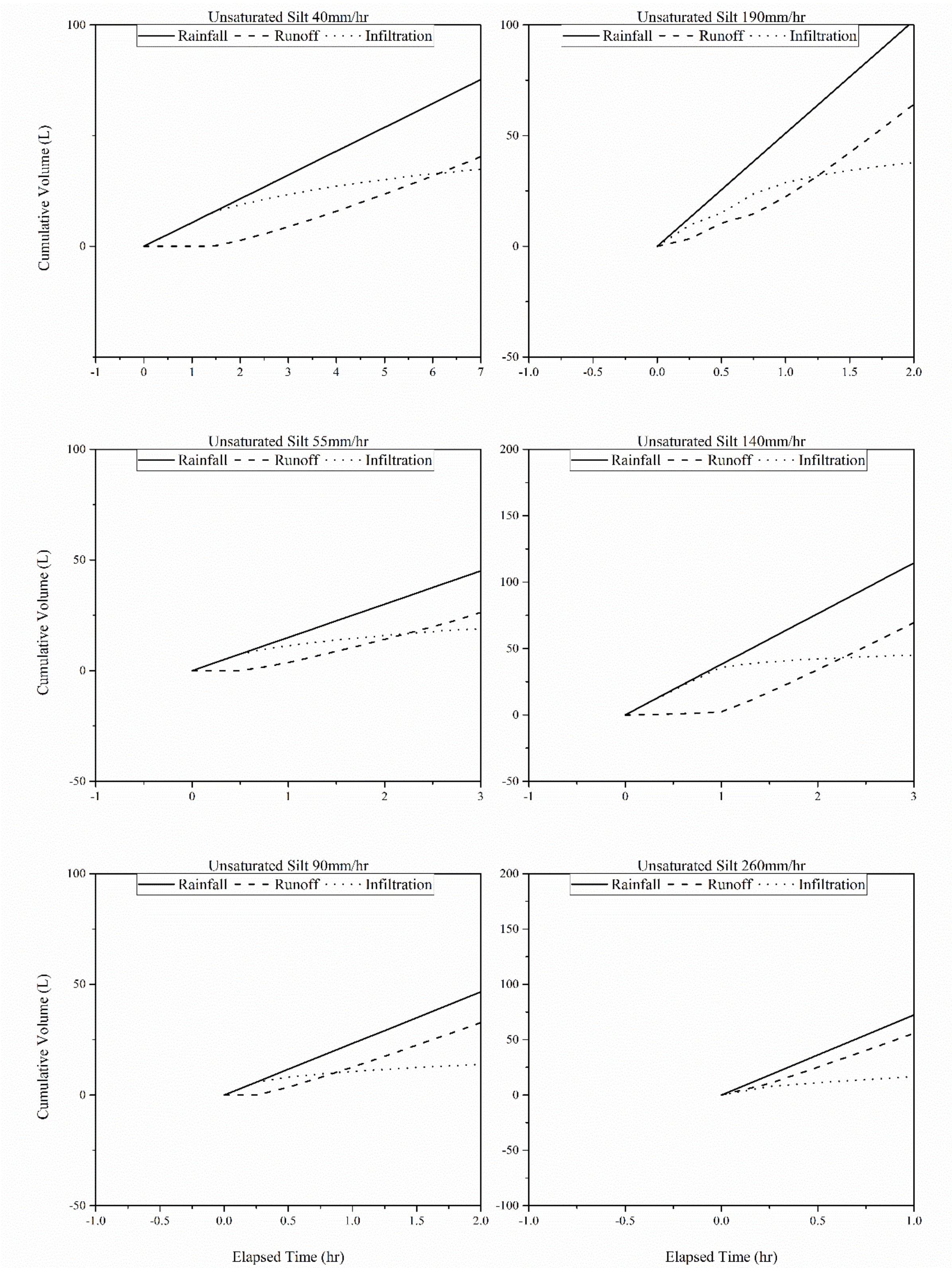

Time to runoff in unsaturated capillary barrier profiles

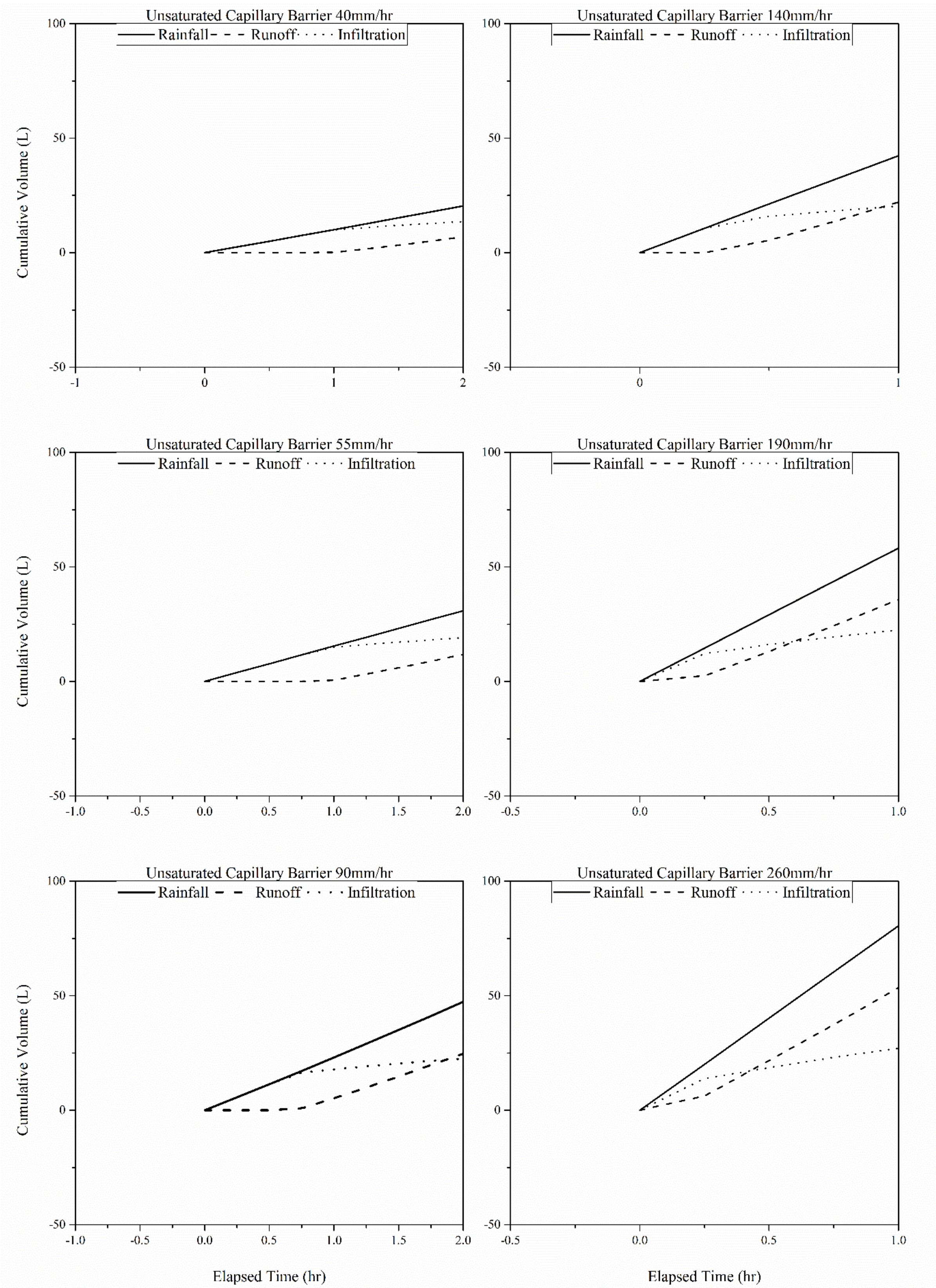

APENDIX II

TDR measurements in unsaturated silt profiles

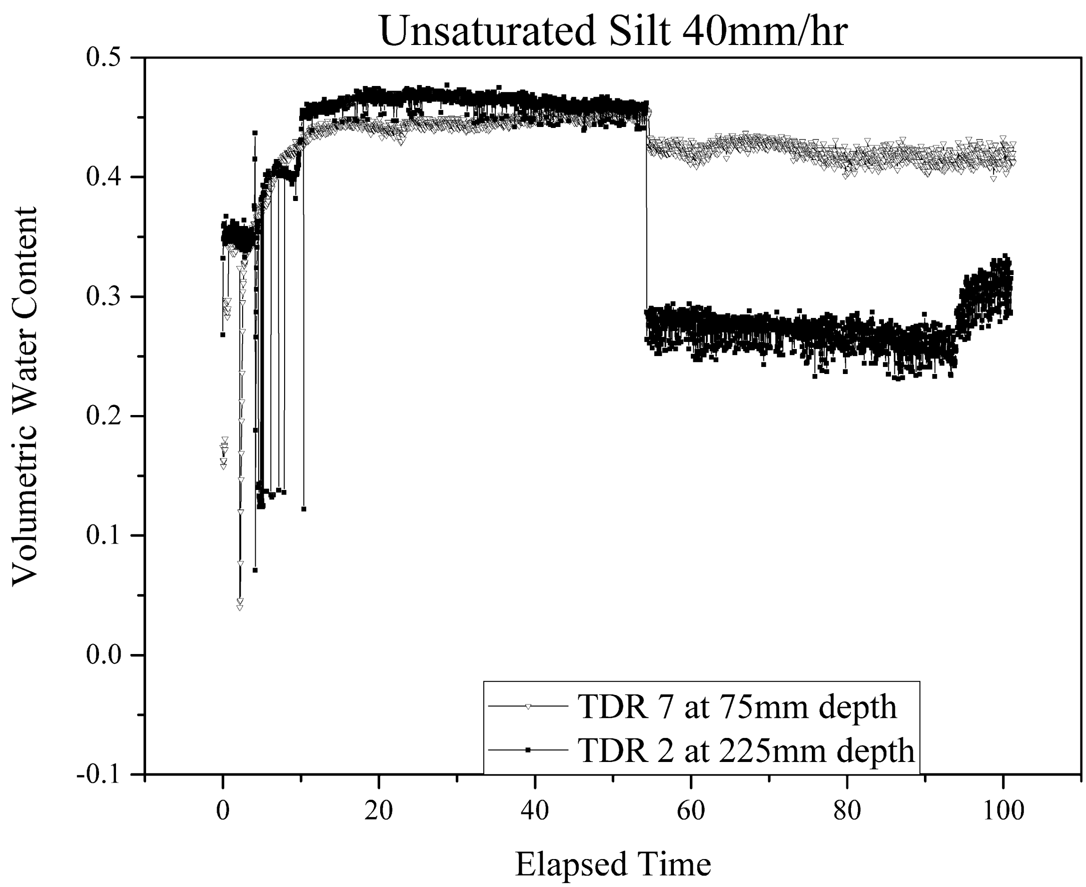

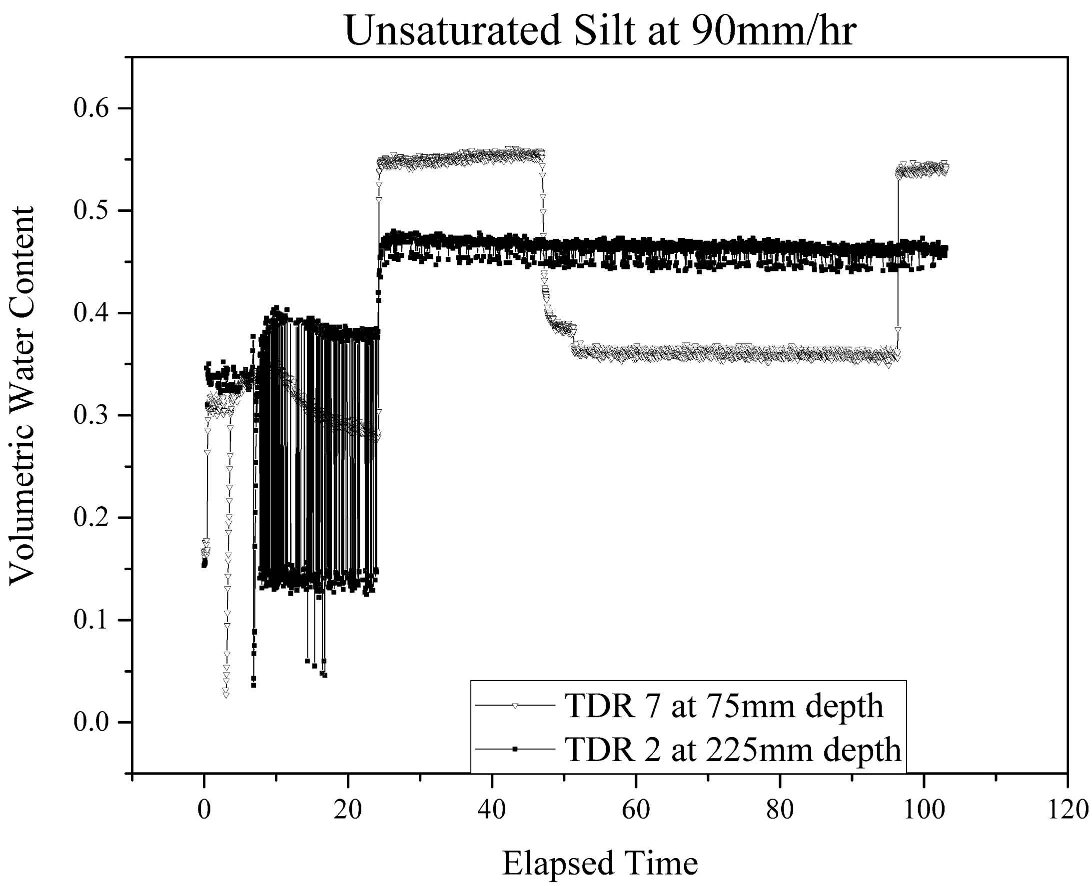

Unsaturated Silt at 90mm/hr
Volumetric Water Content
0.0
0.1
0.2
0.3
0.4
0.5
0.6
0
20
40
60
80
100
120
Elapsed Time
TDR 7 at 75mm depth
TDR 2 at 225mm depth

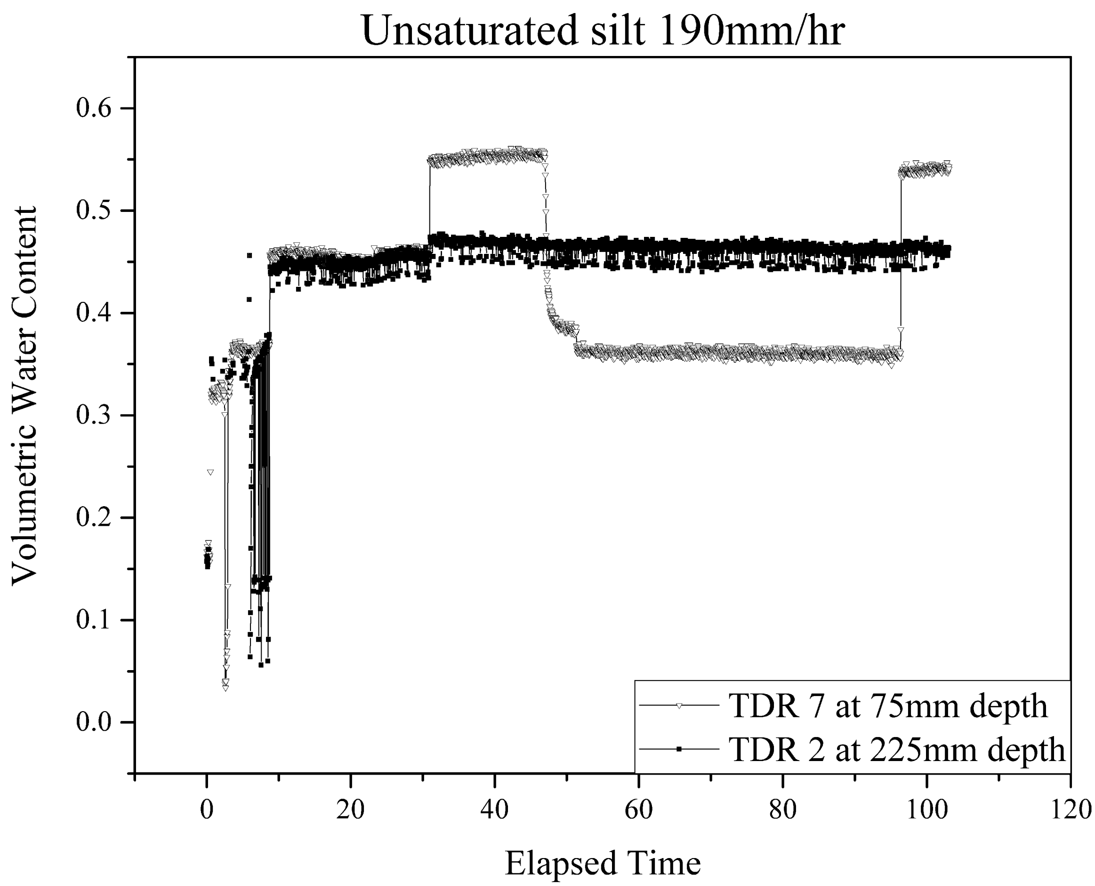

Unsaturated silt 190mm/hr
Volumetric Water Content
0.0
0.1
0.2
0.3
0.4
0.5
0.6
0
20
40
60
80
100
120
Elapsed Time
TDR 7 at 75mm depth
TDR 2 at 225mm depth

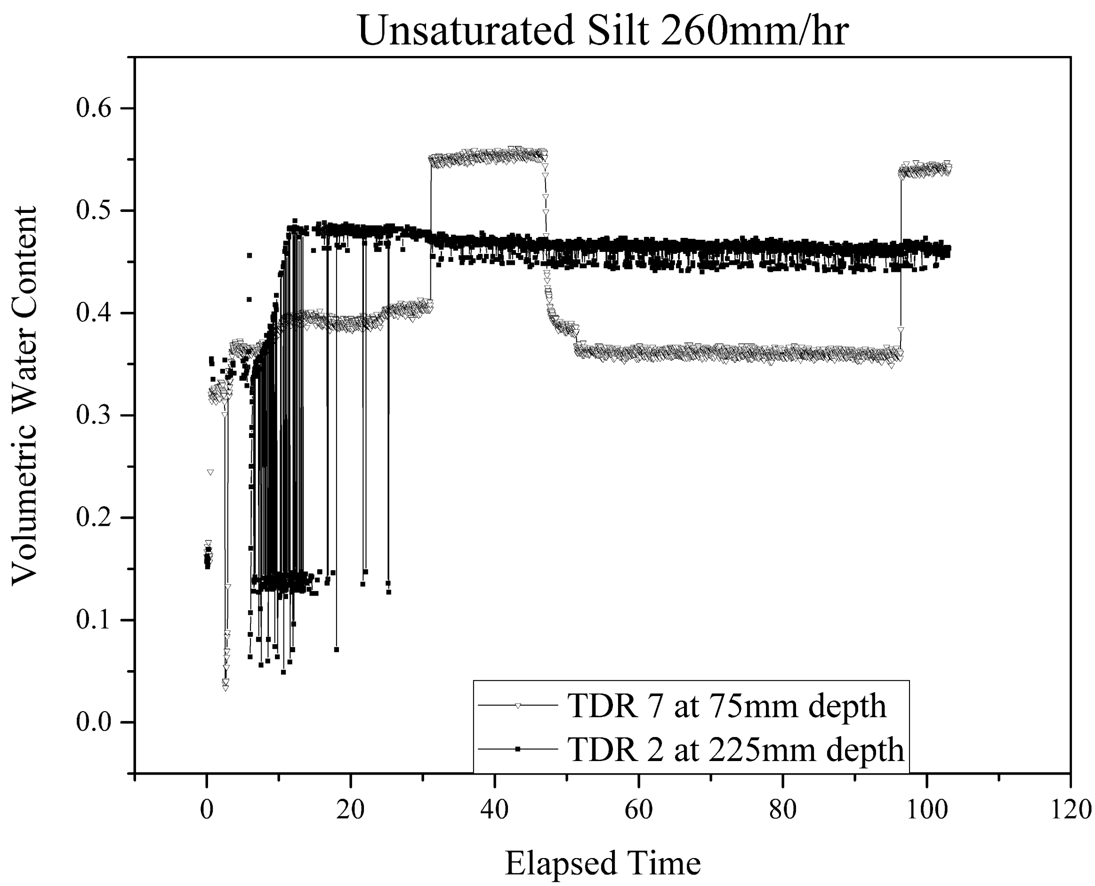
Unsaturated Silt 260mm/hr
Volumetric Water Content
Elapsed Time
0.6
0.5
0.4
0.3
0.2
0.1
0.0
0
20
40
60
80
100
120
TDR 7 at 75mm depth
TDR 2 at 225mm depth

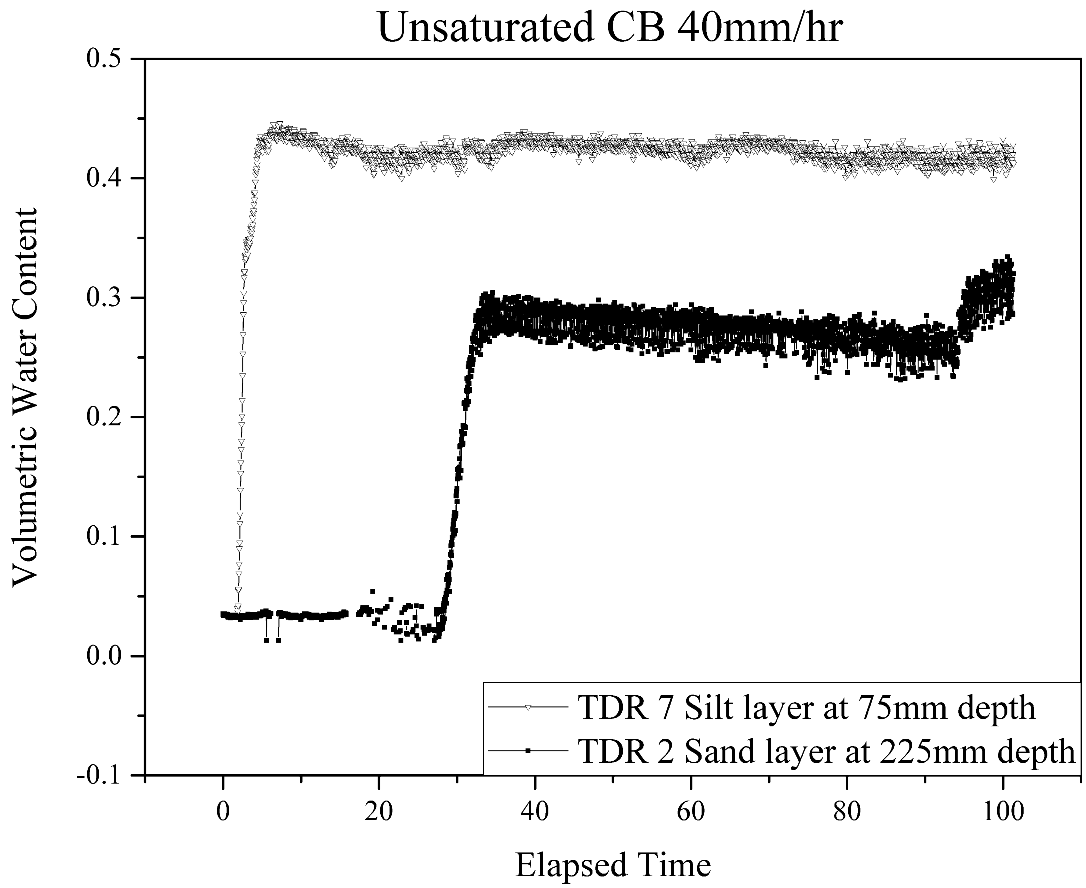
Unsaturated CB 40mm/hr
Volumetric Water Content
0.5
0.4
0.3
0.2
0.1
0.0
-0.1
0
20
40
60
80
100
Elapsed Time
TDR 7 Silt layer at 75mm depth
TDR 2 Sand layer at 225mm depth

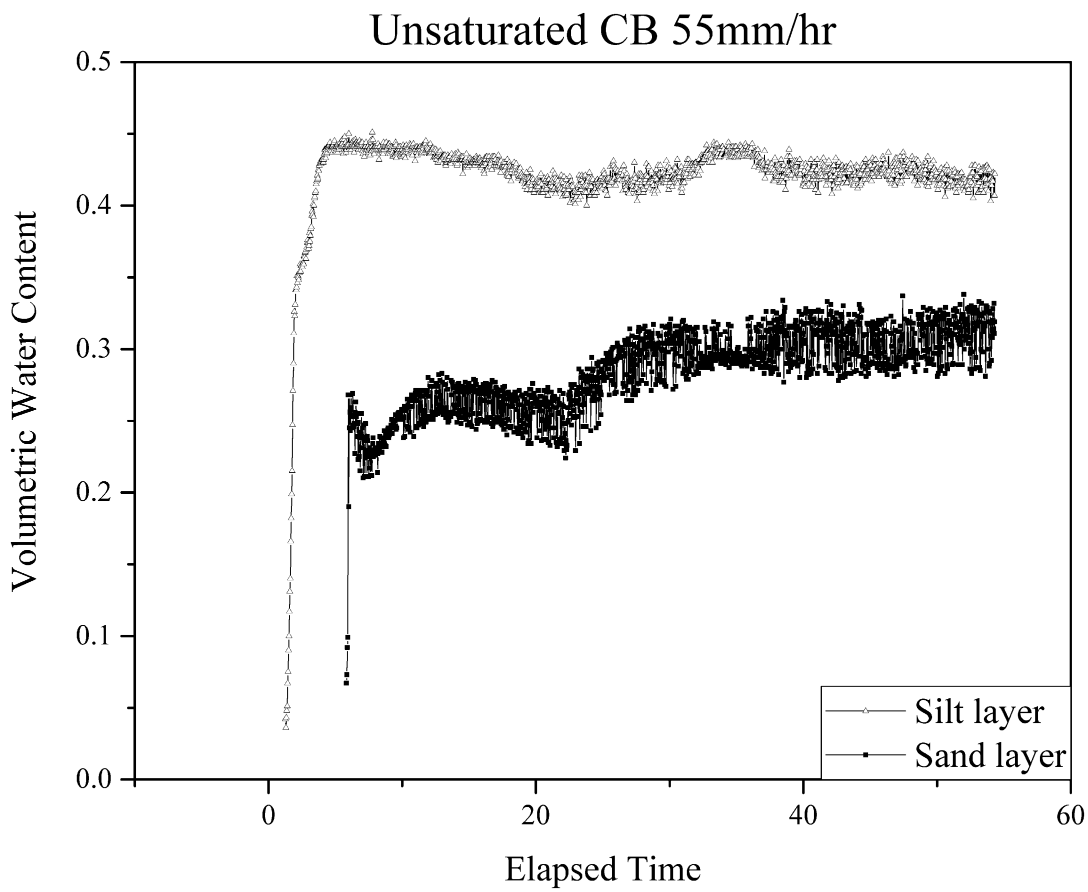
Unsaturated CB 55mm/hr
Volumetric Water Content
0.0
0.1
0.2
0.3
0.4
0.5
0
20
40
60
Elapsed Time
Silt layer
Sand layer

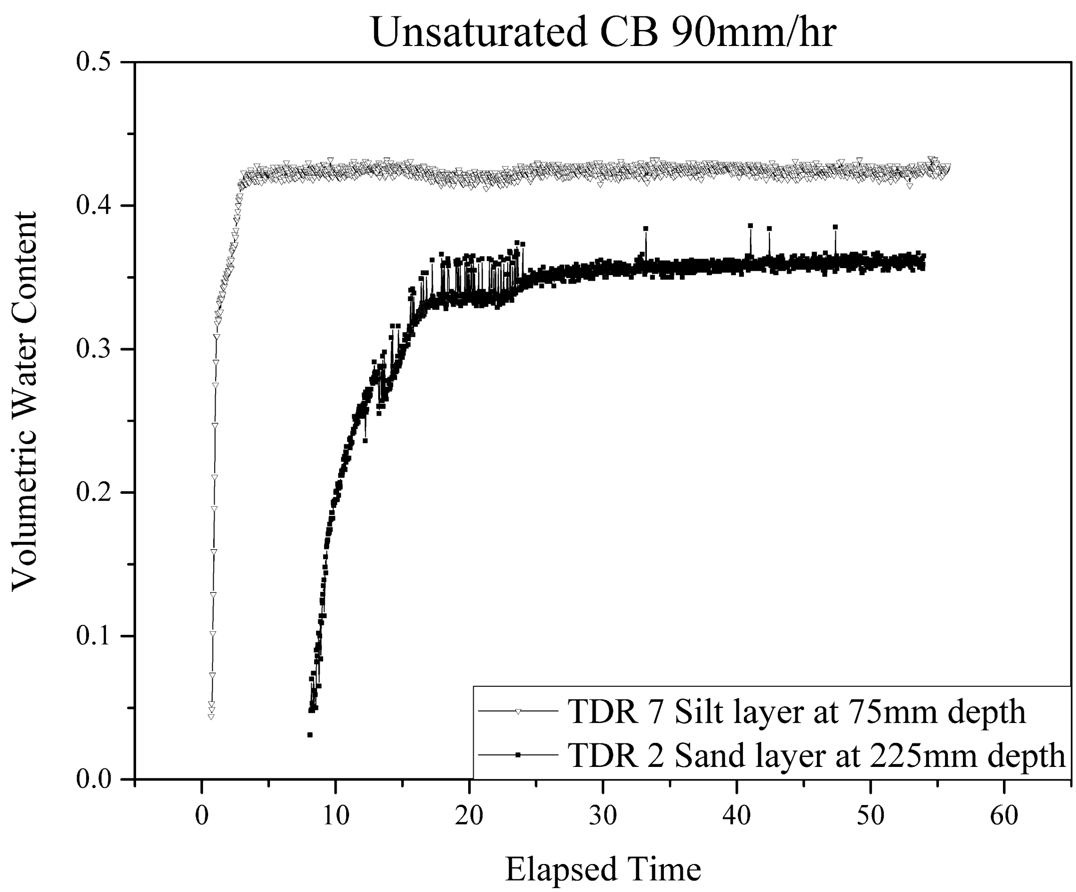

Unsaturated CB 90mm/hr
Volumetric Water Content
Elapsed Time
TDR 7 Silt layer at 75mm depth
TDR 2 Sand layer at 225mm depth
0.0
0.1
0.2
0.3
0.4
0.5
0
10
20
30
40
50
60

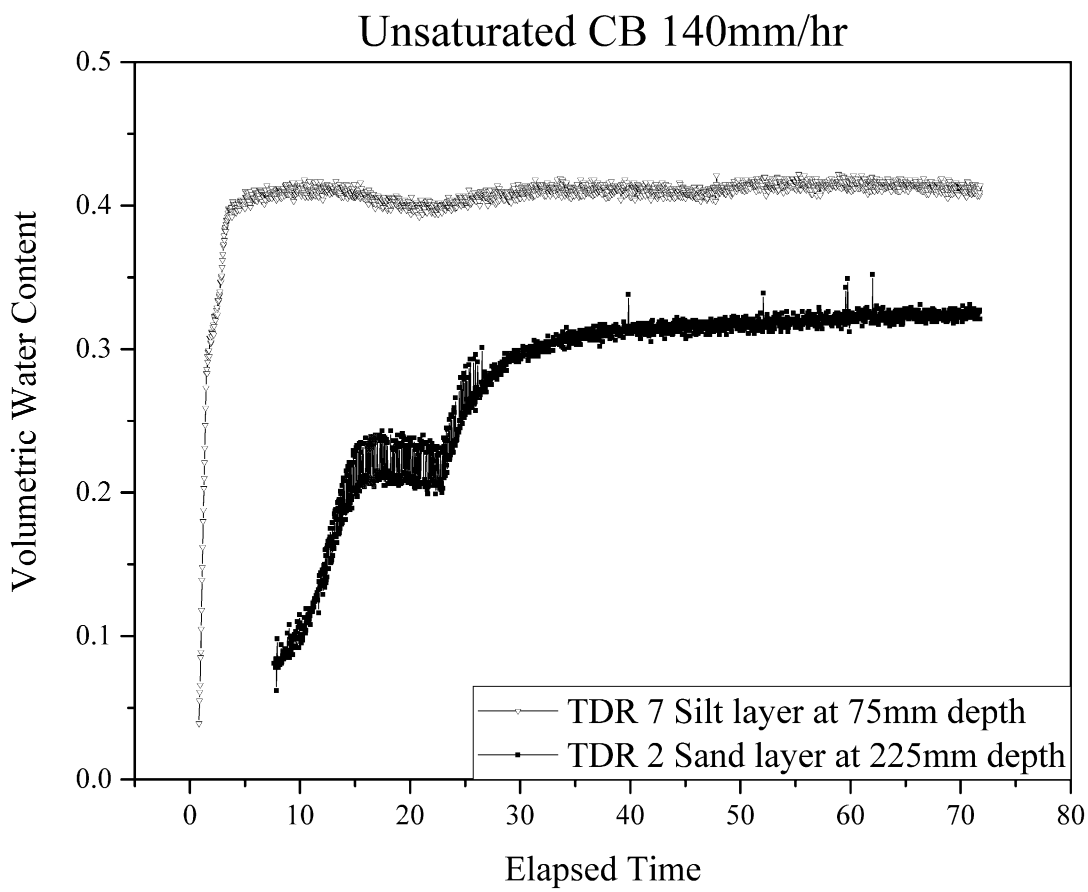

Unsaturated CB 140mm/hr
Volumetric Water Content
0.0
0.1
0.2
0.3
0.4
0.5
0
10
20
30
40
50
60
70
80
Elapsed Time
TDR 7 Silt layer at 75mm depth
TDR 2 Sand layer at 225mm depth

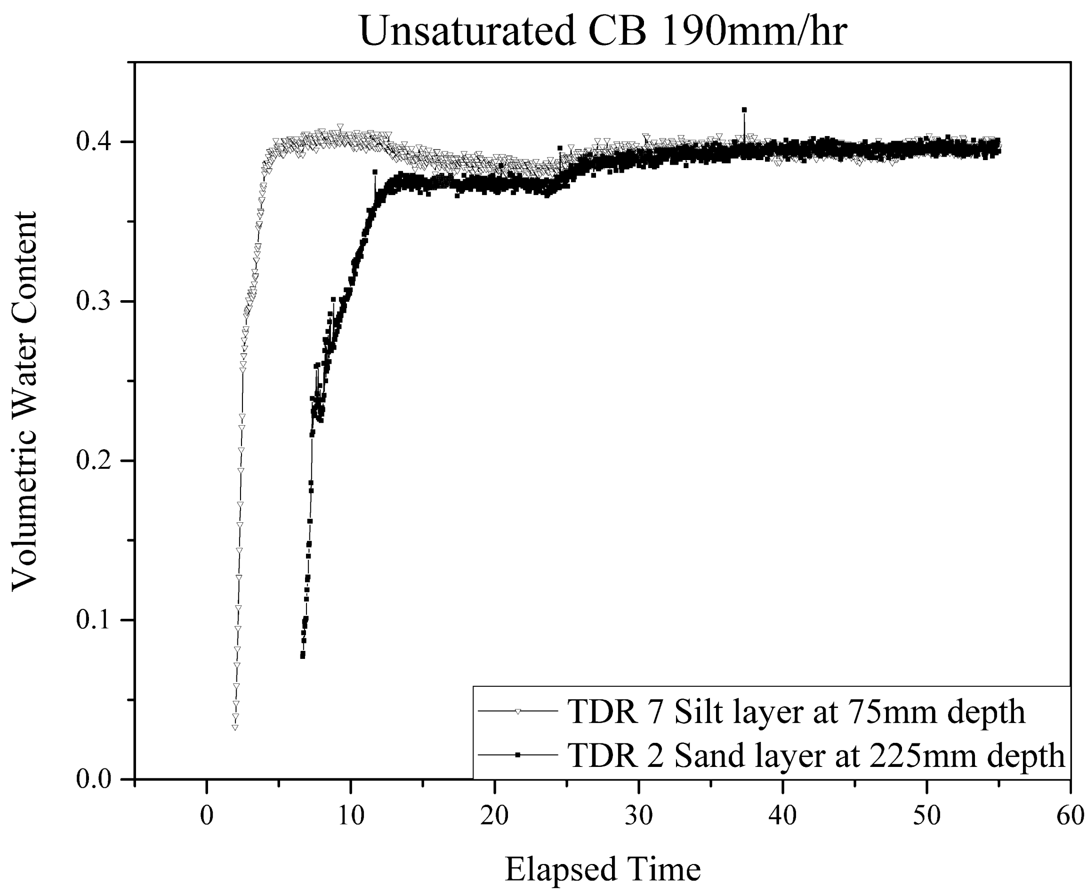
Unsaturated CB 190mm/hr
Volumetric Water Content
0.0
0.1
0.2
0.3
0.4
0
10
20
30
40
50
60
Elapsed Time
TDR 7 Silt layer at 75mm depth
TDR 2 Sand layer at 225mm depth

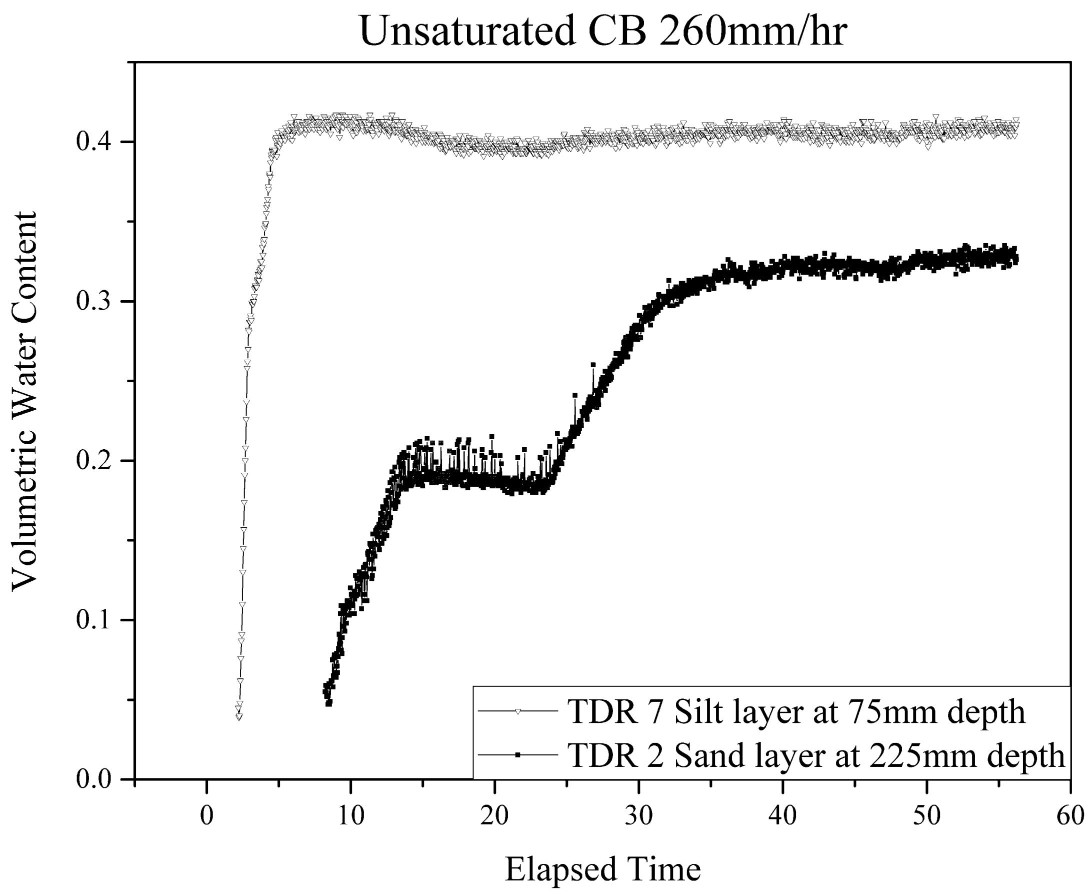

Unsaturated CB 260mm/hr
Volumetric Water Content
0.0
0.1
0.2
0.3
0.4
0
10
20
30
40
50
60
Elapsed Time
TDR 7 Silt layer at 75mm depth
TDR 2 Sand layer at 225mm depth

APPENDIX III

Matric suction profiles for unsaturated silt and unsaturated capillary barrier profiles.

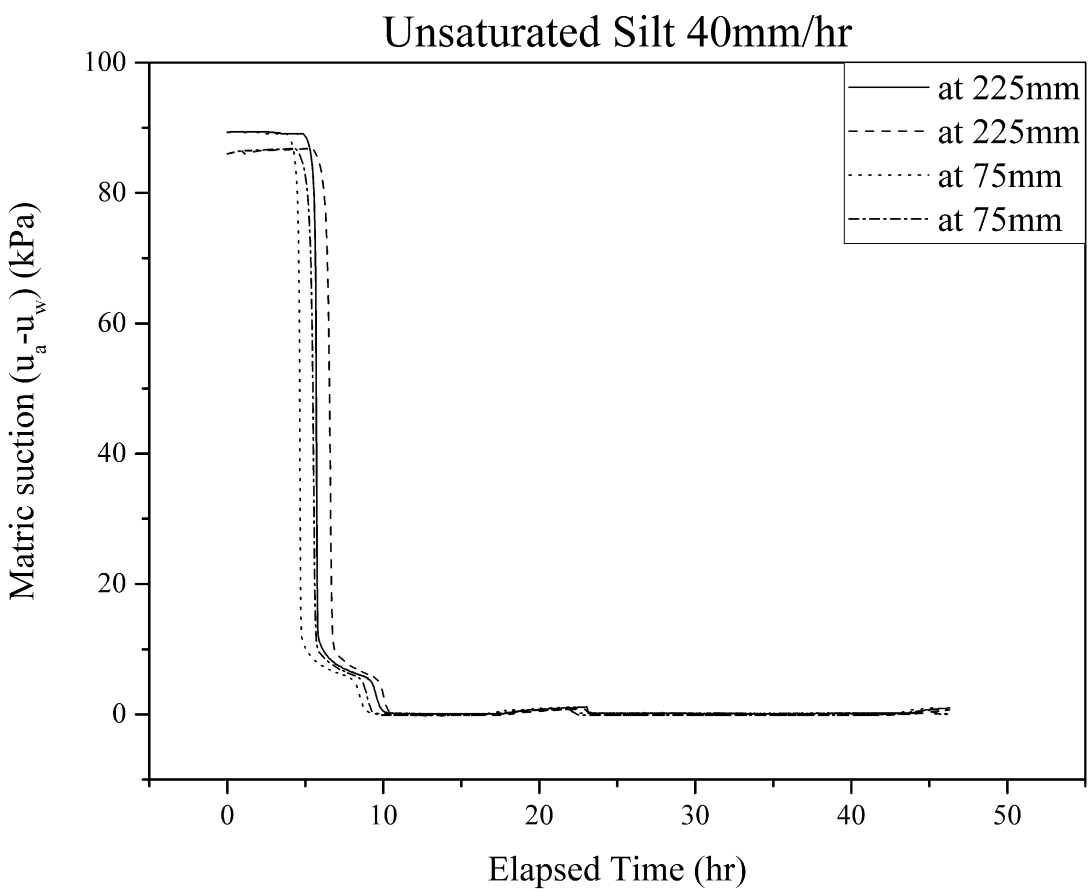

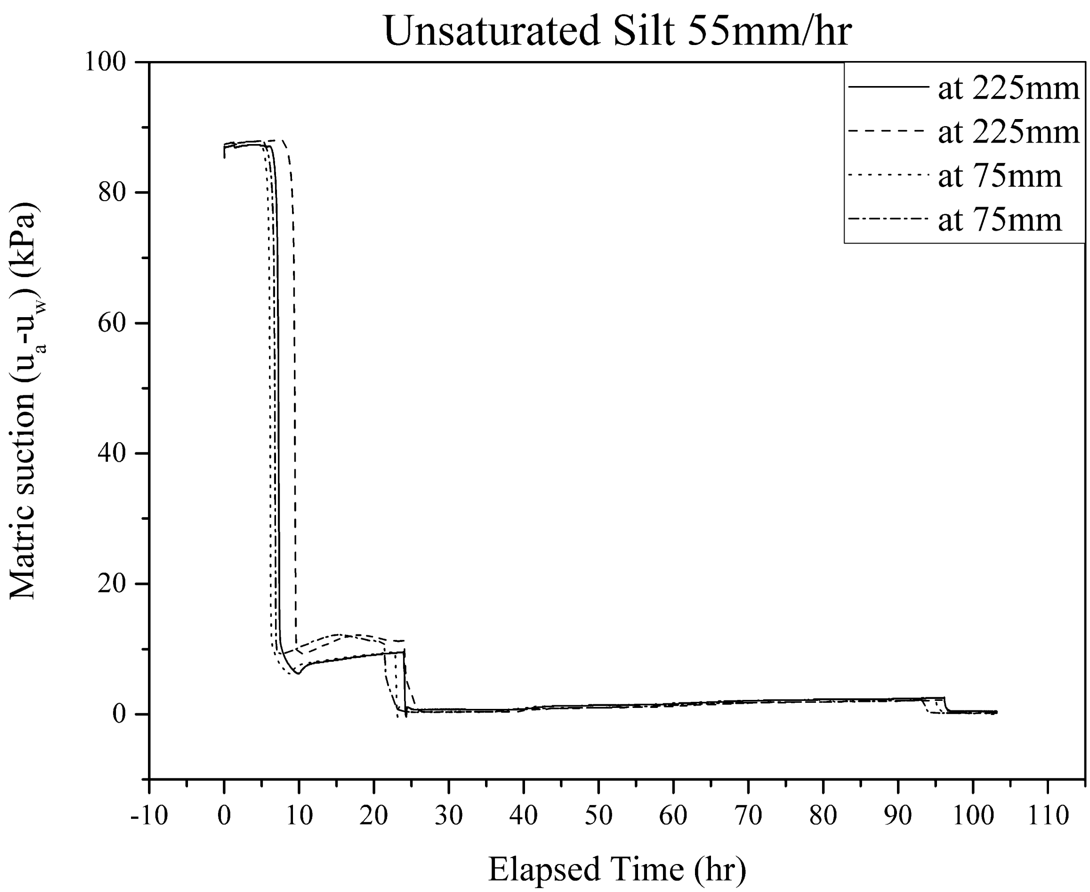

Unsaturated Silt 55mm/hr
Matric suction (u_a-u_w) (kPa)
Elapsed Time (hr)
at 225mm
at 225mm
at 75mm
at 75mm
100
80
60
40
20
0
-10
0
10
20
30
40
50
60
70
80
90
100
110

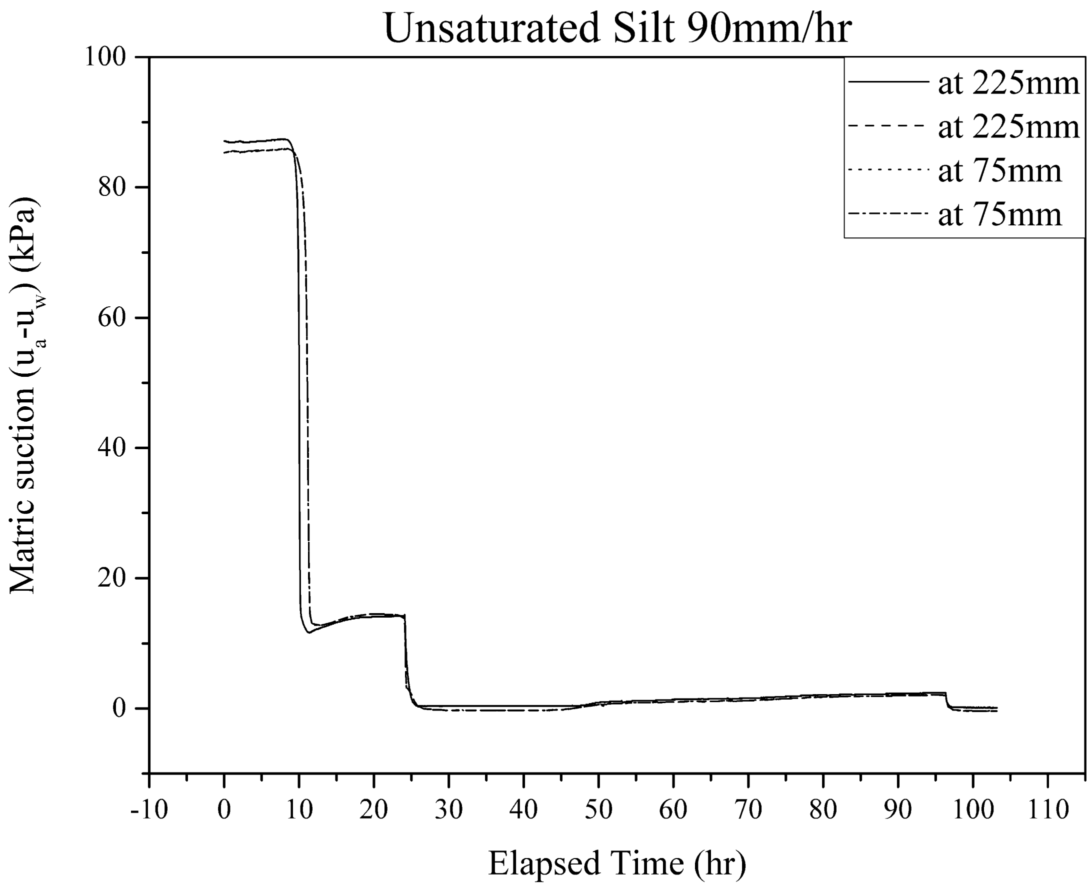
Unsaturated Silt 90mm/hr
at 225mm
at 225mm
at 75mm
at 75mm
Matric suction (u_a-u_w) (kPa)
Elapsed Time (hr)
100
80
60
40
20
0
-10
0
10
20
30
40
50
60
70
80
90
100
110

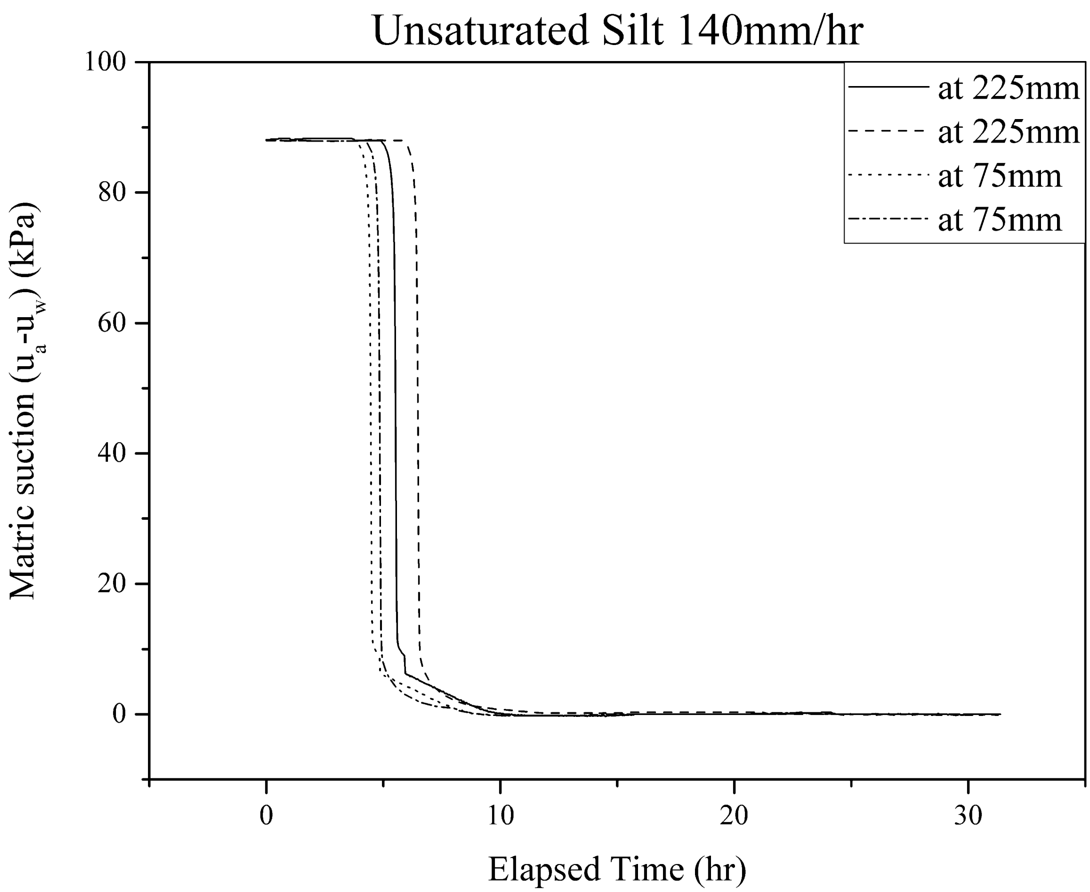

Unsaturated Silt 140mm/hr
at 225mm
at 225mm
at 75mm
at 75mm
Matric suction (u_a-u_w) (kPa)
Elapsed Time (hr)
100
80
60
40
20
0
10
20
30

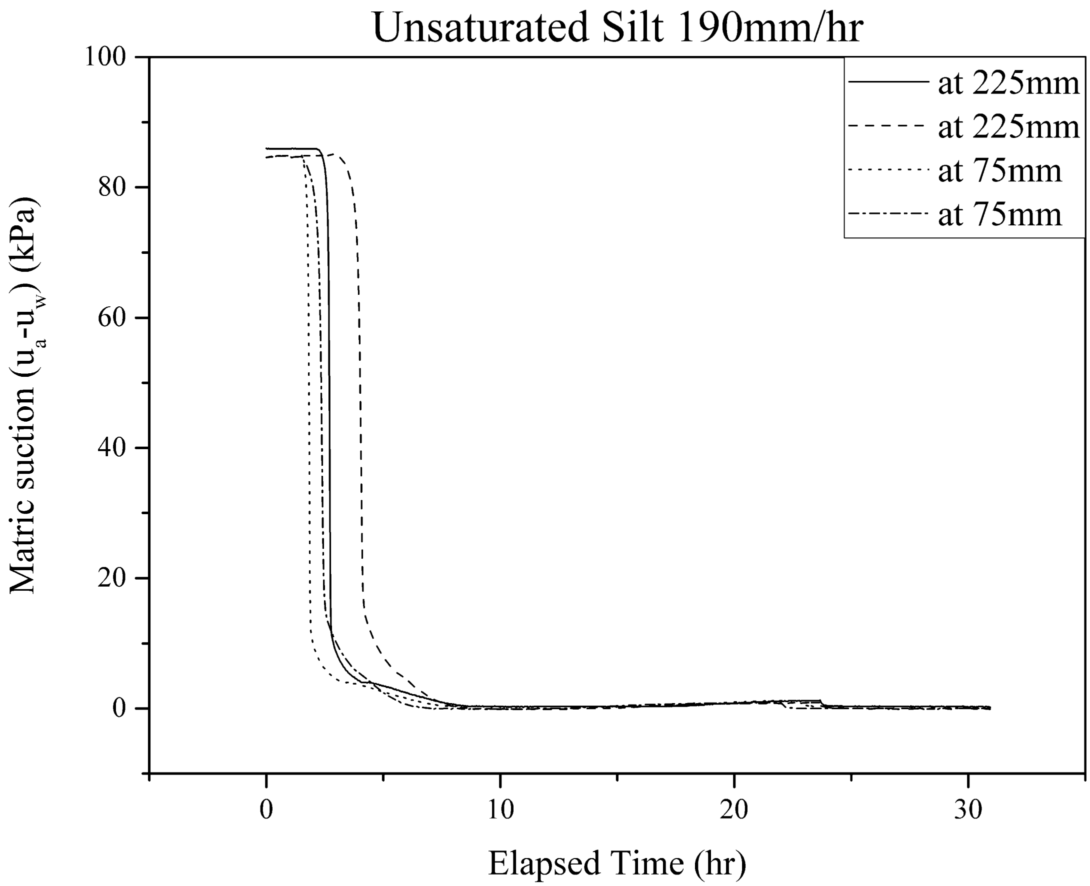

Unsaturated Silt 190mm/hr
at 225mm
at 225mm
at 75mm
at 75mm
Matric suction (u_a-u_w) (kPa)
Elapsed Time (hr)
100
80
60
40
20
0
10
20
30

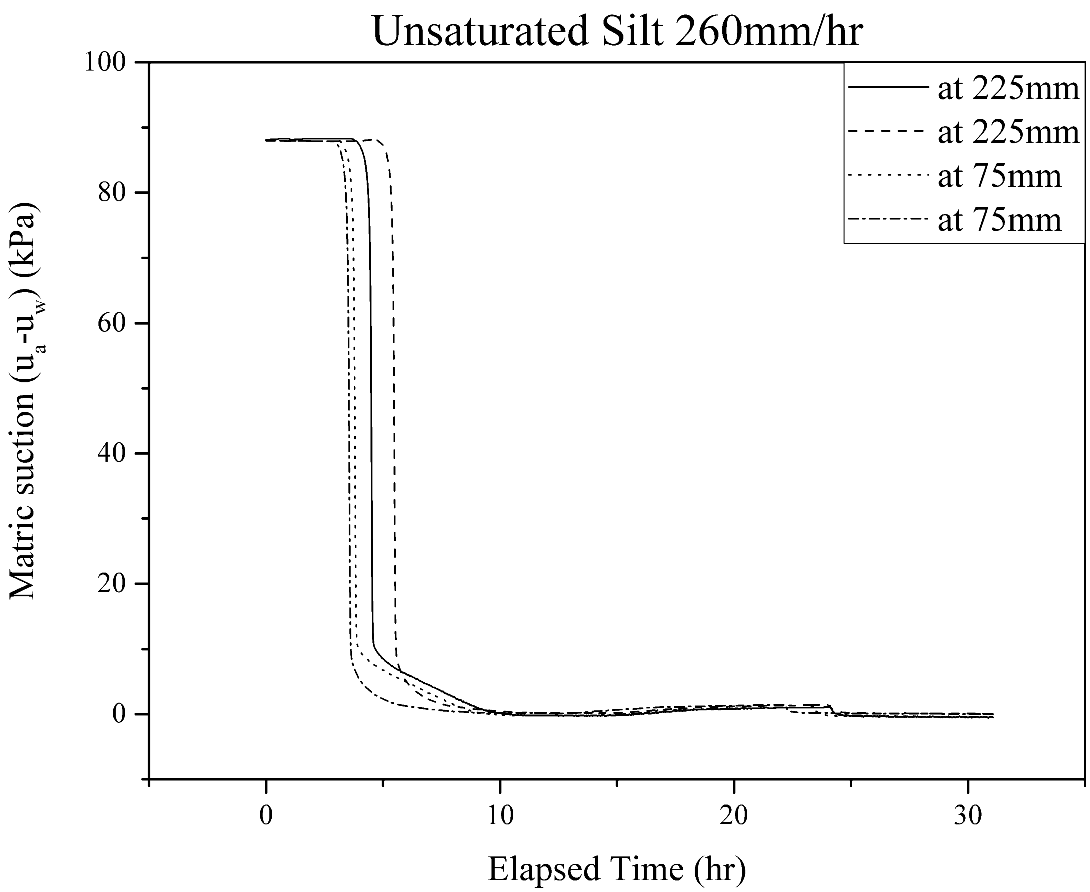

Unsaturated Silt 260mm/hr
at 225mm
at 225mm
at 75mm
at 75mm
Matric suction (u_a-u_w) (kPa)
Elapsed Time (hr)
100
80
60
40
20
0
0
10
20
30

Matric Suction in unsaturated capillary barrier profiles

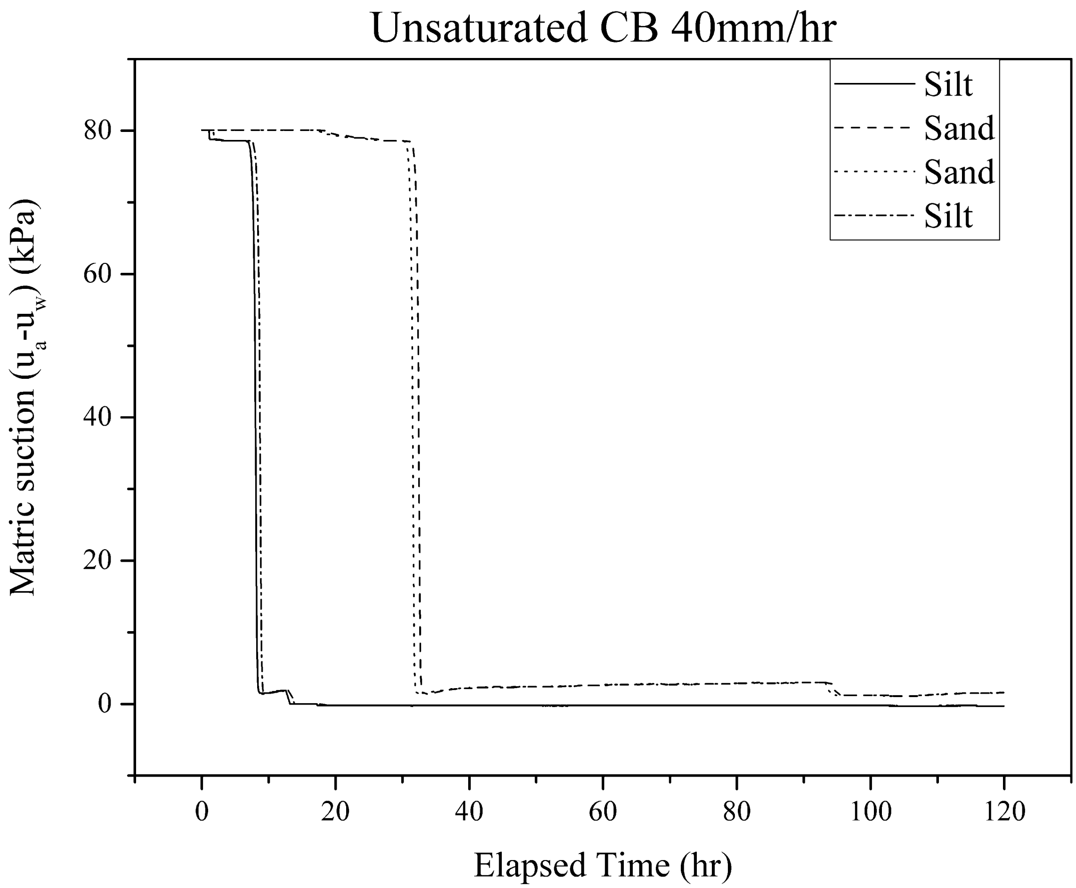

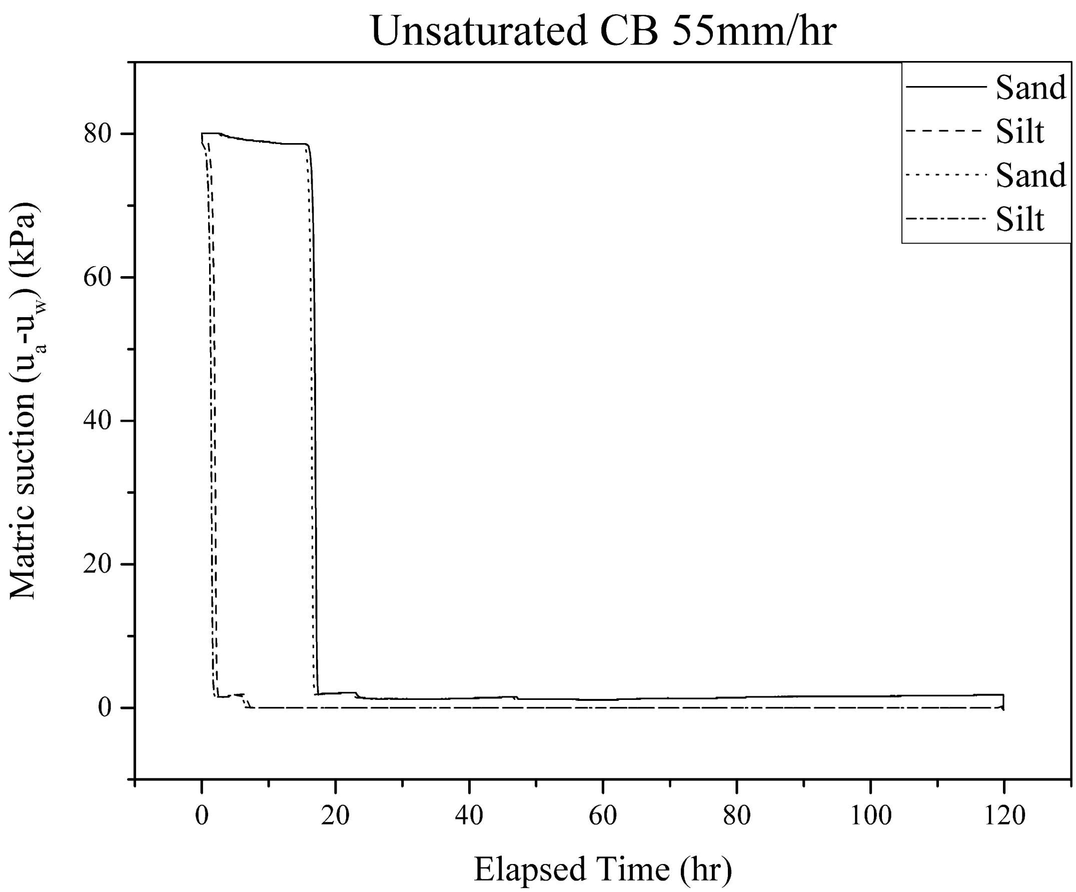
Unsaturated CB 55mm/hr
Sand
Silt
Sand
Silt
Matric suction (u_a-u_w) (kPa)
80
60
40
20
0
0
20
40
60
80
100
120
Elapsed Time (hr)

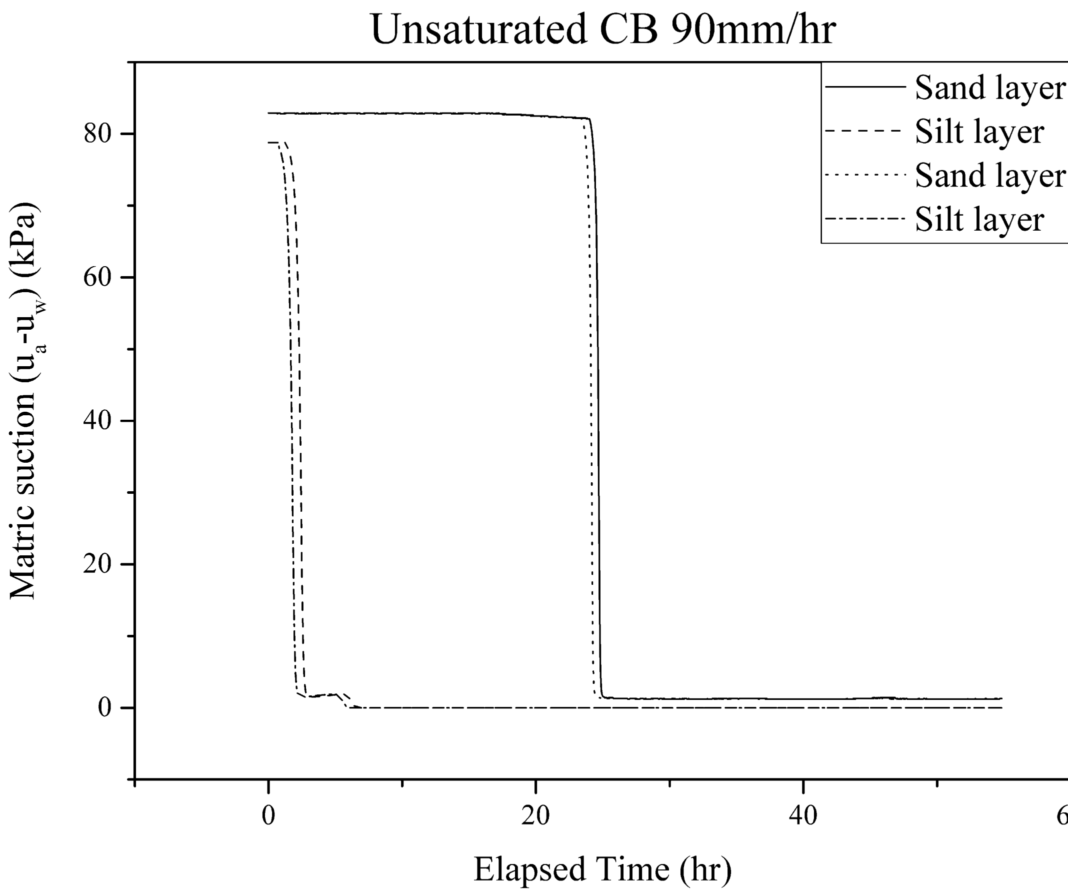
Unsaturated CB 90mm/hr
Sand layer
Silt layer
Sand layer
Silt layer
Matric suction (u_a-u_w) (kPa)
80
60
40
20
0
0
20
40
60
Elapsed Time (hr)

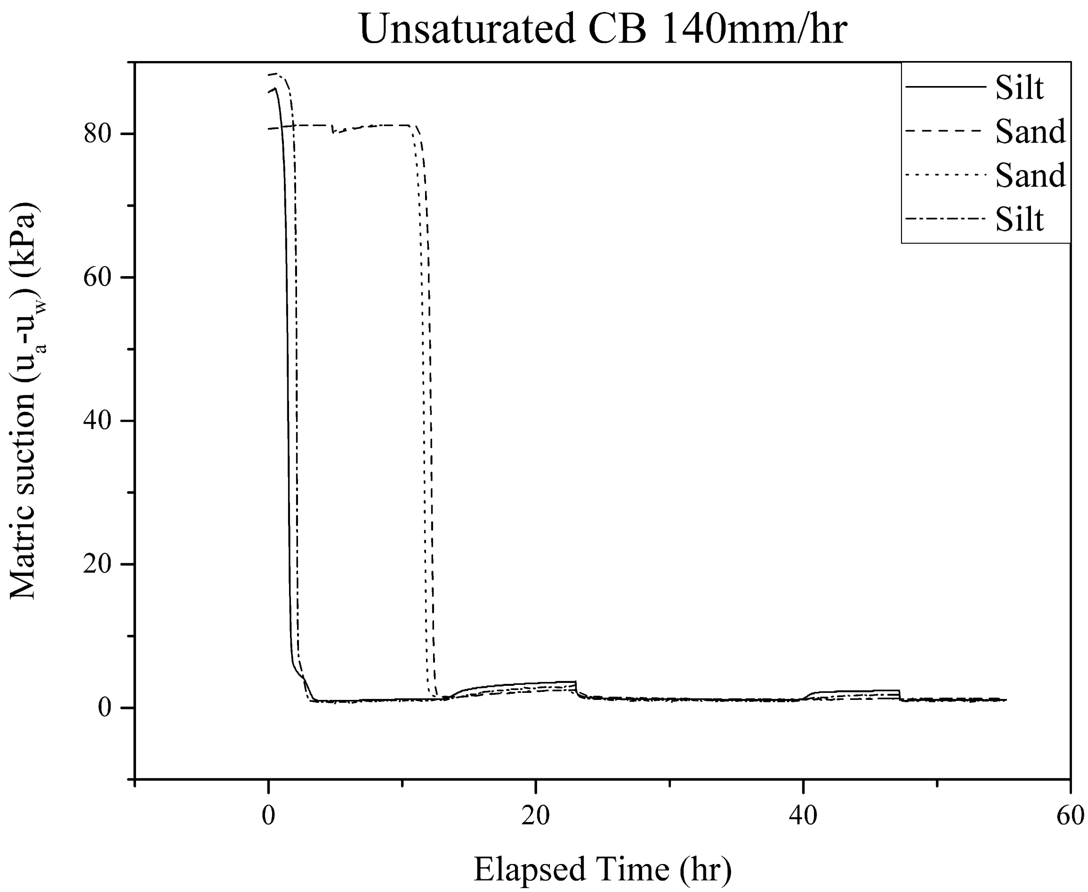
Unsaturated CB 140mm/hr
Silt
Sand
Sand
Silt
Matric suction (u_a-u_w) (kPa)
80
60
40
20
0
0
20
40
60
Elapsed Time (hr)

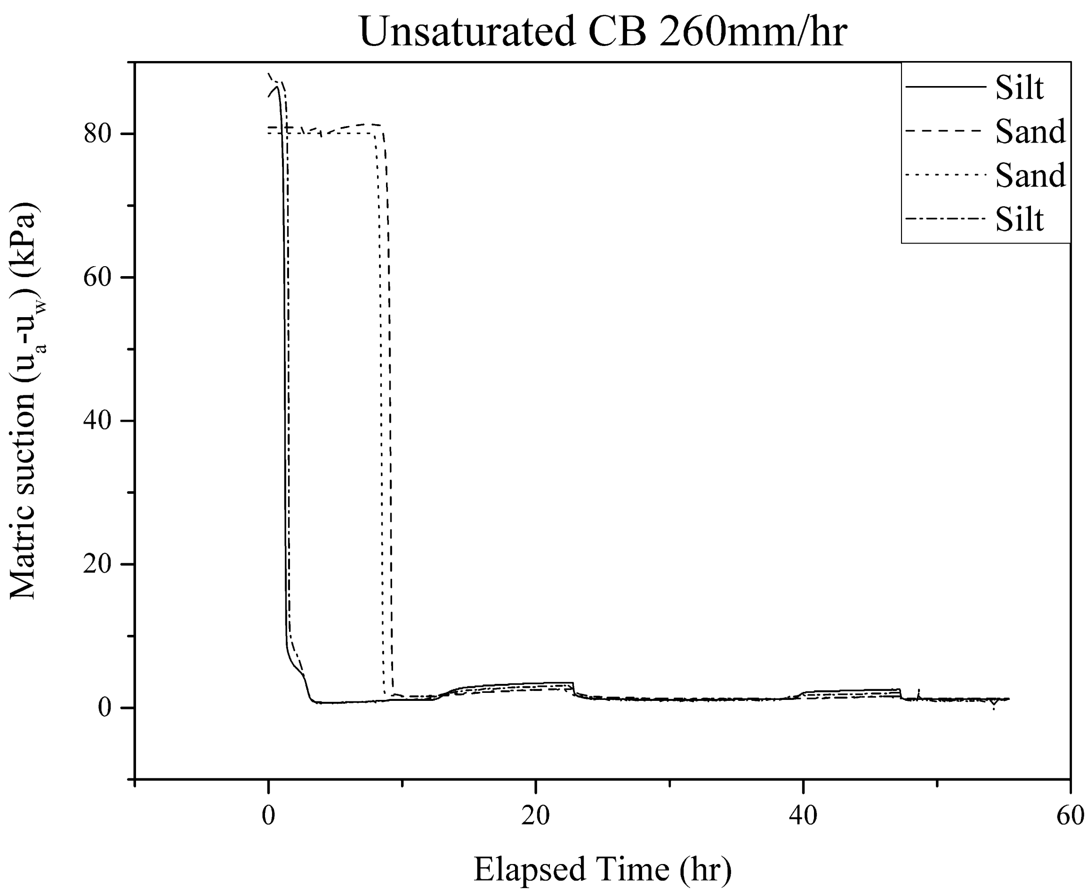
Unsaturated CB 260mm/hr
Silt
Sand
Sand
Silt
Matric suction (u_a-u_w) (kPa)
Elapsed Time (hr)
0
20
40
60
80
0
20
40
60

APPENDIX IV

Calculation of Runoff for saturated profiles using the saturated hydraulic conductivity

Saturated Silt 40mm/hr						
Rainfall rate L/hr	Rainfall rate mm^3/hr	Rainfall rate mm/hr		Infiltration rate L/hr	Infiltration rate mm^3/hr	Infiltration rate mm/hr
12.54362	12543620	46.45785		4.77602	4776020	17.68896
12.40509	12405090	45.94478		2.43349	2433490	9.012926
12.35891	12358910	45.77374		1.68678	1686780	6.247333
12.34212	12342120	45.71156		1.32472	1324720	4.90637
12.33204	12332040	45.67422		1.17028	1170280	4.33437
12.32953	12329530	45.66493		1.00233	1002330	3.712333
12.32413	12324130	45.64493		0.88493	884930	3.277519
12.32008	12320080	45.62993		0.86563	865630	3.206037
12.31693	12316930	45.61826		0.70347	703470	2.605444
12.31441	12314410	45.60893		0.65617	656170	2.430259
12.31464	12314640	45.60978		0.62846	628460	2.32763
12.31273	12312730	45.6027		0.59563	595630	2.206037
12.31112	12311120	45.59674		0.56558	565580	2.094741
12.30974	12309740	45.59163		0.54299	542990	2.011074
12.30854	12308540	45.58719		0.52467	524670	1.943222
12.30591	12305910	45.57744		0.50609	506090	1.874407
12.3036	12303600	45.56889		0.4888	488800	1.81037
12.30154	12301540	45.56126		0.49478	494780	1.832519
12.29837	12298370	45.54952		0.47888	478880	1.77363
12.17084	12170840	45.07719		0.34022	340220	1.260074
12.29414	12294140	45.53385		0.45426	454260	1.682444
12.29518	12295180	45.5377		0.44611	446110	1.652259
12.29284	12292840	45.52904		0.43797	437970	1.622111
12.29174	12291740	45.52496		0.42801	428010	1.585222
12.29074	12290740	45.52126		0.4232	423200	1.567407
12.28884	12288840	45.51422		0.42127	421270	1.560259
12.28615	12286150	45.50426		0.41379	413790	1.532556
12.28365	12283650	45.495		0.40579	405790	1.502926
12.28132	12281320	45.48637		0.40015	400150	1.482037
12.27915	12279150	45.47833		0.39412	394120	1.459704
12.27874	12278740	45.47681		0.38951	389510	1.44263

Saturated Silt 55mm/hr						
Rainfall rate L/hr	Rainfall rate mm^3/hr	Rainfall rate mm/hr		Infiltration rate L/hr	Infiltration rate mm^3/hr	Infiltration rate mm/hr
14.50829	14508290	53.73441		3.14469	3144690	11.647
14.40754	14407540	53.36126		0.07878	78780	0.291778
14.38235	14382350	53.26796		0.12077	120770	0.447296
14.38235	14382350	53.26796		0.15395	153950	0.570185
14.38739	14387390	53.28663		0.11194	111940	0.414593
14.39494	14394940	53.31459		0.14992	149920	0.555259
14.40754	14407540	53.36126		0.1567	156700	0.58037
14.42013	14420130	53.40789		0.18549	185490	0.687
14.43272	14432720	53.45452		0.14228	142280	0.526963
14.45036	14450360	53.51985		0.26184	261840	0.969778
14.46478	14464780	53.57326		0.17424	174240	0.645333
14.481	14481000	53.63333		0.18262	182620	0.67637
14.4986	14498600	53.69852		0.16219	162190	0.600704
14.51548	14515480	53.76104		0.15886	158860	0.58837
14.53348	14533480	53.8277		0.22748	227480	0.842519
14.55237	14552370	53.89767		0.21973	219730	0.813815
14.572	14572000	53.97037		0.42251	422510	1.564852
14.58805	14588050	54.02981		0.18572	185720	0.687852
14.60771	14607710	54.10263		0.24527	245270	0.908407
14.62793	14627930	54.17752		0.28125	281250	1.041667
14.64622	14646220	54.24526		0.22845	228450	0.846111
14.66514	14665140	54.31533		0.19442	194420	0.720074
14.68679	14686790	54.39552		0.28558	285580	1.057704
14.70769	14707690	54.47293		0.28116	281160	1.041333
14.72893	14728930	54.55159		0.29194	291940	1.081259
14.73886	14738860	54.58837		-0.00714	-7140	-0.02644
14.77136	14771360	54.70874		0.65896	658960	2.440593
14.79165	14791650	54.78389		0.27949	279490	1.035148
14.81228	14812280	54.8603		0.33427	334270	1.238037
14.83153	14831530	54.93159		0.29467	294670	1.09137
14.85117	14851170	55.00433		0.32344	323440	1.197926

Saturated Silt 90mm/hr						
Rainfall rate L/hr	Rainfall rate mm^3/hr	Rainfall rate mm/hr		Infiltration rate L/hr	Infiltration rate mm^3/hr	Infiltration rate mm/hr
23.265	23265000	86.16667		3.14469	3144690	11.647
23.27675	23276750	86.21019		0.07878	78780	0.291778
23.28067	23280670	86.2247		0.12077	120770	0.447296
23.28263	23282630	86.23196		0.15395	153950	0.570185
23.2791	23279100	86.21889		0.11194	111940	0.414593
23.28067	23280670	86.2247		0.14992	149920	0.555259
23.27843	23278430	86.21641		0.1567	156700	0.58037
23.27381	23273810	86.1993		0.18549	185490	0.687
23.27022	23270220	86.186		0.14228	142280	0.526963
23.265	23265000	86.16667		0.26184	261840	0.969778
23.265	23265000	86.16667		0.17424	174240	0.645333
23.265	23265000	86.16667		0.18262	182620	0.67637
23.265	23265000	86.16667		0.16219	162190	0.600704
23.265	23265000	86.16667		0.15886	158860	0.58837
23.265	23265000	86.16667		0.22748	227480	0.842519
23.26794	23267940	86.17756		0.21973	219730	0.813815
23.26915	23269150	86.18204		0.42251	422510	1.564852
23.27283	23272830	86.19567		0.18572	185720	0.687852
23.27737	23277370	86.21248		0.24527	245270	0.908407
23.28145	23281450	86.22759		0.28125	281250	1.041667
23.28626	23286260	86.24541		0.22845	228450	0.846111
23.2917	23291700	86.26556		0.19442	194420	0.720074
23.29872	23298720	86.29156		0.28558	285580	1.057704
23.3071	23307100	86.32259		0.28116	281160	1.041333
23.31576	23315760	86.35467		0.29194	291940	1.081259
23.32375	23323750	86.38426		-0.00714	-7140	-0.02644
23.33289	23332890	86.41811		0.65896	658960	2.440593
23.34305	23343050	86.45574		0.27949	279490	1.035148
23.35333	23353330	86.49381		0.33427	334270	1.238037
23.3637	23363700	86.53222		0.29467	294670	1.09137
23.37568	23375680	86.57659		0.32344	323440	1.197926

Saturated Silt 140mm/hr						
Rainfall rate L/hr	Rainfall rate mm^3/hr	Rainfall rate mm/hr		Infiltration rate L/hr	Infiltration rate mm^3/hr	Infiltration rate mm/hr
36.2605	36260500	134.2981		10.3633	10363300	38.38259
36.27225	36272250	134.3417		0.708	708000	2.622222
36.17433	36174330	133.979		0.5673	567300	2.101111
36.19588	36195880	134.0588		0.7073	707300	2.61963
36.19	36190000	134.037		0.6681	668100	2.474444
36.18608	36186080	134.0225		0.7289	728900	2.69963
36.18329	36183290	134.0122		0.6937	693700	2.569259
36.16944	36169440	133.9609		0.6217	621700	2.302593
36.16128	36161280	133.9307		0.6824	682400	2.527407
36.15475	36154750	133.9065		0.6608	660800	2.447407
36.15368	36153680	133.9025		0.6566	656600	2.431852
36.15475	36154750	133.9065		0.7501	750100	2.778148
36.15023	36150230	133.8897		0.9276	927600	3.435556
36.14636	36146360	133.8754		0.934	934000	3.459259
36.143	36143000	133.863		0.55	550000	2.037037
36.13859	36138590	133.8466		0.7293	729300	2.701111
36.12918	36129180	133.8118		0.5393	539300	1.997407
36.12342	36123420	133.7904		0.9159	915900	3.392222
36.12074	36120740	133.7805		1.1245	1124500	4.164815
36.11832	36118320	133.7716		0.1573	157300	0.582593
36.1195	36119500	133.7759		0.6986	698600	2.587407
36.11523	36115230	133.7601		0.6691	669100	2.478148
36.11439	36114390	133.757		0.688	688000	2.548148
36.11362	36113620	133.7541		0.7156	715600	2.65037
36.11574	36115740	133.762		1.0593	1059300	3.923333
36.11588	36115880	133.7625		0.6651	665100	2.463333
36.11515	36115150	133.7598		0.7124	712400	2.638519
36.11782	36117820	133.7697		0.7216	721600	2.672593
36.11464	36114640	133.7579		0.6607	660700	2.447037
36.10853	36108530	133.7353		0.4895	489500	1.812963
36.10206	36102060	133.7113		0.3744	374400	1.386667

Saturated Silt 190mm/hr						
Rainfall rate L/hr	Rainfall rate mm^3/hr	Rainfall rate mm/hr		Infiltration rate L/hr	Infiltration rate mm^3/hr	Infiltration rate mm/hr
48.9505	48950500	181.2981		8.2489	8248900	30.55148
48.93875	48938750	181.2546		2.435	2435000	9.018519
48.93483	48934830	181.2401		2.7482	2748200	10.17852
48.93288	48932880	181.2329		2.4806	2480600	9.187407
48.9364	48936400	181.2459		2.5365	2536500	9.394444
48.94267	48942670	181.2691		2.5988	2598800	9.625185
48.92029	48920290	181.1863		2.3348	2334800	8.647407
48.88294	48882940	181.0479		2.0767	2076700	7.691481
48.87217	48872170	181.008		2.1888	2188800	8.106667
48.83065	48830650	180.8543		1.8478	1847800	6.843704
48.85223	48852230	180.9342		2.4412	2441200	9.041481
48.84083	48840830	180.892		2.1087	2108700	7.81
48.82758	48827580	180.8429		2.0893	2089300	7.738148
48.81454	48814540	180.7946		2.0846	2084600	7.720741
48.7954	48795400	180.7237		2.2115	2211500	8.190741
48.786	48786000	180.6889		2.7154	2715400	10.05704
48.77494	48774940	180.6479		2.1572	2157200	7.98963
48.76119	48761190	180.597		2.0655	2065500	7.65
48.74889	48748890	180.5514		2.4163	2416300	8.949259
48.73665	48736650	180.5061		3.5572	3557200	13.17481
48.72781	48727810	180.4734		2.201	2201000	8.151852
48.71657	48716570	180.4317		2.1933	2193300	8.123333
48.70733	48707330	180.3975		2.1712	2171200	8.041481
48.69298	48692980	180.3444		2.0638	2063800	7.643704
48.67226	48672260	180.2676		1.9954	1995400	7.39037
48.65585	48655850	180.2069		1.8859	1885900	6.984815
48.63891	48638910	180.1441		0.5037	503700	1.865556
48.6215	48621500	180.0796		3.4751	3475100	12.87074
48.60772	48607720	180.0286		1.9912	1991200	7.374815
48.59252	48592520	179.9723		2.1423	2142300	7.934444
48.57753	48577530	179.9168		1.9376	1937600	7.176296

Saturated Silt 260mm/hr						
Rainfall rate L/hr	Rainfall rate mm^3/hr	Rainfall rate mm/hr		Infiltration rate L/hr	Infiltration rate mm^3/hr	Infiltration rate mm/hr
70.2885	70288500	260.3278		11.4781	11478100	42.51148
70.30025	70300250	260.3713		5.3616	5361600	19.85778
70.2415	70241500	260.1537		4.4656	4465600	16.53926
70.2415	70241500	260.1537		4.9459	4945900	18.31815
70.2321	70232100	260.1189		4.8149	4814900	17.83296
70.21408	70214080	260.0521		4.8912	4891200	18.11556
70.21129	70211290	260.0418		4.8997	4899700	18.14704
70.20919	70209190	260.034		5.1181	5118100	18.95593
70.19972	70199720	259.999		4.856	4856000	17.98519
70.19685	70196850	259.9883		4.889	4889000	18.10741
70.18809	70188090	259.9559		4.8113	4811300	17.81963
70.17883	70178830	259.9216		4.8178	4817800	17.8437
70.17462	70174620	259.906		4.8484	4848400	17.95704
70.16261	70162610	259.8615		4.7669	4766900	17.65519
70.15533	70155330	259.8346		4.8423	4842300	17.93444
70.14897	70148970	259.811		4.8299	4829900	17.88852
70.14197	70141970	259.7851		4.8432	4843200	17.93778
70.12792	70127920	259.733		4.7126	4712600	17.45407
70.11534	70115340	259.6864		4.723	4723000	17.49259
70.1052	70105200	259.6489		4.7289	4728900	17.51444
70.0949	70094900	259.6107		4.7574	4757400	17.62
70.08448	70084480	259.5721		4.7207	4720700	17.48407
70.077	70077000	259.5444		4.7525	4752500	17.60185
70.07113	70071130	259.5227		4.784	4784000	17.71852
70.0629	70062900	259.4922		4.7483	4748300	17.5863
70.05802	70058020	259.4741		4.778	4778000	17.6963
70.05089	70050890	259.4477		4.8319	4831900	17.89593
70.04679	70046790	259.4326		4.7984	4798400	17.77185
70.04216	70042160	259.4154		4.8041	4804100	17.79296
70.03783	70037830	259.3994		4.7985	4798500	17.77222
70.03606	70036060	259.3928		4.9006	4900600	18.15037

Saturated capillary barrier 40mm/hr						
Rainfall rate L/hr	Rainfall rate mm^3/hr	Rainfall rate mm/hr		Infiltration rate L/hr	Infiltration rate mm^3/hr	Infiltration rate mm/hr
12.97182	12971820	48.04378		4.48502	4485020	16.61119
12.92144	12921440	47.85719		0.88624	886240	3.28237
12.89626	12896260	47.76393		0.67666	676660	2.506148
12.89626	12896260	47.76393		0.56146	561460	2.079481
12.89626	12896260	47.76393		0.37546	375460	1.390593
12.92144	12921440	47.85719		0.32864	328640	1.217185
12.92144	12921440	47.85719		0.41504	415040	1.537185
12.89626	12896260	47.76393		0.26786	267860	0.992074
12.92144	12921440	47.85719		0.35064	350640	1.298667
12.94663	12946630	47.95048		0.30863	308630	1.143074
12.94663	12946630	47.95048		0.16263	162630	0.602333
12.94663	12946630	47.95048		0.24583	245830	0.910481
12.89626	12896260	47.76393		0.17306	173060	0.640963
12.92144	12921440	47.85719		0.21224	212240	0.786074
12.92144	12921440	47.85719		0.19824	198240	0.734222
12.92144	12921440	47.85719		0.95744	957440	3.546074
12.89626	12896260	47.76393		0.31226	312260	1.156519
12.84588	12845880	47.57733		0.23108	231080	0.855852
12.94663	12946630	47.95048		0.37903	379030	1.403815
12.89626	12896260	47.76393		0.29746	297460	1.101704
12.89626	12896260	47.76393		0.31306	313060	1.159481
12.87107	12871070	47.67063		0.28467	284670	1.054333
12.89626	12896260	47.76393		0.28986	289860	1.073556
12.87107	12871070	47.67063		0.37307	373070	1.381741
12.87107	12871070	47.67063		0.20827	208270	0.77137
12.87107	12871070	47.67063		0.25587	255870	0.947667
12.97182	12971820	48.04378		4.48502	4485020	16.61119
12.92144	12921440	47.85719		0.88624	886240	3.28237
12.89626	12896260	47.76393		0.67666	676660	2.506148
12.89626	12896260	47.76393		0.56146	561460	2.079481
12.89626	12896260	47.76393		0.37546	375460	1.390593

Saturated capillary barrier 55mm/hr						
Rainfall rate L/hr	Rainfall rate mm^3/hr	Rainfall rate mm/hr		Infiltration rate L/hr	Infiltration rate mm^3/hr	Infiltration rate mm/hr
12.77032	12770320	47.29748		9.19072	9190720	34.0397
13.75265	13752650	50.93574		0.21738	217380	0.805111
15.42345	15423450	57.12389		4.21626	4216260	15.61578
14.269	14269000	52.84815		4.21626	4216260	15.61578
14.37227	14372270	53.23063		4.21626	4216260	15.61578
14.45371	14453710	53.53226		4.21626	4216260	15.61578
14.51908	14519080	53.77437		4.21626	4216260	15.61578
14.56811	14568110	53.95596		4.21626	4216260	15.61578
14.61184	14611840	54.11793		4.21626	4216260	15.61578
14.64682	14646820	54.24748		4.21626	4216260	15.61578
14.67773	14677730	54.36196		4.21626	4216260	15.61578
14.7035	14703500	54.45741		4.21626	4216260	15.61578
14.72529	14725290	54.53811		4.21626	4216260	15.61578
14.74577	14745770	54.61396		4.21626	4216260	15.61578
14.76688	14766880	54.69215		4.21626	4216260	15.61578
14.78693	14786930	54.76641		4.21626	4216260	15.61578
14.80758	14807580	54.84289		4.21626	4216260	15.61578
14.83013	14830130	54.92641		4.21626	4216260	15.61578
14.85164	14851640	55.00607		4.21626	4216260	15.61578
14.87225	14872250	55.08241		4.21626	4216260	15.61578
14.8945	14894500	55.16481		4.21626	4216260	15.61578
14.91473	14914730	55.23974		4.21626	4216260	15.61578
14.9332	14933200	55.30815		4.21626	4216260	15.61578
14.95118	14951180	55.37474		4.21626	4216260	15.61578
14.96671	14966710	55.43226		4.21626	4216260	15.61578
14.98492	14984920	55.4997		4.21626	4216260	15.61578
15.00458	15004580	55.57252		4.21626	4216260	15.61578
12.77032	12770320	47.29748		9.19072	9190720	34.0397
13.75265	13752650	50.93574		0.21738	217380	0.805111
15.42345	15423450	57.12389		4.21626	4216260	15.61578
14.269	14269000	52.84815		4.21626	4216260	15.61578

Saturated capillary barrier 90mm/hr						
Rainfall rate L/hr	Rainfall rate mm^3/hr	Rainfall rate mm/hr		Infiltration rate L/hr	Infiltration rate mm^3/hr	Infiltration rate mm/hr
25.28875	25288750	93.66204		10.60435	10604350	39.27537
25.33913	25339130	93.84863		1.32513	1325130	4.907889
25.41469	25414690	94.12848		1.32229	1322290	4.89737
25.41469	25414690	94.12848		1.31909	1319090	4.885519
25.46507	25465070	94.31507		1.32107	1321070	4.892852
25.49026	25490260	94.40837		1.37786	1377860	5.103185
25.49026	25490260	94.40837		1.32066	1320660	4.891333
25.54063	25540630	94.59493		1.44383	1443830	5.347519
25.54063	25540630	94.59493		1.39463	1394630	5.165296
25.49026	25490260	94.40837		1.81346	1813460	6.716519
25.56582	25565820	94.68822		0.94782	947820	3.510444
25.56582	25565820	94.68822		1.43222	1432220	5.304519
25.54063	25540630	94.59493		1.41023	1410230	5.223074
25.64138	25641380	94.96807		1.44378	1443780	5.347333
25.69176	25691760	95.15467		1.44456	1444560	5.350222
25.71695	25716950	95.24796		1.56295	1562950	5.788704
25.76732	25767320	95.43452		1.52012	1520120	5.630074
25.76732	25767320	95.43452		1.50372	1503720	5.569333
25.74214	25742140	95.34126		1.44294	1442940	5.344222
25.84289	25842890	95.71441		1.59729	1597290	5.915889
25.84289	25842890	95.71441		1.74449	1744490	6.461074
25.86808	25868080	95.8077		1.55208	1552080	5.748444
25.89326	25893260	95.90096		1.57886	1578860	5.84763
25.94364	25943640	96.08756		1.57124	1571240	5.819407
25.91845	25918450	95.99426		1.51405	1514050	5.607593
25.96883	25968830	96.18085		2.08563	2085630	7.724556
25.28875	25288750	93.66204		10.60435	10604350	39.27537
25.33913	25339130	93.84863		1.32513	1325130	4.907889
25.41469	25414690	94.12848		1.32229	1322290	4.89737
25.41469	25414690	94.12848		1.31909	1319090	4.885519
25.46507	25465070	94.31507		1.32107	1321070	4.892852

Saturated capillary barrier 140mm/hr						
Rainfall rate L/hr	Rainfall rate mm^3/hr	Rainfall rate mm/hr		Infiltration rate L/hr	Infiltration rate mm^3/hr	Infiltration rate mm/hr
45.59028	45590280	168.8529		17.45588	17455880	64.65141
46.52224	46522240	172.3046		5.26064	5260640	19.48385
46.57261	46572610	172.4911		5.31701	5317010	19.69263
46.67336	46673360	172.8643		5.35776	5357760	19.84356
46.82449	46824490	173.424		5.44489	5444890	20.16626
46.64818	46648180	172.771		5.25778	5257780	19.47326
46.7993	46799300	173.3307		5.3969	5396900	19.98852
46.84968	46849680	173.5173		5.36488	5364880	19.86993
46.97562	46975620	173.9838		5.44922	5449220	20.1823
46.95043	46950430	173.8905		5.60283	5602830	20.75122
47.00081	47000810	174.0771		5.37401	5374010	19.90374
46.97562	46975620	173.9838		5.80642	5806420	21.50526
47.05118	47051180	174.2636		5.26278	5262780	19.49178
47.07637	47076370	174.3569		5.44837	5448370	20.17915
47.07637	47076370	174.3569		5.4	5400000	20
47.10156	47101560	174.4502		5.26064	5260640	19.48385
47.10156	47101560	174.4502		5.31701	5317010	19.69263
47.10156	47101560	174.4502		5.35776	5357760	19.84356
47.20231	47202310	174.8234		5.44489	5444890	20.16626
47.32825	47328250	175.2898		5.25778	5257780	19.47326
47.30306	47303060	175.1965		5.3969	5396900	19.98852
47.30306	47303060	175.1965		5.36488	5364880	19.86993
47.27788	47277880	175.1033		5.44922	5449220	20.1823
47.32825	47328250	175.2898		5.60283	5602830	20.75122
47.429	47429000	175.663		5.37401	5374010	19.90374
47.16201	47162010	174.6741		5.80642	5806420	21.50526
47.30055	47300550	175.1872		5.26278	5262780	19.49178
45.59028	45590280	168.8529		17.45588	17455880	64.65141
46.52224	46522240	172.3046		5.26064	5260640	19.48385
46.57261	46572610	172.4911		5.31701	5317010	19.69263
46.67336	46673360	172.8643		5.35776	5357760	19.84356

Saturated capillary barrier 190mm/hr						
Rainfall rate L/hr	Rainfall rate mm^3/hr	Rainfall rate mm/hr		Infiltration rate L/hr	Infiltration rate mm^3/hr	Infiltration rate mm/hr
65.11098	65110980	241.1518		42.20138	42201380	156.3014
65.917	65917000	244.137		8.2826	8282600	30.6763
66.09331	66093310	244.79		8.78451	8784510	32.53522
66.09331	66093310	244.79		8.77051	8770510	32.48337
66.09331	66093310	244.79		8.73851	8738510	32.36485
66.09331	66093310	244.79		8.73531	8735310	32.353
65.74068	65740680	243.484		8.56348	8563480	31.71659
65.89181	65891810	244.0437		8.69181	8691810	32.19189
65.96737	65967370	244.3236		8.88097	8880970	32.89248
66.04294	66042940	244.6035		9.29654	9296540	34.43163
66.16888	66168880	245.0699		8.95208	8952080	33.15585
66.04294	66042940	244.6035		9.10734	9107340	33.73089
66.06812	66068120	244.6967		8.65852	8658520	32.06859
66.14369	66143690	244.9766		8.70889	8708890	32.25515
66.16888	66168880	245.0699		8.68688	8686880	32.17363
66.21925	66219250	245.2565		8.75645	8756450	32.4313
66.32	66320000	245.6296		8.7484	8748400	32.40148
66.29482	66294820	245.5364		8.82202	8822020	32.67415
66.26963	66269630	245.4431		8.71923	8719230	32.29344
66.26963	66269630	245.4431		8.67443	8674430	32.12752
66.29482	66294820	245.5364		8.61282	8612820	31.89933
66.34519	66345190	245.7229		8.92439	8924390	33.0533
66.39557	66395570	245.9095		8.62717	8627170	31.95248
66.37038	66370380	245.8162		8.73078	8730780	32.33622
66.44594	66445940	246.0961		8.67554	8675540	32.13163
66.52151	66521510	246.376		8.73111	8731110	32.33744
66.42076	66420760	246.0028		8.84316	8843160	32.75244
65.11098	65110980	241.1518		42.20138	42201380	156.3014
65.917	65917000	244.137		8.2826	8282600	30.6763
66.09331	66093310	244.79		8.78451	8784510	32.53522
66.09331	66093310	244.79		8.77051	8770510	32.48337

Saturated capillary barrier 260mm/hr						
Rainfall rate L/hr	Rainfall rate mm^3/hr	Rainfall rate mm/hr		Infiltration rate L/hr	Infiltration rate mm^3/hr	Infiltration rate mm/hr
63.3328	63332800	234.5659		25.58084	25580840	94.74385
75.8816	75881600	281.043		13.66174	13661740	50.59904
76.0676	76067600	281.7319		13.40018	13400180	49.6303
74.9488	74948800	277.5881		14.49379	14493790	53.6807
76.1112	76111200	281.8933		13.3062	13306200	49.28222
76.1616	76161600	282.08		13.20542	13205420	48.90896
75.8748	75874800	281.0178		13.76929	13769290	50.99737
75.7072	75707200	280.397		13.93689	13936890	51.61811
76.2004	76200400	282.2237		13.4185	13418500	49.69815
76.4368	76436800	283.0993		13.20729	13207290	48.91589
76.3356	76335600	282.7244		13.25812	13258120	49.10415
76.3312	76331200	282.7081		13.38846	13388460	49.58689
76.3088	76308800	282.6252		13.38567	13385670	49.57656
76.2504	76250400	282.4089		13.49444	13494440	49.97941
76.0664	76066400	281.7274		13.5525	13552500	50.19444
76.5336	76533600	283.4578		13.16087	13160870	48.74396
76.5112	76511200	283.3748		13.1077	13107700	48.54704
75.0296	75029600	277.8874		14.31224	14312240	53.0083
77.7272	77727200	287.8785		11.74058	11740580	43.48363
76.7404	76740400	284.2237		12.82813	12828130	47.51159
76.4748	76474800	283.24		13.11892	13118920	48.58859
76.5636	76563600	283.5689		13.10568	13105680	48.53956
76.606	76606000	283.7259		13.13884	13138840	48.66237
76.8896	76889600	284.7763		12.65374	12653740	46.8657
74.9236	74923600	277.4948		14.89681	14896810	55.17337
76.062	76062000	281.7111		13.20427	13204270	48.9047
78.3588	78358800	290.2178		12.01574	12015740	44.50274
63.3328	63332800	234.5659		25.58084	25580840	94.74385
75.8816	75881600	281.043		13.66174	13661740	50.59904
76.0676	76067600	281.7319		13.40018	13400180	49.6303
74.9488	74948800	277.5881		14.49379	14493790	53.6807

Saturated Profiles								
	Rain fall Inten sity	Average applied rainfall rate (from lab)	Runoff rate (mm/hr)	Time incre ment	Final Cumulative Runoff Volume mm^3	Calculat ed Final Cumulat ive Runoff Volume L	Measure d Final Cumulati ve Runoff Volume L	Percent differenc e
Saturated silt	40	45.6	45.2	8.0	97713585.0	97.7	95.5	-2%
Saturated silt	55	54.0	53.7	8.0	115901845.0	115.9	116.4	0%
Saturated silt	90	86.3	85.9	8.0	185579167.5	185.6	184.5	-1%
Saturated silt	140	133.9	133.5	8.0	288390690.0	288.4	280.9	-8%
Saturated silt	190	180.7	180.3	7.8	377319527.5	377.3	369.0	-8%
Saturated silt	260	259.8	259.4	7.8	542841421.4	542.8	521.5	-21%
Saturated Capillary Barrier	40	47.8	47.4	6.3	80066759.6	80.1	81.0	1%
Saturated Capillary Barrier	55	54.3	53.9	6.8	98295092.5	98.3	97.6	-1%
Saturated Capillary Barrier	90	95.0	94.6	6.5	166056087.5	166.1	161.7	-4%
Saturated Capillary Barrier	140	174.0	173.6	6.5	304753990.2	304.8	276.9	-28%
Saturated Capillary Barrier	190	245.0	244.6	6.8	445794907.5	445.8	379.0	-67%

Saturated Capillary Barrier	260	280.7	280.4	6.8	510952800.0	511.0	511.6	1%

APPENDIX V

Calculation of Runoff for unsaturated profiles using infiltration rate of each profile

Unsaturated Silt applied rainfall intensity is 40 mm/hr

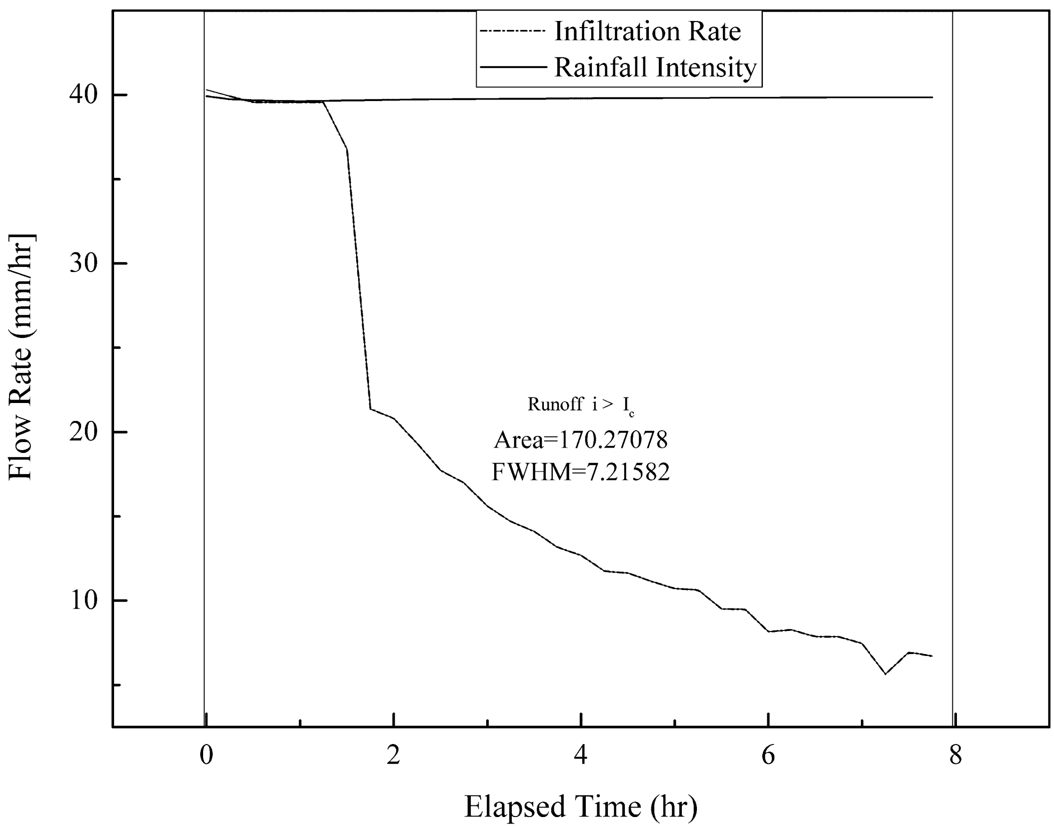

Unsaturated Silt applied rainfall intensity is 55 mm/hr

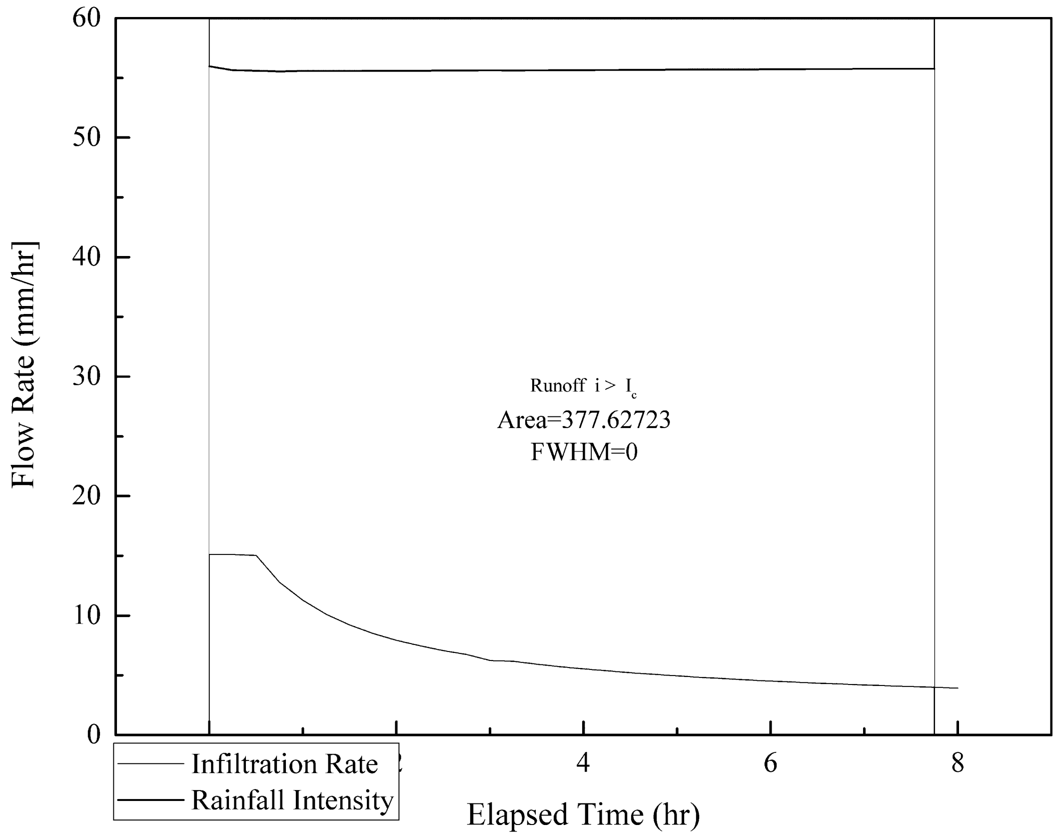

Unsaturated Silt applied rainfall intensity is 90 mm/hr

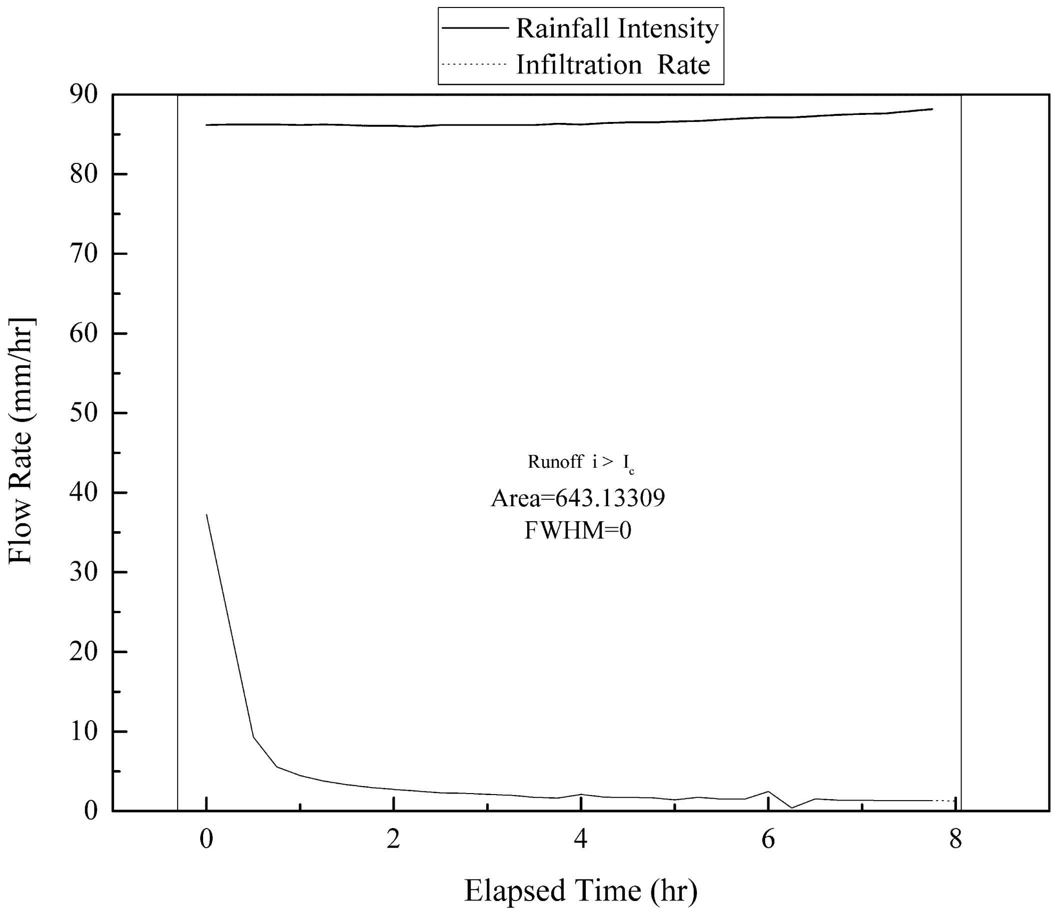

Unsaturated Silt applied rainfall intensity is 140 mm/hr

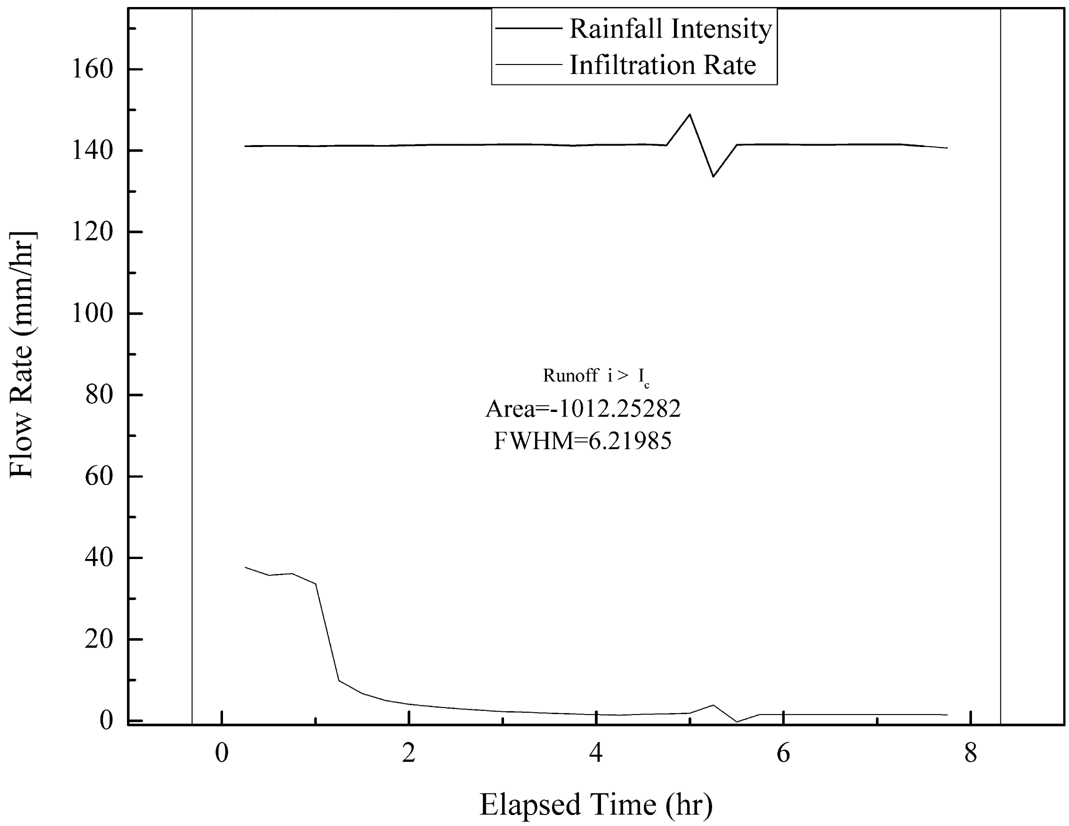

Unsaturated Silt applied rainfall intensity is 190 mm/hr

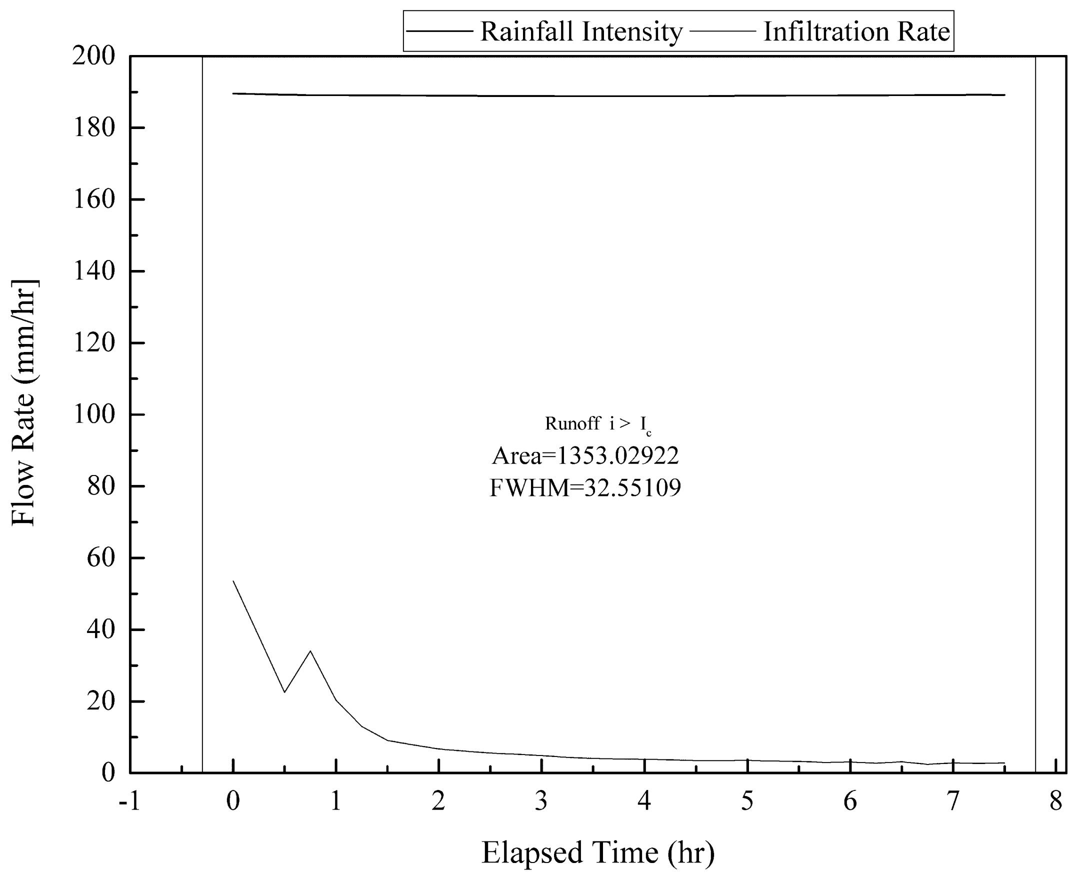

Unsaturated Silt applied rainfall intensity is 260 mm/hr

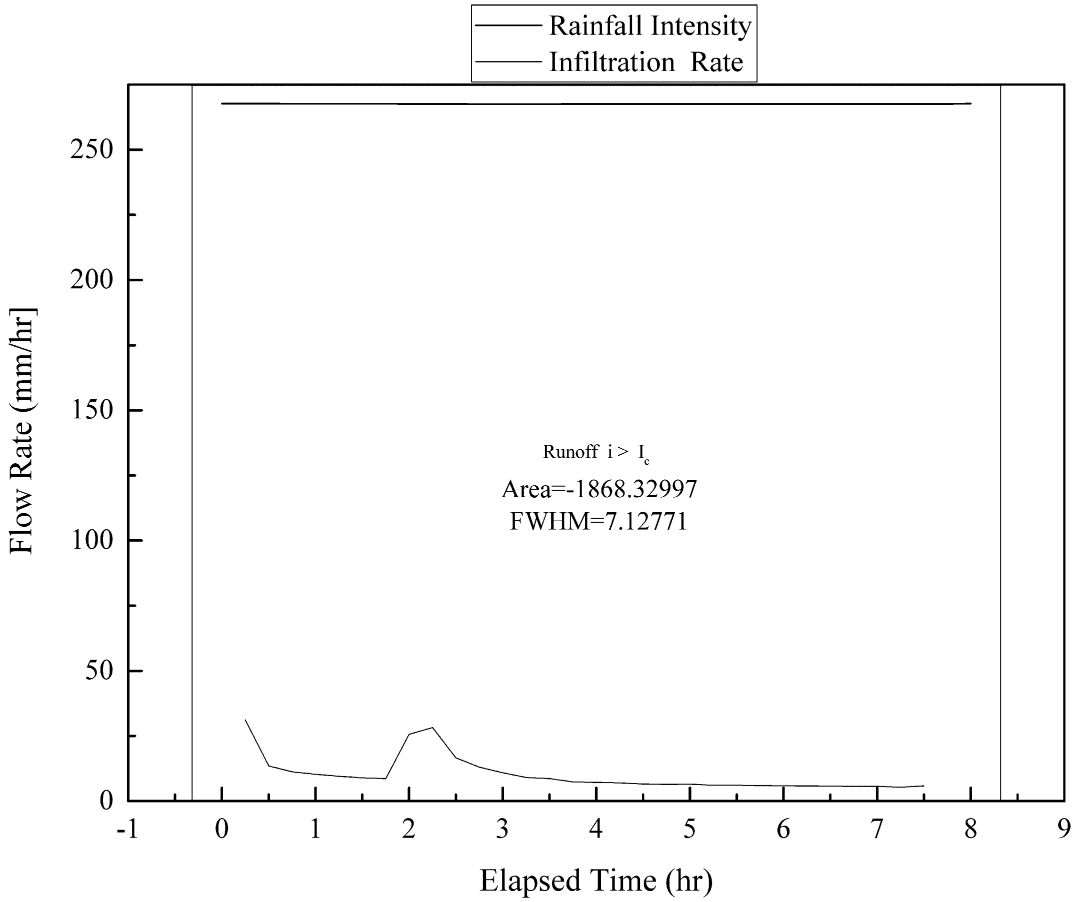

Unsaturated capillary barrier profile applied rainfall intensity is 40 mm/hr

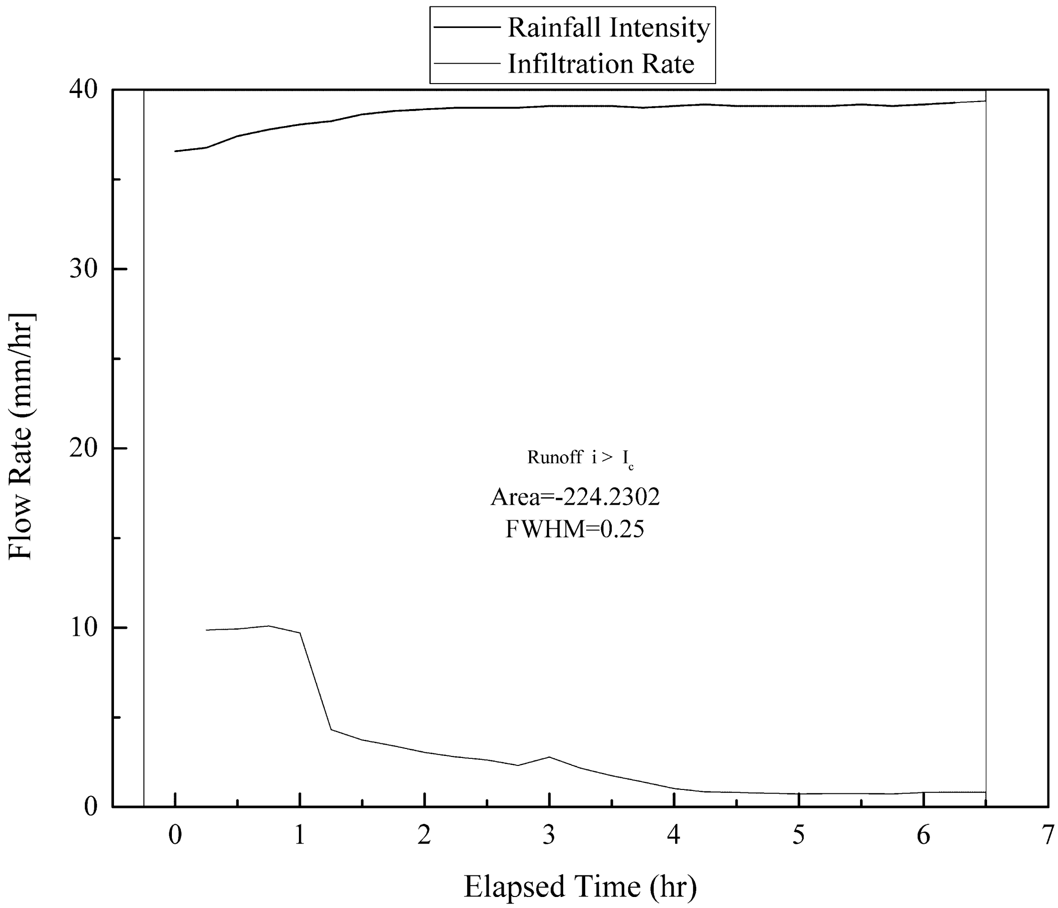

Unsaturated capillary barrier profile applied rainfall intensity is 55 mm/hr

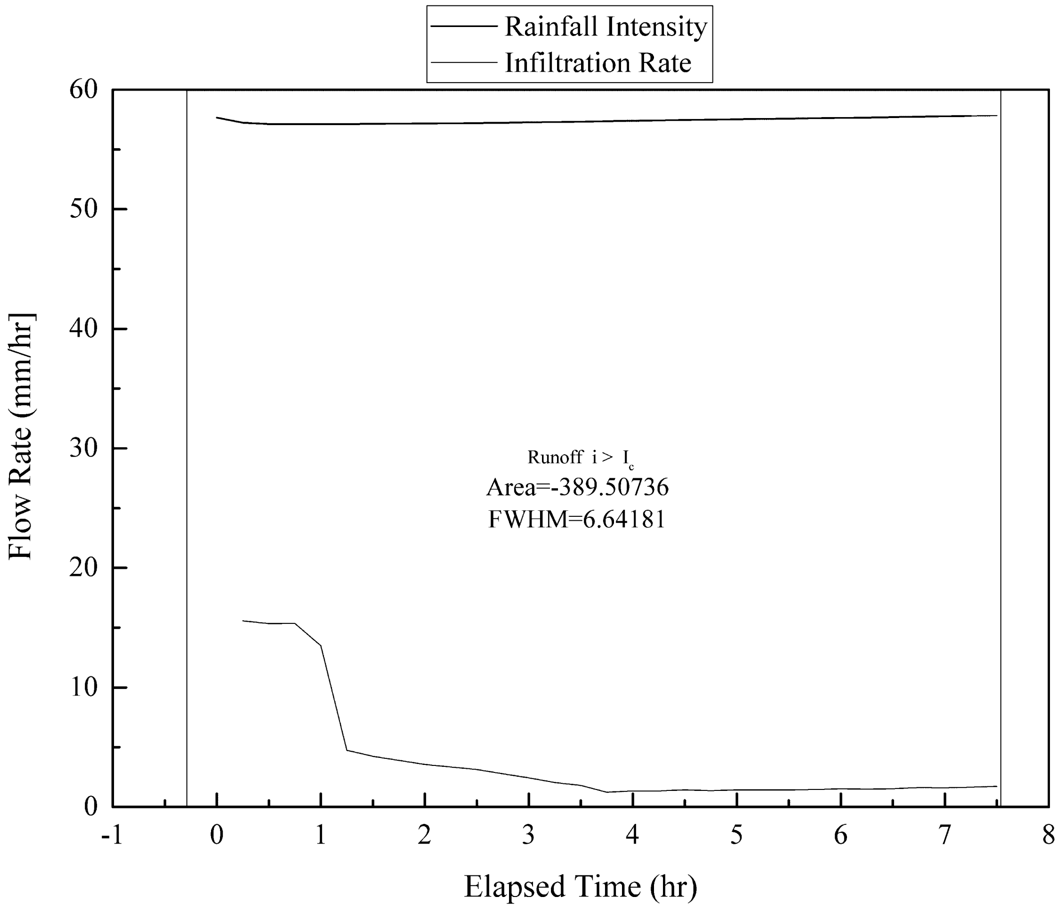

Unsaturated capillary barrier profile applied rainfall intensity is 90 mm/hr

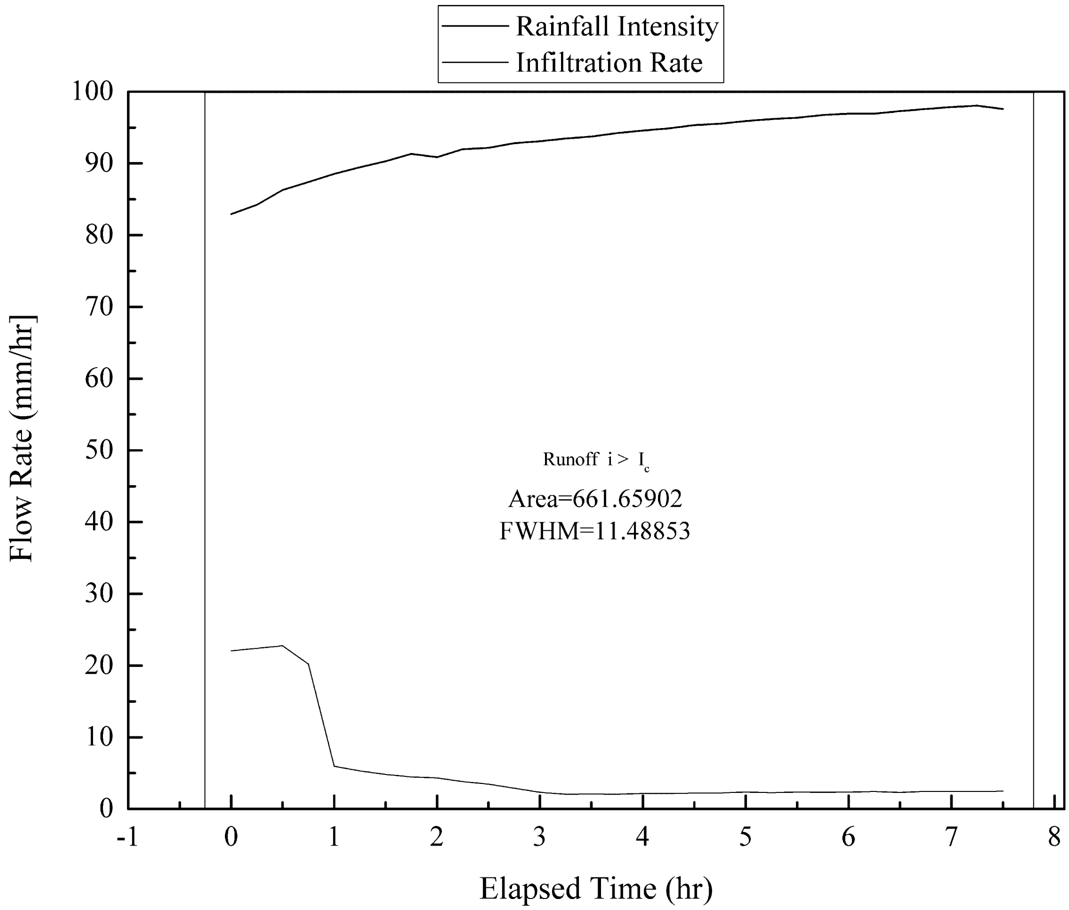

Unsaturated capillary barrier profile applied rainfall intensity is 140 mm/hr

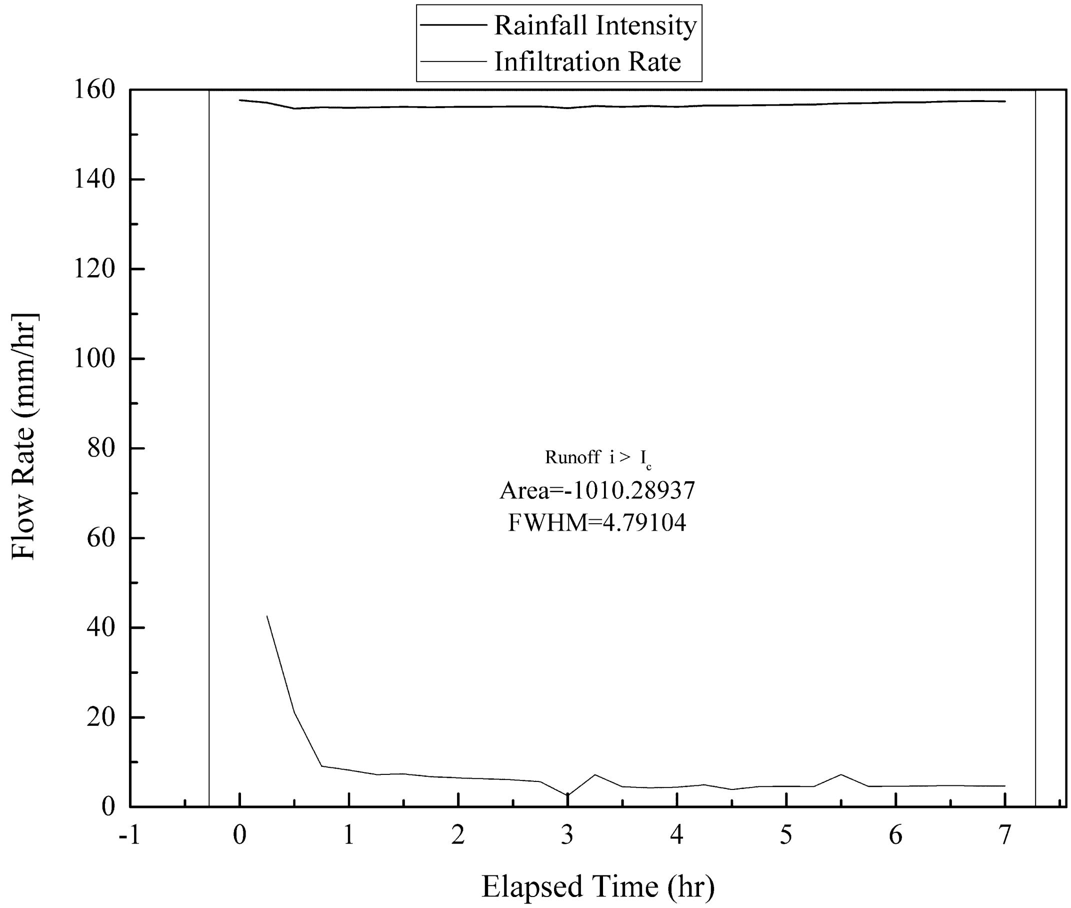

Unsaturated capillary barrier profile applied rainfall intensity is 190 mm/hr

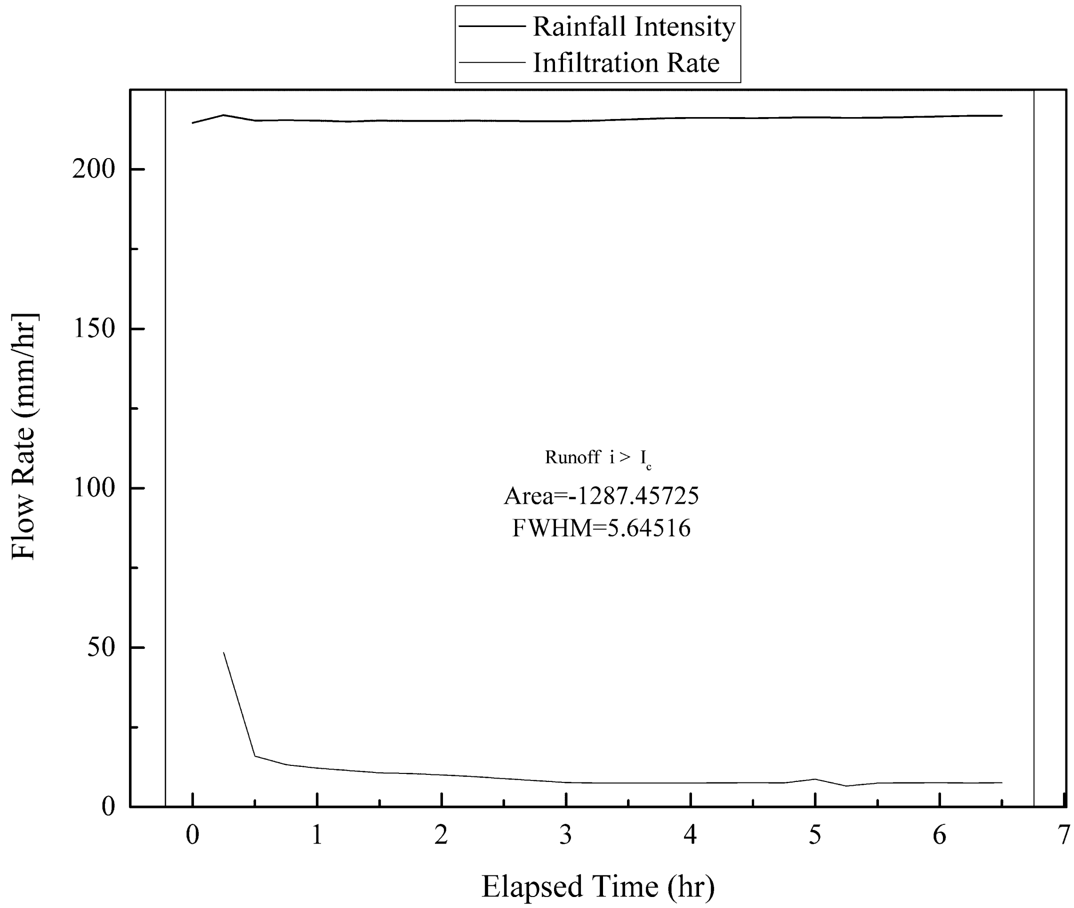

Unsaturated capillary barrier profile applied rainfall intensity is 260 mm/hr

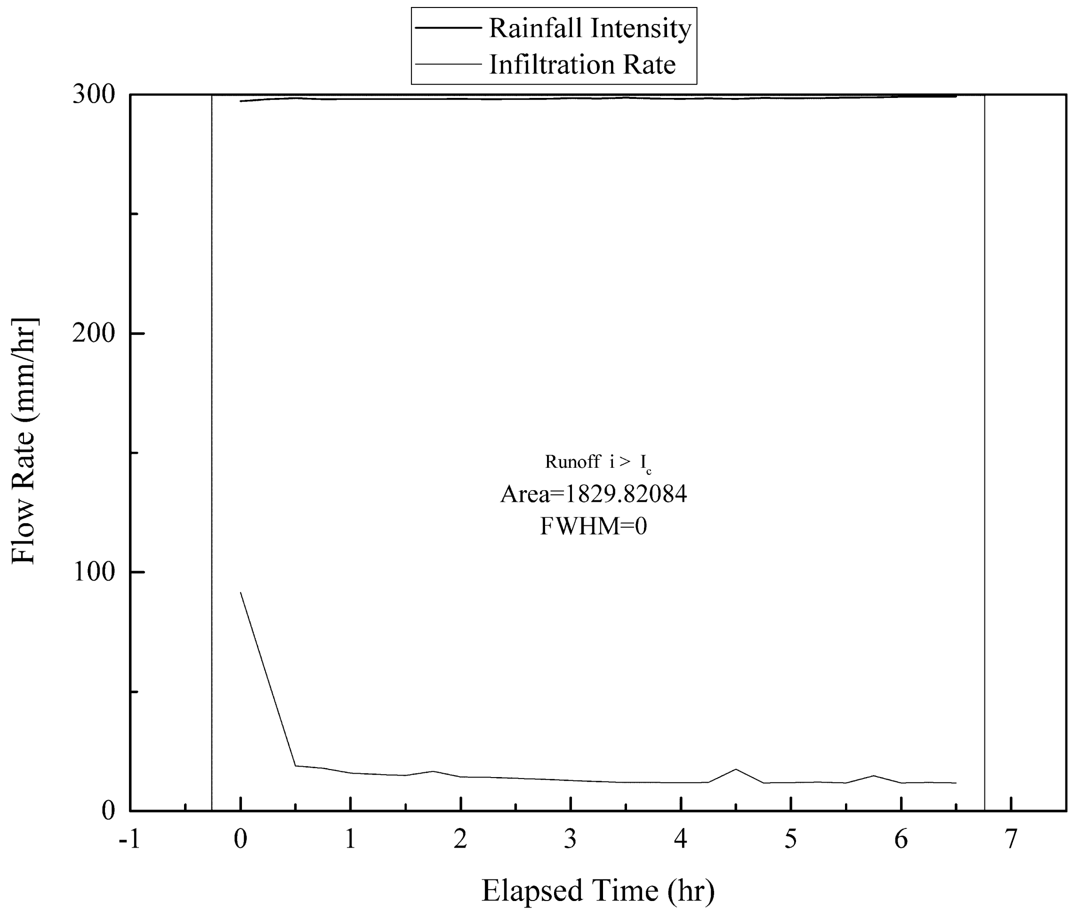

Unsaturated Profile 40mm/hr							
Rainfall rate L/hr	Rainfall rate mm^3/hr	Rainfall rate mm/hr		Infiltration rate L/hr	Infiltration rate mm^3/hr	Infiltration rate mm/hr
10.78046	10780460	39.92763		10.78046	10780460	39.92763
10.73009	10730090	39.74107		10.67971	10679710	39.55448
10.7133	10713300	39.67889		10.67971	10679710	39.55448
10.7049	10704900	39.64778		10.67971	10679710	39.55448
10.69986	10699860	39.62911		10.67971	10679710	39.55448
10.7049	10704900	39.64778		9.92969	9929690	36.77663
10.7121	10712100	39.67444		5.76768	5767680	21.36178
10.71749	10717490	39.69441		5.62048	5620480	20.81659
10.72169	10721690	39.70996		5.21648	5216480	19.3203
10.72505	10725050	39.72241		4.78768	4787680	17.73215
10.73009	10730090	39.74107		4.58406	4584060	16.978
10.73219	10732190	39.74885		4.21128	4211280	15.59733
10.7359	10735900	39.76259		3.96686	3966860	14.69207
10.73908	10739080	39.77437		3.80726	3807260	14.10096
10.74016	10740160	39.77837		3.55328	3553280	13.1603
10.74268	10742680	39.7877		3.42646	3426460	12.69059
10.7449	10744900	39.79593		3.17206	3172060	11.74837
10.74688	10746880	39.80326		3.14126	3141260	11.6343
10.74732	10747320	39.80489		3.00768	3007680	11.13956
10.74898	10748980	39.81104		2.89526	2895260	10.72319
10.75048	10750480	39.81659		2.87246	2872460	10.63874
10.75184	10751840	39.82163		2.56726	2567260	9.50837
10.75309	10753090	39.82626		2.56566	2565660	9.502444
10.75423	10754230	39.83048		2.20526	2205260	8.16763
10.75528	10755280	39.83437		2.23286	2232860	8.269852
10.75721	10757210	39.84152		2.12445	2124450	7.868333
10.75901	10759010	39.84819		2.12405	2124050	7.866852
10.75977	10759770	39.851		2.01486	2014860	7.462444
10.76049	10760490	39.85367		1.52366	1523660	5.643185
10.76031	10760310	39.853		1.87488	1874880	6.944
10.76096	10760960	39.85541		1.81206	1812060	6.711333
10.76157	10761570	39.85767		1.78326	1783260	6.604667

Unsaturated Silt 55 mmm/hr						
Rainfall rate L/hr	Rainfall rate mm^3/hr	Rainfall rate mm/hr		Infiltration rate L/hr	Infiltration rate mm^3/hr	Infiltration rate mm/hr
15.1128	15112800	55.97333		15.1128	15112800	55.97333
15.02464	15024640	55.64681		15.02464	15024640	55.64681
15.01205	15012050	55.60019		12.78351	12783510	47.34633
14.99945	14999450	55.55352		11.27505	11275050	41.75944
15.00701	15007010	55.58152		10.10589	10105890	37.42922
15.00785	15007850	55.58463		9.21245	9212450	34.12019
15.00845	15008450	55.58685		8.50468	8504680	31.49881
15.0089	15008900	55.58852		7.938	7938000	29.4
15.01205	15012050	55.60019		7.47023	7470230	27.66752
15.01205	15012050	55.60019		7.06989	7069890	26.18478
15.01434	15014340	55.60867		6.74328	6743280	24.97511
15.01625	15016250	55.61574		6.23255	6232550	23.08352
15.01786	15017860	55.6217		6.17294	6172940	22.86274
15.01745	15017450	55.62019		5.9365	5936500	21.98704
15.02044	15020440	55.63126		5.72858	5728580	21.21696
15.02307	15023070	55.641		5.54377	5543770	20.53248
15.02538	15025380	55.64956		5.37552	5375520	19.90933
15.02744	15027440	55.65719		5.21886	5218860	19.32911
15.03193	15031930	55.67381		5.08145	5081450	18.82019
15.03472	15034720	55.68415		4.95166	4951660	18.33948
15.03724	15037240	55.69348		4.83156	4831560	17.89467
15.03953	15039530	55.70196		4.72225	4722250	17.48981
15.04162	15041620	55.7097		4.61763	4617630	17.10233
15.04353	15043530	55.71678		4.52087	4520870	16.74396
15.0463	15046300	55.72704		4.43147	4431470	16.41285
15.04789	15047890	55.73293		4.34622	4346220	16.09711
15.04936	15049360	55.73837		4.26606	4266060	15.80022
15.05163	15051630	55.74678		4.1929	4192900	15.52926
15.05287	15052870	55.75137		4.12236	4122360	15.268
15.05403	15054030	55.75567		4.05564	4055640	15.02089
15.05511	15055110	55.75967		3.99218	3992180	14.78585
15.05691	15056910	55.76633		3.93326	3933260	14.56763

Unsaturated silt at 90 mm/hr						
Rainfall rate L/hr	Rainfall rate mm^3/hr	Rainfall rate mm/hr		Infiltration rate L/hr	Infiltration rate mm^3/hr	Infiltration rate mm/hr
23.265	23265000	86.16667		23.265	23265000	86.16667
23.2885	23288500	86.2537		9.2761	9276100	34.35593
23.2885	23288500	86.2537		5.5461	5546100	20.54111
23.2885	23288500	86.2537		4.4601	4460100	16.51889
23.265	23265000	86.16667		3.7754	3775400	13.98296
23.2885	23288500	86.2537		3.3197	3319700	12.29519
23.265	23265000	86.16667		2.977	2977000	11.02593
23.2415	23241500	86.07963		2.7343	2734300	10.12704
23.2415	23241500	86.07963		2.5155	2515500	9.316667
23.218	23218000	85.99259		2.3024	2302400	8.527407
23.265	23265000	86.16667		2.2382	2238200	8.28963
23.265	23265000	86.16667		2.1018	2101800	7.784444
23.265	23265000	86.16667		1.9986	1998600	7.402222
23.265	23265000	86.16667		1.7314	1731400	6.412593
23.265	23265000	86.16667		1.6386	1638600	6.068889
23.312	23312000	86.34074		2.1048	2104800	7.795556
23.2885	23288500	86.2537		1.7577	1757700	6.51
23.3355	23335500	86.42778		1.7051	1705100	6.315185
23.359	23359000	86.51481		1.6862	1686200	6.245185
23.359	23359000	86.51481		1.4134	1413400	5.234815
23.3825	23382500	86.60185		1.7317	1731700	6.413704
23.406	23406000	86.68889		1.5132	1513200	5.604444
23.453	23453000	86.86296		1.501	1501000	5.559259
23.5	23500000	87.03704		2.4536	2453600	9.087407
23.5235	23523500	87.12407		0.3859	385900	1.429259
23.5235	23523500	87.12407		1.5307	1530700	5.669259
23.5705	23570500	87.29815		1.3681	1368100	5.067037
23.6175	23617500	87.47222		1.3595	1359500	5.035185
23.641	23641000	87.55926		1.331	1331000	4.92963
23.6645	23664500	87.6463		1.3273	1327300	4.915926
23.735	23735000	87.90741		1.3326	1332600	4.935556
23.8055	23805500	88.16852		1.2691	1269100	4.70037

Unsaturated Silt 140mm/hr						
Rainfall rate L/hr	Rainfall rate mm^3/hr	Rainfall rate mm/hr		Infiltration rate L/hr	Infiltration rate mm^3/hr	Infiltration rate mm/hr
38.164	38164000	141.3481		37.6624	37662400	139.4904
38.0935	38093500	141.087		35.7383	35738300	132.3641
38.117	38117000	141.1741		36.1454	36145400	133.8719
38.117	38117000	141.1741		33.6382	33638200	124.5859
38.0935	38093500	141.087		9.8919	9891900	36.63667
38.1405	38140500	141.2611		6.6969	6696900	24.80333
38.1405	38140500	141.2611		4.9429	4942900	18.30704
38.117	38117000	141.1741		4.0394	4039400	14.96074
38.164	38164000	141.3481		3.4752	3475200	12.87111
38.1875	38187500	141.4352		3.0155	3015500	11.16852
38.1875	38187500	141.4352		2.6255	2625500	9.724074
38.1875	38187500	141.4352		2.2447	2244700	8.313704
38.211	38211000	141.5222		2.0954	2095400	7.760741
38.211	38211000	141.5222		1.8386	1838600	6.80963
38.1875	38187500	141.4352		1.6843	1684300	6.238148
38.1405	38140500	141.2611		1.5241	1524100	5.644815
38.1875	38187500	141.4352		1.3851	1385100	5.13
38.1875	38187500	141.4352		1.6423	1642300	6.082593
38.211	38211000	141.5222		1.6782	1678200	6.215556
38.164	38164000	141.3481		1.8436	1843600	6.828148
40.2085	40208500	148.9204		3.8785	3878500	14.36481
36.0725	36072500	133.6019		-0.2883	-288300	-1.06778
38.1875	38187500	141.4352		1.5947	1594700	5.906296
38.211	38211000	141.5222		1.5266	1526600	5.654074
38.211	38211000	141.5222		1.5118	1511800	5.599259
38.1875	38187500	141.4352		1.5527	1552700	5.750741
38.1875	38187500	141.4352		1.5315	1531500	5.672222
38.211	38211000	141.5222		1.5558	1555800	5.762222
38.211	38211000	141.5222		1.5202	1520200	5.63037
38.211	38211000	141.5222		1.5606	1560600	5.78
38.0935	38093500	141.087		1.4599	1459900	5.407037

Unsaturated silt 190 mm/hr						
Rainfall rate L/hr	Rainfall rate mm^3/hr	Rainfall rate mm/hr		Infiltration rate L/hr	Infiltration rate mm^3/hr	Infiltration rate mm/hr
0	0	0			0	0
51.183	51183000	189.5667		38.0226	38022600	140.8244
51.136	51136000	189.3926		22.4962	22496200	83.31926
51.09683	51096830	189.2475		34.0469	34046900	126.0996
51.0655	51065500	189.1315		20.3135	20313500	75.23519
51.0561	51056100	189.0967		13.0221	13022100	48.23
51.04983	51049830	189.0734		9.1061	9106100	33.7263
51.03864	51038640	189.032		7.8747	7874700	29.16556
51.02731	51027310	188.99		6.7308	6730800	24.92889
51.02111	51021110	188.9671		6.1055	6105500	22.61296
51.0138	51013800	188.94		5.5664	5566400	20.6163
51.00568	51005680	188.9099		5.2417	5241700	19.4137
51.00088	51000880	188.8921		4.8528	4852800	17.97333
50.995	50995000	188.8704		4.3793	4379300	16.21963
50.99164	50991640	188.8579		4.0456	4045600	14.9837
50.98873	50988730	188.8471		3.9292	3929200	14.55259
50.98913	50989130	188.8486		3.8214	3821400	14.15333
50.99224	50992240	188.8601		3.7052	3705200	13.72296
50.98717	50987170	188.8414		3.453	3453000	12.78889
50.99376	50993760	188.8658		3.4921	3492100	12.9337
51.00205	51002050	188.8965		3.5203	3520300	13.03815
51.01179	51011790	188.9326		3.3449	3344900	12.38852
51.02277	51022770	188.9732		3.2639	3263900	12.08852
51.02974	51029740	188.999		2.999	2999000	11.10741
51.03613	51036130	189.0227		3.1066	3106600	11.50593
51.04482	51044820	189.0549		2.7711	2771100	10.26333
51.05194	51051940	189.0813		3.1592	3159200	11.70074
51.06115	51061150	189.1154		2.4385	2438500	9.031481
51.0697	51069700	189.147		2.8345	2834500	10.49815
51.07684	51076840	189.1735		2.7002	2700200	10.00074
51.08665	51086650	189.2098		2.811	2811000	10.41111

Unsaturated Silt 260 mm/hr						
Rainfall rate L/hr	Rainfall rate mm^3/hr	Rainfall rate mm/hr		Infiltration rate L/hr	Infiltration rate mm^3/hr	Infiltration rate mm/hr
72.286	72286000	267.7259		31.1116	31111600	115.2281
72.286	72286000	267.7259		13.456	13456000	49.83704
72.27817	72278170	267.6969		11.2577	11257700	41.69519
72.25663	72256630	267.6171		10.2888	10288800	38.10667
72.2625	72262500	267.6389		9.506	9506000	35.20741
72.25858	72258580	267.6244		8.931	8931000	33.07778
72.25914	72259140	267.6264		8.6169	8616900	31.91444
72.25369	72253690	267.6063		25.6319	25631900	94.93296
72.24422	72244220	267.5712		28.2465	28246500	104.6167
72.239	72239000	267.5519		16.6168	16616800	61.5437
72.23473	72234730	267.536		13.0348	13034800	48.27704
72.22725	72227250	267.5083		10.8466	10846600	40.17259
72.21731	72217310	267.4715		9.0884	9088400	33.66074
72.21382	72213820	267.4586		8.6221	8622100	31.9337
72.2202	72220200	267.4822		7.3607	7360700	27.26185
72.23019	72230190	267.5192		7.1416	7141600	26.45037
72.23209	72232090	267.5263		6.9673	6967300	25.80481
72.23247	72232470	267.5277		6.5246	6524600	24.16519
72.23158	72231580	267.5244		6.4367	6436700	23.83963
72.23313	72233130	267.5301		6.5133	6513300	24.12333
72.2334	72233400	267.5311		6.1446	6144600	22.75778
72.23473	72234730	267.536		6.0897	6089700	22.55444
72.23491	72234910	267.5367		5.9522	5952200	22.04519
72.23606	72236060	267.541		5.8561	5856100	21.68926
72.239	72239000	267.5519		5.8115	5811500	21.52407
72.2399	72239900	267.5552		5.7433	5743300	21.27148
72.24074	72240740	267.5583		5.6945	5694500	21.09074
72.24152	72241520	267.5612		5.6317	5631700	20.85815
72.24305	72243050	267.5669		5.3836	5383600	19.93926
72.24292	72242920	267.5664		5.8086	5808600	21.51333
72.24658	72246580	267.5799		5.8086	5808600	21.51333
72.24855	72248550	267.5872		5.8086	5808600	21.51333

Unsaturated capillary barrier 40mm/hr						
Rainfall rate L/hr	Rainfall rate mm^3/hr	Rainfall rate mm/hr		Infiltration rate L/hr	Infiltration rate mm^3/hr	Infiltration rate mm/hr
9.8737	9873700	36.56926		9.8737	9873700	36.56926
9.92407	9924070	36.75581		9.92407	9924070	36.75581
10.10039	10100390	37.40885		10.10039	10100390	37.40885
10.20114	10201140	37.782		9.71034	9710340	35.96422
10.2767	10276700	38.06185		4.3127	4312700	15.97296
10.32708	10327080	38.24844		3.73788	3737880	13.844
10.42783	10427830	38.62159		3.41103	3411030	12.63344
10.47821	10478210	38.80819		3.04661	3046610	11.28374
10.5034	10503400	38.90148		2.7926	2792600	10.34296
10.52858	10528580	38.99474		2.62458	2624580	9.720667
10.52858	10528580	38.99474		2.31858	2318580	8.587333
10.52858	10528580	38.99474		2.78978	2789780	10.33252
10.55377	10553770	39.08804		2.16897	2168970	8.033222
10.55377	10553770	39.08804		1.74497	1744970	6.462852
10.55377	10553770	39.08804		1.39657	1396570	5.172481
10.52858	10528580	38.99474		1.03098	1030980	3.818444
10.55377	10553770	39.08804		0.84617	846170	3.133963
10.57896	10578960	39.18133		0.81376	813760	3.013926
10.55377	10553770	39.08804		0.76897	768970	2.848037
10.55377	10553770	39.08804		0.72937	729370	2.70137
10.55377	10553770	39.08804		0.74377	743770	2.754704
10.55377	10553770	39.08804		0.74977	749770	2.776926
10.57896	10578960	39.18133		0.73016	730160	2.704296
10.55377	10553770	39.08804		0.80857	808570	2.994704
10.57896	10578960	39.18133		0.81816	818160	3.030222
10.60415	10604150	39.27463		0.82375	823750	3.050926

Unsaturated capillary barrier 40mm/hr							
Rainfall rate L/hr	Rainfall rate mm^3/hr	Rainfall rate mm/hr		Infiltration rate L/hr	Infiltration rate mm^3/hr	Infiltration rate mm/hr
15.56618	15566180	57.65252		15.56618	15566180	57.65252
15.45284	15452840	57.23274		15.33949	15339490	56.81293
15.42345	15423450	57.12389		15.36468	15364680	56.90622
15.42135	15421350	57.11611		13.49266	13492660	49.97281
15.42513	15425130	57.13011		4.75344	4753440	17.60533
15.42345	15423450	57.12389		4.24946	4249460	15.73874
15.42945	15429450	57.14611		3.89623	3896230	14.43048
15.43395	15433950	57.16278		3.55463	3554630	13.1653
15.43745	15437450	57.17574		3.34863	3348630	12.40233
15.44276	15442760	57.19541		3.13262	3132620	11.6023
15.44711	15447110	57.21152		2.78702	2787020	10.3223
15.45494	15454940	57.24052		2.4298	2429800	8.999259
15.46156	15461560	57.26504		2.0406	2040600	7.557778
15.46903	15469030	57.2927		1.81098	1810980	6.707333
15.47719	15477190	57.32293		1.23417	1234170	4.571
15.48747	15487470	57.361		1.34895	1348950	4.996111
15.49655	15496550	57.39463		1.35615	1356150	5.022778
15.50741	15507410	57.43485		1.43332	1433320	5.308593
15.51713	15517130	57.47085		1.36212	1362120	5.044889
15.52462	15524620	57.49859		1.43334	1433340	5.308667
15.5326	15532600	57.52815		1.42292	1422920	5.270074
15.53985	15539850	57.555		1.43172	1431720	5.302667
15.54647	15546470	57.57952		1.46132	1461320	5.412296
15.55464	15554640	57.60978		1.5309	1530900	5.67
15.56215	15562150	57.63759		1.4925	1492500	5.527778
15.57006	15570060	57.66689		1.53329	1533290	5.678852
15.57924	15579240	57.70089		1.61806	1618060	5.992815
15.58867	15588670	57.73581		1.60365	1603650	5.939444
15.59832	15598320	57.77156		1.65964	1659640	6.146815
15.60816	15608160	57.808		1.72723	1727230	6.397148

Unsaturated capillary barrier 90mm/hr						
Rainfall rate L/hr	Rainfall rate mm^3/hr	Rainfall rate mm/hr		Infiltration rate L/hr	Infiltration rate mm^3/hr	Infiltration rate mm/hr
22.39213	22392130	82.93381		22.39213	22392130	82.93381
22.74476	22744760	84.23985		22.74476	22744760	84.23985
23.2989	23298900	86.29222		20.2061	20206100	74.83741
23.60116	23601160	87.4117		5.96236	5962360	22.08281
23.90341	23903410	88.53115		5.30381	5303810	19.64374
24.15529	24155290	89.46404		4.82129	4821290	17.85663
24.38198	24381980	90.30363		4.45638	4456380	16.50511
24.65905	24659050	91.32981		4.33785	4337850	16.06611
24.53311	24533110	90.86337		3.81431	3814310	14.12707
24.83537	24835370	91.98285		3.46057	3460570	12.81693
24.88574	24885740	92.16941		2.88854	2888540	10.6983
25.06206	25062060	92.82244		2.33406	2334060	8.644667
25.13762	25137620	93.1023		2.05642	2056420	7.61637
25.23838	25238380	93.47548		2.07438	2074380	7.682889
25.31394	25313940	93.75533		2.05354	2053540	7.605704
25.43988	25439880	94.22178		2.16588	2165880	8.021778
25.54063	25540630	94.59493		2.15583	2155830	7.984556
25.6162	25616200	94.87481		2.219	2219000	8.218519
25.74214	25742140	95.34126		2.25534	2255340	8.353111
25.79251	25792510	95.52781		2.34651	2346510	8.690778
25.89326	25893260	95.90096		2.28766	2287660	8.472815
25.96883	25968830	96.18085		2.35323	2353230	8.715667
26.0192	26019200	96.36741		2.332	2332000	8.637037
26.11996	26119960	96.74059		2.36916	2369160	8.774667
26.17033	26170330	96.92715		2.44153	2441530	9.042704
26.17033	26170330	96.92715		2.31073	2310730	8.558259

Unsaturated capillary barrier 140mm/hr						
Rainfall rate L/hr	Rainfall rate mm^3/hr	Rainfall rate mm/hr		Infiltration rate L/hr	Infiltration rate mm^3/hr	Infiltration rate mm/hr
42.56772	42567720	157.6582		42.56772	42567720	157.6582
42.41659	42416590	157.0985		21.08939	21089390	78.10885
42.06396	42063960	155.7924		9.12236	9122360	33.78652
42.13952	42139520	156.0723		8.25272	8252720	30.56563
42.11434	42114340	155.979		7.24034	7240340	26.81607
42.13952	42139520	156.0723		7.34632	7346320	27.20859
42.16471	42164710	156.1656		6.76031	6760310	25.03819
42.13952	42139520	156.0723		6.48672	6486720	24.02489
42.16471	42164710	156.1656		6.28711	6287110	23.28559
42.16471	42164710	156.1656		6.07351	6073510	22.49448
42.1899	42189900	156.2589		5.6391	5639100	20.88556
42.1899	42189900	156.2589		2.5159	2515900	9.318148
42.08915	42089150	155.8857		7.19035	7190350	26.63093
42.21509	42215090	156.3522		4.49109	4491090	16.63367
42.16471	42164710	156.1656		4.30071	4300710	15.92856
42.21509	42215090	156.3522		4.41589	4415890	16.35515
42.16471	42164710	156.1656		4.93831	4938310	18.29004
42.24028	42240280	156.4455		3.88908	3889080	14.404
42.24028	42240280	156.4455		4.54268	4542680	16.82474
42.26546	42265460	156.5387		4.57946	4579460	16.96096
42.29065	42290650	156.632		4.55585	4555850	16.87352
42.31584	42315840	156.7253		7.23624	7236240	26.80089
42.36622	42366220	156.9119		4.59142	4591420	17.00526
42.3914	42391400	157.0052		4.639	4639000	17.18148
42.44178	42441780	157.1918		4.66218	4662180	17.26733
42.44178	42441780	157.1918		4.81498	4814980	17.83326

Unsaturated capillary barrier 190mm/hr						
Rainfall rate L/hr	Rainfall rate mm^3/hr	Rainfall rate mm/hr		Infiltration rate L/hr	Infiltration rate mm^3/hr	Infiltration rate mm/hr
57.9324	57932400	214.5644		48.3924	48392400	179.2311
58.58729	58587290	216.99		15.97849	15978490	59.17959
58.1339	58133900	215.3107		13.2887	13288700	49.21741
58.15909	58159090	215.404		12.18789	12187890	45.14033
58.1339	58133900	215.3107		11.4647	11464700	42.46185
58.05834	58058340	215.0309		10.75554	10755540	39.83533
58.1339	58133900	215.3107		10.4947	10494700	38.86926
58.10872	58108720	215.2175		10.03792	10037920	37.17748
58.10872	58108720	215.2175		9.58872	9588720	35.51378
58.1339	58133900	215.3107		8.8743	8874300	32.86778
58.10872	58108720	215.2175		8.29152	8291520	30.70933
58.08353	58083530	215.1242		7.68673	7686730	28.46937
58.08353	58083530	215.1242		7.49753	7497530	27.76863
58.1339	58133900	215.3107		7.5107	7510700	27.81741
58.23466	58234660	215.6839		7.47306	7473060	27.678
58.31022	58310220	215.9638		7.51182	7511820	27.82156
58.3606	58360600	216.1504		7.585	7585000	28.09259
58.3606	58360600	216.1504		7.5878	7587800	28.10296
58.33541	58335410	216.0571		7.57021	7570210	28.03781
58.38578	58385780	216.2436		8.69658	8696580	32.20956
58.41097	58410970	216.3369		6.60217	6602170	24.45248
58.3606	58360600	216.1504		7.491	7491000	27.74444
58.38578	58385780	216.2436		7.55018	7550180	27.96363
58.43616	58436160	216.4302		7.59416	7594160	28.12652
58.48654	58486540	216.6168		7.46574	7465740	27.65089
58.53691	58536910	216.8034		7.61251	7612510	28.19448

Unsaturated capillary barrier 260mm/hr						
Rainfall rate L/hr	Rainfall rate mm^3/hr	Rainfall rate mm/hr		Infiltration rate L/hr	Infiltration rate mm^3/hr	Infiltration rate mm/hr
80.24897	80248970	297.2184		55.20897	55208970	204.4777
80.47566	80475660	298.058		18.95566	18955660	70.20615
80.6016	80601600	298.5244		17.9952	17995200	66.64889
80.47566	80475660	298.058		15.96006	15960060	59.11133
80.50085	80500850	298.1513		15.34365	15343650	56.82833
80.50085	80500850	298.1513		14.93285	14932850	55.30685
80.50085	80500850	298.1513		16.66085	16660850	61.70685
80.50085	80500850	298.1513		14.29245	14292450	52.935
80.52604	80526040	298.2446		14.11204	14112040	52.26681
80.47566	80475660	298.058		13.70766	13707660	50.76911
80.50085	80500850	298.1513		13.31365	13313650	49.30981
80.52604	80526040	298.2446		12.86604	12866040	47.652
80.6016	80601600	298.5244		12.348	12348000	45.73333
80.55122	80551220	298.3379		12.05402	12054020	44.64452
80.65198	80651980	298.711		11.99518	11995180	44.42659
80.55122	80551220	298.3379		11.83842	11838420	43.846
80.52604	80526040	298.2446		11.98604	11986040	44.39274
80.57641	80576410	298.4311		17.51721	17517210	64.87856
80.52604	80526040	298.2446		11.74364	11743640	43.49496
80.62679	80626790	298.6177		11.98319	11983190	44.38219
80.57641	80576410	298.4311		12.21121	12211210	45.2267
80.6016	80601600	298.5244		11.7856	11785600	43.65037
80.65198	80651980	298.711		14.79718	14797180	54.80437
80.67716	80677160	298.8043		11.80716	11807160	43.73022
80.75273	80752730	299.0842		11.99433	11994330	44.42344
80.77792	80777920	299.1775		11.79832	11798320	43.69748

Unsaturated Profiles						
	Rainfall Intensity	Area under curve (mm/hr)	Final Cumulative Runoff Volume mm^3	Calculated Final Cumulative Runoff Volume L	Measured Final Cumulative Runoff Volume L	Percent difference
Unsaturated silt	40	170.3	45973110.6	46.0	49.8	4%
Unsaturated silt	55	377.6	101959352.1	102.0	89.1	-13%
Unsaturated silt	90	643.1	173645934.3	173.6	163.2	-10%
Unsaturated silt	140	1012.3	273308261.4	273.3	243.2	-30%
Unsaturated silt	190	1353.0	365317889.4	365.3	325.7	-40%
Unsaturated silt	260	1868.3	504449091.9	504.4	499.1	-5%
Unsaturated Capillary Barrier	40	224.2	60542154.0	60.5	48.2	-12%
Unsaturated Capillary Barrier	55	389.5	105166987.2	105.2	89.0	-16%
Unsaturated Capillary Barrier	90	661.7	178647935.4	178.6	164.0	-15%
Unsaturated Capillary Barrier	140	1010.3	272778129.9	272.8	244.5	-28%
Unsaturated Capillary Barrier	190	1287.5	347613457.5	347.6	311.1	-36%
Unsaturated Capillary Barrier	260	1829.8	494051626.8	494.1	424.7	-69%

APPENDIX VI

Infiltration capacity function calculation sheet

$$I_r = \frac{V}{A\,t}$$

I_r	=	Infiltration rate [L/T]
V	=	Volume of water added during each time increment to the soil specimen to maintain ponding depth constant [L^3]
A	=	Surface area of the soil column [L^2]
t	=	Elapsed time increment corresponding to added water volume [T]
$\frac{V}{A}$	=	Wetting front propagation depth [L]

After calculating the infiltration rate corresponding to each time increment, the infiltration capacity function can be constructed by plotting the infiltration rate with cumulative elapsed time.